5-18-2021

Development of a Design Guideline for Pile Foundations Subjected to Liquefaction-Induced Lateral Spreading

Milad Souri
Portland State University

Development of a Design Guideline for Pile Foundations Subjected to Liquefaction-Induced Lateral Spreading

by

Milad Souri

A dissertation submitted in partial fulfillment of the
requirements for the degree of

Doctor of Philosophy
in
Civil and Environmental Engineering

Dissertation Committee:
Arash Khosravifar, Chair
Diane Moug
Thomas Schumacher
Hormoz Zareh

Portland State University
2021

ABSTRACT

Extensive loss of stiffness and strength in liquefied soils can cause large ground deformations during strong earthquake shaking. One of the major sources of damage in pile foundations in liquefied soil is the excessive deformation due to lateral spreading. Pile-supported wharves subjected to earthquake motions are expected to accommodate inertial loads imposed at pile head from the superstructure as well as the kinematic loads imposed on piles from the lateral ground deformations. Current design codes significantly vary on how to combine inertia and kinematic demands. Recent research on soil-foundation-structure interaction suffers from lack of experiment-based data. There is a serious need to fill the knowledge gap and help designers to better evaluate risk and design cost-effective pile foundations.

In this research, the interaction of inertial and kinematic demands is investigated using data from five well-instrumented centrifuge tests on pile-supported wharves. The observations from these tests were used to investigate the time- and depth-dependent nature of kinematic and inertial demands on the deep foundations during earthquake loading. The test results were analyzed to provide the relative contributions of peak inertial loads and peak soil displacements during critical cycles, and the data revealed the depth-dependency of these factors. The results were used to refine existing guidelines for design of pile-supported wharves subjected to foundation deformations.

The observations from centrifuge tests were then used to evaluate the accuracy of the equivalent static analysis (ESA) procedure using p-y models for the design of

pile-supported wharves subjected to lateral ground deformations during earthquake loading. The piles in these centrifuge tests were subjected to the combined effects of wharf deck inertial loads and ground deformations. The experiments included soil properties ranging from nonliquefiable to fully liquefied cases which provided a wide range of conditions against which the ESA method could be evaluated.

Finally, a nonlinear dynamic model of a pile-supported wharf was created and calibrated using recorded data from a centrifuge test. The objective of the numerical modeling was to create a calibrated numerical model that captures key responses of the wharf and the soil in order to be used in subsequent studies that are too costly and time-consuming to do using physical modeling. The calibrated numerical model was then used in an incremental dynamic analysis to evaluate the effects of ground motion duration on the dynamic response of a pile-supported wharf subjected to liquefaction-induced lateral ground deformations. The analysis results provided insights on the relative contribution of inertial and kinematic demands on the response of the wharf with respect to motion duration.

DEDICATION

To my parents for all the love and support.

ACKNOWLEDGEMENTS

I would like to express my sincere appreciation to Prof. Arash Khosravifar for his guidance and support during my research. This was truly a remarkable experience and I am grateful to have this opportunity to work on this project and collaborate with great people. My appreciation also extends to Steve Dickenson, Nason McCullough, and Scott Schlechter for sharing their valuable experimental data and providing comments throughout this research. Support for conducting centrifuge tests was provided by Grant No. CMS-9702744 from the National Science Foundation (NSF) and Grant No. SA2394JB from the Pacific Earthquake Engineering Research Center (S. Dickenson, P.I.). Support for recent analyses of the centrifuge tests was provided by Grant No. CMMI-1761712 from NSF and Grant No. 171126 from the Deep Foundations Institute (A. Khosravifar, P.I.). Any opinions, findings, and conclusions or recommendations expressed in this article are those of the author(s) and do not necessarily reflect the views of the funding agencies. I would like to appreciates the inputs provided by the DFI project advisory board members Dr. Zia Zafir, Mr. Kwabena Ofori-Awuah, Professor Anne Lemnitzer, Dr. Ben Turner, and Dr. Azadeh Bozorgzadeh during this research.

Last, but not least, I would like to thank my dear parents, Ebrahim and Momeneh, my lovely wife Bahareh, and my siblings Mohammad and Atieh for their support and motivation and for putting a smile on my face all the times.

TABLE OF CONTENTS

Page

LIST OF TABLES

LIST OF FIGURES

CHAPTER 1

1.0 OVERVIEW OF RESEARCH

1.1 INTRODUCTION

Liquefaction-induced lateral spreading has been demonstrated to be a major cause of damage to pile-supported wharves (e.g. Hamada et al. 1986, Egan and Wang 1991, Werner et al. 1997, Finn 2005, Rathje et al. 2010, Turner et al. 2016, and Cubrinovski et al. 2017). Lateral ground deformations may be caused by inertial slope movement, and/or by lateral spreading from liquefaction or cyclic softening of foundation soils in the slope or embankment adjacent to the structure and in the backland areas. Studies of the response of piles and pile-supported structures in liquefiable soils using physical models, numerical simulations, and case studies have provided the basis for a number of design recommendations addressing dynamic loads on deep foundations (e.g., Tokimatsu and Asaka 1998, Martin et al. 2002, Dobry et al. 2003, Tokimatsu 2003, Cubrinovski and Ishihara 2006, and Boulanger et al. 2007). Despite insights gleaned from these studies on the consequences of liquefaction-induced slope failure on pile foundations, there is no consensus on how to combine inertial and kinematic loading estimated using uncoupled methods of analysis routinely used in practice. ASCE 61-14 (ASCE 2014) requires that simultaneous application of inertial and kinematic loads be considered, taking into account the phasing and the locations where the loads are applied. The commentary in Section C4.7 of ASCE 61-14 and the Port of Long Beach Wharf Design Criteria (POLB 2015) suggest that the locations of maximum

bending moments from inertia and lateral ground deformations are spaced far enough apart that the two loads do not need to be superimposed. They also suggest that the maximum bending moments from the two loads tend to occur at different times; therefore, they recommend that the loads be treated as uncoupled for typical marginal container wharves. On the other hand, Port of Anchorage Modernization Program Seismic Design Manual (POA 2017) recommends combining the peak inertial loading from earthquake ground motions with 100% of peak kinematic loads from lateral ground displacements. This design manual allows for smaller combination factors (no less than 25%) if justified using peer-reviewed 2-D nonlinear numerical analysis. However, it is recognized that there is limited research and validation of these assumptions; therefore, the design codes indicate that these assumptions should be checked on a project-specific basis.

The lack of consensus on how to combine inertial and kinematic demands is due, in part, to the relatively limited quantity of experimental data on the phasing of lateral spreading and superstructure inertia, the lack of well-documented field case histories of wharf behavior during earthquakes with strong motion records at both the superstructure and the ground, and the site- and project-specific aspects of the seismic performance of deep foundations in laterally moving grounds. While many of the previous studies focused on soil profiles and pile geometries that are typical to pile-supported bridges, this study attempts to contribute data to enhancing current guidelines for pile-supported wharves and piers. This was done by analyzing data from a series of centrifuge tests on pile-supported wharves (McCullough et al. 2000, Schlechter et al. 2000a,b, and Boland et al. 2001a,b) in

conjunction with equivalent static analysis using LPILE. While these centrifuge models represent common wharf and waterfront configurations at major port facilities in the western United States, the findings are useful for similar structures that are supported by piles in liquefiable soils.

The results of five centrifuge tests were used to evaluate the accuracy of an equivalent static analysis (ESA) procedure using p-y models for the design of pile-supported wharves subjected to lateral ground deformations during earthquake loading. The comparison provided a systematic way to evaluate the accuracy of the proposed load combinations in estimating bending moments demands and provided insights on the circumstances under which each load combination controls the pile design.

Finally, a nonlinear dynamic model of a pile-supported wharf was created and calibrated using recorded data from a centrifuge test. The objective of the numerical modeling was to create a calibrated numerical model that captures key responses of the wharf and the soil in order to be used in subsequent studies that are too costly and time-consuming to do using physical modeling. The calibrated numerical model was then subjected to a suite of spectrally matched ground motions covering a wide range of strong motion durations. The nonlinear dynamic analyses were performed for three loading cases: (a) a case with combined effects of liquefaction-induced lateral spreading and wharf deck inertia, (b) a case with liquefaction but without wharf deck inertia, and (c) a case with inertia only in the absence of liquefaction. Incremental dynamic analyses were performed by linearly scaling seven motions that were spectrally matched to have the same response

spectra. These dynamic analyses provided insights on the effects of motion duration on the contribution of soil lateral spreading and wharf deck inertia in pile demands. The data from this study suggests that the behavior of wharf structures supported on relatively flexible, small-diameter piles, such as the ones studied here, is heavily influenced by the kinematic loads in long duration motions and less so by the inertial loads.

1.2 DISSERTATION OUTLINE

This PhD dissertation follows the multi-paper format per Portland State University's electronic thesis and dissertation (ETD) formatting and is composed of nine chapters. Chapters 2 to 8 represent manuscripts that have been submitted or have been published in peer-reviewed journals and conference proceedings. Chapter 9 summarizes the main conclusions and recommendations for practice. The abstract and acknowledgement sections from each paper have been removed from the chapters. A summary of each chapter is presented below.

Chapter 2 is based on a paper entitled "Inertial and Liquefaction-Induced Kinematic Demands on a Pile-Supported Wharf: Physical Modeling" which is presented and published in the proceedings of the Geotechnical Earthquake Engineering and Soil Dynamics V, June 2018, Austin, TX, authored by M. Souri, A. Khosravifar, S. Schlechter, N. McCullough, and S.E Dickenson. In this paper the results of a centrifuge test on a pile-supported wharf were used to investigate the time-, depth-, and row-dependent nature of kinematic and inertial loading on wharf piles in sloping rockfill. P-y models were calibrated against recorded bending moments in

different piles and different depths. It was found that full kinematic demands and full superstructure inertia should be combined to estimate bending moments at pile head and shallow depths (less than 10 diameters below the ground surface). However, it was found that applying full kinematic demands alone was adequate to estimate pile bending moments at large depths (greater than 10 diameters deep).

Chapter 3 is based on a paper entitled “Seismic Performance of Pile-Supported Piers and Wharves Subjected to Foundation Deformations” which is presented and published in the proceedings of the ASCE PORTS 2019 conference, Pittsburgh, PA, authored by M. Souri, A. Khosravifar, S. Schlechter, N. McCullough, and S.E Dickenson. In this paper the interaction of inertial and kinematic demands is investigated using data from five physical models of pile-supported wharves using a large-scale geotechnical centrifuge. The wharf structures in this study were subjected to superstructure inertia, and earthquake-induced slope deformations of varying magnitudes. The observations from these tests were used to provide insights on how to estimate large bending moments that developed at pile head and at depths significantly below a commonly assumed point of fixity that are associated with deep-seated ground deformations. Design recommendations are proposed on how to combine inertial and kinematic demands in a manner that is representative of the global structure.

Chapter 4 is based on a paper entitled “Pile-supported wharves subjected to inertial loads and lateral ground deformations: observations from centrifuge tests” which has been submitted to the ASCE Journal of Geotechnical and

Geoenvironmental Engineering and is currently under review. This paper is authored by M. Souri, A. Khosravifar, S. Schlechter, N. McCullough, and S.E Dickenson. This paper describes the analysis of measured data from five dynamic large-scale centrifuge tests on pile-supported wharves. These tests were used to investigate the time- and depth-dependent nature of kinematic and inertial demands on the deep foundations during earthquake loading. The wharf structures in the physical experiments were subjected to a suite of recorded ground motions and imposed superstructure inertial demands on the piles. Partial to full liquefaction in loose sand resulted in slope deformations of varying magnitudes that imposed kinematic demands on the piles. It was found that the wharf inertia and soil displacements were always in-phase during the critical cycle when bending moments were at their maximum values. The test results were analyzed to provide the relative contributions of peak inertial loads and peak soil displacements during critical cycles, and the data revealed the depth-dependency of these factors. The results are used to refine existing guidelines for design of pile-supported wharves subjected to foundation deformations.

Chapter 5 is based on a paper entitled “Pile-supported wharves subjected to inertial loads and lateral ground deformations: design recommendation” which has been submitted to the ASCE Journal of Geotechnical and Geoenvironmental Engineering and is currently under review. This paper is authored by M. Souri, A. Khosravifar, S. Schlechter, N. McCullough, and S.E Dickenson. This paper describes an equivalent static analysis (ESA) procedure that is proposed for the design of pile-supported wharves subjected to combined inertial and kinematic

loads during earthquakes. The accuracy of the ESA procedure is evaluated against measurements from five large-scale centrifuge tests. It is shown that large bending moments at depths greater than 10 pile diameters are primarily induced by kinematic demands and can be estimated by applying soil displacements only (i.e., 100% kinematic). In contrast, the large bending moments at the pile head are primarily induced by wharf deck inertia and can be estimated by applying superstructure inertial loads at the pile head only (i.e., 100% inertial). The large bending moments at depths shallower than 10 pile diameters are affected by both inertial and kinematic loads; therefore, the evaluation of pile performance should include soil displacements and a portion of the peak inertial load at the pile head that coincides with the peak kinematic loads. Proposed ranges for inertial and kinematic load combinations in uncoupled analyses are provided.

Chapter 6 is based on a paper entitled “Development of Experimental P-Y Curves from Centrifuge Tests for Piles Subjected to Static Loading and Liquefaction-Induced Lateral Spreading” which was published in the Deep Foundation Institute (DFI) Journal, Vol. 14, No. 1 December 2020, and was authored by M. Souri, A. Khosravifar, S. Schlechter, N. McCullough, and S.E Dickenson. This paper describes the results of five centrifuge models were used to evaluate the response of pile-supported wharves subjected to inertial and liquefaction-induced lateral spreading loads. The centrifuge models contained pile groups that were embedded in rockfill dikes over layers of loose to dense sand and were shaken by a series of ground motions. The p-y curves were back-calculated for both dynamic and static loading from centrifuge data and were compared against commonly used

American Petroleum Institute p-y relationships. It was found that liquefaction in loose sand resulted in a significant reduction in ultimate soil resistance. It was also found that incorporating p-multipliers that are proportional to the pore water pressure ratio in granular materials is adequate for estimating pile demands in pseudo-static analysis. The unique contribution of this study is that the piles in these tests were subjected to combined effects of inertial loads from the superstructure and kinematic loads from liquefaction-induced lateral spreading.

Chapter 7 is based on a paper entitled “2D Numerical Modeling of a Centrifuge Test on a Pile-Supported Wharf Subjected to Liquefaction-Induced Ground Deformations.” which has been submitted to the Soil Dynamics and Earthquake Engineering Journal and is currently under review. This paper is authored by M. Souri, A. Khosravifar, S. Schlechter, N. McCullough, and S.E Dickenson. In this paper a 2D nonlinear dynamic model of a pile-supported wharf was created and calibrated using recorded data from a centrifuge test in prototype scale. The piles in the centrifuge test and the numerical model were subjected to the combined effects of inertial loads from the superstructure mass and kinematic loads from liquefaction-induced ground deformations during earthquake loadings. The numerical model was created in FLAC. Pressure-dependent multi-yield surface constitutive model was used to simulate undrained cyclic behavior of sands with different relative densities and the rockfill. The objective of the numerical modeling was to create a calibrated numerical model that captures key responses of the wharf and the soil in order to be used in subsequent studies. Practical simplifications were made to simulate the 3D response of piles, wharf, soils and

the centrifuge container in a 2D analysis. The implications of these simplifications are discussed.

Chapter 8 is based on a paper entitled “Effects of Long Duration Earthquakes on the Interaction of Inertial and Liquefaction-Induced Kinematic Demands on Pile-Supported Wharves.” which has been submitted to the Soil Dynamics and Earthquake Engineering Journal and is currently under review. This paper is authored by M. Souri, A. Khosravifar, S. Schlechter, N. McCullough, and S.E Dickenson. This paper describes nonlinear dynamic analyses that were performed to evaluate the effects of ground motion duration on the dynamic response of a pile-supported wharf subjected to liquefaction-induced lateral ground deformations. The calibrated numerical model used in an incremental dynamic analysis using a suite of spectrally matched motions with different durations. The nonlinear dynamic analyses were performed for three loading scenarios: combined effects of inertial loads from the wharf deck and kinematic loads from ground deformations, inertial loads only in the absence of liquefaction, and kinematic loads only in the absence of deck mass. The analysis results provided insights on the relative contribution of inertial and kinematic demands on the response of the wharf with respect to motion duration. It was found that the interaction of peak inertial and kinematic loads increases with motion duration. However, the response of the wharf supported by relatively flexible piles having a small diameter (0.6 m) was found to be primarily governed by kinematic demands in long-duration motions. The differences between the effects of motion duration on the response of small-diameter flexible piles and stiff shafts with a large-diameter (2 m) are discussed.

REFERENCES

ASCE (American Society of Civil Engineers). 2014. *Seismic Design of Piers and Wharves,* ASCE/COPRI 61-14. ASCE Standards Committee on Seismic Design of Piers and Wharves. Reston, Va.: ASCE. https://doi.org/10.1061/9780784413487.

Brandenberg, S. J., Boulanger, R. W., Kutter, B. L., and D. Chang. 2005. "Behavior of pile foundations in laterally spreading ground during centrifuge tests." *J. Geotech. Geoenviron. Eng*. 131(11): 1378–1391. https://doi.org/10.1061/(ASCE)1090-0241(2005)131:11(1378).

Brandenberg, S. J., Boulanger, R. W., Kutter, B. L., and D. Chang. 2007. "Static pushover analyses of pile groups in liquefied and laterally spreading ground in centrifuge tests." *J. Geotech. Geoenviron. Eng.* 133 (9): 1055–1066. https://doi.org/10.1061/(ASCE)1090-0241(2007)133:9(1055).

Boland, C.B., Schlechter S. M., McCullough, N. J., Dickenson, S. E., Kutter, B. L. and D. W. Wilson. 2001a. *Pile-Supported Wharf — Centrifuge Model SMS02.* Report No. GEG04-2000, Oregon State University/University of California at Davis.

Boland, C. B., Schlechter S. M., McCullough, N. J., Dickenson, S. E., Kutter, B. L. and D. W. Wilson. 2001b. *Pile-Supported Wharf — Centrifuge Model JCB01.* Report No. GEG05-2000, Oregon State University/University of California at Davis.

Boulanger, R. W., Chang, D., Brandenberg, S. J., Armstrong, R. J., and B. L. Kutter. 2007. "Seismic design of pile foundations for liquefaction effects." In *Proc. of 4th International Conference on Earthquake Geotechnical Engineering*, 277–302. Dordrecht, Germany: Springer. https://doi.org/10.1007/978-1-4020-5893-6_12.

Cubrinovski, M., and K. Ishihara. 2006. "Assessment of pile group response to lateral spreading by single pile analysis." In *Seismic Performance and Simulation of Pile Foundations in Liquefied and Laterally Spreading Ground*, GSP 145, Boulanger, R., and K. Tokimatsu, eds., 242–254. Reston, Va.: ASCE. https://doi.org/10.1061/9780784408223.

Cubrinovski, M., Bray, J. D., de la Torre, C., Olsen, M. J., Bradley, B. A., Chiaro, G., Stocks, E. and L. Wotherspoon. 2017. "Liquefaction effects and associated damages observed at the Wellington Centreport from the 2016 Kaikoura earthquake." *Bull. N. Z. Soc. Earthq. Eng.*, 50 (2): 152–173.

Dobry, R., Abdoun, T., O'Rourke, T. D., and S. H. Goh. 2003. "Single piles in lateral spreads: Field bending moment evaluation." *J. Geotech. Geoenviron. Eng.* 129, 879–889. https://doi.org/10.1061/(ASCE)1090-0241(2003)129:10(879)

Egan, J. A., and Wang, Z. L. 1991. “Liquefaction-related ground deformation and effects on facilities at Treasure Island, San Francisco, during the 17 October 1989 Loma Prieta Earthquake.” In Proceedings of the 3rd Japan–US workshop on earthquake resistant design of lifeline facilities and countermeasures for soil liquefaction. Technical Report NCEER-91–0001 (pp. 57-76).

Finn, W. D. L. 2005. “A study of piles during earthquakes: Issues of design and analysis.”
B. Earthq. Eng., 3(2), 141–234. https://doi.org/10.1007/s10518-005-1241-3

Hamada, M., Yasuda, S., Isoyama, R., and Emoto, K. 1986. ‘‘Study on liquefaction induced permanent ground displacements.’’ Research Rep., Association for Development of Earthquake Prediction, Japan, November, 87.

Khosravifar, A., Boulanger, R. W., and S. K. Kunnath. 2014. “Design of Extended Pile Shafts for the Effects of Liquefaction.” *Earthq. Spectra* 30 (4): 1775–1799. https://doi.org/10.1193/032512EQS107M

Martin, G. R., March, M. L., Anderson, D. G., Mayes, R. L., and M. S. Power. 2002. “Recommended design approach for liquefaction induced lateral spreads,” In *Proc. of 3rd National Seismic Conf. on Bridges and Highways*, MCEER-02-SP04, Buffalo, N.Y.: University at Buffalo.

McCullough, N. J., Dickenson, S. E., Kutter, B. L. and D. W. Wilson. 2000. *Pile-Supported Wharf — Centrifuge Model NJM01.* Report No. GEG01-2000, Oregon State University/ University of California at Davis.

McCullough, N. J., S. E. Dickenson, and S. M. Schlechter. 2001. “The seismic performance of piles in waterfront applications.” In *Ports Conference 2001*, 1–10. Reston, VA: ASCE. https://doi.org/10.1061/40555(2001)83

MCEER (Multidisciplinary Center for Earthquake Engineering Research). 2003. *Recommended LRFD Guidelines for the Seismic Design of Highway Bridges.* MCEER/ATC-49, Report No. MCEER-03-SP03. Buffalo, N.Y.: University at Buffalo.

POA (Port of Anchorage). 2017. “Anchorage Port Modernization Project Seismic Design Manual”.

POLB (Port of Long Beach). 2015. “Port of Long Beach Wharf Design Criteria,” Version 4.0 (May). Long Beach, CA: POLB.

Rathje, E., Bachhuber, J., Cox, B., French, J., Green, R., Olson, S., Rix, G., Wells, D., and Suncar, O. 2010. “Geotechnical engineering reconnaissance of the 2010 Haiti earthquake.” GEER Association, Report No. GEER-021.

Schlechter, S. M., McCullough, N. J., Dickenson, S. E., Kutter, B. L., and D. W. Wilson, 2000a. *Pile-Supported Wharf — Centrifuge Model NJM02.* Report No. GEG02-2000, Oregon State University/University of California at Davis.

Schlechter S. M., McCullough, N. J., Dickenson, S. E., Kutter, B. L., and D.W. Wilson. 2000b. *Pile-Supported Wharf — Centrifuge Model SMS01.* Report No. GEG03-2000, Oregon State University/University of California at Davis.

Souri, M., Khosravifar, A., Schlechter, S., McCullough, N. and S. E. Dickenson. 2019. "Seismic Performance of Pile-Supported Piers and Wharves Subjected to Foundation Deformations." In *PORTS '19*. Reston, VA: ASCE. https://doi.org/10.1061/9780784482612.058

Souri, M., A. Khosravifar, S. E. Dickenson, S. Schlechter, and N. McCullough. 202X. "Pile-supported wharves subjected to inertial loads and lateral ground deformations: design recommendations." (companion paper)

Tokimatsu, K., 2003. "Behavior and design of pile foundations subjected to earthquakes." In *Proc. of 12th Asian Regional Conference on Soil Mechanics and Geotechnical Engineering*, 1065–1096. Klong Luang, Thailand: Association of Geotechnical Societies in Southeast Asia.

Turner, B. J., Brandenberg, S. J., and J. P. Stewart. 2016. "Case study of parallel bridges affected by liquefaction and lateral spreading." *J. Geotech. Geoenviron. Eng.* 142.7 (2016): 05016001. http://dx.doi.org/10.1061/(ASCE)GT.1943-5606.0001480

Werner, S. D., Dickenson, S. E., and Taylor, C. E. (1997). "Seismic risk reduction at ports: Case studies and acceptable risk evaluation." Journal of waterway, port, coastal, and ocean engineering, 123(6), 337-346.

CHAPTER 2

2.0 INERTIAL AND LIQUEFACTION-INDUCED KINEMATIC DEMANDS ON A PILE-SUPPORTED WHARF: PHYSICAL MODELING

Note: The contents in this chapter have been published in proceedings of the Geotechnical Earthquake Engineering and Soil Dynamics V (GEESDV) conference with the following citation:

Souri, M., Khosravifar, A., Schlechter, S., McCullough, N. & Dickenson, S. E. (2018). "Inertial and Liquefaction-Induced Kinematic Demands on a Pile-Supported Wharf: Physical Modeling" Geotechnical Earthquake Engineering and Soil Dynamics V, Austin, Texas, June 10–13, 2018, https://doi.org/10.1061/9780784481479.040

2.1 INTRODUCTION

Pile foundations in sloping soils should be designed to sustain loading due to both permanent ground deformation (kinematic) and inertia of the structure during shaking. Current design recommendations vary significantly on how to combine inertia and kinematic loads. For example, AASHTO (2014) recommends designing piles for simultaneous effects of inertia and ground deformation (e.g., lateral spreading) only for large magnitude earthquakes (M>8). Caltrans (2012) and ODOT (Ashford et al. 2012) recommend combining 100% lateral spreading with 50% inertia. Washington DOT recommend combining 100% lateral spreading with 25% inertia (WSDOT 2015). The Port of Long Beach Wharf Design Criteria (POLB 2015) suggests that for their common wharf configurations and soils the locations of maximum bending moments from inertia and lateral spreading are spaced far enough apart that the two loads do not need to be superimposed. It also assumes

that the maximum bending moments from the two loads tend to occur at different times; therefore, it recommends that the two loads be treated as uncoupled for typical marginal container wharves at the Port of Long Beach. For other types of wharves, both POLB (2015) and ASCE COPRI 61-14 (2014) recommend evaluating this assumption on a project-specific basis. Tokimatsu et al. (2005) recommended in-phase and out-of-phase combination of inertia and lateral spreading based on the natural periods of soil and structure.

The objective of this study is to identify inertial and kinematic loads on piles (i.e., bending moments) at different depths. For piles in nonliquefied conditions (minimal kinematic demands) the contribution of inertial forces from superstructure is known to attenuate within approximately 8 to 10-diameter depth below the ground surface (depending on the relative stiffness of soil and pile). Data from a large-scale centrifuge test on a pile-supported wharf and practice-oriented p-y models were used to investigate whether the same attenuation occurs in liquefied conditions where kinematic demands are large. The piles in this centrifuge test were subjected to liquefaction-induced lateral spreading combined with wharf deck inertia. P-y models were calibrated to measured response in the centrifuge test, then applied to provide insights on how kinematic and inertial demands should be combined in design of similar pile-supported wharf configurations. It will be shown that large bending moments at depth (above and below the liquefiable layer) are primarily induced by kinematic demands and can be estimated by applying kinematic demands only. On the contrary, large bending moments at shallow depths (pile head or at ground surface) are induced by the combination of

kinematics and inertia; therefore, both demands should be combined to more accurately estimate pile bending moments at shallow depths.

2.2 CENTRIFUGE TEST

A series of five centrifuge tests was conducted by Dickenson, McCullough, Schlechter and coworkers at the UC Davis Center for Geotechnical Modeling (McCullough et al. 2001). These tests were conducted on pile-supported wharfs and foundation soils that included rockfill, saturated sand deposits, and soft marine clay. This paper focuses on the results of one of these centrifuge tests (NJM01; McCullough et al. 2000). The cross section of the physical model is shown in Figure 1. The dimensions discussed in this paper are in prototype scale, unless noted otherwise.

The centrifuge acceleration was 40.1 g. The soil layers include rockfill dikes that deformed due to liquefaction of the underlying loose sand. Loose to dense Nevada sand was used with relative densities (D_R) ranging from 39% to 82%. The piles were aluminum tubes with prototype diameter of 0.64 m. Table 1 lists the pile and deck properties used in this test. The model was constructed in a flexible shear beam container, which was designed to have a shear modulus compatible to that of liquefied soils. The pore fluid was a mixture of methylcellulose, which has a higher viscosity than that of water. This was done to reconcile different time scales for the dynamic and diffusion equations. The test was subjected to multiple, scaled input motions. The results presented in this paper are for the 1989 Loma Prieta earthquake motions recorded at the Port of Oakland Outer Harbor Wharf station scaled to a PGA of 0.15 g. The centrifuge model used in this study simulates a

typical pile-supported wharf embedded in rock dikes over liquefiable layers. This cross section represents the common layout of major port facilities in California. The findings from this test can be applied to other port facilities with similar subsurface conditions and structural properties. Data from the other four centrifuge tests are being analyzed to evaluate the time-, depth-, and row-dependent nature of kinematic and inertial loading on wharf piles in sloping rockfill.

Table 1. Pile and Deck Properties in Centrifuge Test NJM01 [1]

	Values in Prototype Scale	**Values in Model Scale**
Pile	Pile group (3-by-7) Pile b = 0.64 m, t = 0.036 m, L = 27.23 m EI = 2.134e5 kPa-m^4	Pile group (3-by-7) Pile b = 15.9 mm, t = 0.899 mm, L = 679 mm, EI = 82.536 Pa-m^4
Wharf Deck	Dimensions: 33.68m x 15.24m x 0.25m Mass = 350445 kg	Dimensions: 839.9mm x 380.1mm x 6.2mm, Mass = 5.43 kg

1. Centrifuge Scale Factor = 40.1

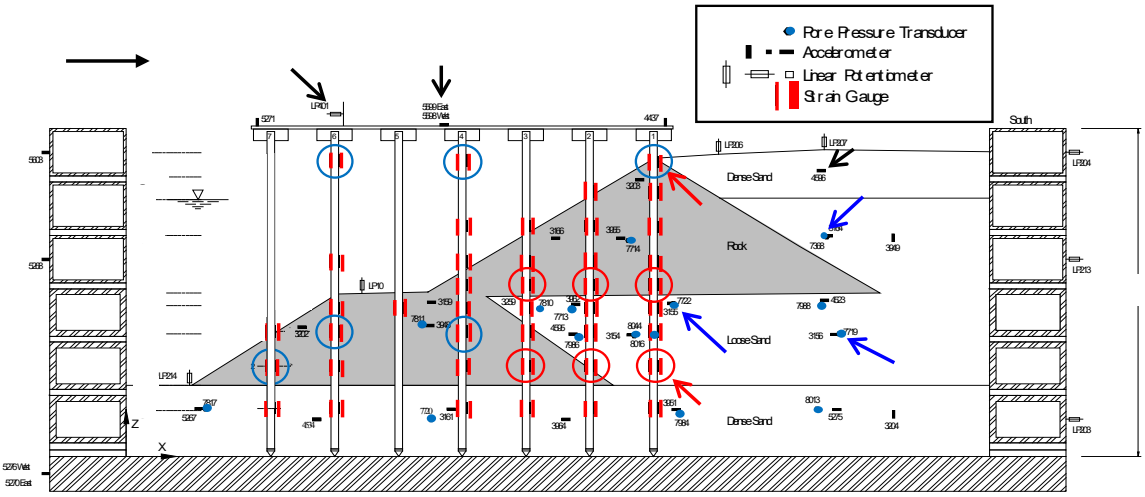

Figure 1. Cross section of pile-supported wharf centrifuge test NJM01 (prototype scale)

2.3 MEASUREMENTS AND DATA PROCESSING

The instrumentation data used in this analysis included accelerometers (mounted on the wharf deck, centrifuge box, and within the soil), Linear Variable Differential Transformers (LVDT; mounted on the wharf deck and centrifuge box in the horizontal direction and to the ground surface in the vertical direction), strain gauges (SG; mounted on the piles at various depths), and pore-water-pressure transducers (PPT; located within the soil at various depths). This centrifuge test did not include a horizontal LVDT at the ground surface; therefore, the horizontal soil displacement profiles were calculated by double-integrating accelerations within and near the ground surface. The pile bending moments were calculated from strain gauge measurements. To calculate the lateral soil reaction (p), the bending moments were approximated using the Smooth Cubic Spline method and were double differentiated as described in Brandenberg et al. (2010). The bending moments and shear forces at pile tips were assumed to be zero.

2.4 OBSERVATIONS BASED ON INSTRUMENTATION ARRAY

The time histories of soil and pile responses, and input motions are shown in Figure 2 for the first main event in the NJM01 testing sequence, i.e., Oakland Outer Harbor Wharf motion scaled to PGA of 0.15 g. The figure shows soil and pile displacements, wharf accelerations, excess pore-water-pressures at three key locations in the model, bending moments at two critical locations along Pile #1 (the

rightmost pile on the cross section), and the soil reaction on Pile #1 from the laterally spreading rockfill (13.2 m from pile head).

Displacements and Accelerations. The wharf deck displacement was measured using an LVDT that captured both transient and permanent displacements. Maximum wharf deck displacement was measured 0.17 m downslope. As previously described, the ground surface displacement at the upper dike was calculated by double integrating accelerations because this test did not include a horizontal LVDT at the ground surface. Therefore, the ground surface displacement measured here includes the transient component only. It is observed that the transient component of soil displacement is rather large in both directions with maximum downslope displacement being equal to 0.07 m. These relatively large transient soil displacements are attributed to the inertia of the crust over the liquefied layer and contribute significantly to the bending moments at deeper elevations in the piles, as will be described later. To be consistent with the soil displacements, the wharf deck displacement was also calculated by double integrating accelerations at wharf deck to include the transient component only (black dashed-line in Figure 2 with maximum downslope displacement of 0.11 m). The wharf accelerations are plotted as an indicative of the inertial force.

Pore-Water-Pressure. The excess pore-water-pressures ratios (r_u) are shown for three locations within the loose sand layer showing partial liquefaction (Point B, r_u = 75%) to full liquefaction (Point A, r_u = 100%). The r_u values were later used in the p-y analysis to estimate p-multipliers.

Pile Bending Moments. The data from two strain gauges on Pile #1 are plotted in Figure 2: SG1-9 at ground surface and SG1-2 at the bottom of the liquefied zone. SG1-2 experienced the maximum bending moment of all instrumented piles in the test. The deeper strain gauge (SG1-2) exhibited a combination of transient and permanent (end-of-shaking) components, while the response of the shallower strain gauge (SG1-9) was governed by a transient component with very small permanent component. We attributed the transient component of the bending moment in the deep strain gauge (SG1-2) to the transient component of soil displacements. It will be shown later that the bending moment at this strain gauge location can be reasonably estimated by considering soil displacements only (kinematics). The bending moment in the shallow strain gauge (SG1-9) can be reasonably estimated by combining kinematics with inertia.

Lateral Soil Reaction. The lateral soil reaction within the rockfill was back-calculated by double-integrating bending moments (Figure 2). The magnitude of back-calculated soil reaction was found sensitive to the method of approximating (or interpolating) bending moments and the noise in recorded data. Therefore, the soil reactions were primarily used to understand the direction of loading from soil on the piles. It was found that the soil reactions within the top nonliquefiable layer (rockfill) was not uniformly downslope. Instead, the soil reaction was maximum at the interface of rockfill and loose liquefiable sand and reduced in the top half of the rockfill indicating that full passive crust load was not mobilized. The soil reaction at

the bottom of rockfill (13.2 m from pile head) was used as an indicative of the lateral spreading force (LSF).

Time of Peak Values. It is observed that the displacements, bending moments, and soil reactions in Figure 2 maximize during the strong shaking, and not necessarily at the end of shaking. For example, the residual wharf deck displacement (end-of-shaking) is 58% of its peak value during shaking (0.10 m compared to 0.17 m). Similarly, the residual bending moment at depth (SG1-2) is 62% of its maximum value (474 kN-m compared to 768 kN-m). The residual bending moment at the shallow strain gauge (SG1-9) is 9% of its peak value (38 kN-m compared to 437 kN-m).

The maximum bending moments do not necessarily occur at the same time along the length of the pile. They also do not occur at the same time at the same elevation for various rows of piles. In order to compare the magnitude of moments at the same time, we identified a critical time (i.e., loading cycle) at which the soil and pile displacements, bending moments, and wharf accelerations are maximum, or close to maximum. The critical time (t = 21.6 sec) is marked with a vertical dashed line in Figure 2. At this time, the wharf acceleration is 0.13 g, which is 90% of the peak wharf acceleration in the positive direction (resulting in downslope inertia) and 48% of the peak wharf acceleration in both directions. In the following section, we

estimate pile bending moments recorded at 21.6 sec by combining inertia and kinematics.

2.5 CONTRIBUTION OF INERTIA AND KINEMATICS AT DIFFERENT DEPTHS

Approach. The objective of this study was to identify inertial and kinematic loads on piles (i.e., bending moments) at different depths. To study this combination, key strain gauges were identified among all piles where bending moments were large at some point during the shaking. These strain gauges are circled in Figure 1. We used p-y models, calibrated to the results of the centrifuge test, to find the relative contribution of inertia and kinematics in bending moments at those key strain gauges. The p-y models were subjected to two loading conditions:

(a) Kinematic demands only (100% Kinematics)

(b) Combined kinematic and inertial demands (100% Kinematics + 100% Inertia)

The kinematic demands were imposed by applying soil displacements to the end nodes of p-y springs. The soil displacements were calculated by double integrating accelerometers in soil. As described earlier, these soil displacements include the transient component only. The inertial demands can be applied as a shear load or an imposed displacement at pile head. While the total inertial load of the wharf deck can be calculated by multiplying total mass and the recorded acceleration, the relative distribution of the inertial load between seven rows of piles depends on the relative lateral stiffness of piles. This is difficult to do, because the lateral stiffness of the piles changes during shaking due to changes in soil

properties. Therefore, it was decided to apply the inertial demand as an imposed displacement at pile head rather than a shear force.

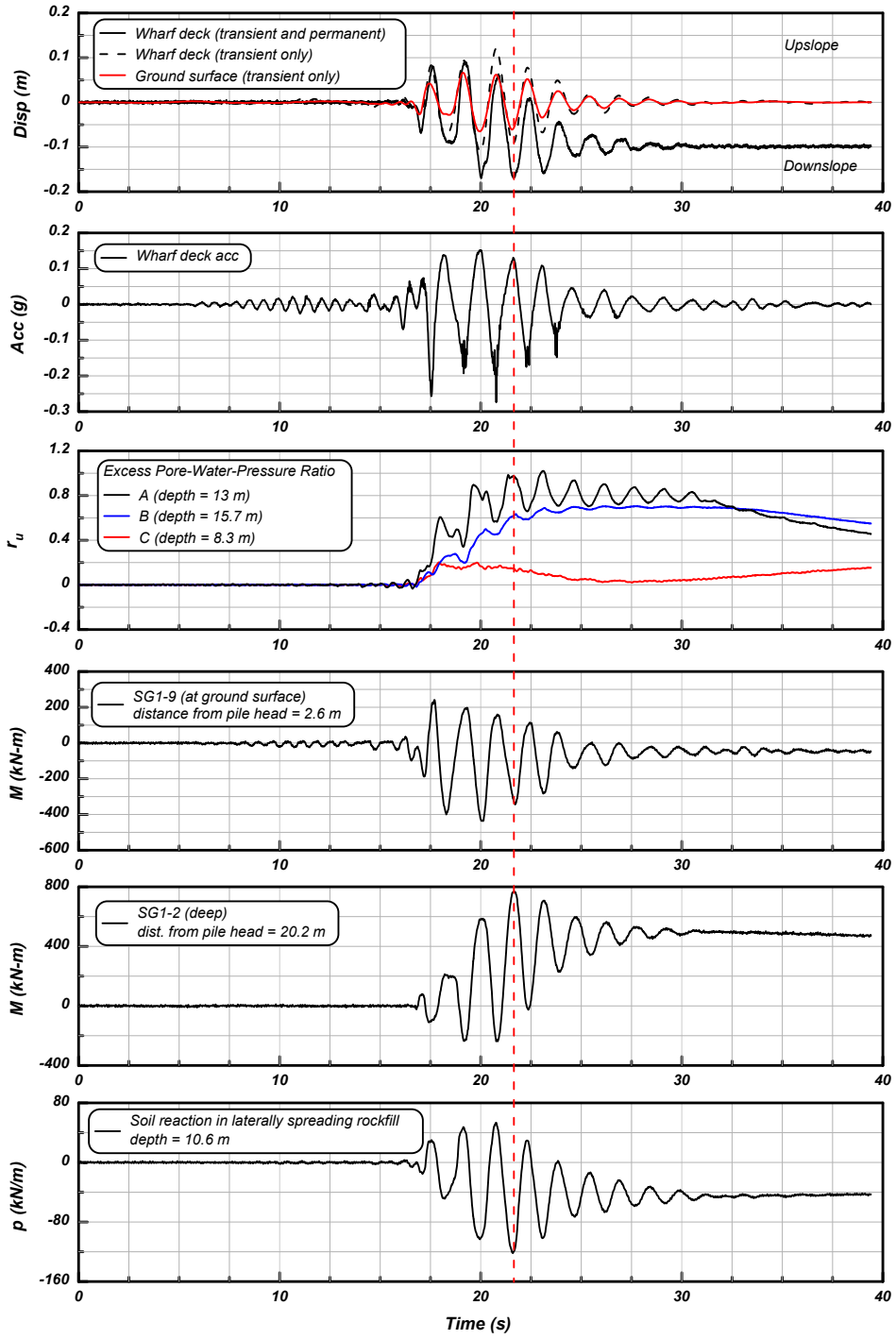

Figure 2. Representative time histories from the Loma Prieta Outer Harbor Wharf motion scaled to PGA of 0.15 g

Assuming that the deck was relatively rigid during the test, the imposed pile head displacements were the same for all piles and were equal to the wharf displacement. To be consistent with the imposed soil displacements, only the transient component of the wharf displacement was applied (calculated by double integrating accelerations at wharf deck). The pile head was fixed against rotation to simulate the rigid pile-to-deck connection in the centrifuge test. The soil and pile displacements were extracted at 21.6 sec which resulted in peak (or close to peak) bending moments.

The p-y model was created using LPILE (Ensoft 2014). The soil spring properties were calibrated based on a series of monotonic lateral load tests on piles in two other centrifuge tests conducted using similar soil and pile properties to those in the centrifuge test discussed in this paper. The Sand p-y curves in LPILE (Reese et al. 1974) were used with modifications based on the monotonic lateral load tests. The details of the calibration process and the recommended soil properties are provided in Dickenson and McCullough (2006). Two main adjustments were made to the soil springs: (i) the stiffness was reduced in sloping rockfill to account for the softer response observed in the centrifuge tests with monotonic loading, and (ii) p-multipliers were used in the liquefied zone based on recorded pore-water-pressure (PWP) following recommendations in Caltrans (2012), i.e. the p-multipliers for full liquefaction (r_u = 100%) were scaled by a factor of 100/r_u for units where liquefaction did not fully trigger. The pile spacing was

approx. 8 diameters; therefore, group reduction factors were not applied. Table 2 lists key properties used in p-y models.

Results. Figure 3a shows the snapshot of recorded bending moments at 21.6 sec and the results of the p-y analyses for the two loading conditions described above, i.e. kinematics only (green lines) and kinematics plus inertia (blue lines). Figure 3b shows the snapshot of soil displacements at 21.6 sec and pile displacements from the p-y analyses for the two loading conditions. It is observed that the effects of inertia attenuate within 5 to 6 m from the ground surface (approximately 8 to 10 pile diameters). The location of maximum (or large) recorded bending moments varied in different pile rows. In piles #1, #2 and #3, large bending moments were recorded at pile head, and above and below the loose liquefiable layer. This was expected since the failure shear plane passed through the liquefied layer imposing significant curvature (and moment) in the piles. In piles #4, #6, and #7, which did not pass through the loose liquefiable layer, large bending moments were recorded at pile head and at shallow depths (less than 10 diameters deep).

The location of strain gauges with large recorded bending moments are circled on Figure 1. Focusing on these strain gauges, it is observed that the magnitude of large bending moments above and below the liquefied zone (generally deeper than 10 diameters and marked with red circles in Figure 1) can be reasonably estimated by applying kinematic demands only in the p-y model. This indicates that these deep bending moments are primarily governed by soil displacements (100% Kinematics). Conversely, the magnitude of large bending moments at pile head and shallow depths (marked with blue circles in Figure 1)

can only be captured if both kinematics and inertia are applied in the p-y model. This indicates that inertia and kinematics fully interact at pile head and shallow depths, and that combined loads should be considered in design (100% Kinematics + 100% Inertia). These results show that at depth of approximately 10 diameters we transition from “inertia + kinematics” to “kinematics only” in rockfill. It should be noted that this range may be valid only for the rockfill and the configuration of this test. Although the relative locations of the maximum bending moments were accurately predicted to form above and below the liquefied sand, the exact locations of the deeper maximum moments were inaccurately predicted and were approximately 2 m off (3 pile diameter). The uncertainty in predicting the location of maximum moments should be considered in design.

Table 2. Soil Properties Used in P-Y Models (LPILE)

Material	P-Y Model	Effective Unit Weight γ′(kN/m^3)	Friction Angle (deg)	Subgrade Reaction, k (kN/m3)
Loose Nevada Sand (D_R = 39 %)	Sand (Reese et al. 1974)	9.6	33	5430 [1]
Dense Nevada Sand (D_R = 82%)	Sand (Reese et al. 1974)	10.6	37	33900
Rockfill	Sand (Reese et al. 1974)	10.7	45	16300 [1]

1. Softened due to sloping ground

2.6 DISCUSSION

Pile demands (displacements, shear forces and bending moments) are shown in Figure 4 for Pile #1 at time=21.6 sec. The results of a sensitivity analysis with the p-y model are also shown on this figure for comparison. The magnitude of bending moments above and below the liquefied layer (SG1-2 and SG1-5) is governed by

kinematics (soil displacements) and are relatively unaffected by the inertia applied at top of the pile. To investigate the contribution of inertia at deeper locations, pile #1 is analyzed by combining kinematics and different magnitudes of inertial demands. The inertial load at 21.6 sec is estimated to range between 200 kN (calculated by double integrating bending moments in the centrifuge test) and 320 kN (by imposing wharf displacement of 0.09 m at pile head in the p-y model). Given this uncertainty, various magnitudes of inertial loads were applied at pile head in the sensitivity analysis (i.e., 0, 160, 320, and 480 kN). The objective of these analyses was to investigate how the inertial contribution dissipates with depth. It was found that the effects of pile head inertia are negligible at depths larger than 10 diameters below the ground surface. This depth corresponds to z/T of approximately 4 if depth (z) is normalized by the relative stiffness factor (T) in rockfill (i.e., $T = (EI/k)^{(1/5)}$ where EI is the pile bending stiffness and k is the subgrade reaction).

The piles – having elastic stiffness representative of 24-in diameter steel pipe-piles or 24-in square/octagonal prestressed concrete piles – are relatively flexible and follow the soil displacements pattern with depth. Therefore, the bending moments, which are the product of curvature in pile, were heavily dependent on the soil displacement pattern. This behavior may be different than the behavior reported for stiffer foundations (e.g. large diameter drilled shafts used for bridge foundations) where laterally spreading crust moves around the pile to the extent that it can mobilize full passive earth pressure (Boulanger et al. 2007; Caltrans 2012).

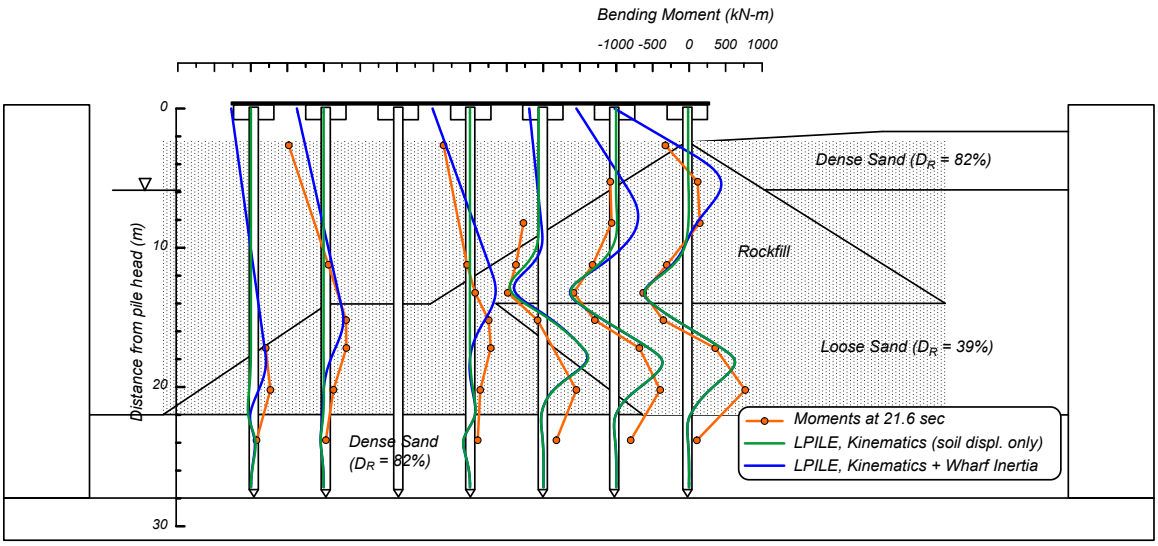

Figure 3. Bending moments at the critical time (21.6 sec) and moment profiles from p-y solutions (LPILE) –prototype scale

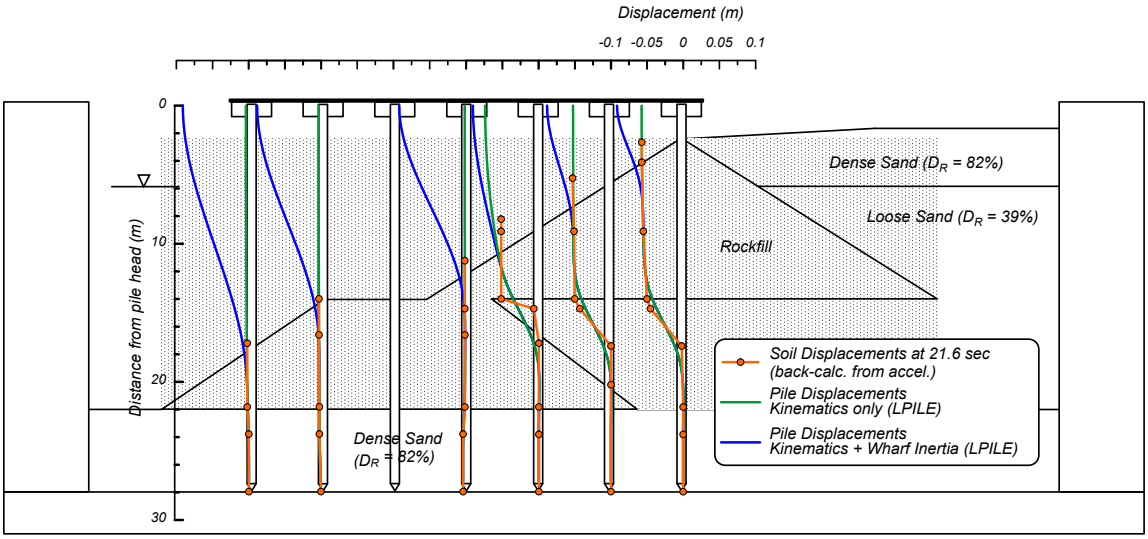

Figure 3b. Soil displacement profiles at the critical time (21.6 sec) calculated from accelerometers and pile displacements from p-y solutions (LPILE) – prototype scale

For the piles studied in this centrifuge test and the range of deformations observed, full passive pressure was not mobilized along the entire pile in the rockfill. Therefore, applying kinematic demands by imposing full passive pressure

on piles will over-estimate pile demands. Applying kinematic demands by imposing soil displacements to the end nodes of p-y springs will estimate pile bending moments more accurately. Given the uncertainty in estimating the magnitude and pattern of soil displacements, sensitivity analysis is necessary to estimate the magnitude and location of kinematic demands. The uncertainties in the selection of soil spring properties should be considered in design as recommended in ASCE COPRI 61-14 by incorporating upper- and lower-bound spring stiffness for dynamic soil-structure-interaction (SSI) analysis. The soil displacement profiles in this study were calculated from acceleration recordings in the centrifuge test; however, the location of maximum bending moments were not estimated accurately. It is recommended that the uncertainties in the location of maximum bending moments be considered in design.

2.7 CONCLUSIONS

The physical modeling has provided a valuable data set for analysis of the time-, depth-, and row-dependent nature of kinematic and inertial loading on wharf piles in sloping rockfill. It was observed that pile bending moments were relatively large at soil interfaces with significant stiffness contrasts or at the shear failure plane. We found that 100% of kinematics (soil displacements) and 100% of inertia (wharf deck displacements) conservatively estimated bending moments at pile head and shallow depths (less than 10 diameters below the ground). On the contrary, applying 100% of kinematics was adequate to estimate pile bending moments at large depths (deeper than 10 diameters and above/below the liquefiable layer).

These combination factors may be different for stiff shafts that are often used in bridge foundations and for significantly different soil profiles. For flexible piles, the flexibility of the foundation elements and the ability of the structure to move will have a significant impact on the pattern of kinematic loading on the structure. Therefore, uncertainties in the magnitude and patter of soil displacements with depth and soil spring properties should be considered in design as recommended in ASCE COPRI 61-14.

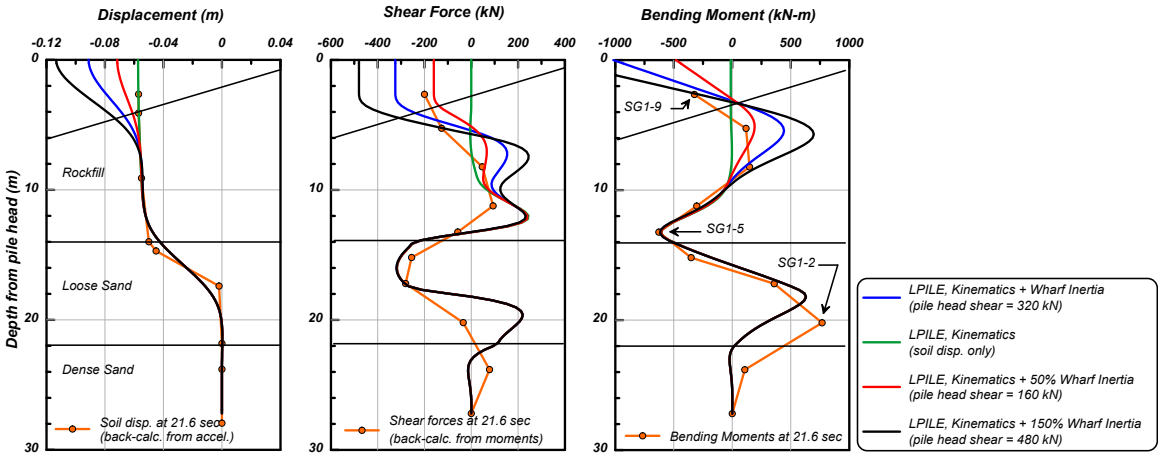

Figure 4. Comparison of displacement, shear force, and bending moment profiles recorded in and calculated from the centrifuge test and results of p-y analyses combining full kinematic demands and varying contributions of wharf inertia

REFERENCES

AASHTO (2014). “Guide Specifications for LRFD Seismic Bridge Design.” Second Edition with 2014 Interim, AASHTO, Washington, D.C.

ASCE/COPRI 61-14 (2014). “Seismic Design of Piers and Wharves, prepared by the ASCE Standards Comm. on Seismic Design of Piers and Wharves.” ASCE, Reston, VA.

Ashford, S.A., Scott, M.H., and Rayamajhi, D., (2012). “Reducing Seismic Risk to Highway Mobility: Assessment and Design Examples for Pile Foundations Affected by Lateral Spreading”, ODOT

Brandenberg, S.J., Wilson, D.W., and Rashid, M.M. (2010). “A Weighted Residual Numerical Differentiation Algorithm Applied to Experimental Bending Moment Data.”, J. Geo. and Geoenv. Engr., 136(6), 854-863

Boulanger, R.W., Chang, D., Brandenberg, S.J., Armstrong, R.J., and Kutter, B.L. (2007). “Seismic design of pile foundations for liquefaction effects.” 4th International Conference on Earthquake Geotechnical Engineering, The Netherlands, 277-302.

California Department of Transportation (Caltrans) (2012). “Guidelines for Foundation Loading and Deformation Due to Liquefaction Induced Lateral Spreading.” Sacramento, CA.

Dickenson, S.E., and McCullough, N.J. (2006). "Modeling the Seismic Performance of Pile Foundations for Port and Coastal Infrastructure," ASCE, Geo. Special Pub. No. 145, 173 - 191.

Ensoft, (2014). “User’s Technical Manual for LPile 2013”

McCullough, N.J., Dickenson, S.E., Kutter, B.L. and Wilson, D.W. (2000). “Pile-Supported Wharf — Centrifuge Model NJM01.” Report No. GEG01-2000, OSU-Geotechnical Engr.

McCullough, N. J., Dickenson, S. E., & Schlechter, S. M. (2001). “The seismic performance of piles in waterfront applications.” In Ports' 01: America's Ports: Gateway to the Global Economy (pp. 1-10).

Port of Long Beach (POLB) (2015). “Port of Long Beach Wharf Design Criteria,” POLB WDC Version 4, May 2015.

Tokimatsu, K., Suzuki, H., Sato, M. (2005). “Effects of inertial and kinematic interaction on seismic behavior of pile with embedded foundation.” Soil Dyn. EQ. Eng. 25, 753-762.

Reese, L. C.; Cox, W. R.; and Koop, F. D., 1974. “Analysis of Laterally Loaded Piles in Sand,” Proceedings, 6th Offshore Technology Conference, Vol. II, pp. 473-484.

Washington Department of Transportation (WSDOT) (2015). “Geotechnical Design Manual.” M 46-03.11, May 2015.

CHAPTER 3

3.0 SEISMIC PERFORMANCE OF PILE-SUPPORTED PIERS AND WHARVES SUBJECTED TO FOUNDATION DEFORMATIONS

Note: The contents in this chapter have been published in proceedings of the PORTS '19 conference with the following citation:

Souri, M., Khosravifar, A., Schlechter, S., McCullough, N. & Dickenson, S. E. (2019), “Seismic Performance of Pile-Supported Piers and Wharves Subjected to Foundation Deformations” PORTS '19, Pittsburgh, PA https://doi.org/10.1061/9780784482612.058

3.1 INTRODUCTION

Pile-supported wharves subjected to earthquake motions are designed to accommodate inertial loads imposed at pile head from the superstructure as well as the kinematic loads imposed on piles from the lateral ground deformations adjacent to the structure. The ground deformations are caused by shear strains in the weak, cyclically degradable foundation soils, the slope or embankment, and the backland areas.

ASCE 61-14 (Section 4.7) requires that simultaneous application of inertial and kinematic loads be considered taking into account the phasing and the locations where these loads are applied. The commentary of ASCE 61-14 (Section C4.7) suggests that these two loads (inertia and kinematics) are often considered to act at different times during the ground motion; therefore, they can be assumed uncoupled in design. This commentary mentions that this assumption should be checked on a project-specific basis. It also suggests that the inertial load tends to

result in large bending moments at pile head while the kinematic loads tend to result in large bending moments at depth. The ASCE 61-14 (Section 4.7.2) specifically refers to the permanent portion of lateral ground deformations to be used to estimate the kinematic demands on piles. The commentary for this section describes different methods with various complexities to estimate the permanent lateral ground deformations, including the simplified Newmark sliding block analysis to more detailed two-dimensional dynamic soil-structure interaction analyses of the entire soil-structure system.

Other design codes provide varying recommendations on the combination of inertia and kinematics. Pertinent examples include;

- ASCE 7-16 does not require combining lateral spreading and inertia;
- AASHTO (2014) recommends designing piles for simultaneous effects of inertia and lateral spreading only for large magnitude earthquakes (M>8);
- California and Oregon DOT's recommend 100% lateral spreading + 50% inertia (Caltrans 2012, ODOT 2014);
- Washington DOT recommends 100% lateral spreading + 25% inertia (WSDOT, 2015).

While numerical modeling is often used in design to develop bracketed load combination factors from synchronous timing of inertia and kinematics, we use physical modeling in this paper to evaluate the time-dependent interaction of inertia and kinematics noting that while the peak loads induced by these two conditions may not occur simultaneously there is always at least a portion of both loads acting on piles throughout the duration of the seismic loading. The physical modeling has

been completed using the large-scale geotechnical centrifuge at UC Davis (McCullough et al. 2001). Centrifuge modeling is widely used to model soil-foundation-structure-interaction (SFSI) for transportation systems, tunnels, and offshore structures (e.g., Dobry et al. 2003, Brandenberg et al. 2005, Chou et al. 2011, and Zhou et al. 2017). The centrifuge tests provide useful case-study simulations that are commonly used as the basis for calibrating simplified and complex numerical models that are used in practice (e.g. Travasarou et al. 2011).

The following section of this paper provides an overview of the five centrifuge tests that were used in this study. This section is followed by a summary of the analyzed data on the relative magnitude of inertial and kinematic demands at the time(s) when the peak bending moments are observed at the pile head and at depth. Implications for design are provided based on the results of pseudo-static analyses in *LPILE* to provide insights on when to combine inertial and kinematic loads in design to estimate peak bending moments in piles. Concluding remarks are provided based on the observations from these centrifuge tests.

3.2 EXPERIMENTAL STUDY

Centrifuge Tests. Table 1 lists the five tests analyzed in this study along with the key pile, superstructure, and soil properties and the applied ground motions. All tests included a wharf deck supported by 21 piles in a 7-by-3 setup. The piles were steel pipe piles with outer diameters ranging from 0.38 m (1.25 ft) to 0.64 m (2 ft) (in prototype scale). Figure 1 shows the cross sections of the five centrifuge models. Figure 1a shows the cross section of the first centrifuge model (NJM01) and Figure 1b shows a photo of the model before shaking. The subsurface

conditions in NJM01 included multi-lift rock dikes, a loose sand layer that liquefied during shaking and resulted in lateral spreading, a dense sand layer above the water table and a dense sand layer at pile tips. The inferred failure surface during cyclic loading was determined based on the soil displacement profiles and is shown with a red dashed line. The envelopes of maximum bending moment distributions during the ground motions are shown along the instrumented piles in gray. The locations where large bending moments were observed are color-coded according to the following categories: top of pile (blue), shallow locations with depth < 10D (red), deep locations with depth > 10D (green), and piles subjected to minimal kinematic demands (orange). The locations of maximum bending moments above and below grade are shown in this figure, which will be discussed later in the paper. It should be noted that while the envelopes of the maximum pile moments are useful for highlighting zones of importance, the plots do not demonstrate the time-dependent nature of the maximum moments as functions of depth or pile row (i.e., the peak moments are not experienced at the same time along a single pile or in all piles simultaneously).

Table 3. Pile geometries, superstructure geometries, soil properties and ground motions in five centrifuge tests

Test ID [1]	Pile properties [2]	Superstructure properties	Soil properties	Applied ground motion at base	PGA at base (g)
NJM01	Pile D = 0.64 m, t = 0.036 m, L = 27.23 m, EI = 2.134e5 kPa-m4	Wharf deck 33.7 m × 15.2 m × 0.25 m, mass = 714774 kg	Nevada loose sand D_R = 39 % Nevada dense sand, D_R = 82 % Rockfill, friction angle =45 deg	Event 11. Loma Prieta [3]	0.15
NJM02	Pile D = 0.38 m, t = 0.036 m, L = 25.063 m, EI = 4.113e4 kPa-m4	Wharf deck 24.9 m × 12.2 m × 0.25 m, mass = 265727 kg	Nevada loose sand D_R = 45 % Nevada dense sand, D_R = 85 % Bay Mud, undrained shear strength = 38 kPa Rockfill, friction angle = 45 deg	Event 42. Loma Prieta [3]	0.19
SMS01	Pile D = 0.38 m, t = 0.036 m, L = 25.063 m, EI = 4.113e4 kPa-m4	Wharf deck 24.9 m × 12.2 m × 0.25 m, mass = 265727 kg	Nevada loose sand D_R = 30 % Nevada dense sand, D_R = 70 % CDSM, unconfined compressive strength = 0.9 MPa Rockfill, friction angle = 45 deg	Event 25. Loma Prieta [3]	0.42
SMS02	Pile D = 0.64 m, t = 0.036 m, L = 24.26 m, EI = 2.134e5 kPa-m4	Wharf deck 28.1 m × 12.0 m × 0.78 m, mass = 951549 kg	Nevada dense sand, D_R = 70 % Rockfill, friction angle = 45 deg	Event 35. Northridge [4]	0.56
JCB01	Pile D = 0.64 m, t = 0.036 m, L = 24.26 m, EI = 2.134e5 kPa-m4	Wharf deck 28.1 m × 12.0 m × 0.78 m, mass = 951549 kg	Nevada loose sand D_R = 40 % Nevada dense sand, D_R = 74 % Rockfill, friction angle = 45 deg	Event 23. Loma Prieta [3]	0.15

1. The centrifuge scale factor was 40.1 for all tests.
2. Pile group consists of 21 piles (in a 3-by-7 setup).
3. 1989 Loma Prieta Outer Harbor Station.
4. 1994 Northridge Rinaldi Station. This time history was recorded less than 10 km from the fault and included a velocity pulse.

Figures 1c to 1f show the cross sections of the other four centrifuge models (NJM02, SMS01, SMS02 and JCB01) illustrating similar information as those in Figure 1a for NJM01. In NJM02 a relatively soft Bay Mud layer was included. In

SMS01 a cement-deep-soil-mixing unit (CDSM) was incorporated. In SMS02 a single monolithic rock dike was supported by dense sand. In JCB01, the rock dikes were replaced with a thin layer of rock face.

In general, the observed zone of shear failure in the liquefied sand in the vicinity of piles can be characterized as broad, diffuse shear failure combined with a localized shear plane at the interface of weak and resistant layers such as the liquefied sand and the upper rockfill. Localized shear planes were also developed above Bay Mud in NJM02 and below CDSM in SMS01, which contributed to the large bending moments that developed at depth in those tests.

The location of the shear planes explain how large bending moments developed below grade. It is significant that the large bending moments that were observed at depth (color-coded green) are below a typically assumed depth of fixity. The depth of fixity ranges from 5D to 7D for the piles studied here. The 10D depth that was used to distinguish deep bending moments (color-coded green) corresponds to z/T of 3 if depth (z) is normalized by the relative stiffness factor (T) (i.e., $T = (EI/k)^{(1/5)}$ where EI is the pile bending stiffness and k is the subgrade reaction in rockfill). The 10D depth is aligned with the definition of “deep in-ground” plastic hinge location per ASCE 61-14.

Representative Time Histories. Figure 2 provides representative time histories of pile moment, displacement, and wharf deck acceleration from test NJM01 to illustrate the time- and depth-dependent nature of the inertial and displacement demands on two piles (one which experienced the greatest inertial loading at the pile head and one that experienced the greatest kinematic loading at depth during

shaking). Figure 2a shows the maximum transient bending moments below and above grade recorded in the test. The maximum moment above grade was recorded at the top of Pile 6 and the maximum moment below grade was recorded 17 m (56 ft) deep (26D) in Pile 1 above the interface between the loose liquefied sand and the underlying dense sand. These maximum transient moments both occurred at approximately the same time, as denoted with a vertical dashed line. The residual (end of shaking) moments are denoted in this figure showing that the residual bending moments were significantly smaller than the maximum transient bending moments.

Figure 2b shows the wharf deck and soil displacements. The maximum transient displacement and the permanent (end of shaking) displacements are also denoted in this figure suggesting that the maximum transient soil displacement (0.13 m or 5 in bayward) is approximately 1.3 times larger than the permanent soil displacement (0.1 m or 4 in bayward). This difference highlights the need for considering maximum transient soil displacements in design rather than the end of shaking, residual displacements. It is worthwhile noting that existing design methods (e.g., Newmark sliding block, and linear/nonlinear time-history analysis) provide an estimate of maximum transient and/or permanent soil displacements with various levels of conservatism.

Figure 2c shows the wharf acceleration, which is directly correlated with superstructure inertia. As plotted, positive wharf acceleration corresponds to bayward inertia. It is significant to note that in this model test the wharf inertia and the soil displacement were always in-phase. In addition, the peak moments at both

the pile head and at depth were synchronous with the peak transient soil and wharf deck displacements. At this time the wharf acceleration was approximately 85% of its peak in the corresponding direction (i.e., the peak moment at the pile head did not occur at the time of peak inertial loading).

Range of Inertial and Kinematic Demands. Figure 3a shows the peak acceleration at wharf deck (superstructure) versus the peak ground acceleration (PGA) at ground surface for the five tests analyzed here. The wharf peak accelerations (indicative of the peak inertial demand) in this study range from 0.25g to 0.7g. The data supports a nonlinear relationship between the wharf deck peak acceleration and the ground surface PGA across the 5 tests evaluated.

Figure 3b shows the maximum transient and permanent (end of shaking) soil displacements measured by a Linear Variable Differential Transformers (LVDT) installed in the backland behind the wharf deck. The maximum transient soil displacements in the backland (indicative of the kinematic demands) range from 0.07 m to 0.4 m (2.8 to 15.7 in), and the permanent soil displacements range from 0.06 m to 0.3 m (2.4 to 11.8 in). It is observed from these tests that the maximum transient soil displacements are 1.3 to 2.7 times larger than the permanent soil displacements. It is acknowledged that this ratio depends on soil properties, layering, and ground motion characteristics; however, it is noticed that in all five tests, this ratio was greater than one suggesting that the maximum transient soil displacements should be considered in design to estimate kinematic demands rather than the permanent (end of shaking) displacements. The soil displacements in SMS02 follow a noticeably different trend than other tests as the

subsurface conditions in SMS02 included rockfill and dense sand that did not liquefy.

Location of Maximum Bending Moments. From a design perspective, it is important to estimate the location of maximum moments in the entire pile group and to determine whether the maximum moment occurs above the grade (e.g. at the pile head) or below the grade. The bending moments below grade can develop at the typical depth of fixity in cases with minimal kinematic demands or at large depths driven by significant soil deformations. The location and magnitude of maximum bending moments above and below grade were previously shown in the cross sections in Figure 1. Figure 4 shows a comparison of the magnitude of the maximum transient bending moments above and below grade observed in any pile within the group (i.e., the maximum moments were not necessarily experienced in the same pile). With the exception of NJM01, the bending moments above grade (at pile head) were equal to or larger than the maximum bending moments below grade. This ratio was approximately 1 for tests NJM02, SMS01, and JCB01, where liquefaction was triggered and significant kinematic demands were imposed. The ratio was approximately 1.9 in SMS02, where liquefaction was not triggered and kinematic demands were small. It should also be noted that maximum bending moments below grade in SMS02 were encountered at typical depth of fixity rather than at more significant depths in other tests with liquefiable soils.

3.3 COINCIDENCE OF INERTIAL AND KINEMATIC DEMANDS

Wharf Inertia at the Time of Maximum Bending Moments. Figure 5(a) shows a comparison of the normalized wharf acceleration (Acceleration at time = t /

maximum wharf acceleration) at the time of maximum bending moment for locations above grade and below grade. The wharf accelerations at time t are normalized by the maximum wharf acceleration in the corresponding direction, i.e. positive accelerations are normalized by the maximum positive acceleration and negative accelerations are normalized by the maximum negative acceleration. This figure demonstrates that when pile head bending moments are at the maximum value, the wharf acceleration is, on average, at 92% of its peak (ranging between 84% to 100%). This relationship confirms, as expected, that peak moments at the pile-deck connection and near the pile head are synchronous with, and well-correlated with peak wharf deck acceleration. Conversely, peak moments at depth are not well-correlated with peak wharf deck PGA, as indicated by the significant variability in the normalized acceleration at the time of the peak moments at depth.

Maximum Transient and Residual Bending Moments. The physical model tests outlined in this paper indicate that the residual, end of shaking bending moments due to permanent soil displacement are smaller than the maximum moments that the piles experience during shaking. This is due, in part, to the fact that the peak transient pile moment reflects the synchronous application of inertial and kinematic effects, while the residual, post-shaking, pile moment is in response to only the permanent pile curvature demand related to the final soil displacement. The difference between the peak, transient and residual moments is a function of both the soil conditions and slope configuration, and the characteristics of the strong ground motions, therefore the timing and extent of the seismically-induced slope

deformation. Figure 5b shows the residual bending moments normalized by the maximum transient bending moments for two locations along a single pile (one above and one below grade). This figure shows that the residual moments are approximately 14% and 48% of their peak transient values for above grade and below grade locations, respectively. These ratios suggest that both the transient and residual moments should be evaluated in seismic design. This conclusion applies to relatively flexible piles, such as the ones studied here, where the piles follow the soil displacement patterns closely, reducing the relative displacement between soil and pile such that the ultimate soil reactions (i.e. the p_{ult} in p-y springs) do not mobilize. In these cases, the soil reaction, and therefore the bending moments, are proportional to soil displacements.

The kinematic demands on flexible piles can be best estimated by imposing the soil displacements to the end nodes of p-y springs, rather than imposing them as a lateral spreading pressure. This conclusion may not apply to the relatively stiff piles, such as large diameter pile shafts, where the laterally spreading soil flows around the pile and the ultimate soil reactions mobilize. In those cases, the soil reactions, and therefore the bending moments, are not necessarily dependent on the soil displacements in which case imposing the permanent (end of shaking) soil displacements may be adequate in design.

3.4 IMPLICATIONS OF THE PHYSICAL MODELING FOR COMBINING INERTIAL AND KINEMATIC DEMANDS

The physical model tests provided a very worthwhile data set that highlights the depth-, pile row-, and time-dependent interaction of inertial and kinematic effects

leading to the cumulative loads on piles for five different prototypes of wharf and waterfront configurations. The data clearly demonstrates that the moments resisted along a single pile reflect a complex interaction of ground motion characteristics, wharf – pile stiffness and dynamic response, and the combination of transient and accumulated permanent ground deformation. As addressed in ASCE 61-14, it is therefore necessary to approximate the primary lateral loads (inertia and kinematics) acting on a single pile and combine these loads in a manner that satisfies performance objectives for all piles supporting the wharf throughout the entirety of the design seismic load application (i.e. duration of shaking).

The use of inertial and kinematic Load Combinations is commonly applied in practice as addressed in the Introduction; however, a broad range of scaling factors to peak loads have been proposed. To investigate whether inertial demands applied at the pile head should be combined with kinematic demands to estimate large bending moments at various locations along a pile pseudo-static analyses of the five centrifuge models addressed herein were performed with *LPILE*. Each of the five models were analyzed for two earthquake load sequences, thus 10 earthquake loading scenarios were evaluated. The bending moments computed using *LPILE* were compared against the measured moments from the centrifuge tests. The profiles of moment along the pile were compared; however, for the sake of brevity the results presented in this paper focus on the portion of the piles where large bending moments were observed during the centrifuge tests. This comparison provided a practical approach to determine whether inertial and

kinematic demands should be combined in order to estimate bending moments at different depths. The following three load combinations were evaluated:

- Kinematic demand only: Soil displacement profiles were extracted at the time of maximum bending moments at depth from centrifuge tests and were applied to the end nodes of p-y springs. The soil displacement profiles were calculated by combining the transient component (from accelerometers) and the permanent component (from LVDT at ground surface).
- Wharf inertial demand only: Inertial forces at the pile head were extracted at the time of the maximum bending moment at depth in the centrifuge tests, and were applied to the pile head as shear forces. The inertial force was calculated from the slope of the bending moment profiles above the grade for the piles that were instrumented. The pile-deck connection was modeled as fixed-head given the non-yielding connection and the in-plane rigidity of the wharf deck.
- Combined kinematic and inertial demands.

It is important to note that these demands (i.e. the inertial load applied at pile head and soil displacements imposed along the piles) are often estimated in practice on the basis of decoupled analyses. In this study, these demands were not estimated; they were directly extracted from the centrifuge tests. In the absence of strong motion records at design-level seismic loads on well-instrumented wharves in North America, the physical modeling results provide useful data for evaluating how inertial and kinematic loads from decoupled analyses (i.e., *LPILE*) should be combined to yield a representative approximation

of the measured, coupled behavior of wharf – pile – soil interaction. The goal of this on-going investigation is to develop rational procedures for combining the individual loads for a practice based analysis.

The comparison of bending moments at the pile heads obtained from *LPILE* and the corresponding centrifuge tests is provided in Figure 6a. The trends from the 10 tests evaluated demonstrate the following general conclusions;

- Applying combined inertial and kinematic demands provides the best agreement between the *LPILE* simulation and the physical modeling results,
- Applying inertial demands only will slightly underestimate the bending moments,
- Applying kinematic demand only will grossly underestimate the bending moments, as expected.

Although it is anticipated that the bending moments at pile heads are primarily driven by the inertial forces due to the wharf deck, as evidenced by the majority of data points that are reasonably estimated by applying inertial demands only, the data trends support combining inertial and kinematic demands to capture the response.

The comparison of the bending moments from physical and numerical models for deep locations (>10D) associated with deep-seated ground deformation is provided in Figure 6b. As anticipated, the effects of the inertial loads decreases with depth. The data trends support the application of kinematic loading

only as the combination of inertial and kinematic demands did not improve the accuracy of estimated bending moments at depth.

3.5 CONCLUDING REMARKS

Physical modeling of the dynamic response of five well-instrumented wharf – foundation configurations has provided an extensive database for evaluating complex soil-foundation-structure interaction and for calibrating numerical models routinely used in practice for wharf design. This paper has focused on a subset of the instrumentation array data that supports the investigation of dynamic loading of the wharf foundation piles. The primary results of the investigation are summarized as follows, with suggestions for the seismic analysis of pile supported wharves in practice.

1. Practice-oriented procedures for combining Inertial and Kinematic loads on piles are considered necessary approximations of complex soil-foundation-structure-interaction (SFSI) that has been shown by the physical modeling to be dependent on factors such as; pile row, location along the pile, wharf – foundation stiffness, soil profile and site configuration, and ground motion characteristics. This complexity has led to the development of Load Combination factors that are derived from envelopes of maximum response along a pile, therefore do not explicitly account for the timing of the respective loads. The results of the physical modeling and subsequent pseudo-static analyses support the following practical approximations for seismic wharf design;

a. Peak bending moments adjacent to the pile head (roughly in the upper 3D to 6D) approximated using only peak wharf deck inertial loads (100% I + 0% K) provide estimates that generally fall within 0.70 to 0.85 x Peak Measured Moment; however, substantially smaller ratios were observed. Peak moment estimates at the pile head were improved by incorporating the effects of kinematic loading, which largely accrues due to rotation at the pile-deck connection in response to global ground displacement.
b. In general, peak pile moments at depth (> 10D) can be reasonably evaluated using the displacement demand (i.e., soil displacement profile) without the contribution of inertial loading, thus 100% K + 0% I.

2. Although in all five tests studied here the inertial load and soil displacements were in-phase (in bayward or landward directions) at the time of maximum bending moments, the soil reaction along the nonliquefiable crust (i.e. rockfill) was not necessarily in-phase with the wharf inertia. For relatively flexible piles, such as those studied here, the piles closely follow the soil deformations. As a result, the sign of the lateral soil reaction changes through the rockfill and non-liquefiable, near-surface soils. Therefore, it is overly conservative to assume that the near-surface soils apply a uniformly bayward pressure on the piles. In these cases, the kinematic demands can be best estimated by imposing the soil displacements to the end nodes of p-y springs, rather than imposing them as a lateral spreading pressure. Applying kinematic demands using a uniformly

bayward passive pressure from the rockfill in pseudo-static analysis significantly overestimated bending moments in piles.

3. In almost all tests (except SMS02 where kinematic demands were minimal) large bending moments developed at depths greater than 10D, which is below the typically assumed equivalent depth of fixity.
4. Transient, peak moments at both the pile head and at depth are often greater than the end of shaking residual moments. This is attributed to the difference between the maximum transient and permanent (end of shaking) soil displacements. The data from the five centrifuge tests suggest that the maximum transient soil displacements were 1.3 to 2.7 times larger than the permanent soil displacements. When existing design methods are used to estimate soil displacements, the uncertainties in the estimated values should be considered in design. If the results of 2D nonlinear dynamic analysis are used by the designer in supplementary pseudo-static (uncoupled) analysis, the computed peak transient displacement should be considered as opposed to the end of shaking residual ground displacement. If the Newmark sliding block analysis is used to estimate soil displacements, the built-in conservatism in computing the accumulated permanent displacement should be considered in design. There is also considerable uncertainty in estimating the soil displacement distribution with depth which was found to significantly affect the estimated bending moments in *LPILE* analyses for the flexible piles that were studied here. Additional work is needed to assess the accuracy of existing design methods in estimating maximum transient soil displacements and their

distribution with depth in layered and challenging soil profiles. This should be noted in dynamic geotechnical analyses in which peak kinematic loads are often evaluated using the end of shaking, residual soil displacement profile.

5. It is important to note that this investigation did not include important aspects of pile response and performance due to loads associated with dynamic p-Δ effects for piles supporting crane rails and therefore additional vertical loading imposed by gantry cranes.

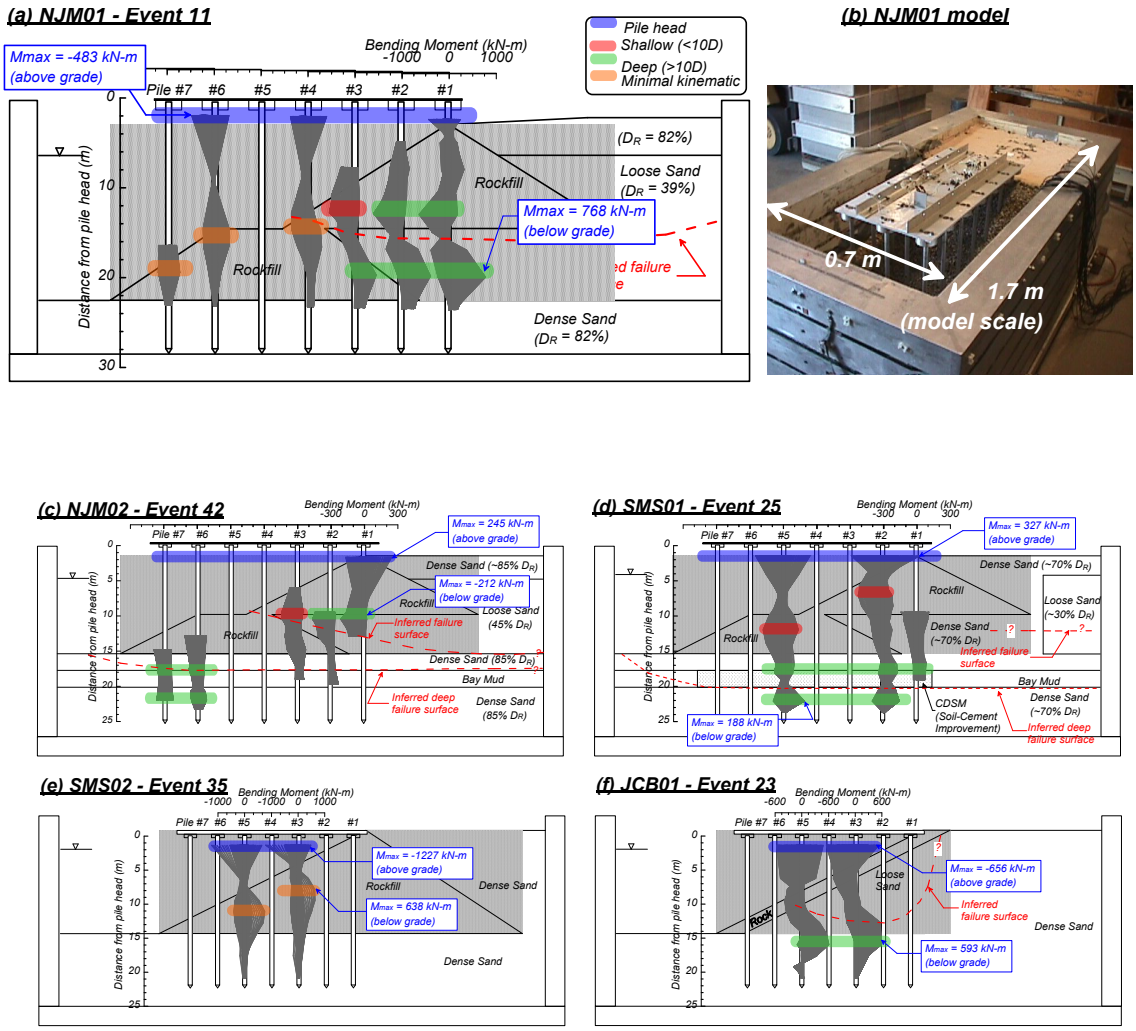

Figure 1. Cross sections of five centrifuge tests along with envelopes of bending moment profiles, and inferred failure surfaces.

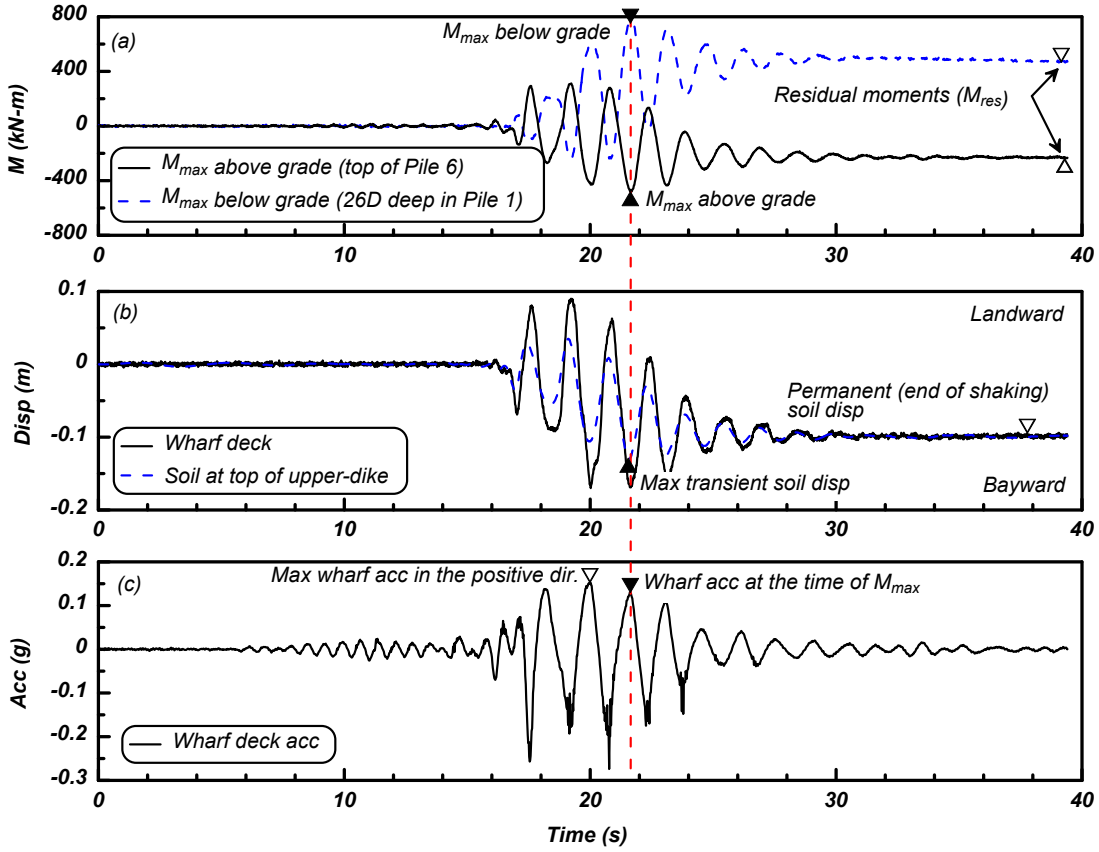

Figure 2. Representative time histories of (a) bending moments, (b) soil and wharf deck displacements, and (c) wharf deck inertia for the first major shaking in NJM01

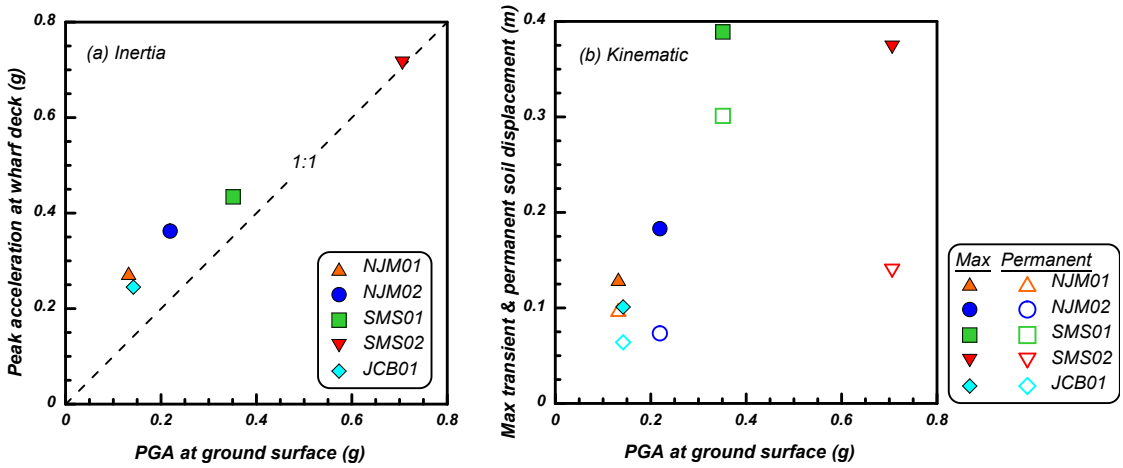

Figure 3. (a) Comparison of the peak acceleration at wharf deck (superstructure inertia) and peak acceleration at the ground surface (PGA), and (b) comparison of maximum transient and permanent soil displacements, and ground surface PGA

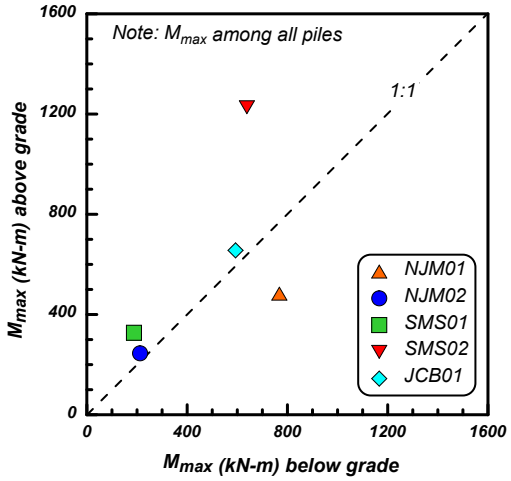

Figure 4. Comparison of the maximum bending moments above and below grade

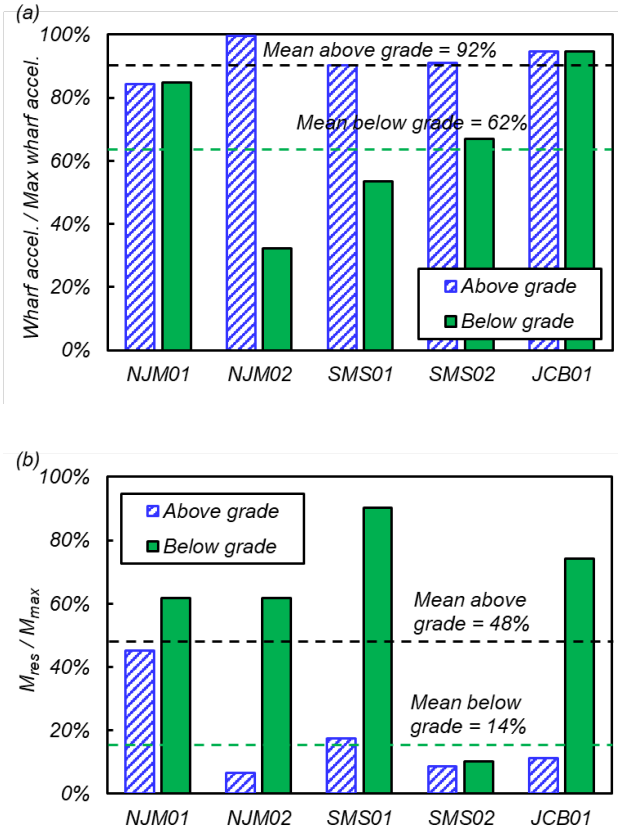

Figure 5. (a) Normailized wharf accelerations at the time of maximum bending moments, and (b) ratios of residual bending moment to maximum transient moments above and below grade

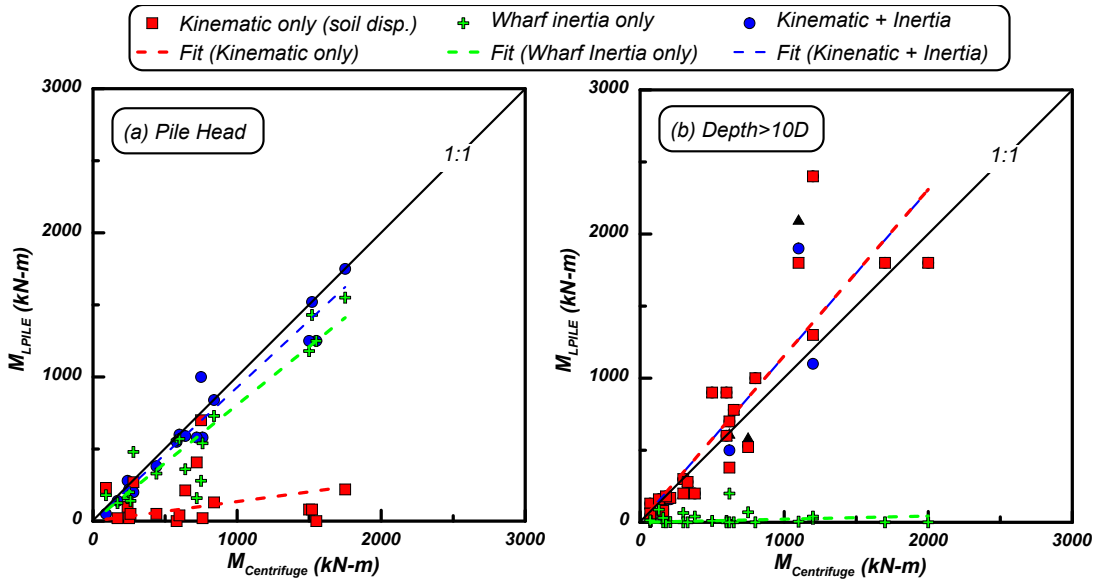

Figure 6. Comparison of bending moments recorded in the centrifuge tests and estimated from LPILE models

REFERENCES

AASHTO (2014). “Guide Specifications for LRFD Seismic Bridge Design.” Second Edition with 2014 Interim, AASHTO, Washington, D.C.

ASCE/COPRI 61-14 (2014). “Seismic Design of Piers and Wharves, prepared by the ASCE Standards Comm. on Seismic Design of Piers and Wharves.” ASCE, Reston, VA.

Brandenberg, S. J., Boulanger, R. W., Kutter, B. L., and Chang, D. (2005). “Behavior of pile foundations in laterally spreading ground during centrifuge tests.” Journal of Geotechnical and Geoenvironmental Engineering, ASCE, 131(11), 1378-1391.

California Department of Transportation (Caltrans) (2012). “Guidelines for Foundation Loading and Deformation Due to Liquefaction Induced Lateral Spreading.” Sacramento, CA.

Chou, J. C., Kutter, B. L., Travasarou, T., & Chacko, J. M. (2011). “Centrifuge modeling of seismically induced uplift for the BART Transbay Tube.” Journal of Geotechnical and Geoenvironmental Engineering, 137(8), 754-765.

Dobry, R., Abdoun, T., O'Rourke, T.D., and Goh, S.H. (2003). “Single piles in lateral spreads: Field bending moment evaluation”, J. Geotech. Geoenviron. Eng. 129, 10, 879-889.

McCullough, N. J., Dickenson, S. E., & Schlechter, S. M. (2001). “The seismic performance of piles in waterfront applications.” In Ports' 01: America's Ports: Gateway to the Global Economy (pp. 1-10).

Oregon Dept. of Transportation (2014). Geotechnical design manual. Tech. Services Branch, Salem, OR.

Travasarou, T., Chen, W. Y., & Chacko, J. M. (2011). “Liquefaction-induced uplift of buried structures: insights from the study of an immersed railway tunnel.” In Proc. of 5th International Conference on Earthquake Geotechnical Engineering, Chile, January.

Washington Department of Transportation (WSDOT) (2015). “Geotechnical Design Manual.” M 46-03.11, May 2015.

Zhou, Y. G., Chen, J., Chen, Y. M., Kutter, B. L., Zheng, B. L., Wilson, D. W., and Clukey, E. C. (2017). “Centrifuge modeling and numerical analysis on seismic site response of deep offshore clay deposits.” Engineering Geology, 227, 54-68.

CHAPTER 4

4.0 PILE-SUPPORTED WHARVES SUBJECTED TO INERTIAL LOADS AND LATERAL GROUND DEFORMATIONS: OBSERVATIONS FROM CENTRIFUGE TESTS

Note: The contents in this chapter have been submitted as a technical paper to ASCE Journal of Geotechnical and Geoenvironmental Engineering and is currently under review with the following citation:

Souri, M.; Khosravifar, A.; Dickenson, S. E.; Schlechter, S. & McCullough, N. “Pile-supported wharves subjected to inertial loads and lateral ground deformations: observations from centrifuge tests.” ASCE Journal of Geotechnical and Geoenvironmental Engineering (under review)

4.1 INTRODUCTION

Liquefaction-induced lateral spreading has been demonstrated to be a major cause of damage to pile-supported wharves (e.g. Hamada et al. 1986, Egan and Wang 1991, Werner et al. 1997, Finn 2005, Rathje et al. 2010, Turner et al. 2016, and Cubrinovski et al. 2017). Studies of the response of piles and pile-supported structures in liquefiable soils using physical models, numerical simulations, and case studies have provided the basis for a number of design recommendations addressing dynamic loads on deep foundations (e.g., Tokimatsu and Asaka 1998, Martin et al. 2002, Dobry et al. 2003, Tokimatsu 2003, Cubrinovski and Ishihara 2006, and Boulanger et al. 2007). Despite insights gleaned from these studies on the consequences of liquefaction-induced slope failure on pile foundations, there is no consensus on how to combine inertial and kinematic loading estimated using uncoupled methods of analysis routinely used

in practice. ASCE 61-14 (ASCE 2014) requires that simultaneous application of inertial and kinematic loads be considered, taking into account the phasing and the locations where the loads are applied. The commentary in Section C4.7 of ASCE 61-14 and the Port of Long Beach Wharf Design Criteria (POLB 2015) suggest that the locations of maximum bending moments from inertia and lateral ground deformations are spaced far enough apart that the two loads do not need to be superimposed. They also suggest that the maximum bending moments from the two loads tend to occur at different times; therefore, they recommend that the loads be treated as uncoupled for typical marginal container wharves. On the other hand, Port of Anchorage Modernization Program Seismic Design Manual (POA 2017) recommends combining the peak inertial loading from earthquake ground motions with 100% of peak kinematic loads from lateral ground displacements. This design manual allows for smaller combination factors (no less than 25%) if justified using peer-reviewed 2-D nonlinear numerical analysis. However, it is recognized that there is limited research and validation of these assumptions; therefore, the design codes indicate that these assumptions should be checked on a project-specific basis.

The design recommendations on the basis of highway transportation research for pile-supported bridges also vary significantly. MCEER/ATC (2003) noted that, for most earthquakes, peak inertia is likely to occur early in the ground motion while the maximum lateral spreading load will develop near the end of motion, and it was recommended to design piles for independent effects of inertia and lateral spreading. They suggested that for large magnitude and long duration

earthquakes the two loads may interact. Boulanger et al. (2007) used a series of 14 centrifuge tests and numerical simulations on piles in liquefiable soils and recommended combining the lateral spreading load with 65% to 85% of the peak inertial load combined with an additional factor ranging between 0.35 to 1.4 if the peak inertial loads are estimated for nonliquefied conditions. Their study was the basis for the design guidelines by transportation agencies in California and Oregon that required combining 100% lateral spreading with 50% inertia (Caltrans 2012; ODOT 2014); Caltrans later retracted this recommendation in favor of higher performance criteria (Caltrans 2016). Other design codes for highway bridge structures recommend different load combinations: Washington State DOT recommends 100% lateral spreading + 25% inertia (WSDOT 2015), while AASHTO (2014) recommends designing piles for the simultaneous effects of inertia and lateral spreading only for large magnitude earthquakes (M>8). Numerical studies by one of the co-authors showed that the two loads need to be combined in design, particularly in cases where the piles are expected to yield (Khosravifar et al. 2014) and subjected to long-duration earthquakes (Nasr and Khosravifar 2018). Brandenberg et al. (2007) suggest that the simultaneous application of lateral spreading and structure inertial forces is most reasonable for stiffer pile foundations but slightly conservative for more flexible pile groups.

The lack of consensus on how to combine inertial and kinematic demands is due, in part, to the relatively limited quantity of experimental data on the phasing of lateral spreading and superstructure inertia, the lack of well-documented field case histories of wharf behavior during earthquakes with strong motion records at

both the superstructure and the ground, and the site- and project-specific aspects of the seismic performance of deep foundations in laterally moving grounds. While many of the previous studies focused on soil profiles and pile geometries that are typical to pile-supported bridges, this study attempts to contribute data to enhancing current guidelines for pile-supported wharves and piers. This was done by analyzing data from the centrifuge tests of McCullough et al. (2001) on pile-supported wharves that was performed using a large geotechnical centrifuge. While these centrifuge models represent common wharf and waterfront configurations at major port facilities in the western United States, the findings are useful for similar structures that are supported by piles in liquefiable soils. This paper summarizes the results of the five centrifuge tests, focusing on locations of large bending moments along the piles and the phasing of inertial and kinematic demands. The centrifuge data were analyzed to evaluate the relative contributions of peak wharf inertia, peak soil displacement, and peak bending moments during the critical cycles. The analysis results in this paper are summarized to provide a basis for the development of design guidelines which are presented in the companion paper (Souri et al. 202X).

4.2 CENTRIFUGE TESTS

Details about the centrifuge tests employed in this study can be found in data reports in McCullough et al. (2000), Schlechter et al. (2000a,b), and Boland et al. (2001a,b). For brevity, only a summary of the results is provided in this paper. Five models were tested at a centrifugal acceleration of 40.1 g and subjected to a sequence of shaking events having various amplitudes. The cross sections of the

five models are shown in Fig. 1. The dynamic response of the wharf and ground was recorded during the shaking using accelerometers, linear variable differential transformers (LVDT), pore water pressure transducers, and pile-mounted strain gauges. All measurements reported in this paper are in prototype scale.

The wharf decks were supported by 21 piles in a 7-by-3 configuration, where the piles were rigidly attached to the wharf deck. The wharf deck was made from an aluminum plate (for dimensions, see Table 1); the piles were aluminum pipes with outer diameters ranging from 0.38 m to 0.64 m. Subsurface conditions in model NJM01 included multi-lift rock dikes, a loose sand layer that liquefied during shaking and resulted in lateral spreading, a dense sand layer above the water table, and a dense sand layer at the pile tips. In NJM02, a relatively soft Bay Mud layer was included. In SMS01, a cement-deep-soil-mixing unit (CDSM) was incorporated as a ground improvement method for the soft Bay Mud. In SMS02, a single monolithic rock dike was supported by dense sand. In JCB01, the rock dikes were replaced with a thin layer of rock face. Key soil, pile, and superstructure properties for the centrifuge models are listed in Table 1.

Each model was subjected to a series of three to five input motions, sequentially increasing in amplitude. Peak ground acceleration (PGA) at the base was calculated as the average of the readings from two accelerometers attached to the outside of the centrifuge box, while the PGA at the ground surface was extracted from accelerometers in the backland immediately behind the wharf deck. Wharf deck acceleration was computed as the average of readings from two accelerometers attached to the deck (East side and West side). Horizontal soil

displacements at the ground surface were measured from LVDTs attached to the ground surface in the backland behind the deck. As these measurements are likely affected by the wharf deck response, they should be considered as pile-restrained displacements. All displacements (soil and wharf) were adjusted to be relative to the container base; displacements have negative values in the bayward direction and positive values in the landward direction. The input ground motions are listed in Table 1.

4.3 OBSERVATIONS FROM CENTRIFUGE TESTS

4.3.1 Slope Deformations and Pile Bending Moments

The profiles on the right in Fig. 1 show the envelopes of maximum bending moment distributions during ground motions along the instrumented piles (shown in gray) for the first large shaking event in all five tests. The locations of strain gauges where large bending moments were observed during the test are color-coded: the top of pile is in blue, shallow locations with depths < 10D are in red, and deep locations with depths > 10D are in green; the locations of maximum bending moments among all piles above and below grade are indicated in blue callouts. Measurements from these strain gauges were later used to determine the critical cycles. It should be noted that while the envelopes of the maximum pile moments are useful for highlighting zones of importance, the plots do not demonstrate the time-dependent nature of the maximum moments as functions of depth or pile row (i.e., the peak moments are not experienced at the same time along a single pile or in all piles simultaneously). The profiles on the left in Fig. 1 show the maximum

landward and bayward transient soil displacement profiles for all five tests; these are used to identify the inferred zone of shear failure in the ground (shown by dashed red lines). The transient soil displacements within the soil are calculated through double integration of the readings from the embedded accelerometers.

Characterizing the zone of shear failure aids in understanding how kinematic demands are exerted on the piles in each centrifuge test. In NJM01, a localized shear failure plane developed through the liquefied loose sand beneath the rockfill, which contributed to large bending moments at those depths in Piles 1 to 3. The shear strains in rockfill were minimal. The large bending moments at shallow depths in Piles 4, 6 and 7 are typical for piles loaded with inertial demands at the top and minimal kinematic effects. In NJM02, a broad, diffuse shear failure developed within the liquefied soil unit. A deeper shear failure plane also developed above the soft Bay Mud and resulted in relatively large bending moments in Piles 6 and 7. In SMS01, a shear failure plane developed in the loose sand in the backland area and was extended through the dense sand underneath the upper rock dike. A deeper shear failure plane developed below the cement-deep-soil-mixing (CDSM) layer, which was used as a ground improvement method to improve the Bay Mud. The relatively large bending moments at depth are an indication that a slight slippage might have occurred below the CDSM unit at the interface with the dense sand layer. It is speculated that this slippage occurred because the CDSM was not keyed in the underlying dense sand layer. The rockfill deformed substantially more in this test than in the first two tests.

The zones of failure in the last two tests were somewhat different. In SMS02, no liquefiable layer was present. Despite noticeable deformations in the rockfill (due to a very large input motion at the base), the strains were uniform and the stresses imposed on the piles from soil deformations were small. The large bending moments at shallow depths show the typical response expected from piles loaded at the top by superstructure inertia under nonliquefied conditions. In contrast, for JCB01, the shear failure plane developed through the loose liquefied sand, resulting in large bending moments at the interface between the loose sand and the underlying dense sand. Large bending moments developed at pile head as well—which was also the case for the pile heads in the other four tests.

4.3.2 Time Histories

The time histories of wharf and ground response were used to investigate the depth-dependency of the interaction of inertia and kinematic demands on the piles. We found that the peak inertial load from the superstructure and the peak kinematic loads from soil displacements are more likely to be synchronous when the bending moments are at their peak value at the pile head rather than when they are at peak value at depth. This is demonstrated in Fig. 2, using the time histories for NJM02 as an example. The strain gauges where maximum bending moments were recorded above and below grade (marked with callouts in Fig. 1) are highlighted in the time histories corresponding to the pile head (SG1-4) and a deep location above the liquefied layer (SG1-2) in Pile 1. All other strain gauges are plotted in the background to show the range of recorded bending moments at other locations. Excess pore water pressure ratios are presented at representative

locations within each soil unit: PPT7367 is in the upper rockfill, PPT8016 is in the loose sand between Piles 1 and 2, PPT7817 is in the loose sand in the free field, and PPT8013 is in the dense sand layer below the loose sand layer. The PPT in the free field shows that the pore water pressure ratio (R_u) reached 100%, indicating that liquefaction was triggered during shaking. However, the PPT at the same elevation within the loose sand in between the piles shows the maximum R_u of 50%. The lower R_u in the loose sand below the rockfill is attributed to the drainage of excess pore water pressure into the rockfill, which has a much higher permeability. The time histories shown here correspond to the first large shaking event (Event 42) with a base input PGA of 0.19 g.

For NJM02, the maximum bending moment above grade, 245 kN-m, occurred at the pile head in Pile 1 (SG1-4) at t = 17.6 sec, which is indicated by a vertical dashed red line. This bending moment was also the maximum recorded moment during the test. At that time, the soil and the wharf deck were both moving landward. The wharf deck acceleration was −0.32 g (99% of PGA at wharf deck), the wharf displacement was 0.14 m (83% of the peak wharf displacement), and soil displacement was 0.06 m (34% of the peak soil displacement). The maximum bending moment below grade was −212 kN-m and occurred 9 m (23D) below grade in Pile 1 (SG1-2) at t = 22.9 sec, when the soil and the wharf deck were moving bayward. At this critical cycle, the wharf deck acceleration was 0.12 g (32% of PGA at wharf deck), the wharf displacement was −0.13 m (76% of the peak wharf displacement), and soil displacement was −0.12 m (73% of the peak soil displacement). The maximum residual moment below grade for NJM02 was −131

kN-m, which is 62% of M_{max} below grade. The residual moment above grade was negligible (16 kN-m, which is 7% of M_{max} above grade). The residual wharf deck displacement of −0.07 m is 43% of its peak value during the ground motion. Similarly, the residual soil displacement of −0.07 m is 43% of its peak value during the ground motion.

The critical cycle corresponding to the maximum bending moment above grade (t = 17.6 sec) for NJM02 occurred early during the time history when liquefaction was not yet triggered. However, at the critical cycle corresponding to the maximum bending moment below grade (t = 22.9 sec), liquefaction was triggered in the free field while the near-field R_u adjacent to the piles only reached approximately 40%. The pore pressures at the time of maximum bending moments show transient drops, and this finding was attributed to the dilative behavior of sand; this observation is consistent with those for the centrifuge tests conducted by Brandenberg et al. (2005). Both critical cycles corresponding to maximum bending moments below and above grade occurred within the strong motion portion of the earthquake and not necessarily at the end of motion.

A similar analysis on the time history data was performed for the other centrifuge tests. In the key time history plots for NJM01 (Fig. 3a), the maximum bending moments above grade (SG6-9) and below grade (SG1-2) both occurred at t = 21.6 sec. At that time, both the soil and the wharf deck were moving bayward; wharf deck acceleration was 0.13 g (or 47% of PGA at the wharf deck), and the soil displacement was −0.13 m (or 99% of peak soil displacement). The residual

soil displacement was −0.1 m which is 77% of its peak value during the ground motion.

For SMS01 (Fig. 3b), the maximum bending moment above grade (SG2-15) occurred at t = 17.8 sec. At that time, the soil and wharf deck were moving landward, wharf deck acceleration was 0.39 g (90% of PGA at wharf deck), and soil displacement was 0.19 m (54% of peak soil displacement). The maximum deep bending moment (SG5-2) occurred at t = 23 sec, when the soil and the wharf deck were moving bayward; wharf deck acceleration was 0.2 g (45% of PGA at wharf deck), and soil displacement was −0.35 m (99% of peak soil displacement). The subsequent cycles produced deep bending moments of a similar magnitude (but slightly smaller) that corresponded to even smaller deck accelerations. The results confirm that deep moments are not affected by or correlated to deck inertia. The residual soil displacement for SMS01 was −0.30 m which is 85% of its peak value during the ground motion.

Key time history plots for SMS02, where no liquefiable soil was present, are shown in Fig. 3c. While transient soil displacements were large due to the large applied accelerations at the base, soil deformations were more uniform through the rockfill; they exerted smaller curvature and bending moments below grade and negligible bending moments at depths greater than 10D. The maximum bending moment above grade (SG3-13) and below grade (SG3-8) for SMS02 occurred at t = 7.4 sec. At that time, the soil and the wharf deck were moving bayward, the wharf deck acceleration was 0.48 g (67% of PGA at wharf deck) just slightly after it was at its peak value, and the soil displacement was −0.28 m (99% of peak soil

displacement). The residual soil displacement for SMS02 was −0.14 m which is 47% of its peak value during the ground motion.

For JCB01 (Fig. 3d), the maximum bending moments above grade (SG3-13) and below grade (SG3-4) occurred at t = 22.9 sec, when the soil and wharf deck were moving bayward. Wharf deck acceleration was 0.23 g (95% of PGA at wharf deck), and soil displacement was −0.15 m (99% of peak soil displacement). The residual soil displacement for JCB01 was −0.1 m which is 67% of its peak value during the ground motion.

In these tests, the peak inertia and peak soil displacement cycles occurred during the strong motion portion of the earthquake and were not necessarily decoupled, as suggested by some studies (e.g. MCEER 2003, ASCE 61 2014).

4.3.3 Location and Magnitude of Maximum Bending Moments

From a design perspective, it is sometimes useful to estimate the largest bending moments that develop below and above grade for the entire pile group. This is the case when, for example, following the ASCE 61-14 standards (Section 3.9), where different strain limits are defined for plastic hinges that form at the top of pile, in ground shallower than 10D, and deep in ground deeper than 10D. The magnitude and location of the maximum bending moments (M_{max}) above and below grade for the first major shaking in each test are presented in Table 2. Note that the maximum moments correspond to the entire pile group and were not necessarily experienced in the same pile. The data shows that the large bending moments that develop below grade were encountered at depths between 8.8D and 16.8D, which are deeper than the typical depth of fixity. This was true for all tests

with partial to full liquefaction (NJM01, NJM02, SMS01, and JCB01). In SMS02, which corresponds to a nonliquefied soil profile, the maximum moment below grade occurred at a depth of 5.4D, which is typical for piles subjected to inertial load at the top in nonliquefied ground. Fig. 4 shows the magnitude of the maximum bending moments above and below grade for all major shaking events in each test. In all tests with partial to full liquefaction, the bending moments below grade were comparable to or larger than those at the pile head. The distinction is more obvious when comparing the results from these tests to those for SMS02, where liquefaction was not triggered and the kinematic demands were small due to uniform soil deformations. This observation regarding large bending moments below grade is compatible with the recommendations in POLB (2015) which states that deep inground plastic hinges may form in the piles due to the kinematic loading from the lateral movement of dikes on weak soils.

4.3.4 Phasing of Inertial Load and Soil Displacement during Critical Cycle

To estimate the peak bending moments in a pseudo-static analysis, it is important to know the phasing of the deck inertial force and the soil displacements during the critical cycle. The directions of wharf inertial load and soil displacement movement at the time when peak bending moments above and below grade were measured in each centrifuge test are listed in Table 2. In all models, the maximum bending moments below grade occurred when the wharf deck inertia and soil displacements were acting in the bayward direction. On the other hand, the maximum bending moments above grade occurred sometimes when the two loads were in the bayward direction and at other times when they were in the landward

direction. It was observed that the two loads were always in-phase during the critical cycle. This finding is consistent with observations from centrifuge tests on piles in liquefiable sloped grounds that were described in Brandenberg et al. (2005), Chang et al. (2005), and Brandenberg et al. (2007), where the superstructure inertial load and soil displacements were in-phase and downslope at the time of peak bending moments for tests where the inertial load from the superstructure or pile cap was significant. The finding is also consistent with those from a series of large-scale shake table tests by Tokimatsu et al. (2005), where the authors concluded that soil displacements and inertial loads are in-phase when the natural period of the structure is smaller than the natural period of the soil profile after liquefaction. The natural period of the wharf in the centrifuge tests in this study ranged between 0.5 to 1.0 sec, and the natural period of the ground after liquefaction ranged from 1.4 to 1.7 sec. For comparison, the natural period of nonliquefied ground, estimated from small amplitude events where liquefaction was not triggered, ranged from 0.8 to 1.1 sec.

4.4 INTERACTION OF INERTIAL AND KINEMATIC DEMANDS

Time histories of soil and wharf responses were analyzed to characterize the interaction between peak soil displacement (indicative of kinematic demands) and peak wharf deck acceleration (indicative of superstructure inertia) for different pile rows and at different locations along the piles where maximum bending moments were recorded.

4.4.1 Portion of Peak Soil Displacements at Time of Peak Inertial Loads

The normalized soil displacements (soil displacement at time *t* / peak soil displacement) during the critical cycle at which the peak wharf acceleration is recorded for all major events in all five tests are shown in Fig. 5. It can be seen that at peak inertia, the soil displacements ranged from 67% to 100% of the peak soil displacements. This finding is consistent with the recommendations in POA (2017) which assumes that the peak kinematic loading from lateral ground displacements on piles occur at the same time as peak inertial loading from earthquake ground motions. The POA recommendations allow for reducing the peak kinematic loading at the time of peak inertia to 50% if 2-D nonlinear numerical analysis is performed and to 25% if more stringent independent peer review is performed due to various uncertainties associated with numerical modeling.

The normalized bending moment (bending moment at a particular strain gauge at time *t* / maximum bending moment in the same strain gauge) versus depth normalized with pile diameter for all key strain gauges in all five tests are shown in Fig. 6. Only the first event in each test is used in producing the data shown in this figure. The bending moment (M) is extracted at the time of peak wharf acceleration. The depth is measured from the ground surface; thus, the data points with negative depth/diameter ratios indicate strain gauges that are mounted at, or very close to, the pile head. Consistent with the color-coded categories for the strain gauges in Fig. 1, the mean M/M_{max} ratios were calculated for three categories: pile head (depth/diameter <0), shallow locations (0 ≤ depth/diameter <10), and deep locations (depth/diameter ≥10). The results

suggest that at the time of peak wharf acceleration, the M/M_{max} ratio is, on average, 93%, 74%, and 67% for the pile head, shallow locations, and deep locations, respectively (all mean values reported in this figure and subsequent figures correspond to the geometric mean). The gray shading in Fig. 6 merely indicates the range of plotted data points in the three categories. These findings confirm, as expected, that the maximum bending moments at the pile head correlate well with peak wharf deck acceleration (i.e. peak inertia). Conversely, the maximum bending moments at depth do not correlate well with peak wharf deck acceleration, as indicated by the variability in the normalized bending moments at depth. This finding is attributed to the notion that deep bending moments are more influenced by the soil displacements (i.e. kinematic demands) than the superstructure inertia.

4.4.2 Portion of Peak Inertial Loads at Time of Peak Soil Displacements

The normalized wharf deck acceleration (acceleration at time *t* / peak wharf acceleration) during the critical cycle at which the peak ground surface soil displacement is recorded are shown in Fig. 7. This figure shows that when soil displacement is at the maximum value, the wharf acceleration ranges from 48% to 100% of its peak. This wide range of inertial combination factors highlights the site- and project-specific nature of the interaction between inertial and kinematic loads. It is noted that although a portion of the inertial load coincides with kinematic load during the ground motion, the effect of inertial load attenuates with depth. It was shown by Souri et al. (2019) that applying soil displacements only is sufficient for estimating large pile bending moments that develop at depths greater than 10D. This is also consistent with the observations of Abdoun and Dobry (2002), who

reported that the influence of superstructure inertia diminished to a minimal level at depths greater than 2 to 3 m for 0.6-m-diameter piles.

The normalized bending moment (M/M_{max}) versus normalized depth for all key strain gauges in five tests are presented in Fig. 8. Only the first event in each test is shown in this figure. The results suggest that at the time of peak soil displacement, the M/M_{max} ratio is, on average, 85%, 69%, and 72% for the pile head, at shallow locations, and at deep locations, respectively. Ratios below one can be explained by considering that soil reactions, and thus pile bending moments, are a function of the relative displacement between the soil and the pile rather than soil displacements only. Therefore, while there is a strong correlation between maximum bending moments and peak soil displacements, their peaks do not necessarily occur at the same time.

4.4.3 Portion of Peak Inertial Loads and Peak Soil Displacements at Time of Maximum Pile Bending Moments

The normalized wharf deck acceleration (acceleration at time *t* / peak wharf acceleration) at the time of maximum pile bending moments at the pile head, shallow locations (<10D), and deep locations (>10D) is presented in Fig. 9 for the first shaking event in each test. This figure provides a basis to combine a fraction of the peak inertial load with the kinematic loads in the companion paper that outlines the proposed design recommendations. The data points for each test correspond to the key strain gauges that were highlighted in Fig. 1. A clear difference can be noticed between the data points for the pile head and those below grade, which suggests that the interaction of inertia and kinematics reduces

with depth. There is also a noticeable difference between the acceleration ratios calculated for the first three tests (NJM01, NJM02 and SMS01) where the acceleration ratio ranges between 0.2 to 1.0 (0.3 to 0.6 for shallow bending moments where the two loads need to be combined) and the last two tests (JCB01 and SMS02) where the acceleration ratio ranges between 0.9 to 1.0. The kinematic demands in the first three tests are driven by a large nonliquefiable rockdike overlying loose liquefiable sand which takes time to mobilize the kinematic loads on piles. As a result, the peak kinematic demands and the peak wharf accelerations are less likely to occur during the same cycle as indicated by the low acceleration ratios in Fig. 9 for the first three tests. In contrast, the kinematic loads in the last two tests are relatively small: the nonliquefiable layer in JCB01 consists of a thin layer of rock facing displacing in response to underlying loose sand that liquefied early in the motion, and the soil profile in SMS02 did not have a liquefiable soil and represented nonliquefied conditions. In the last two tests, the inertial loads and the small kinematic loads were synchronous as indicated by acceleration ratios that are close to 1 in Fig. 9. These differences further highlight that inertial and kinematic combination factors are dependent on soil profiles. The range of values shown in Fig. 9 is comparable to the values recommended by Boulanger et al. (2007) using a different set of centrifuge tests and numerical analyses on piles in gently sloped liquefiable ground. The values recommended by Boulanger et al. (2007) range from 0.65 to 0.85 for the pile cap and superstructure, respectively, and are shown in Fig. 9 for comparison purposes.

The normalized soil displacement (soil displacement at time *t* / peak soil displacement) at the time when bending moments are at their maximum value at various locations along the pile is presented in Fig. 10 for the first shaking in each test. Ratios that are close to one for deep bending moments confirm that, as was shown in previous figures, the peak bending moments at depth are highly correlated with peak soil displacements. Data points below 0.5 for the pile head are related to the critical cycles corresponding to landward movement. As the bending moments in these cases are primarily developed due to deck inertia and generally occur earlier in the ground motion—at a time when very little soil displacement has developed—the resulting soil displacement ratios are low. The wharf acceleration and soil displacement ratios are approximately 100% in the case of SMS02; this result is expected, since this test represents a nonliquefied soil profile.

From Figs. 9 and 10, the relative contribution of inertial and kinematic demands at the critical time when pile bending moments are maximum at various locations along the pile can be quantified. The mean (geometric) and mean + 1σ ratios in Figs. 9 and 10 (listed in Table 3) are used in the companion paper as the basis for developing bracketed load combination factors for design. It is worth noting that while the mean values from the five tests provide a measure of the portion of the peak inertial load that interacts with kinematic demands, the individual ratios could be as high as 100%, indicating that a larger combination factor may be conservatively used in design (e.g. values corresponding to mean + 1σ in Table 3). For completeness, Table 3 also includes the mean and mean + 1σ

ratios of soil displacements at the time of peak inertial load (from Fig. 5) and inertial loads at the time of peak soil displacement (from Fig. 7).

4.5 RESIDUAL VERSUS PEAK KINEMATIC DEMANDS

4.5.1 Residual versus Peak Soil Displacements

The physical test results indicate that the residual bending moments at the end of shaking are smaller than the peak transient moments that the piles experience during shaking since, in part, the peak pile bending moment reflects the synchronous application of inertial and kinematic effects, while the residual bending moment is only the response to the permanent soil displacements. The magnitude of peak and residual soil displacements for the first major shaking in each test and the ratio of peak transient to residual soil displacement are shown in Fig. 11. It can be noticed that the peak transient soil displacements are 1.2 to 2.2 times larger than residual soil displacements, with an average of 1.7 for the five tests. The displacements shown in Fig. 11 (and throughout the paper) are relative to the centrifuge base. The considerably large transient component of the soil displacement is attributed to the inertia of soil mass.

4.5.2 Residual versus Peak Bending Moments

A plot of the residual bending moments normalized by the peak bending moments for key strain gauges along the piles are shown in Fig. 12. This figure shows that residual moments are, on average, 17%, 28% and 69% of their peak transient values at the pile head, shallow locations (<10D) and deep locations (>10D), respectively. The small ratios for $M_{residual}/M_{max}$ above the ground surface

suggest that the bending moments at the pile head are primarily dominated by deck inertia, which is entirely transient and drops to zero at the end of ground motion. Conversely, the large ratios for $M_{residual}/M_{max}$ at depth (>10D) suggest that the effects of deck inertia attenuate with depth and that bending moments at depth are primarily dominated by soil displacements. It is important to note that the $M_{residual}/M_{max}$ ratios at depth are still below one (69% on average), which is attributed to the transient portion of the soil displacements shown previously in Fig. 11. Similar observations were reported by Abdoun et al. (2003) using a series of centrifuge tests where the maximum moment during shaking decreased towards the end of shaking. However, they attributed this behavior to the strain softening of the soils around the pile as the soil free-field displacements continued to increase during their tests. It is worth noting that the low ratios in Fig. 12 correspond to SMS02, which exhibited very small residual moments since liquefaction was not triggered and the permanent kinematic demands were small compared to peak transient kinematic demands.

The $M_{residual}/M_{max}$ ratios suggest that both the transient and residual moments should be evaluated in seismic design. Relatively flexible piles, such as the ones studied here, follow the soil displacement pattern closely, and the relative displacements between the soil and pile are small enough that the ultimate soil reactions (i.e. the p_{ult} in the p-y springs) do not mobilize. Therefore, soil reactions (and bending moments) are highly correlated and are proportional to soil displacements (as shown in Fig. 10). This highlights the importance of accurately estimating soil displacements in design when imposing them to the end nodes of

p-y springs in pseudo-static analysis. This conclusion may not apply to relatively stiff piles, such as large-diameter pile shafts, where the large relative displacement between the soil and pile mobilizes the ultimate soil reactions such that the calculated bending moments may not be sensitive to the imposed soil displacements as long as soil displacements are large enough to mobilize the ultimate soil reactions in the p-y springs. The difference between the peak transient moments and residual moments is also expected to be a function of the characteristics of the strong ground motions and, thus, the timing and extent of the seismically-induced slope deformation.

4.6 CONCLUDING REMARKS

The observations from the centrifuge tests on pile-supported wharves subjected to foundation deformations provided valuable insights for understanding the mechanism of interaction between superstructure inertia and kinematic demands from ground deformations. The time histories from centrifuge tests were analyzed to quantify the coincidence of peak wharf acceleration (indicative of superstructure inertia), peak soil displacement (indicative of kinematic demands), and peak bending moments during the ground motion. The primary conclusions of the investigation are summarized as follows:

- In cases involving liquefaction of foundation soils the maximum bending moments (M_{max}) below grade were always comparable to or larger than the M_{max} at the pile head. The location of the maximum loading varied significantly based on the varying soil profiles between tests. The large bending moments

below grade often developed at depths greater than 8D, which is below the typically assumed equivalent depth of fixity. This observation is consistent with the recommendations in POLB (2015) that deep inground plastic hinges may develop in piles due to kinematic loadings from the lateral movement of dikes underlain by weak soils.

- M_{max} below grade only occurred when the wharf deck inertia and the soil displacements were acting in the bayward direction; M_{max} above grade sometimes occurred when the two loads were in the bayward direction and at other times in the landward direction. Wharf inertia and soil displacements were always in-phase during the critical cycle.
- At maximum wharf accelerations, the soil displacements were 67% to 100% of the peak soil displacement which is consistent with the recommendations in POA (2017) that assume that peak kinematic loads occur at the same time as the peak inertial loads from earthquake ground motions. At peak soil displacements, the wharf accelerations ranged from 48% to 100% of the peak wharf acceleration during the entire shaking. At the time of peak bending moments, the wharf accelerations ranged from 20% to 100% of the peak wharf accelerations. These wide ranges of inertial ratios highlight the site- and project-specific nature of the interaction between inertial and kinematic loads on piles, which is also acknowledged by ASCE 61-14. The range of inertial load ratios observed in this study is comparable to the inertial multipliers recommended by Boulanger et al. (2007) which range from 0.65 to 0.85.

- The maximum bending moments at the pile head were more correlated in time with the peak wharf inertia than the maximum bending moments at depth. The wharf acceleration that was acting at the wharf deck was, on average, 84%, 51%, and 52% of the peak wharf acceleration when the bending moments were maximum at pile head, shallow locations (<10D), and deep locations (>10D), respectively. Conversely, the maximum bending moments at depth were more correlated in time with the peak soil displacement than the maximum bending moment at the pile head. Mobilized soil displacements were, on average, 67%, 63%, and 93% of the peak soil displacements at the time when bending moments were at their maximum at the pile head, shallow locations (<10D), and deep locations (>10D), respectively.
- Peak, transient bending moments at both the pile head and at depth were always greater than the residual moments at the end of shaking. This is attributed to the transient portion of deck inertia as well as the transient portion of the soil displacements. The maximum transient soil displacements were 1.2 to 2.2 times larger than the permanent soil displacements in the centrifuge tests studied here. This implies that if the results of 2D nonlinear dynamic analysis are used by the designer in supplementary pseudo-static (uncoupled) analysis, the computed peak transient displacement should be considered as opposed to the residual ground displacement at the end of shaking. If Newmark sliding block analysis is used to estimate the soil displacements, the built-in conservatism in computing the accumulated permanent displacement should be considered in design.

The above conclusions are applicable for relatively flexible, small-diameter piles such as the ones studied here. The interaction of inertia and kinematics could be different for pile shafts with larger diameters. The contribution factors that were developed in this study are used as a basis for developing design guidelines in the companion paper (Souri et al. 202X).

Table 1. Pile, superstructure, and soil properties and input ground motions in the five centrifuge tests

Test ID	Pile properties	Superstructure properties	Soil properties	Shaking Event	PGA at base (g)
NJM01	Pile D = 0.64 m, t = 0.036 m, L = 27.23 m, EI = 2.134e5 kPa-m^4	Wharf deck 33.7 m × 15.2 m × 0.25 m, mass = 714.8 Mg	Nevada loose sand D_R = 39 % Nevada dense sand, D_R = 82 % Rockfill, friction angle = 45 deg	Event 11: L Event 12: L Event 13: N Event 14: N	−0.15 −0.36 0.73 −0.82
NJM02	Pile D = 0.38 m, t = 0.036 m, L = 25.063 m, EI = 4.113e4 kPa-m^4	Wharf deck 24.9 m × 12.2 m × 0.25 m, mass = 265.8 Mg	Nevada loose sand D_R = 45 % Nevada dense sand, D_R = 85 % Bay Mud, undrained shear strength = 38 kPa Rockfill, friction angle = 45 deg	Event 42: L Event 49: N Event 55: N	−0.19 0.57 0.72
SMS01	Pile D = 0.38 m, t = 0.036 m, L = 25.063 m, EI = 4.113e4 kPa-m^4	Wharf deck 24.9 m × 12.2 m × 0.25 m, mass = 265.8 Mg	Nevada loose sand D_R = 30 % Nevada dense sand, D_R = 70 % CDSM, unconfined compressive strength = 0.9 MPa Rockfill, friction angle = 45 deg	Event 25: L Event 43: L Event 44: N	−0.42 −0.42 0.40
SMS02	Pile D = 0.64 m, t = 0.036 m, L = 24.26 m, EI = 2.134e5 kPa-m^4	Wharf deck 28.1 m × 12.0 m × 0.78 m, mass = 951.6 Mg	Nevada dense sand, D_R = 70 % Rockfill, friction angle = 45 deg	Event 30: L Event 31: L Event 32: N Event 35*: N Event 36: L	−0.20 −0.43 0.52 0.56 −0.47
JCB01	Pile D = 0.64 m, t = 0.036 m, L = 24.26 m, EI = 2.134e5 kPa-m^4	Wharf deck 28.1 m × 12.0 m × 0.78 m, mass = 951.6 Mg	Nevada loose sand D_R = 40 % Nevada dense sand, D_R = 74 % Rockfill, friction angle = 45 deg	Event 18: L Event 19: L Event 20: L Event 23*: L	−0.15 −0.50 −0.15 −0.15

L: 1989 Loma Prieta Earthquake Outer Harbor Station
N: 1994 Northridge Earthquake Rinaldi Station
* Shaking event after the battered piles were detached

Table 2. Location and magnitude of maximum bending moments above and below grade and the phasing of wharf inertial load and soil displacements

	Above Grade				Below Grade			
Test / Event	M_{max} (kN-m)	Location	Height above ground surface (m)	Dir. of inertia / soil displacement at the time of M_{max}	M_{max} (kN-m)	Location	Depth below ground surface (m)	Dir. of wharf inertia / soil displacement at the time of M_{max}
NJM01 / Event 11	−483	Pile 6 head	12.1	yward/Bayward	767*	Pile 1 below liq. layer	16.8	Bayward/Bayward
NJM02 / Event 42	245*	Pile 1 head	0.0	andward/Landward	−212	Pile 1 above liq. layer	8.8	Bayward/Bayward
SMS01 / Event 25	327*	Pile 2 head	3.2	andward/Landward	187	Pile 5 below CDSM	11.8	Bayward/Bayward
SMS02 / Event 35	−1227*	Pile 3 head	2.7	yward/Bayward	638	Pile 3 in rockfill	5.4	Bayward/Bayward
JCB01 / Event 23	−655*	Pile 3 head	2.6	yward/Bayward	592	Pile 3 below liq. layer	12.0	Bayward/Bayward

* Maximum bending moment during the test (above or below the grade).

Table 3. Interaction of peak inertial load and peak soil displacements during critical cycles

Critical cycle based on the time of	Portion of peak soil displacement acting during the critical cycle[1] mean (mean + 1σ)	Portion of peak wharf acceleration acting during the critical cycle[2] mean (mean + 1σ)
Maximum bending moments at pile head	0.67 (1.12)	0.84 (1.01)
Maximum bending moments at shallow locations (<10D)	0.63 (0.87)	0.51 (0.86)
Maximum bending moments at deep locations (>10D)	0.93 (1.02)	0.52 (0.79)
Peak inertial load at wharf deck	0.95 (1.06)	1.00 (1.00)
Peak soil displacement at ground surface	1.00 (1.00)	0.89 (1.08)

1. Ratio of the soil displacement during the critical cycle to the peak soil displacement.
2. Ratio of the wharf acceleration during the critical cycle to the peak wharf acceleration

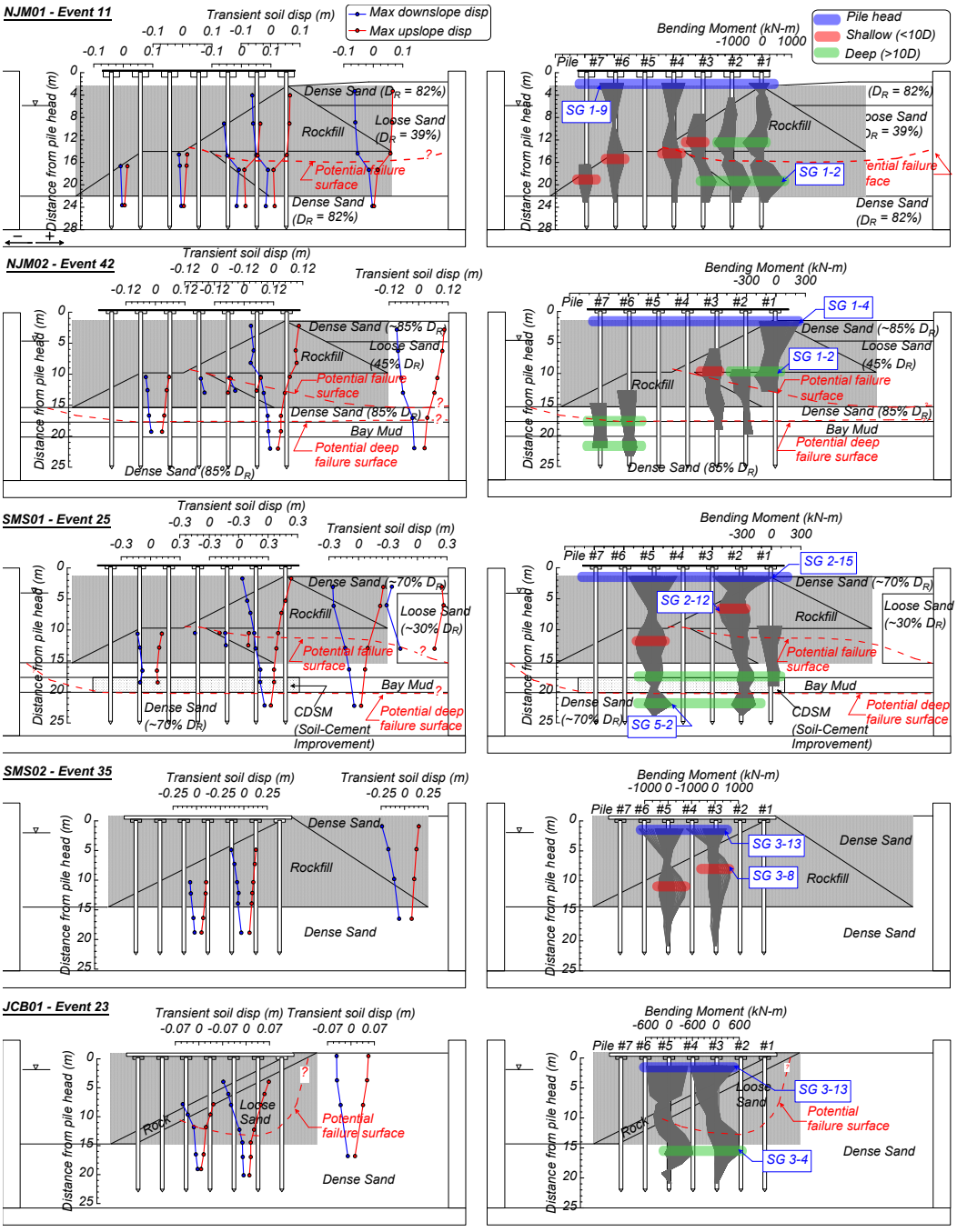

Figure 1. Bending moment profiles and maximum landward and bayward transient soil displacements for all five tests during the first large shaking.

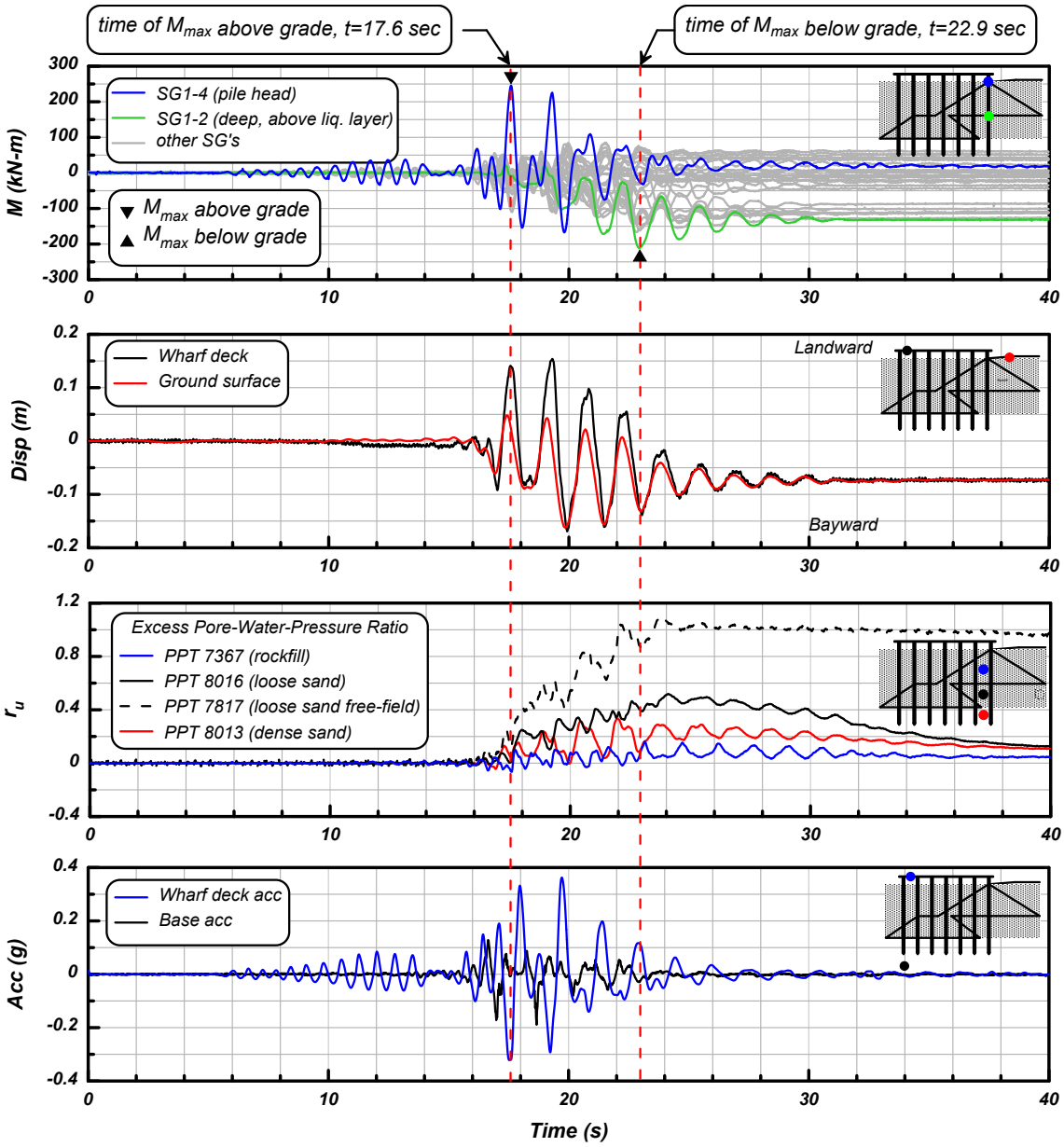

Figure 2. Time histories of bending moments, soil and wharf deck displacements

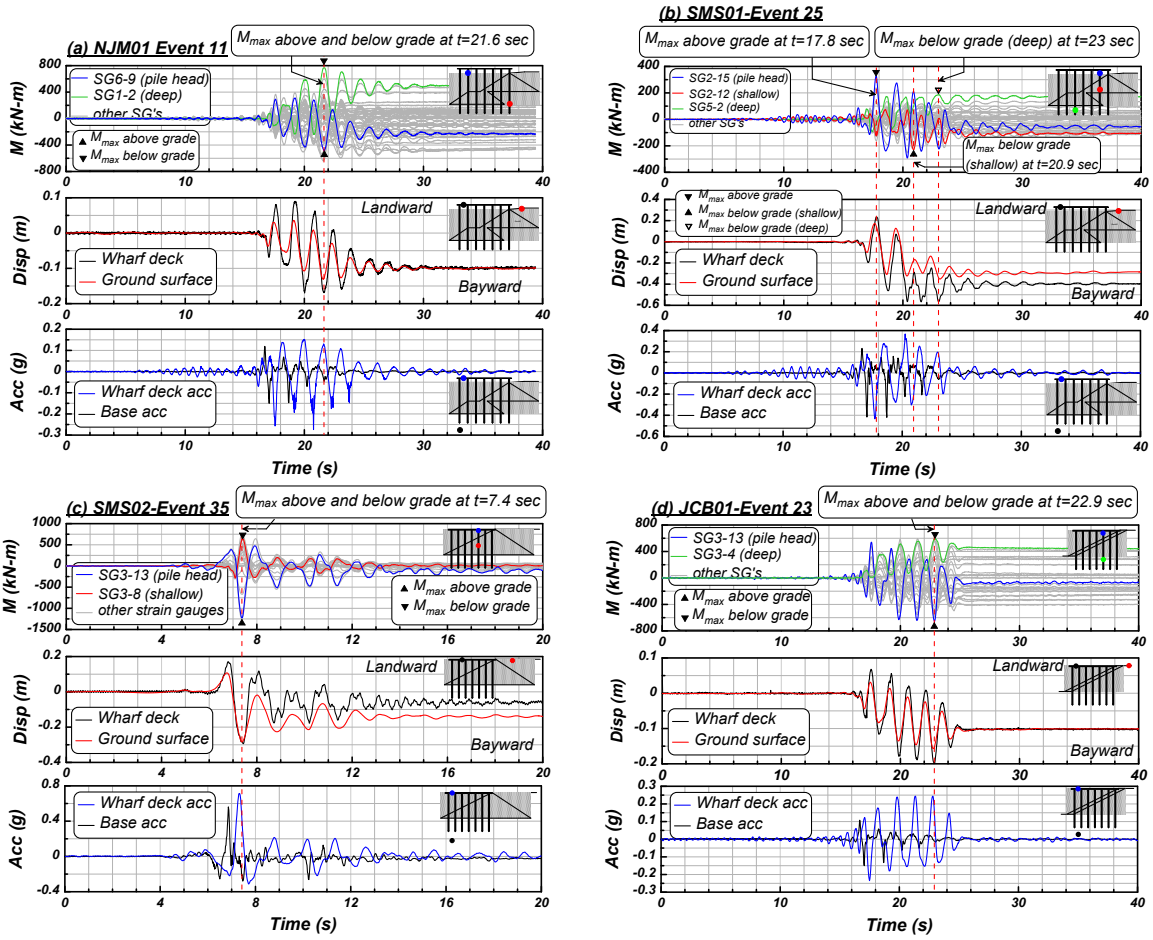

Figure 3. Time histories of moments, displacements, and accelerations for the first large shaking in NJM01, SMS01, SMS02, and JCB01

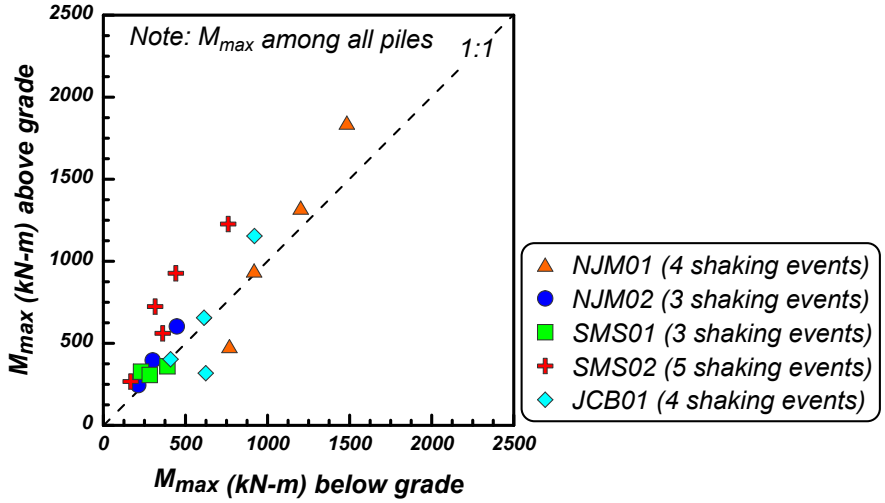

Figure 4. Comparison of the maximum bending moments above and below grade for all major shakings in five tests.

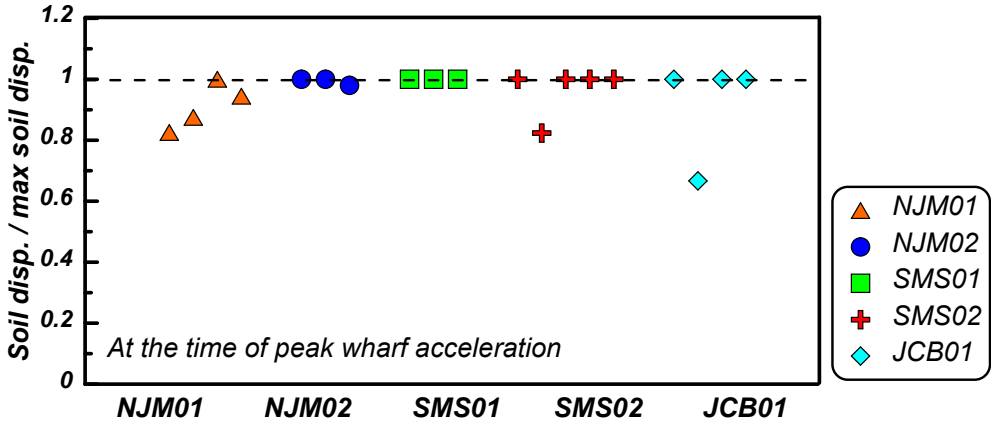

Figure 5. Normalized soil displacements at the time of peak wharf deck accelerations in all major shakings in five tests.

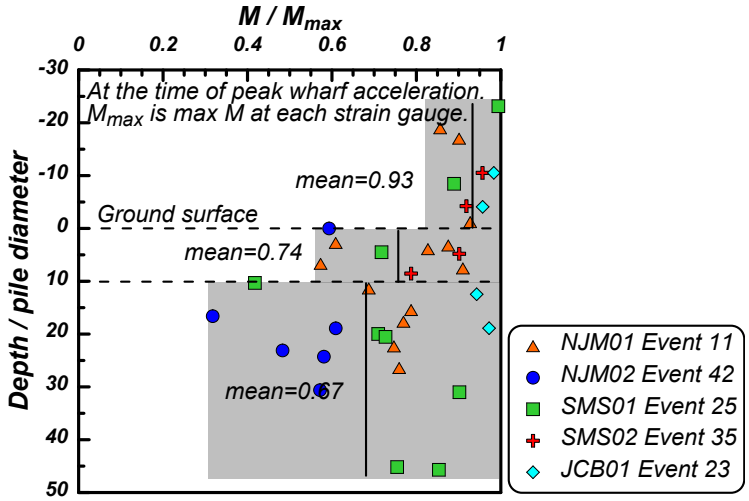

Figure 6. Normalized pile bending moments at the time of peak wharf deck accelerations.

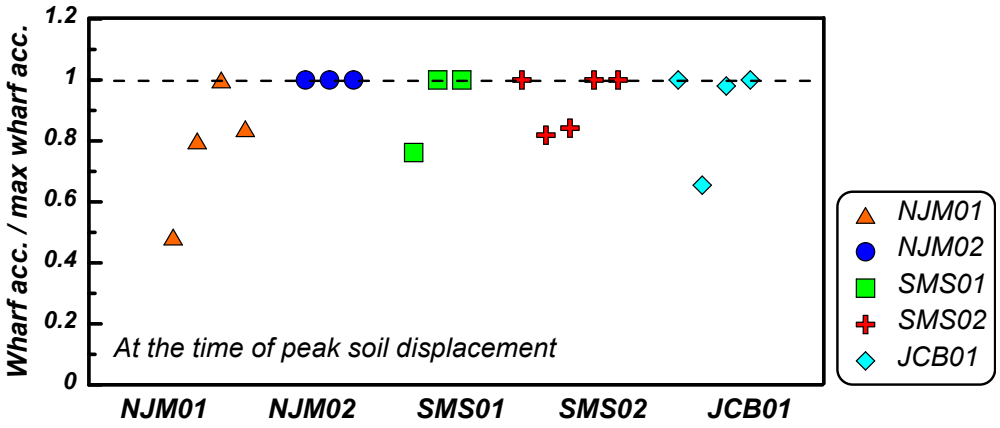

Figure 7. Normalized wharf deck accelerations at the time of peak soil displacements in all major shakings in five tests.

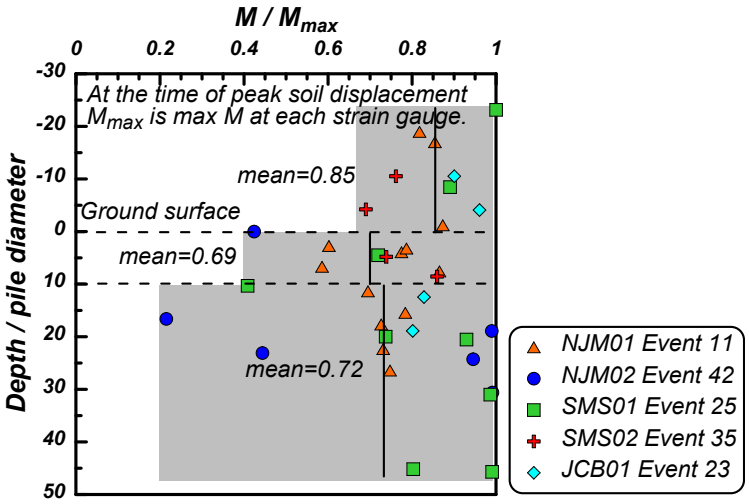

Figure 8. Normalized pile bending moments at the time of peak soil displacements in the first large shaking in each test.

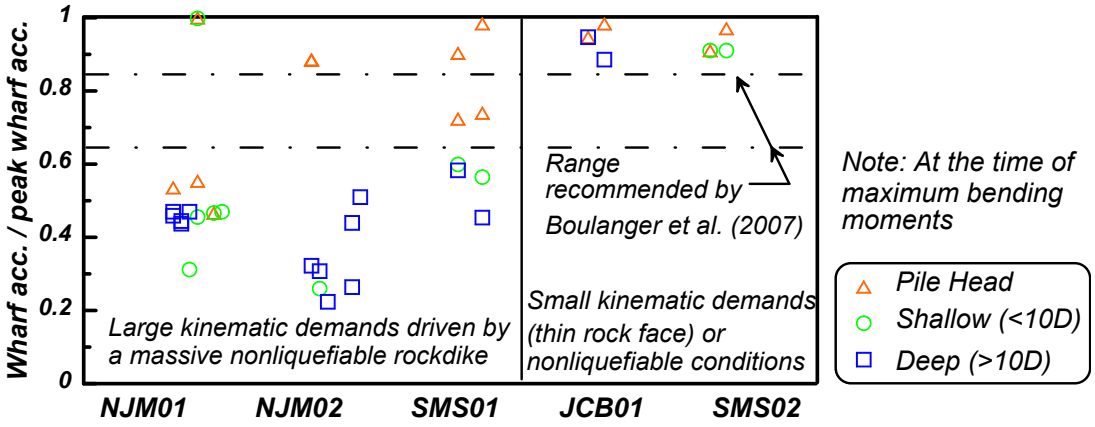

Figure 9. Normalized wharf deck accelerations at the time of maximum pile bending moments in the first large shaking in each test.

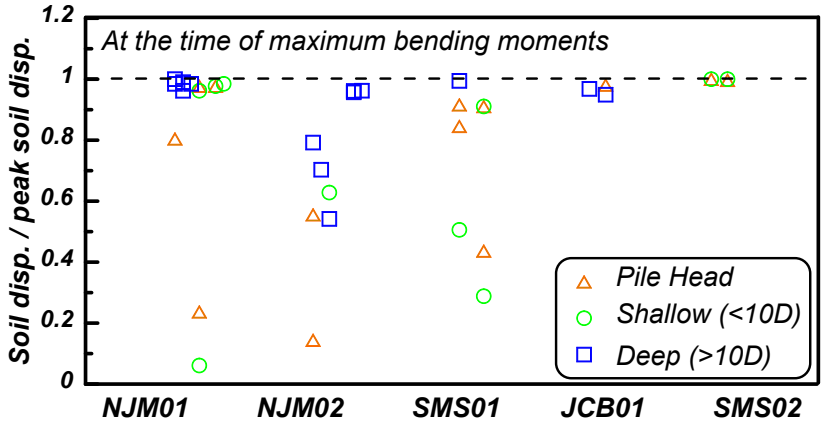

Figure 10. Normalized soil displacements at the time of maximum pile bending moments in the first large shaking in each test.

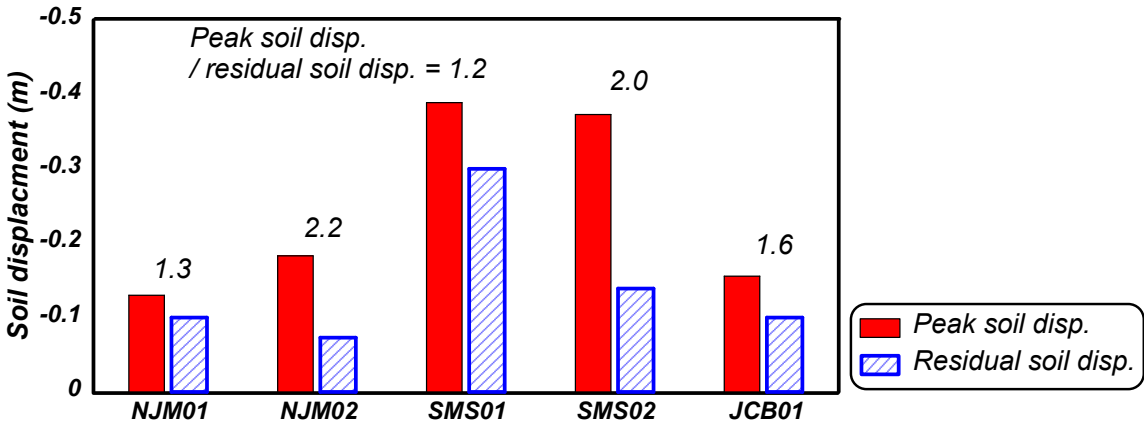

Figure 11. Peak and residual soil displacements in the first large shaking in each test.

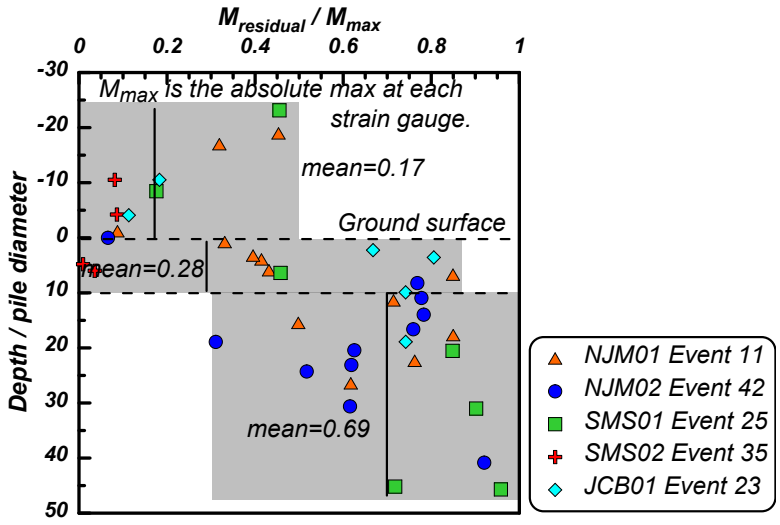

Figure 12. Ratio of residual bending moments (at the end of shaking)

REFERENCES

AASHTO (American Association of State Highway and Transportation Officials). 2014. *Guide Specifications for LRFD Seismic Bridge Design*. 2nd ed. with 2014 Interim. Washington, DC: AASHTO.

Abdoun, T., and R. Dobry. 2002. "Evaluation of pile foundation response to lateral spreading." *Soil Dyn. and Earthq. Eng.* 22: 1051–1058. https://doi.org/10.1016/S0267-7261(02)00130-6.

Abdoun, T., Dobry, R., O'Rouke, T. D., and S. H. Goh. 2003. "Pile response to lateral spreads: Centrifuge modelling." *J. Geotech. Geoenviron. Eng*. 129(10): 869–878.https://doi.org/10.1061/(ASCE)1090-0241(2003)129:10(869).

ASCE (American Society of Civil Engineers). 2014. *Seismic Design of Piers and Wharves,* ASCE/COPRI 61-14. ASCE Standards Committee on Seismic Design of Piers and Wharves. Reston, Va.: ASCE. https://doi.org/10.1061/9780784413487.

Brandenberg, S. J., Boulanger, R. W., Kutter, B. L., and D. Chang. 2005. "Behavior of pile foundations in laterally spreading ground during centrifuge tests." *J. Geotech. Geoenviron. Eng*. 131(11): 1378–1391. https://doi.org/10.1061/(ASCE)1090-0241(2005)131:11(1378).

Brandenberg, S. J., Boulanger, R. W., Kutter, B. L., and D. Chang. 2007. "Static pushover analyses of pile groups in liquefied and laterally spreading ground in centrifuge tests." *J. Geotech. Geoenviron. Eng.* 133 (9): 1055–1066. https://doi.org/10.1061/(ASCE)1090-0241(2007)133:9(1055).

Boland, C.B., Schlechter S. M., McCullough, N. J., Dickenson, S. E., Kutter, B. L. and D. W. Wilson. 2001a. *Pile-Supported Wharf — Centrifuge Model SMS02.*

Report No. GEG04-2000, Oregon State University/University of California at Davis.

Boland, C. B., Schlechter S. M., McCullough, N. J., Dickenson, S. E., Kutter, B. L. and D. W. Wilson. 2001b. *Pile-Supported Wharf — Centrifuge Model JCB01.* Report No. GEG05-2000, Oregon State University/University of California at Davis.

Boulanger, R. W., Chang, D., Brandenberg, S. J., Armstrong, R. J., and B. L. Kutter. 2007. "Seismic design of pile foundations for liquefaction effects." In *Proc. of 4th International Conference on Earthquake Geotechnical Engineering*, 277–302. Dordrecht, Germany: Springer. https://doi.org/10.1007/978-1-4020-5893-6_12.

Caltrans (California Department of Transportation). 2012. *Guidelines for Foundation Loading and Deformation Due to Liquefaction Induced Lateral Spreading*. Sacramento, CA: Caltrans.

Caltrans (California Department of Transportation). 2016. *Bridge Memo to Designer (MTD) 20-4: Seismic Retrofit Guidelines for Bridges in California*. Sacramento, CA: Caltrans.

Chang, D., Boulanger, R. W., Kutter, B. L., and S. J. Brandenberg. 2005. "Experimental observations of inertial and lateral spreading loads on pile groups during earthquakes." In *Earthquake Engineering and Soil Dynamics*, GSP 133, Boulanger, R., Dewoolker, M., Gucunski, N., Juang, C. H., Kalinsky, M., Kramer, S., Manzari, M., and J. Pauschke, eds., 1–15. Reston, Va.: ASCE. https://doi.org/10.1061/40779(158)17.

Cubrinovski, M., and K. Ishihara. 2006. "Assessment of pile group response to lateral spreading by single pile analysis." In *Seismic Performance and Simulation of Pile Foundations in Liquefied and Laterally Spreading Ground*, GSP 145, Boulanger, R., and K. Tokimatsu, eds., 242–254. Reston, Va.: ASCE. https://doi.org/10.1061/9780784408223.

Cubrinovski, M., Bray, J. D., de la Torre, C., Olsen, M. J., Bradley, B. A., Chiaro, G., Stocks, E. and L. Wotherspoon. 2017. "Liquefaction effects and associated damages observed at the Wellington Centreport from the 2016 Kaikoura earthquake." *Bull. N. Z. Soc. Earthq. Eng.*, 50 (2): 152–173.

Dobry, R., Abdoun, T., O'Rourke, T. D., and S. H. Goh. 2003. "Single piles in lateral spreads: Field bending moment evaluation." *J. Geotech. Geoenviron. Eng.* 129, 879–889. https://doi.org/10.1061/(ASCE)1090-0241(2003)129:10(879)

Egan, J. A., and Wang, Z. L. 1991. "Liquefaction-related ground deformation and effects on facilities at Treasure Island, San Francisco, during the 17 October 1989 Loma Prieta Earthquake." In Proceedings of the 3rd Japan–US workshop on earthquake resistant design of lifeline facilities and countermeasures for soil liquefaction. Technical Report NCEER-91–0001 (pp. 57-76).

Finn, W. D. L. 2005. “A study of piles during earthquakes: Issues of design and analysis.” *B. Earthq. Eng.*, 3(2), 141–234. https://doi.org/10.1007/s10518-005-1241-3

Hamada, M., Yasuda, S., Isoyama, R., and Emoto, K. 1986. ‘‘Study on liquefaction induced permanent ground displacements.’’ Research Rep., Association for Development of Earthquake Prediction, Japan, November, 87.

Khosravifar, A., Boulanger, R. W., and S. K. Kunnath. 2014. “Design of Extended Pile Shafts for the Effects of Liquefaction.” *Earthq. Spectra* 30 (4): 1775–1799. https://doi.org/10.1193/032512EQS107M

Martin, G. R., March, M. L., Anderson, D. G., Mayes, R. L., and M. S. Power. 2002. “Recommended design approach for liquefaction induced lateral spreads,” In *Proc. of 3rd National Seismic Conf. on Bridges and Highways*, MCEER-02-SP04, Buffalo, N.Y.: University at Buffalo.

McCullough, N. J., Dickenson, S. E., Kutter, B. L. and D. W. Wilson. 2000. *Pile-Supported Wharf — Centrifuge Model NJM01.* Report No. GEG01-2000, Oregon State University/ University of California at Davis.

McCullough, N. J., S. E. Dickenson, and S. M. Schlechter. 2001. “The seismic performance of piles in waterfront applications.” In *Ports Conference 2001*, 1–10. Reston, VA: ASCE. https://doi.org/10.1061/40555(2001)83

MCEER (Multidisciplinary Center for Earthquake Engineering Research). 2003. *Recommended LRFD Guidelines for the Seismic Design of Highway Bridges.* MCEER/ATC-49, Report No. MCEER-03-SP03. Buffalo, N.Y.: University at Buffalo.

Nasr, J., and A. Khosravifar. 2018. “The Effects of Long-Duration Subduction Earthquakes on Inelastic Behavior of Bridge Pile Foundations Subjected to Liquefaction-Induced Lateral Spreading.” In *Proc. Geotechnical Earthquake Engineering and Soil Dynamics V*, Geotechnical Special Publication 290, Brandenberg, S. J. and M. T. Manzari, eds., 617–625, Reston, VA: ASCE.

OCOT (Oregon Department of Transportation). 2014. *Geotechnical Design Manual.* Tech. Services Branch, Salem, OR

POA (Port of Anchorage). 2017. “Anchorage Port Modernization Project Seismic Design Manual”.

POLB (Port of Long Beach). 2015. “Port of Long Beach Wharf Design Criteria,” Version 4.0 (May). Long Beach, CA: POLB.

Rathje, E., Bachhuber, J., Cox, B., French, J., Green, R., Olson, S., Rix, G., Wells, D., and Suncar, O. 2010. “Geotechnical engineering reconnaissance of the 2010 Haiti earthquake.” GEER Association, Report No. GEER-021.

Schlechter, S. M., McCullough, N. J., Dickenson, S. E., Kutter, B. L., and D. W. Wilson, 2000a. *Pile-Supported Wharf — Centrifuge Model NJM02.* Report No. GEG02-2000, Oregon State University/University of California at Davis.

Schlechter S. M., McCullough, N. J., Dickenson, S. E., Kutter, B. L., and D.W. Wilson. 2000b. *Pile-Supported Wharf — Centrifuge Model SMS01.* Report No. GEG03-2000, Oregon State University/University of California at Davis.

Souri, M., Khosravifar, A., Schlechter, S., McCullough, N. and S. E. Dickenson. 2019. "Seismic Performance of Pile-Supported Piers and Wharves Subjected to Foundation Deformations." In *PORTS '19*. Reston, VA: ASCE. https://doi.org/10.1061/9780784482612.058

Souri, M., A. Khosravifar, S. E. Dickenson, S. Schlechter, and N. McCullough. 202X. "Pile-supported wharves subjected to inertial loads and lateral ground deformations: design recommendations." (companion paper)

Tokimatsu, K., 2003. "Behavior and design of pile foundations subjected to earthquakes." In *Proc. of 12th Asian Regional Conference on Soil Mechanics and Geotechnical Engineering*, 1065–1096. Klong Luang, Thailand: Association of Geotechnical Societies in Southeast Asia.

Tokimatsu, K., and Y. Asaka. 1998. "Effects of liquefaction-induced ground displacements on pile performance in the 1995 Hyogoken-Nambu earthquake." *Soils Found.* 38 (suppl.): 163–177. https://doi.org/10.3208/sandf.38.Special_163

Tokimatsu, K., Suzuki, H., and M. Sato. 2005. "Effects of inertial and kinematic interaction on seismic behavior of pile with embedded foundation." *Soil Dyn. Earthq. Eng.* 25 (7–10): 753–762. https://doi.org/10.1016/j.soildyn.2004.11.018

Turner, B. J., Brandenberg, S. J., and J. P. Stewart. 2016. "Case study of parallel bridges affected by liquefaction and lateral spreading." *J. Geotech. Geoenviron. Eng.* 142.7 (2016): 05016001. http://dx.doi.org/10.1061/(ASCE)GT.1943-5606.0001480

WSDOT (Washington Department of Transportation). 2015. *Geotechnical Design Manual.* M 46-03.11, May 2015.

Werner, S. D., Dickenson, S. E., and Taylor, C. E. (1997). "Seismic risk reduction at ports: Case studies and acceptable risk evaluation." Journal of waterway, port, coastal, and ocean engineering, 123(6), 337-346.

CHAPTER 5

5.0 PILE-SUPPORTED WHARVES SUBJECTED TO INERTIAL LOADS AND LATERAL GROUND DEFORMATIONS: DESIGN RECOMMENDATIONS

Note: The contents in this chapter have been submitted as a technical paper to ASCE Journal of Geotechnical and Geoenvironmental Engineering and is currently under review with the following citation:

Souri, M.; Khosravifar, A.; Dickenson, S. E.; Schlechter, S. & McCullough, N. “Pile-supported wharves subjected to inertial loads and lateral ground deformations: design recommendation.” ASCE Journal of Geotechnical and Geoenvironmental Engineering (under review)

5.1 INTRODUCTION

Pile-supported wharves are designed to accommodate superstructure inertial loads imposed at the pile head and kinematic loads imposed on the piles from the lateral ground deformations when subjected to earthquake motions. Lateral ground deformations may be caused by inertial slope movement, and/or by lateral spreading from liquefaction or cyclic softening of foundation soils in the slope or embankment adjacent to the structure and in the backland areas. Different design guidelines provide varying recommendations on how to combine superstructure inertial and kinematic ground deformation loads to estimate the lateral demands on piles. The design guidelines provided in commonly used codes are summarized in Table 1 and explained in more detail in the companion paper (Souri et al. 202X). The varying recommendations provided by highway and maritime transportation agencies highlight the site- and project-specific assumptions that are made to combine inertial and kinematic demands. It is recognized that there is limited research and validation of these assumptions, and

most design codes indicate that these assumptions should be evaluated on a project-specific basis.

This paper summarizes the development of an equivalent static analysis (ESA) procedure using p-y models for the design of pile-supported wharves subjected to lateral ground deformations during earthquake loading. The accuracy of the proposed ESA procedures in estimating pile demands is evaluated against the results of five centrifuge tests on pile-supported wharves. The piles in these centrifuge tests were subjected to the combined effects of wharf deck inertial loads and ground deformations. The experiments included soil properties ranging from nonliquefiable to fully liquefied cases which provided a wide range of conditions against which the ESA method could be evaluated. Additionally, these tests included the system-level response of the wharf deck and all rigidly-connected piles, as opposed to single piles, as had been used in most previous centrifuge tests. This is important because the restraining effects of the superstructure affect how inertial and kinematic loads interact, as reported by Turner et al. (2016). The following section of this paper provides an overview of the five centrifuge tests that were used in this study. The paper is then followed by two sections where peak inertial and peak kinematic demands are estimated and compared with centrifuge measurements. Next, load factors to combine peak inertial and peak kinematic loads are proposed. Concluding remarks are provided based on a comparison of the demands estimated from ESA to those measured in the centrifuge tests.

5.2 CENTRIFUGE TESTS

Details for the centrifuge tests can be found in a series of data reports in

McCullough et al. (2000), Schlechter et al. (2000a, b), and Boland et al. (2001a, b). The pile, superstructure, and soil properties and the applied input motions are provided in the companion paper (Souri et al. 202X). All tests included a wharf deck supported by 21 piles configured in a 7-by-3 setup. The piles consisted of aluminum pipe piles with outer diameters ranging from 0.38 m to 0.64 m (in prototype scale). The centrifuge scale factor was 40.1 for all tests.

Fig. 1 shows the cross sections of the five centrifuge models. The subsurface conditions in model NJM01 included a multi-lift rock dike, a loose sand layer that liquefied during shaking and resulted in lateral spreading, a dense sand layer above the water table, and a dense sand layer at the pile tips. A relatively soft Bay Mud layer was included in model NJM02, while a cement-deep-soil-mixing (CDSM) unit was incorporated into model SMS01. Model SMS02 featured a single, monolithic rock dike supported by a dense layer of sand. In model JCB01, the rock dikes were replaced with a thin layer of rock face. The failure surface, which was determined based on the soil displacement profiles interpreted from accelerometer data, is indicated in Fig. 1 by a red dashed line. In general, the observed zone of shear failure in the liquefied sand in the vicinity of piles can be characterized as broad, diffuse shear failure combined with a localized shear plane at the interface of weak and resistant layers (such as liquefied sand and upper rockfill). Localized shear planes were also developed above the Bay Mud layer in NJM02 and below the CDSM unit in SMS01, which contributed to the large pile bending moments that developed at depth in these two models. The overall objective of the current study was to develop guidelines for combining inertial and kinematic demands in

ESA and to evaluate its accuracy in estimating the large bending moments that were observed in the centrifuge tests.

5.3 ESTIMATING PEAK KINEMATIC DEMANDS

The kinematic demands on piles can be estimated using different methods with varying levels of complexity, including the simplified Newmark sliding block analysis (Newmark 1965) to a more detailed two- or three-dimensional dynamic analysis that incorporates soil–structure interaction. In the subsequent analysis, the soil displacements were computed using the Newmark method and were applied to the end nodes of p-y springs using beam on nonlinear Winkler foundation (BNWF) approach. One pertinent question is whether the permanent soil displacement (at the end of shaking) or the peak transient soil displacement (which occurs during shaking) should be used in design to evaluate the kinematic pile demands. ASCE 61-14 (Section 4.7.2) specifically requires that the permanent portion of the lateral ground deformations be used to estimate the kinematic demands on piles. However, it has been shown in Souri et al. (2019) that the peak transient bending moments at both the pile head and at depth are often greater than the residual bending moments at the end of shaking; this result was attributed, partly, to the difference between the peak transient soil displacement and the permanent soil displacement. The following section provides practical recommendations for design by comparing the estimated soil displacements against the measurements obtained from the centrifuge tests.

5.3.1 Estimating Soil Displacements at the Ground Surface

5.3.1.1 Estimation of Soil Displacements using the Newmark Sliding Block Method

Permanent ground displacements were estimated using the Newmark sliding block method (hereafter referred to as *Newmark analysis*). The yield accelerations for each test were determined by using pseudo-static limit equilibrium analysis and were assumed to be constant during the motion in the Newmark analysis. The beneficial resistance of the piles against the laterally moving ground (i.e., the pile pinning effects) were considered by including the piles as reinforcement elements in the limit equilibrium analysis. Thus, the soil displacements calculated here are pile-restrained displacements and not free-field displacements. The residual strength for liquefied soils in the limit equilibrium analysis was determined using correlations and were consistent with the weighted approach proposed by Kramer (2008). If liquefaction was not triggered, an equivalent friction angle was calculated proportional to the pore water pressure ratio using the relationship by Ebeling and Morrison (1992). Full details for these analyses are provided in McCullough et al. (2001). Newmark analyses are typically performed in practical applications using accelerations that are obtained from site response modeling; however, in this study, the recorded accelerations from centrifuge tests were used as input for the Newmark analysis. Thus, uncertainties in ground motion estimation associated with site response analysis are minimized.

5.3.1.2 Comparison between the Soil Displacements from Centrifuge Tests and Newmark Analysis

The accuracy of the Newmark method in estimating soil displacements was evaluated by comparing the results of the Newmark analysis to the measured displacements obtained from the centrifuge tests. Fig. 2 shows a comparison of median Newmark displacements for all accelerometers within the failure mass against the permanent displacement (end of shaking) and peak transient displacement measured at the ground surface in the centrifuge tests. The error bars show the Newmark median + 1σ and Newmark median − 1σ values. The Newmark displacements include the pile-pinning effects. The centrifuge displacements were calculated by combining data from the linear variable differential transformer (LVDT) with accelerometer data collected by sensors installed in the vicinity of the piles; therefore, the displacements shown in Fig. 2 can be considered pile-restrained. All displacements are adjusted to be relative to the base of the model. This figure suggests that the permanent (end of shaking) displacements from the centrifuge tests are better estimated using the median Newmark displacements. This figure also suggests that the peak transient displacements from the centrifuge tests are better estimated using the median + 1σ displacements from the Newmark analysis (as indicated by the top error bars). The measured peak transient displacements were found to be between 1.2 and 2.2 times larger than the permanent displacements in most cases (with an average of 1.8). Similarly, the median + 1σ displacements from Newmark were, on average, 1.8 times larger than the median Newmark displacements.

The difference between the permanent displacement and peak transient displacement should be considered in conjunction with the distribution of soil displacements with depth in the pseudo-static analysis. While Fig. 2 suggests that the median Newmark displacements underestimate the peak transient soil displacements, it will be shown that the distinct transitions in the idealized soil displacement profiles overestimate the predicted pile bending moments such that the combination of median Newmark displacements and an idealized soil displacement profile is sufficient to obtain a reasonable estimate of the peak pile bending moments.

5.3.2 Estimating Soil Displacements with Depth

5.3.2.1 Idealized Soil Displacement Profile with Depth

To estimate soil displacements with depth, Armstrong et al. (2014) proposed integrating the maximum shear strains in all soil layers to develop the soil displacement profile and then scaling it down to match the ground surface displacement estimated from the Newmark method. Applying this method to the five sets of centrifuge models resulted in approximately linear deformations with depth within the loose sand layer and negligible deformations in the rockfill and dense sand layers. Therefore, the idealized soil displacement profiles in this study were simply assumed to vary linearly with depth within the loose sand units and remain constant within the rockfill and the dense sands units. The idealized soil displacements profiles are referred to as “design” soil displacements hereafter.

5.3.2.2 Soil Displacement Profiles Obtained from Centrifuge Tests

To measure the accuracy of the developed design soil displacement profiles, it was necessary to develop soil displacement profiles from the results of the centrifuge tests. The horizontal soil displacements at a given depth below the ground surface were calculated by combining the high-frequency and low-frequency components of the displacements. The high-frequency soil displacements were calculated by double integration of the recorded accelerations from the embedded accelerometers and were filtered by applying a high-pass Butterworth filter. The low-frequency soil displacements at a given depth were calculated by applying a low-pass Butterworth filter to the recorded LVDT displacement at the ground surface and then distributing it with depth based on an assumed profile. This profile was developed using the shape of the maximum transient displacements with depth obtained from the accelerometer data as a guide. No permanent soil displacement was considered below the shear failure plane. The pattern of the permanent accumulated soil displacements with depth generally agreed with the measurements on the dissected model, which were collected after the tests were completed.

5.3.3 Comparison Between Centrifuge and Design Soil Displacement Profiles

A comparison of soil displacement profiles from centrifuge tests and design is shown in Fig. 3 for Event 11 of model NJM01. The soil displacements were interpreted at the pile locations to be applied to the end nodes of p-y springs. The

design soil displacements were estimated using the mean Newmark displacements, and the centrifuge soil displacements correspond to the peak transient displacement during motion (which occurred at time t = 21.6 sec). It can be observed from this figure that for Piles 1, 2 and 3 (where the kinematic effects are large), the peak transient soil displacements are underestimated by the mean Newmark displacements. While the design soil displacement profile follows the general trends observed in the centrifuge tests, it lacks the smooth curvature of the displacements from the centrifuge test.

The same trend for soil displacements interpreted from centrifuge tests and estimated in design for model NJM01 was consistently observed in other centrifuge tests. In the results for all five test sets shown in Fig. 4, the peak transient soil displacements from the centrifuge tests were generally underestimated when evaluated using the mean Newmark values, but we found that the distinct transitions in the design soil displacement profiles at layer boundaries above and below the loose sand layer over-predict the pile bending moments. These two effects have an approximately equal and opposite influence on the estimated bending moments, such that the combination of idealized soil displacement profiles and mean Newmark displacements is able to estimate the peak transient pile bending moments reasonably well (a comparison of bending moments is presented in a later section). The discrepancy between the curvature of the estimated and interpreted soil displacement profiles at layer boundaries was also reported in other studies involving centrifuge tests and numerical analyses (e.g., Brandenberg et al. 2007; McGann et al. 2011; Armstrong et al. 2014). Caltrans

(2012) recommends tapering the p-y spring properties over a transitional zone that extends one to two pile diameters from the interface between the liquefied and nonliquefied layers; this approach was adopted in this study.

5.3.4 Lateral Soil Reactions on Piles during the Critical Cycle

The lateral soil reactions back-calculated from the centrifuge tests showed that the nonliquefied rockfill does not apply a uniformly bayward pressure. Rather, the direction of the lateral soil reaction changes throughout the rockfill. The cross sections of two tests where the pile instrumentation was dense enough to accurately compute the soil reactions are shown in Fig. 5. The soil reactions were computed by fitting a spline curve to the bending moments and double differentiating it with depth (Souri et al. 2020). The profiles show the lateral soil reactions that occur at the time of maximum bending moments. In Piles 1 and 2 of NJM01 and in Piles 2 and 5 of SMS01, where a thick nonliquefiable crust (rockfill) was present, the top portion of the crust was resisting the inertial load, as indicated by positive (landward) soil reactions. The inertial force at the pile head was bayward. In these models, the effect of inertia was resisted by the resisting lateral soil pressure from the nonliquefied crust, and it did not contribute to the bending moments that developed at depth (~20 m below the pile head in NJM01 and ~22 m below the pile head in SMS01). It is important to note that in both tests the rockfill moved almost uniformly over the liquefied soils. This observation is further analyzed in Fig. 6 for Pile 1 in NJM01 Event 11, as an example. The soil and pile displacement profiles are plotted at the critical cycle (left figure) showing that the pile has moved more than the soil in the top half portion of the rockfill resulting in

a positive (landward) soil reaction (middle two figures). Conversely, the soil has moved more than the pile in the bottom half portion of the rockfill resulting in a negative (bayward) soil reaction. The inertial force at the pile head was bayward as indicated by the slope of the bending moments at the pile head (right figure). The two middle figures show the same data but at different scales. The ultimate soil reaction (p_u) calculated based on API is plotted as a reference to show that the soil reactions are significantly smaller than the full passive pressure. This is expected for relatively flexible piles used in this study as the piles follow soil deformations closely. This conclusion is likely to be different for relatively stiff piles such as large diameter shafts as the soil deformations could be much larger than the pile deformations to the extent that full passive pressure may develop throughout the nonliquefied crust. This finding is consistent with those in Boulanger et al. (2007), which showed that in relatively flexible piles, the nonliquefiable crust load can, in fact, apply a resisting upslope reaction while the inertia is downslope.

The observations made regarding models NJM01 and SMS01 suggest that it is overly conservative to estimate the kinematic demands by applying a bayward limiting pressure throughout the rockfill. Thus, for such piles, it is more appropriate to apply kinematic demands by imposing the estimated soil displacements to the end nodes of the p-y springs.

5.4 ESTIMATING THE PEAK INERTIAL DEMANDS

Equivalent non-linear static analysis (ESA) was used to estimate the peak inertial demands associated with the dynamic response of the deck mass. The ESA procedure included developing p-y models for a single row of piles,

developing a lateral force-displacement relationship (pushover curve) for the entire pile group, calculating the equivalent stiffness and natural period of the wharf, and estimating the peak inertial force using the acceleration response spectra at the ground surface. The ESA was performed for both liquefied and nonliquefied conditions. The estimated inertial demands were then compared against the measured demands from the centrifuge tests to evaluate the accuracy of the ESA procedures. It is worth noting that there are other important variables in performing ESA that were not evaluated in this study, such as the uncertainties associated with the p-y spring properties in the design as recommended by ASCE 61-14 (ASCE 2014), the effect of pile head fixity on the lateral stiffness of the pile group, and the uncertainties associated with site response analysis. Incorporating these uncertainties in design may introduce bias in estimating inertial demands that could affect how the inertial and kinematic demands are combined. This is a complex, project-specific issue, which warrants additional investigation of the sensitivity of the proposed load combinations to these uncertainties.

5.4.1 Properties for the Developed p-y Models

The p-y models were created in *LPILE* v. 2019 (Ensoft 2016) and were calibrated using four static lateral load pile tests that were performed for SMS02 and JCB01. These calibrations are provided in detail in Souri et al. (2020) and are not repeated here for brevity.

Soil Properties. The moduli of the subgrade reaction for sand were modified from the API recommendations to match the results of the four static lateral load tests. The rockfill was modeled by incorporating a pseudo-cohesion of 15 kPa to

account for additional resistance caused by the interlocking and movement of rock particles near the ground surface, thus simply modeled as a φ'-c' soil as applied in calibration studies from field load tests in rockfill (e.g. McCullough and Dickenson 2004; Dickenson et al. 2016). No modifications were made to the p-y springs in regard to the ground slope as the p-y models reasonably captured the pushover curves and pile demands from the four static lateral load tests as described in Souri et al. (2020).

Pile Properties. The wharf deck in the centrifuge tests was supported by three rows of seven piles (for a total of 21 piles) with diameters ranging from 0.38 m to 0.64 m. Considering the rigidity of the wharf deck, all piles were assumed to have zero rotation at the pile head. The piles remained elastic in the centrifuge tests and were modeled as elastic in the *LPILE* models. While the piles in the centrifuge tests were hollow aluminum pipes, their stiffness properties in prototype scale represented those of prestressed concrete piles.

P-multipliers. The p-y springs were modified using p-multipliers (P_m) proportional to the pore water pressure ratio R_u generated during the ground motion*:* $P_m = 1.2 - 1.1*Ru$ for $Ru > 0.2$ and $P_m = 1.0$ for $Ru \leq 0.2$, as the effect of liquefaction is assumed to be negligible when *Ru* is below 0.2. These practice-oriented relationships account for the first-order softening effect of liquefaction and generally agree with the nonlinear relationship proposed by Liu and Dobry (1995). For details on the development of the proposed R_u-proportional p-multipliers for liquefiable soils and their effectiveness in predicting peak pile demands, see Souri et al. (2020). In this study, the *Ru* values recorded in the vicinity of piles were used.

In practice, these values can be estimated from simplified correlations with the factor of safety against liquefaction.

5.4.2 Pile Group Force–Displacement Relationships

Force–displacement relationships (i.e., pushover curves) were developed for the entire pile group for each centrifuge test under the two conditions shown in Fig. 7. In the nonliquefied condition (Case A), regular p-y springs were used with no soil displacements. For the liquefied condition (Case B), soil displacements were imposed to the end nodes of the p-y springs, and the p-y curves for the liquefiable soils were softened using p-multipliers. The mean Newmark soil displacements were distributed with depth using an idealized profile, as this combination better predicted the peak bending moments in the centrifuge tests. The idealized soil displacements used in Case A analyses are the ones labeled as “Design” in Fig. 4. To develop pushover curves using *LPILE* models, displacements were imposed incrementally at the top of individual piles while maintaining zero rotation at the pile head to simulate the rigid connection between the piles and the wharf deck. The total shear force for the pile group was calculated by summing the pile head shear forces of all seven piles in one row multiplied by three rows in the transverse direction. No group reduction factor was considered based on AASHTO (2014), since the pile spacing was greater than six times the pile diameter. Some studies have shown that the sequence of applying inertial and kinematic demands can affect the estimated demands on piles (e.g. Chang 2007). However, this topic was not investigated in this study; thus, the full soil

displacement was applied in *LPILE,* and the pile head displacements were incrementally increased to reach 1 m.

The pushover curves are shown in Fig. 8 for all five sets of centrifuge test models. The pushover curves for the liquefied condition are different for each shaking because the soil displacements are different. For plotting purposes, the pushover curves in Fig. 8 are only shown for one event in each centrifuge test. The pushover curves for liquefied conditions exhibit a non-zero displacement at zero shear force due to the application of soil displacements. They also show a softer response as compared to pushover curves for the nonliquefied condition due to softened p-y springs in the liquefied soils and the application of soil displacements. The soil displacements had a more pronounced effect on the pushover curves for liquefied conditions in the cases analyzed in this study due to the fact that flexible piles follow the ground deformations more closely. The variations in p-multipliers had a minor effect on the pushover curves for liquefied conditions, likely because the majority of the piles (except for those in JCB01) were not embedded in liquefied soils.

The equivalent natural period of the soil–wharf system was computed for both conditions in each test using the initial stiffness of the pushover curves and the total wharf mass including the deck and the piles (the deck mass constitutes 74% of the total wharf mass). The effect of initial versus secant stiffness on the equivalent natural period was insignificant. Fig. 9 shows the equivalent natural period of the wharf calculated based on the pushover curves for liquefied and nonliquefied conditions. The wharf natural periods ranged from 0.5 sec to 1 sec in

the nonliquefied condition but were elongated to values between 0.8 sec and 1.1 sec in the liquefied condition (an average increase of 25%).

5.4.3 Estimate Peak Inertia using Equivalent Static Analysis

Equivalent static analyses (ESAs) were performed for liquefied and nonliquefied conditions in order to estimate peak superstructure inertial demands. The pushover curves (Cases A or B) were used to estimate the lateral stiffness and natural period of the wharf system. The acceleration response spectra (ARS) at the ground surface was then used to extract the spectral acceleration at the corresponding natural period of the wharf. The peak inertial load at the wharf deck was estimated by multiplying the spectral acceleration and the wharf mass.

The ESA for nonliquefied conditions included pushover curves (Case A in Fig. 8) combined with the ARS in the lower rock dike, which were representative of a nonliquefied site response. While there were no liquefied soils underlying the lower rock dike, the liquefaction of soils in the backland may have affected the recorded accelerations in the lower rock dike; however, this effect is believed to be minimal. The use of nonliquefied ARS is consistent with procedures proposed by Caltrans (2012), where the peak inertial loads are estimated in the absence of liquefaction and then reduced by 50% to account for the effects of liquefaction on site response and the asynchronous timing of peak inertial and peak kinematic demands.

The ESA for liquefied conditions included a pushover curve (Case B in Fig. 8) combined with an ARS in the backland representative of the accelerations in the liquefied ground. This approach is sometimes used in practice when the effects of

liquefaction is already included in the design spectra. It should be noted that the peak inertial demand estimated using this approach will only need to be multiplied by a potential reduction factor due to asynchronous timing of peak inertial and peak kinematic loads. There is considerable damping associated with soil-pile-fluid interaction that should be accounted for in estimating inertial demands. This complex behavior was approximated in the ESA analyses by developing the ARS for 14% damping ratio (as opposed to the typical 5% damping ratio). The equivalent damping ratio of 14% was calculated based on a dashpot coefficient of $c = 4*B*\rho*Vs$ proposed by Wang et al. (1998), where B is the pile diameter and ρ and Vs are the density and shear wave velocity in the rockfill. The damping ratio of 14% reasonably estimated the peak acceleration at the wharf deck as explained in the next section. For comparison, using 5% damping ratio overestimated the wharf accelerations by a factor of 1.5.

Fig. 10 shows how spectral accelerations were extracted using the ESA approaches described above, using the first event in NJM01 as an example. The natural period of the wharf changed slightly from 0.94 sec in nonliquefied conditions to 0.95 sec in liquefied conditions. The spectral accelerations were calculated from accelerations time histories recorded in the centrifuge test. A black line shows the spectra in the backland that are representative of liquefied conditions; three lines in different shades of blue show the spectra for three different accelerometers in the lower rock dike that are representative of nonliquefied conditions. The base spectra are also shown for comparison purposes. The nonliquefied spectra in the lower rock dike confirm that the lower

rock dike moves fairly rigidly and that the extracted spectral acceleration is not sensitive to the location of the selected accelerometer. The spectral acceleration at the natural period of the structure increased from 0.2 g in the nonliquefied condition to 0.24 g in the liquefied condition.

5.4.4 Comparison Between Peak Inertial Demands from Centrifuge Tests and ESA

The accuracy of the ESA methods in estimating inertial demands was evaluated by comparing the estimated peak deck acceleration and peak pile head shear forces with those measured in the centrifuge tests. Fig. 11 shows that ESA for both liquefied and nonliquefied conditions reasonably estimated peak deck accelerations (slightly overestimated by a factor of 1.1.)

The pile head shear in ESA was calculated by distributing the peak deck inertial force (i.e., spectral acceleration multiplied by the wharf mass) between individual piles in the pile group based on their relative lateral stiffness. The pile head shear forces in centrifuge tests were calculated using the measured bending moments from the top two strain gauges in each pile (for piles with two strain gauges located above the ground surface). Fig. 12 shows that the nonliquefied ESA underestimates the measured pile head shear forces by a factor of 0.9, and the liquefied ESA overestimates the measured pile head shear forces by a factor of 1.2. This indicates that the pile head shear forces were, on average, estimated reasonably well. This comparison confirms that no significant bias was introduced in estimating inertial demands that would affect the load combination factors that are proposed next.

Overall, Figs. 11 and 12 show no significant difference between the inertial forces at pile head estimated using ESA for liquefied or nonliquefied conditions. In the subsequent analyses, the liquefied ESA was used to evaluate the accuracy of design methods in estimating pile bending moments. However, it should be noted that performing the ESA for liquefied conditions requires estimation of soil displacement profiles, which includes significant uncertainty and could greatly affect the results for flexible piles. In addition, performing ESA for liquefied conditions requires estimating the response spectra in liquefied soils using effective-stress site response analysis, which also include significant uncertainty. Thus, it is sometimes desirable for design purposes to perform ESA for nonliquefied conditions and the results of this study show that the pile head inertial loads can be reasonably captured using ESA for nonliquefied conditions.

5.5 COMBINING PEAK INERTIAL AND PEAK KINEMATIC DEMANDS IN DESIGN

5.5.1 Proposed Load Combinations

As the peak inertial and peak kinematic demands do not always occur during the same cycle, Boulanger et al. (2007) recommends combining the peak kinematic demand with a fraction of the peak inertial demand, defined as parameter *Ccc*, which ranges from 0.65 to 0.85. The proposed values in Boulanger et al (2007) were developed primarily for bridge structures with a pile cap and an elevated superstructure. The *Ccc* parameters in this study were calculated for pile-supported wharf structures where the pile cap is rigidly fixed to the superstructure.

The back-calculated *Ccc* parameters from the centrifuge tests are described in detail in the companion paper (Souri et al. 202X). The data from this study suggests that *Ccc* decreases with depth, which can be attributed to the finding that the bending moments at the pile head are heavily influenced by, and correlated with, the deck inertia, resulting in *Ccc* values closer to 1. In contrast, the bending moments that develop at depth are less correlated with deck inertia as they are more influenced by kinematic demands and thus will have smaller *Ccc* values.

There is also a noticeable dependence between the *Ccc* values and different soil profiles, as discussed in the companion paper. The *Ccc* values calculated for the first three tests (NJM01, NJM02, and SMS01) range from 0.3 to 0.6, while the *Ccc* values calculated for the last two tests (JCB01 and SMS02) range from 0.9 to 1.0. In the first three tests, the kinematic demands are driven by a large overlying nonliquefiable rockfill. The time-dependent mobilization of slope deformation and corresponding application of kinematic loads on piles associated with this soil profile and configuration resulted in a lower likelihood for the peak kinematic loads to coincide with peak inertial loads. In contrast, the kinematic loads in the last two tests are relatively small and mobilized earlier in the motion. The kinematic loads in JCB01 were driven by a thin layer of rock face underlain by a loose sand layer that liquefied early in the motion and the soil profile in SMS02 did not include a liquefiable layer. The peak kinematic loads in the last two tests were more likely to coincide with peak inertia which resulted in larger *Ccc* values. The difference between the calculated *Ccc* values among different soil profiles

highlights the site-specific nature of inertial and kinematic interaction and the subsequent load combination factors.

For the sake of comparison of the tests performed in this study, a *Ccc* value of 85% was used based on the median + 1σ values among all five tests. This multiplier resulted in a better match between the average recorded and estimated bending moments in all five tests, as presented in the next section. However, it is acknowledged that lower combination factors may be used for soil profiles that resemble those in NJM01, NJM02 and SMS1. Table 2 shows the proposed load combinations for design. It will be shown in the next section that two uncoupled load combinations are adequate to estimate the bending moments that develop at the pile head (Case A) and at deep locations (Case C, where depth >10D). However, the bending moments at shallow depths (<10D) can only be accurately estimated when the two loads are combined (Case B). Therefore, the proposed inertial multiplier in Table 2 were selected primarily based on the *Ccc* values that were back-calculated for bending moments at shallow locations. Fig. 13 shows a schematic diagram of the proposed ESA load combinations in the p-y analysis. The proposed inertial multipliers in Table 2 are applicable when decoupled analysis is performed in ESA where peak inertial and peak kinematic demands are estimated separately. As suggested in POA (2017) more refined multipliers may be used if nonlinear dynamic analysis is adopted in design.

5.5.2 Comparison of Estimated and Measured Maximum Bending Moments

Equivalent static analyses were performed in *LPILE* using the three proposed load combinations listed in Table 2 and an inertial multiplier of 85% as

an average for all tests. The estimated bending moments from the ESA were compared to the measured bending moments in the centrifuge tests. Fig. 14 shows the measured and estimated bending moments for NJM01 Event 11, as an example. The bending moments were compared for key strain gauges where large moments were exhibited during the motion. The large measured bending moments are classified into three categories based on their location: bending moments that develop at the pile head (highlighted in blue in Fig. 14), bending moments that develop shallower than 10D (highlighted in red), and bending moments that develop deeper than 10D (highlighted in green). It was observed that the location of large recorded bending moments varied for different pile rows. In Piles #1, #2 and #3, large bending moments were recorded at the pile head as well as above and below the loose liquefiable layer. This was expected, as the failure shear plane passed through the liquefied layer, imposing significant curvature (and moment) in the piles. In Piles #4, #6, and #7, which did not pass through the loose liquefiable layer, large bending moments were recorded at the pile head and at shallow depths (depths <10D).

The estimated bending moments from ESA using the three proposed load combinations are also shown in Fig. 14. As an example, for Pile #1, it is observed that applying inertia only (indicated by a green line) accurately estimates the measured bending moment at the pile head, while applying kinematics only (indicated by a red line) accurately estimates the measured bending moment at depth. The effects of inertia attenuate within 5 to 6 m from the ground surface (approximately 8 to 10 pile diameters). Fig. 14 also shows that while the p-y

analysis may not always accurately capture the location of maximum moments, it is capable of capturing the magnitude of the maximum moment with reasonable accuracy (note the location of the estimated and measured deep bending moments in Pile #1). This analysis was performed for two main shaking events for each of the five tests, producing a total of 10 different experimental results that are used to evaluate the accuracy of the proposed load combinations in estimating the pile bending moments. Similar plots for the other tests are provided in the Supplemental Appendix.

Plots of the peak bending moments measured in the centrifuge tests and those estimated in the ESA are provided in Fig. 15 for all five tests and two shaking events for each test. In this figure, the dashed lines indicate the mean residual between the estimated and measured values providing a measure of accuracy for each ESA load combination. At the pile head, it can be seen that applying inertia only (Case A) adequately estimates the bending moments; while the combined case (Case B) slightly underestimates the bending moments, and applying kinematics only (Case C) grossly underestimates them (Fig. 15a). This is expected, as pile head bending moments are primarily affected by wharf inertia; thus, it is necessary to apply full inertial load to estimate the demands at this location. For shallow locations (depth <10D), a combination of the two loads (Case B) estimates the bending moments with reasonable accuracy, while applying inertia only (Case A) or kinematics only (Case C) significantly underestimate some of the bending moments and will be inadequate for design (Fig. 15b). For deep locations with depth >10D, it is clear that applying kinematics only (Case C) can

capture the bending moments with reasonable accuracy, while applying inertia only (Case A) will result in grossly underestimated bending moments, and the combination of inertia and kinematics (Case B) will not improve the accuracy (Fig. 15c). Note that the soil displacements in Case C are estimated using Newmark mean values, which were shown to reasonably estimate permanent soil displacements but underestimate the peak soil displacements (Fig. 2). However, this underestimation is compensated by the overestimation of pile curvatures using idealized soil displacement profiles with distinct transitions at layer boundaries.

5.6 CONCLUDING REMARKS

5.6.1 General Conclusions

The combination of inertial and kinematic demands in pile foundations subjected to liquefaction-induced lateral spreading was investigated using the experimental data from five centrifuge tests on pile-supported wharves in conjunction with equivalent static analysis using *LPILE*. The peak kinematic demands were estimated from the Newmark sliding block method using recorded accelerations time histories in centrifuge tests. The peak inertial demands were estimated using the natural period of the wharf–foundation system and the spectral acceleration at the ground surface. The analysis was performed for three loading cases: soil displacement only, peak inertia only, and soil displacement combined with 85% of peak inertia. The bending moments estimated from ESA were compared to the peak bending moments measured in the centrifuge tests. The comparison provided a systematic way to evaluate the accuracy of the proposed

load combinations in estimating bending moment demands and provided insights on the circumstances under which each load combination controls the pile design. The primary conclusions of the analyses are summarized as follows.

- Bending moments adjacent to the pile head can be reasonably estimated by applying the peak inertial load only, while bending moments at deep locations (>10D) can be reasonably estimated by applying the kinematic demands only.
- Bending moments at shallow locations (<10D) can be reasonably estimated by combining kinematic demands with a portion of peak deck inertial load. The portion of the peak inertia that was acting at the deck during the critical cycle (*Ccc*) ranged from 0.2 to 1.0, and appeared to be generally correlated with soil profile and the dynamic response of each soil unit.
- Median soil displacements calculated using the Newmark sliding block method are well correlated with permanent displacements from the centrifuge tests, but underestimate the peak transient displacements. Newmark median + 1σ values are better correlated with the peak transient displacements from the centrifuge tests.
- There is considerable uncertainty in predicting the pattern of soil displacement with depth, and this significantly affects the estimated bending moments in the equivalent static analysis of flexible piles. The distribution of soil displacements in multi-layered soils based on the expected maximum shear strain in each layer resulted in idealized soil displacement profiles with distinct transitions. The overestimation of bending moments due to distinct transitions in idealized soil displacement profiles, when combined with the underestimation of peak

transient soil displacements using the Newmark mean values, resulted in a reasonably accurate estimation of the maximum bending moments below grade.

- The peak deck accelerations and the peak shear forces at pile head were reasonably estimated by ESA methods using pushover analyses for both liquefied and nonliquefied conditions.
- The analyses in this study suggest that higher damping ratios (i.e. 14%) may be required in estimating deck accelerations to approximate the complex soil-structure-fluid interactions.

5.6.2 Recommendations for Practice

- It is recommended that the median displacements computed using Newmark-type analysis be applied in combination with an idealized soil displacement profile with distinct transitions.
- The modeling completed in this investigation supports the use of damping ratios significantly greater than the 5% routinely used in practice as the basis for defining the spectral acceleration at the fundamental period of vibration of the wharf structure. This appears to reflect the combined influence of radiation damping, nonlinear soil behavior and inelastic pile performance consistent with the cyclically-induced permanent deformations. Given the range of tolerable and anticipated displacements defined in port standards and codes for design-level ground motions, a damping ratio of approximately 10% to 15% appears to more suitably represent aspects of wharf – pile foundation – soil behavior.

Project-specific estimates of the structural damping deemed representative of the response of the wharf structure, and therefore the inertial loading, should be made in conjunction with structural analysis.

- The five tests were subdivided into two general categories: Profile B1 is characterized as configurations that include deep-seated liquefaction underlying significant nonliquefiable crust (i.e. rockfill), Profile B2 is characterized as configurations that include generally smaller kinematic demands associated with either nonliquefiable profiles or weak/softened soils closer to the ground surface, and thin nonliquefiable crust (i.e. sliver rockfill). Inertial multipliers (*Ccc*) of 0.3 to 0.6 are recommended as an initial baseline for soil profiles that resemble Profile B1 and *Ccc* values of 0.9 to 1.0 are recommended for soil profiles that resemble Profile B2.
- The wide range of *Ccc* values observed in this research highlights the benefit of performing coupled nonlinear dynamic analysis that capture complex soil-pile-structure interaction for varying soil profiles.
- The load combination factors proposed here are appropriate for decoupled analysis using the p-y spring approach and are not necessarily appropriate for use with the simplified equivalent fluid pressure for lateral spreading load.

These conclusions are applicable only for relatively flexible piles with small diameters (up to about 0.7 m). The interaction of inertial and kinematic loads could be different for pile shafts with larger diameters. Incorporating uncertainties in design (e.g. uncertainties associated with estimating ground motions) may introduce bias in estimating inertial demands that could affect how the inertial and

kinematic demands are combined. The sensitivity of the proposed load combinations to these uncertainties is an important issue that needs to be evaluated in future studies.

Table 1. Design guidelines on combination of inertial and kinematic demands on piles

Design Code	Recommendation
ASCE 61-14 (2014) Section C4.7 and Port of Long Beach Wharf Design Criteria (POLB 2015)	Locations of maximum bending moment from inertial and lateral ground deformation are spaced far enough apart that the two loads do not need to be superimposed. Maximum bending moments occur at different times. The two loads should be treated uncoupled for marginal wharves.
Port of Anchorage Modernization Program Seismic Design Manual (POA 2017)	Combine peak inertial loading from earthquake ground motion with 100% peak kinematic demands from lateral ground displacements. Smaller factors are allowed if peer-reviewed 2-D nonlinear numerical analysis is used (no less than 25%).
AASHTO (2014)	Design the piles for the simultaneous effects of inertial and lateral spreading loads only for large magnitude earthquakes (M>8).
MCEER/ATC (2003)	For most earthquakes, peak inertia is likely to occur early in the ground motion. Design piles for independent effects of inertia and lateral spreading. For large magnitude and long-duration earthquakes the two loads may interact.
PEER (2011)	100% kinematic + (65% to 85%) inertial (multiplied by 0.35 to 1.4 to account for the effects of liquefaction on peak inertial load)
Caltrans (2012) and ODOT (2014)	100% kinematic + 50% inertial
WSDOT (2015)	100% kinematic + 25% inertial

Table 2. Proposed load combinations for design of piles subjected to combined inertial load and kinematic load from lateral ground deformations

(Case) Load combination	Portion of permanent soil displacements applied at end nodes of p-y springs[1]	Portion of peak deck inertial force applied at deck[2]	Applicability
(A) Inertia only	NA	100%	Adequate to estimate bending moments at pile head.
(B1) Combined kinematic and inertial demands-Profile B1[3]	100%	0.3 to 0.6[5]	Suitable to estimate bending moments below grade down to depth of 10D.
(B2) Combined kinematic and inertial demands-Profile B2[4]	100%	0.9 to 1.0[5]	Suitable to estimate bending moments below grade down to depth of 10D.
(C) Kinematic only	100%	NA	Adequate to estimate pile bending moments deeper than 10D.

1. Soil displacement profiles in this study were estimated using the mean Newmark values and distributed with depth using an idealized profile based on estimated shear strains in each soil unit following Armstrong et al. (2014).
2. Peak deck inertial forces were estimated in this study using ESA performed for liquefied conditions. If ESA is performed for nonliquefied conditions, an additional multiplier may be needed (*Cliq* per Boulanger et al. 2007) to account for the effects of liquefaction on the wharf peak inertial demands.
3. Profile B1 is defined as configurations that include deep-seated liquefaction underlying significant nonliquefiable crust (i.e. rockfill).
4. Profile B2 is defined as configurations that include generally smaller kinematic demands/loads associated with either nonliquefiable profile or weak/softened soils closer to the ground surface, and thin nonliquefiable crust (i.e. sliver rockfill).
5. These ranges provide an initial baseline for preliminary analysis subject to refinement on a project-specific basis. The load combination factors proposed here are appropriate for decoupled analysis using the p-y spring approach and are not necessarily appropriate for use with the simplified equivalent fluid pressure for lateral spreading load.

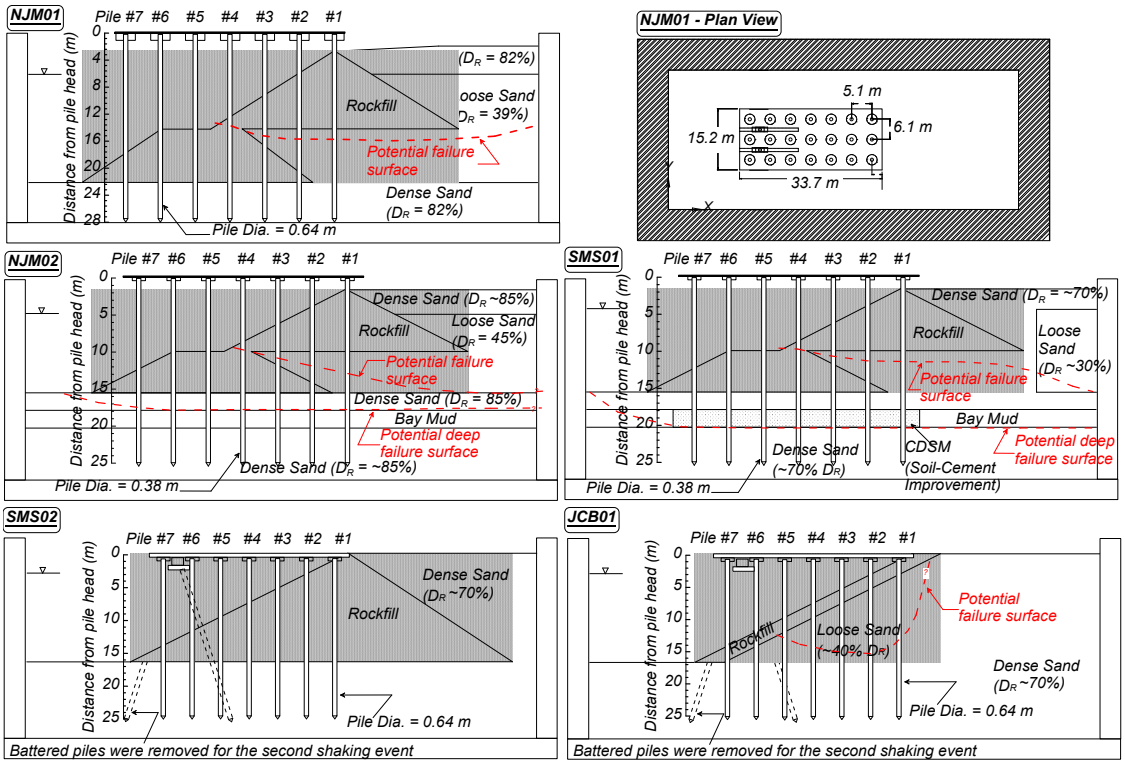

Figure 1. Cross sections and plan view of five centrifuge tests on pile-supported wharves.

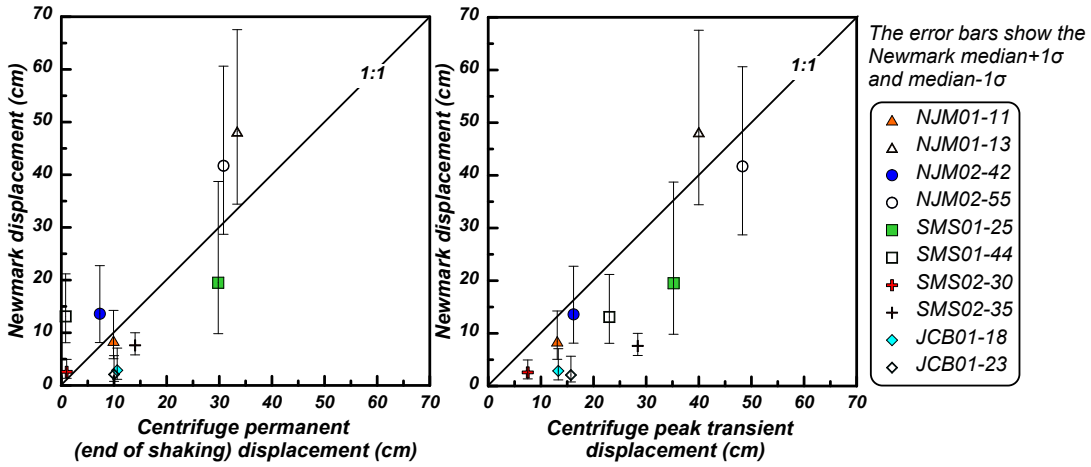

Figure 2. Comparison of estimated and measured ground surface soil displacements.

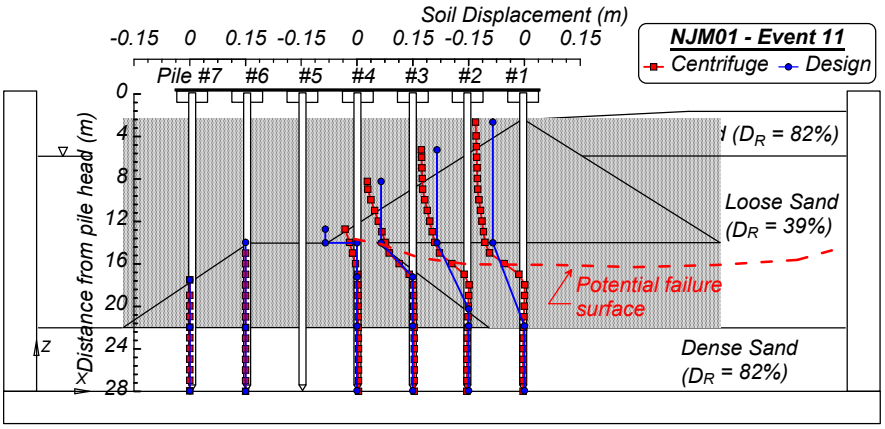

Figure 3. Comparison of soil displacements at pile locations estimated in design (mean Newmark) and interpreted from centrifuge test results (peak transient) for NJM01 Event 11.

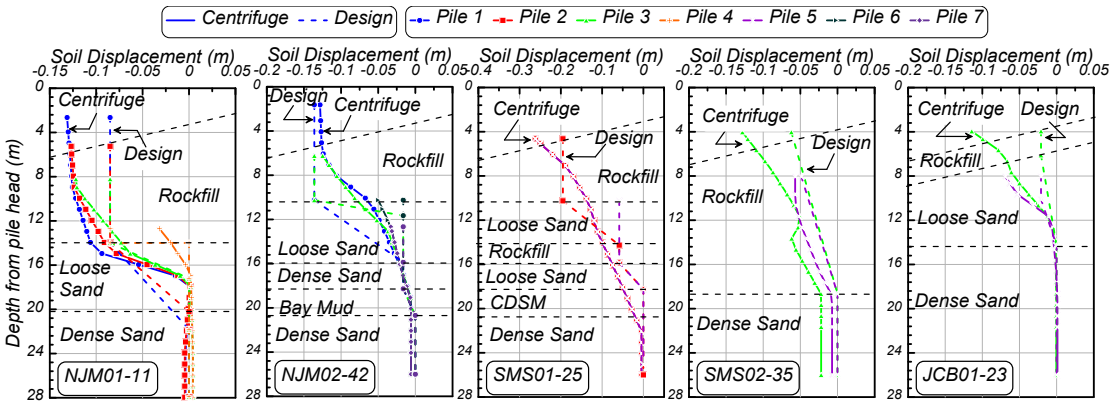

Figure 4. Comparison of soil displacement profiles at the pile locations interpreted from centrifuge tests (peak transient) and estimated in design (mean Newmark).

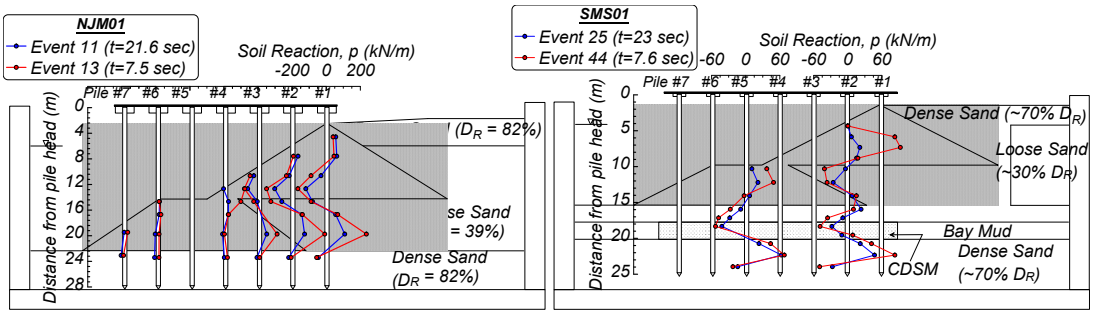

Figure 5. Soil reaction profiles at the time of maximum bending moment in NJM01 and SMS01.

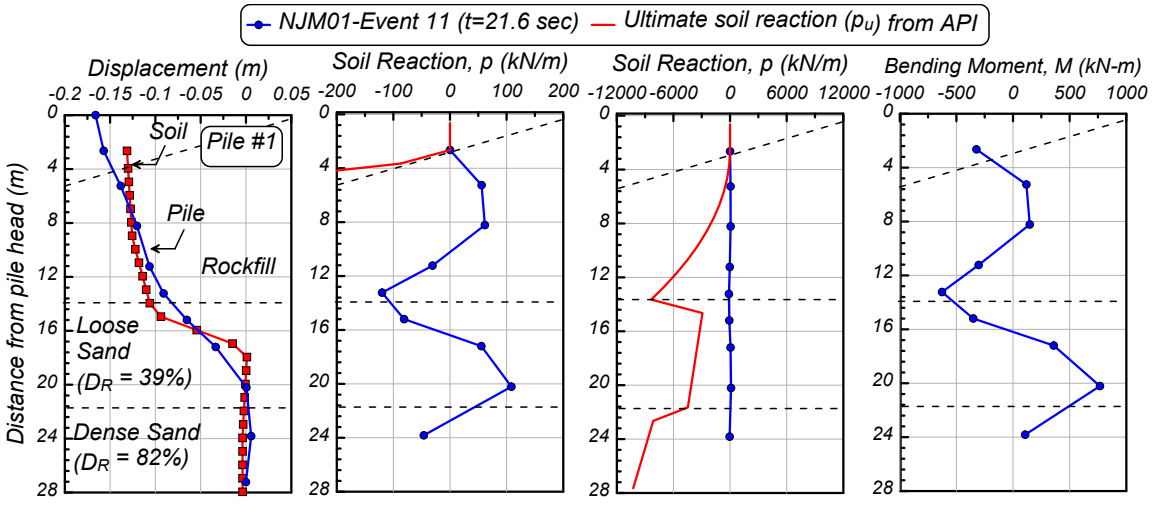

Figure 6. Displacement, soil reaction, and bending moment profiles at the time of maximum bending moment for Pile 1 in NJM01 Event 11.

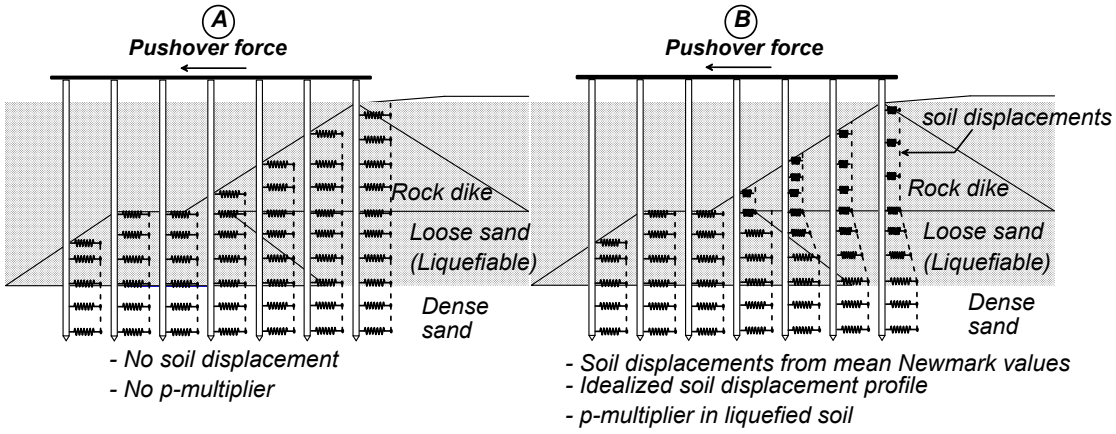

Figure 7. Schematic of (a) nonliquefied and (b) liquefied pushover analyses.

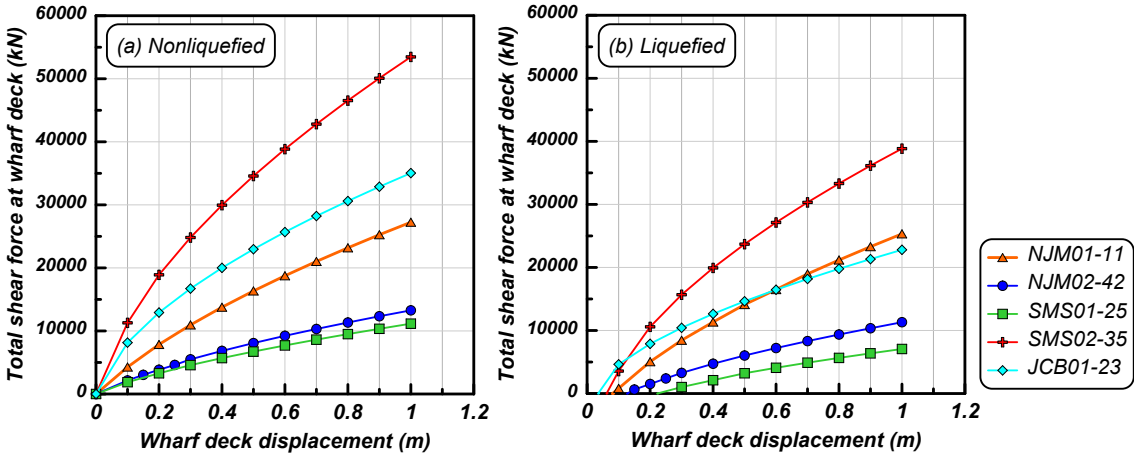

Figure 8. Pile group force–displacement relationships (pushover curves) for nonliquefied and liquefied conditions.

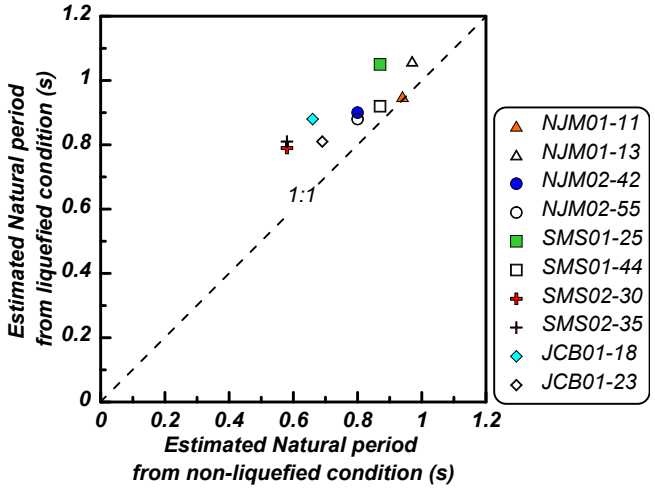

Figure 9. Comparison of estimated natural period in liquefied condition against nonliquefied condition from pushover analyses.

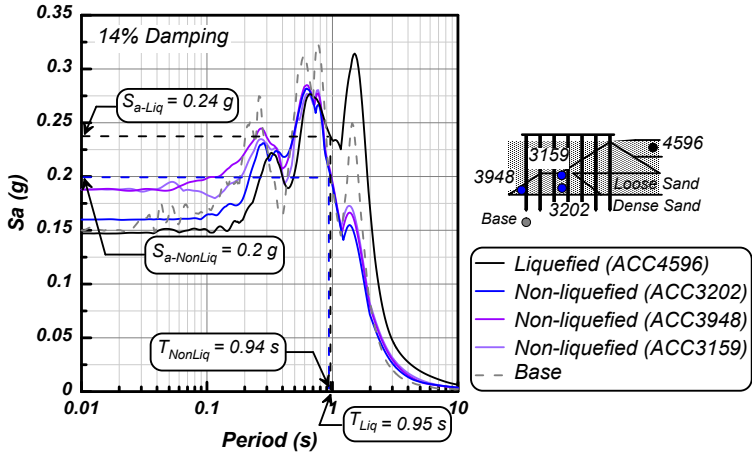

Figure 10. Spectral accelerations for liquefied and nonliquefied conditions for NJM01 Event 11.

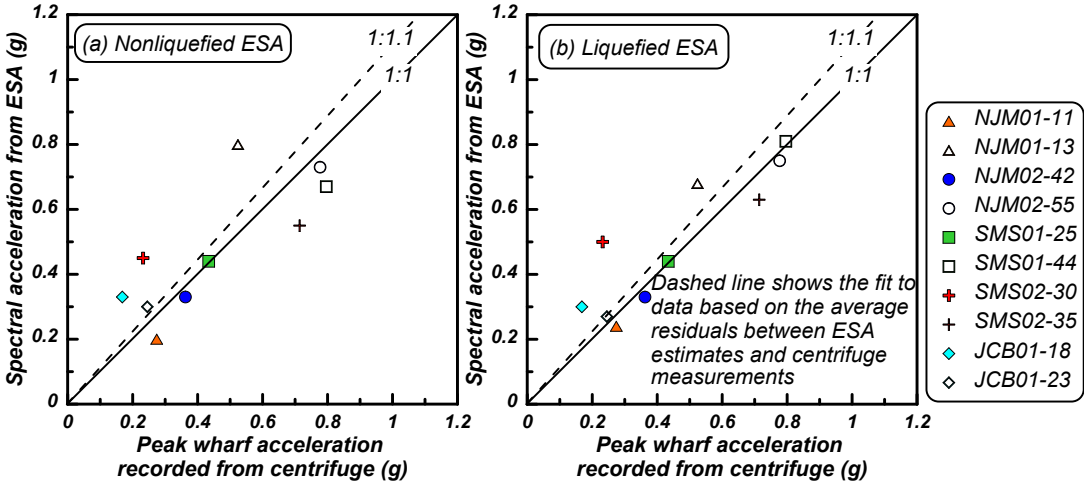

Figure 11. Comparison of estimated spectral acceleration from design method to peak wharf acceleration measured in the centrifuge tests.

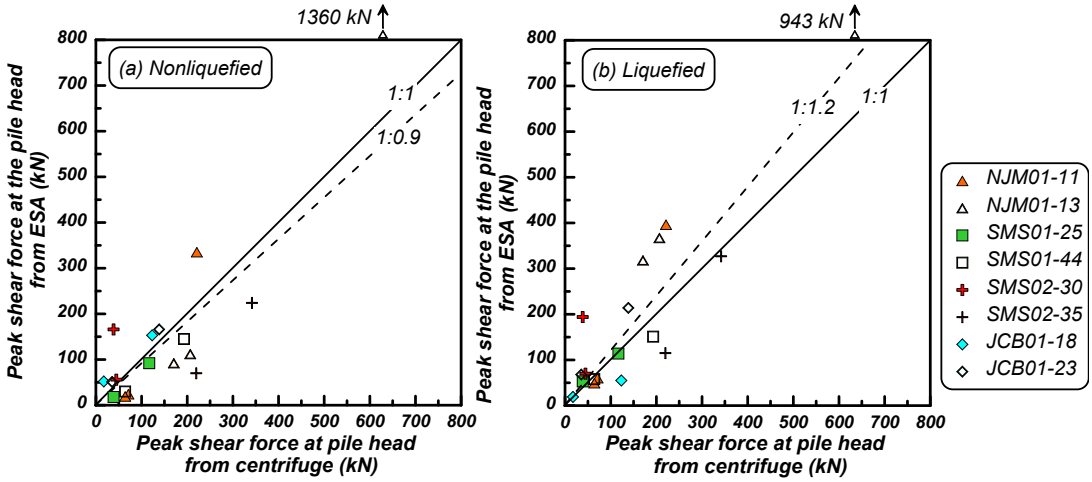

Figure 12. Comparison of estimated shear force from pushover analysis to the peak shear force at the pile head calculated from the centrifuge test results.

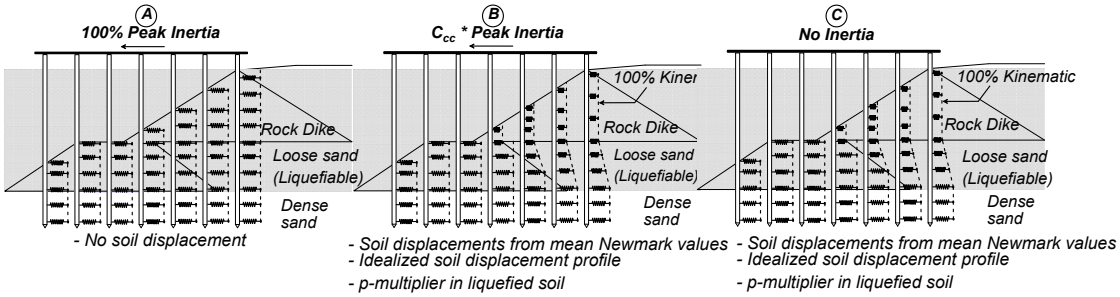

Figure 13. Schematic of proposed ESA load combinations for piles subjected to ground deformations: (a) inertia only, (b) combined inertia and kinematic, and (c) kinematic only.

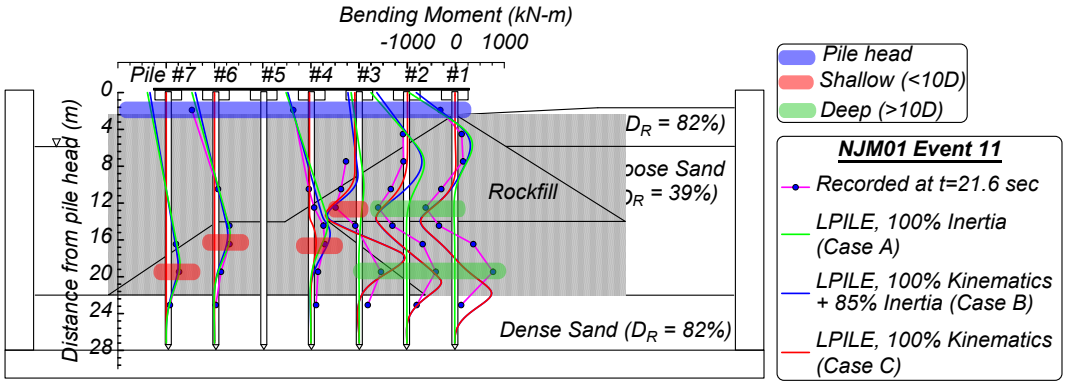

Figure 14. Comparison of measured and estimated bending moments for NJM01

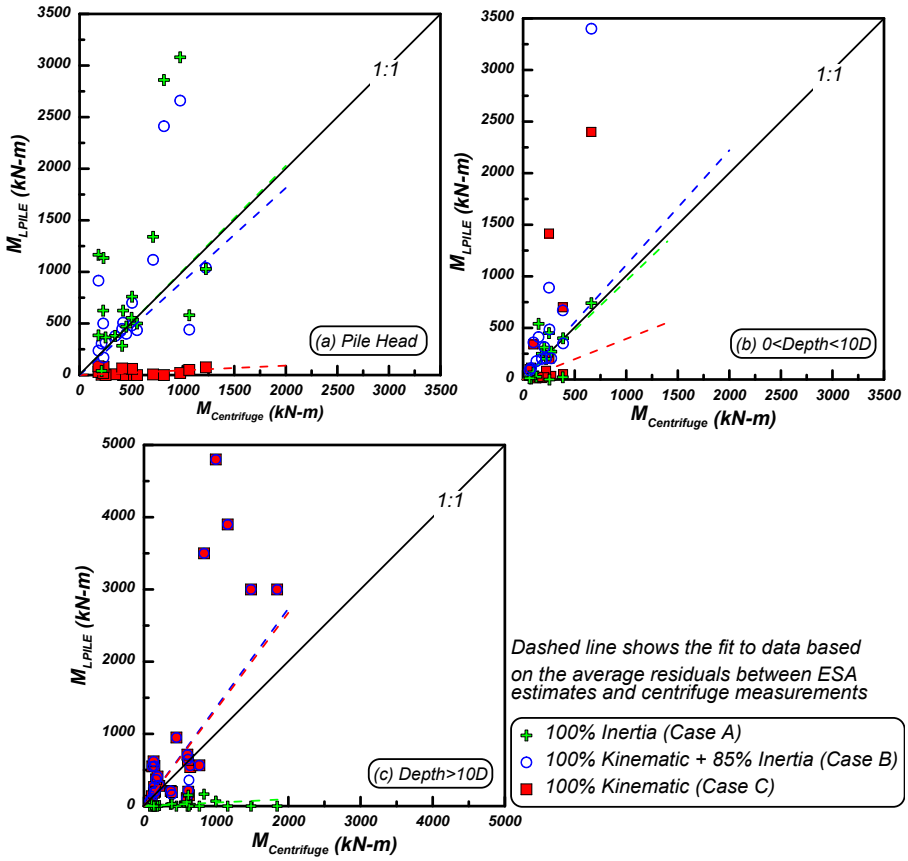

Figure 15. Peak bending moments measured in centrifuge tests and estimated from ESA analyses in LPILE at (a) the pile head, (b) locations shallower than 10D, and (c) locations deeper than 10D.

REFERENCES

AASHTO (American Association of State Highway and Transportation Officials). 2014. *Guide Specifications for LRFD Seismic Bridge Design*. 2nd ed. with 2014 Interim. Washington, DC: AASHTO.

Armstrong, R. J., R. W. Boulanger, and M. H. Beaty. 2014. "Equivalent static analysis of piled bridge abutments affected by earthquake-induced liquefaction." *J. Geotech. Geoenviron. Eng.* 140 (8): 04014046. https://doi.org/10.1061/(ASCE)GT.1943-5606.0001152

ASCE (American Society of Civil Engineers). 2014. *Seismic Design of Piers and Wharves*. *ASCE/COPRI 61-14.* Reston, VA: ASCE Standards Committee on Seismic Design of Piers and Wharves. https://doi.org/10.1061/9780784413487

Brandenberg, S. J., R. W. Boulanger, B. L. Kutter, and D. Chang. 2007. "Static pushover analyses of pile groups in liquefied and laterally spreading ground in centrifuge tests." *J. Geotech. and Geoenviron. Eng.* 133 (9): 1055–1066. https://doi.org/10.1061/(ASCE)1090-0241(2007)133:9(1055)

Boland, C. B., S. M. Schlechter, N. J. McCullough, S. E. Dickenson, B. L. Kutter, and D. W. Wilson. 2001a. *Pile-Supported Wharf — Centrifuge Model SMS02. Report No. GEG04-2000.* Oregon State University/University of California at Davis.

Boland, C.B., S. M. Schlechter, N. J. McCullough, S. E. Dickenson, B. L. Kutter, and D.W. Wilson. 2001b. *Pile-Supported Wharf — Centrifuge Model JCB01. Report No. GEG05-2000*. Oregon State University/University of California at Davis.

Boulanger, R. W., D. Chang, S. J. Brandenberg, R. J. Armstrong, and B. L. Kutter. 2007. "Seismic design of pile foundations for liquefaction effects." In *Proc. of 4th International Conf. on Earthq. Geotech. Eng.*, 277–302. Dordrect, Germany: Springer. https://doi.org/10.1007/978-1-4020-5893-6_12

Caltrans (California Department of Transportation). 2012. *Guidelines for Foundation Loading and Deformation Due to Liquefaction Induced Lateral Spreading*. Sacramento, CA: Caltrans.

Chang, D., 2007. "Seismic Performance of Pile-Supported-Structures in Liquefied and Laterally Spreading Ground*." Ph.D. Thesis,* University of California, Davis

Dickenson, S., Yang, S., Schwarm, D., & Rees, M. 2016. "Design Considerations for the Kinematic Loading of Piles." In *Proc. Ports 2016 Conference* (pp. 213-222).

Ebeling, R. M., and E. E. Morrison, Jr. 1992. *The Seismic Design of Waterfront Retaining Structures. Tech. Rep. No. ITL-92-11*. Port Hueueme, CA: U.S. Naval Civil Engineering Lab.

Kramer, S.L. 2008. “Evaluation of Liquefaction Hazards in Washington State.” Washington State Department of Transportation (WSDOT), WA-RD 668.1.

Liu, L., and R. Dobry. 1995. “Effect of liquefaction on lateral response of piles by centrifuge model tests.” *NCEER Bulletin* 91: 7–11.

LPILE. 2016. “LPILE: A program for the analysis of piles and drilled shafts under lateral loads.” Version 2016.9.10 [computer program]. Austin, Texas: Ensoft Inc.

McCullough, N.J., S.E. Dickenson, B. L. Kutter, and D.W. Wilson. 2000. *Pile-Supported Wharf — Centrifuge Model NJM01. Report No. GEG01-2000*. Oregon State University/University of California at Davis.

McCullough, N., and S. Dickenson. 2004. “The Behavior of Piles in Sloping Rock Fill at Marginal Wharves.” In *Proc. Ports Conference 2004*, Reston, VA: ASCE. https://doi.org/10.1061/40727(2004)86

McCullough, N. J., S. E. Dickenson, and S. M. Schlechter. 2001. “The seismic performance of piles in waterfront applications.” In *Ports Conference 2001*, 1–10. Reston, VA: ASCE. https://doi.org/10.1061/40555(2001)83

MCEER (Multidisciplinary Center for Earthquake Engineering Research). 2003. *Recommended LRFD Guidelines for the Seismic Design of Highway Bridges.* MCEER/ATC-49, Report No. MCEER-03-SP03. Buffalo, N.Y.: University at Buffalo.

McGann, R., P. Arduino, and P. Mackenzie-Helnwein. 2011. “Applicability of conventional p–y relations to the analysis of piles in laterally spreading soil.” *J. Geotech. Geoenviron. Eng.* 137 (6): 557–567. https://doi.org/10.1061/(ASCE)GT.1943-5606.0000468

Newmark, N.M. 1965. “Effects of Earthquakes on Dams and Embankments.” *Geotechnique* 15 (2): 139–160. https://doi.org/10.1680/geot.1965.15.2.139

ODOT (Oregon Department of Transportation). 2014. *Geotechnical Design Manual*. Salem, OR: ODOT Technical Services Branch.

POLB (Port of Long Beach). 2015. “Port of Long Beach Wharf Design Criteria,” Version 4.0 (May). Long Beach, CA: POLB.

POA (Port of Anchorage) 2017. “Anchorage Port Modernization Project Seismic Design Manual”.

Schlechter, S. M., N. J. McCullough, S. E. Dickenson, B. L. Kutter, and D. W. Wilson. 2000a. *Pile-Supported Wharf — Centrifuge Model NJM02. Report No. GEG02-2000*. Oregon State University/University of California at Davis.

Schlechter, S. M., N. J. McCullough, S. E. Dickenson, B. L. Kutter, and D. W. Wilson. 2000b. *Pile-Supported Wharf — Centrifuge Model SMS01*. *Report No. GEG03-2000*. Oregon State University/University of California at Davis.

Souri, M., A. Khosravifar, S. Schlechter, N. McCullough, and S. E. Dickenson. 2019. “Seismic Performance of Pile-Supported Piers and Wharves Subjected

to Foundation Deformations" In *PORTS '19*. Reston, VA: ASCE. https://doi.org/10.1061/9780784482612.058

Souri, M., A. Khosravifar, S. Schlechter, N. McCullough, and S. E. Dickenson. 2020. "Development of experimental p-y curves from centrifuge tests for piles subjected to static loading and liquefaction-induced lateral spreading." *DFI Journal*, 14(1): 1-15.

Souri, M., A. Khosravifar, S. E. Dickenson, S. Schlechter, and N. McCullough. 202X. "Pile-supported wharves subjected to inertial loads and lateral ground deformations: observations from centrifuge tests." (companion paper)

Turner, B. J., Brandenberg, S. J., and J. P. Stewart. 2016. "Case study of parallel bridges affected by liquefaction and lateral spreading." *J. Geotech. Geoenviron. Eng.* 142.7 (2016): 05016001.

Wang, S., Kutter, B. L., Chacko, J., Wilson, D. W., Boulanger, R. W., and Abghari, A. 1998. "Nonlinear seismic soil-pile-structure interaction." Earthquake Spectra, Earthquake Engineering Research Institute, 14(2), 377-396.

WSDOT (Washington State Department of Transportation). 2015. *Geotechnical Design Manual. M 46-03.11.* Olympia, WA: WSDOT.

CHAPTER 6

6.0 DEVELOPMENT OF EXPERIMENTAL P-Y CURVES FROM CENTRIFUGE TESTS FOR PILES SUBJECTED TO STATIC LOADING AND LIQUEFACTION-INDUCED LATERAL SPREADING

Note: The contents in this chapter have been published in the DFI Journal with the following citation:

Souri, M., Khosravifar, A., Schlechter, S., McCullough, N. & Dickenson, S. E. (2020). “Development of Experimental P-Y Curves from Centrifuge Tests for Piles Subjected to Static Loading and Liquefaction-Induced Lateral Spreading,” Journal of Deep Foundations Institute, 14 (1), 1-15.

6.1 INTRODUCTION

Liquefaction-induced ground deformations can cause severe damage to pile-supported wharves and other waterfront structures. A common approach in analyzing the lateral behavior of piles against seismic loads is using the beam on nonlinear Winkler foundation (BNWF) simulation or p-y spring analysis. One common p-y relationship for sand is the one proposed by the American Petroleum Institute, also known as the API sand model (API 1993). While the API sand model was originally developed for static loading conditions, it is common to modify the API sand curves to account for the effects of cyclic loading. A number of studies have shown that complex pile behavior under dynamic loading conditions is not captured by the API curves. Observations from a series of dynamic centrifuge tests reported by Wilson (1998) indicate that peak values of soil reaction for the experimentally derived p-y curves were significantly greater than those recommended by the API p-y curve at depths that are less than approximately

three times the pile diameter. Yang et al. (2011) performed a series of shaking table tests on dry and saturated dense sand deposits and found that the API p-y curve underpredicts the ultimate soil resistance (smaller than one third of experimental p-y curves) at shallow depths. Yoo et al. (2013) carried out a centrifuge test for a single pile in dry sand under sine wave loading and found that pseudo-static analysis using the API curve overestimated the maximum bending moment and pile displacements as compared to those measured from the centrifuge test. They also found that the subgrade reaction modulus at shallow depths could be overestimated by the API sand curve within an elastic pile displacement of 1% of the pile diameter. On the other hand, when the displacement of the pile was greater than 1% of the pile diameter, which may occur during earthquake loading, the API sand relation significantly underestimated the ultimate soil reaction at shallow depths.

Existing p-y curves have been widely used in pseudo-static analysis to predict the response of pile foundations in liquefied soils. However, there is no consensus on how to modify the static p-y curves to account for the effects of liquefaction and pore water pressure generation in loose granular soils. In previous studies, the p-y springs of piles in liquefying soils were back-calculated from case histories, centrifuge model studies (e.g., Wilson et al. 2000; Brandenberg et al. 2005; Abdoun et al. 2003), full-scale tests (e.g., Rollins et al. 2005; Chang and Hutchinson 2013), and numerical analyses (e.g., McGann et al. 2011).

One approach to account for the effect of partial/full liquefaction on the p-y curve is to apply a p-multiplier to degrade the ultimate soil resistance of liquefied

soil. Liu and Dobry (1995) investigated the effect of excess pore water pressure on the p-y curve in partially/fully liquefied sands by performing a series of centrifuge tests, and they defined a dimensionless degradation parameter, C_u, that changes more or less linearly with the excess pore water pressure ratio R_u to degrade the p-y curves. Wilson (1998) performed a series of dynamic centrifuge tests in complement with pseudo-static analyses of pile-supported structures. They concluded that the p-multiplier strongly correlated to initial relative density (D_R) of the soil. They found that a range of 0.1–0.2 for relatively loose sand (D_R = 35%) and about 0.25–0.35 for medium dense sand (D_R = 55%) would be reasonable to predict the measured pile demands. Tokimatsu (1999) evaluated the field performance of pile foundations subjected to lateral ground spreading during the 1995 Kobe earthquake. They compared the pseudo-static analysis results to values in well-documented case histories and concluded that *p*-multipliers ranging from 0.05 to 0.2 are reasonable for predicting the observed pile performance in liquefied soils in the field.

Another approach proposed in other studies uses an upward concave shape for p-y curves in liquefied soils (e.g., Rollins et al. 2005; Franke and Rollins 2013; Chang and Hutchinson 2013). Rollins et al. (2005) performed full-scale tests on a large drilled shaft using blast-induced liquefaction, and they proposed an upward concave shape for the p-y curve to capture the dilative behavior of liquefied soils during shearing. Reasonably good agreement was demonstrated between measured and predicted pile response by implementing the proposed p-y curve in the lateral pile analysis. Franke and Rollins (2013) developed a simplified hybrid

p-y model by incorporating aspects of the p-y curve of Rollins et al. (2005) and the p-y curve for liquefied soils proposed by Wang and Reese (1998); they evaluated the applicability of the proposed hybrid model against various published case histories and observed a reasonable computed response for piles in liquefied soils under both kinematic and inertial loadings. Chang and Hutchinson (2013) conducted sequential loading on a single-pile specimen in a saturated sand deposit and observed an inverted S-shaped p-y curve from the back-calculated experimental data even at low levels of pore water pressure ratios (R_u > 10–15%).

The studies mentioned above provide varying and sometimes contradicting recommendations on how to modify the static p-y curves to capture the complex behavior of soil during the liquefaction process, which highlights the need for further investigation. The focus of this study is to evaluate the effectiveness of the p-multiplier approach in modifying p-y springs in partially/fully liquefied soils to predict the lateral response of piles. This was done by using the results of five centrifuge tests that simulate pile-supported wharves in sloping ground (McCullough et al., 2001). The p-y curves were back-calculated in loose sands, dense sands and sloping rockfill dikes. The p-y curves were back-calculated for both piles subjected to cyclic static push/pull forces at the pile head as well as for piles subjected to dynamic transient earthquake shaking. The static p-y curves were approximated using the API relationships for sands, and the input parameters for the API curves were back-calculated. The dynamic p-y curves were compared against the static p-y curves to provide insight on the applicability of the *p*-multiplier approach in developing p-y curves for liquefied zones. What differentiates this

study from previous studies on piles in liquefied soils is that the piles in these centrifuge tests were subjected to both kinematic loads from laterally spreading soils as well as inertial loads from the superstructure mass. Therefore, the back-calculated p-y curves in liquefied zones represent a more realistic loading condition for pile-supported structures. To evaluate the effectiveness of using *p*-multipliers in the API sand curves, the piles from the centrifuge tests were modeled in *LPILE* (version 2016.9.10; Ensoft, Inc.), and the predicted maximum bending moments in each pile were compared against the values measured in the centrifuge tests. It will be shown that the maximum bending demands in piles were reasonably captured using *p*-multipliers that are proportional to the pore water pressure ratio in partially/fully liquefied zones.

6.2 DESCRIPTION OF CENTRIFUGE TESTS

6.2.1 Centrifuge models and cross sections

Data from a series of five centrifuge tests were analyzed to back-calculate pile lateral behavior (i.e., the p-y springs) for static and dynamic loading conditions. These tests were performed on pile-supported wharves by Dickenson, McCullough, Schlechter, and coworkers at the UC Davis Center for Geotechnical Modeling (McCullough et al. 2001). These centrifuge models represent the typical layout of major port facilities in California, and the findings can be used to represent other similar pile-supported wharves embedded in rock dikes over native soils and potentially liquefiable artificial fill soils. The cross sections of all models and key soil properties are shown in Figure 1. Uniform fine Nevada was used in all five

centrifuge experiments. The sand had a specific gravity of (Gs) 2.67, mean grain size (D_{50}) of 0.15 mm, coefficient of uniformity (Cu) of 1.6, minimum dry unit weight of 13.98 kN/m^3, and maximum dry unit weight of 16.76 kN/m^3. The parameters discussed in this paper are all in prototype scale unless noted otherwise.

6.2.2 Dynamically loaded piles

The wharf deck in these tests was supported by three rows of seven piles (for a total of 21 piles). The pile diameters ranged from 0.38 m to 0.68 m. Each centrifuge model was subjected to a sequence of scaled input motions with the peak base acceleration values ranging from 0.15 g to 0.82 g. The pile group was subjected to the combined effects of inertial and liquefaction-induced kinematic demands during earthquake shaking (these piles are referred to as *dynamic piles*).

6.2.3 Static cyclically loaded piles

Two of the five tests (SMS02 and JCB01) included two single piles that were statically pushed by two to seven cycles of loads using actuators attached to their pile heads (these piles are referred to as *static piles*). The static loads, which were applied prior to earthquake shaking, provided key data for the comparison of p-y springs under static and dynamic loading conditions. In these two tests, the static pile at the back of the wharf was placed in dense sand with no slope; the static pile at the front of the wharf was placed in sloping rockfill in SMS02 and in a sloping rock face overlying loose sand in JCB01. The layout for the static piles is shown in Figure 1. The structural properties of the static piles were the same as those for the dynamic piles.

6.2.4 Sensors and instruments

Measurements for all centrifuge tests conducted in this study were obtained using a suite of sensors and instrumentation. Linear volt displacement transducers (LVDT) mounted on the wharf deck, ground surface and the shear box container were used to measure the horizontal and vertical displacements. Pore pressure transducers (PPT) were embedded within the soil model at various depths to measure pore fluid pressures. Accelerometers were embedded within the soil model and attached to the wharf deck and the shear box to measure horizontal ground shaking accelerations. Strain gauges were attached to static and dynamic piles to back-calculate pile bending moments.

6.3 PROCEDURES TO BACK-CALCULATE P-Y CURVES

6.3.1 Lateral soil reactions

Bending moments were back-calculated at discrete locations along the pile where strain gauges were attached. The bending moments were interpolated along the pile length using a cubic spline fitting method before being numerically double-differentiated to back-calculate the lateral soil reactions, p (Haiderali and Madabhushi 2016; Brandenberg et al. 2010). For the piles where the bending moment at the pile head was not measured, the bending moments were extrapolated assuming a constant shear force above the ground surface. The bending moments and shear forces at the pile tips were assumed to be zero.

6.3.2 Horizontal pile displacements

The horizontal pile displacements were estimated by double-integrating the bending moments along the pile and dividing by the pile flexural stiffness (*EI*). The rotations at the pile head were assumed to be zero as the piles were rigidly connected to a relatively rigid wharf deck. The displacement at the pile head was set to be equal to the measured displacement from the LVDT at the wharf deck and the pile tip was allowed to have a non-zero rotation.

6.3.3 Horizontal soil displacements

Total horizontal soil displacements were calculated by combining the transient (high-frequency) and permanent (low-frequency) components of displacement following the methods described by Wilson et al. (2000). Transient soil displacements were calculated by double-integrating the recorded accelerations. A high-pass Butterworth filter was applied to remove the low-frequency motions from the recorded accelerations. The permanent soil displacements were calculated based on the displacements recorded using LVDTs at the ground surface after applying a low-pass Butterworth filter. The pattern of distributing the permanent component of the soil displacement with depth was a major source of uncertainty in our analyses. The estimated pile bending moments in our consecutive pseudo-static analyses were also found to be very sensitive to the assumptions made regarding the pattern of permanent soil displacements with depth, which warranted investigating this issue methodically. After considering various patterns of permanent soil displacement with depth and investigating their

effects on the estimated bending moments, we used the normalized shape of the maximum transient soil displacements with depth as a guide to determine where the subsurface shear failure zones formed as well as to distribute the permanent component of the soil displacement from the ground surface down to the shear failure plane. No permanent soil displacement was considered below the shear failure plane.

6.3.4 Back-calculated p-y curves

Lateral pile behavior is commonly characterized using p-y curves at various depths along the pile. The *p* in these relationships corresponds to the lateral soil reaction, and the *y* corresponds to the relative displacement between the soil and pile (i.e. *y* = horizontal pile displacement – horizontal soil displacement). As described earlier, there is some uncertainty in estimating the horizontal soil displacements and pile displacements for dynamic piles. Therefore, the dynamic p-y curves were used primarily for estimating ultimate lateral soil reaction, and the relative soil–pile displacement (*y*) was only used qualitatively.

6.4 EXPERIMENTAL P-Y CURVES FROM STATIC PILES

Experimental p-y curves were extracted from the results of statically loaded piles in SMS02 (penetrating dense sand and rockfill) and JCB01 (penetrating dense sand, loose sand and a thin rockfill) prior to shaking. Given that these soil and rockfill units are made from granular materials, the back-calculated p-y curves were approximated using API sand relationships. It was assumed that the behavior of rockfill can be modeled as a granular material; therefore, an API sand with a

friction angle was used for rockfill with the properties that are tabulated in Table 1. The API sand model recommends a hyperbolic tangent function to characterize the ultimate soil reaction (p_{ult}) and initial stiffness (k_T). In the API sand model, the ultimate lateral reaction (p_{ult}) increases with depth, pile diameter and internal friction angle. Internal friction angles of 33°, 37° and 45° were used to develop API curves for loose sand (D_R = 30%), dense sand (D_R = 70% to 80%) and rockfill, respectively. It will be discussed later that the API sand models are modified with reduced stiffness for all soil units and a pseudo-cohesion for rockfill to better approximate the p-y curves calculated from the centrifuge tests.

As an example, a comparison between the experimental p-y curve and the API relationship for loose sand is shown in Figure 2a for the front pile in JCB01 at a depth of 3.05 m, which is approximately five times the pile diameter (D). This static pile was subjected to seven cycles of static loading. Different loading cycles are plotted with different colors on this figure to help understand how p and y evolve in the experimental p-y curve. As can be noticed from this figure, the API sand curve using a friction angle of 33° captures the ultimate resistance of the experimental p-y curve reasonably well. The comparison is not that favorable at other depths; however, it will be shown later that the overall pile demands are reasonably captured using the API sand curves. Figure 2b shows the 6th cycle of the same experimental p-y curve compared to the same API curve used in Figure 2a, which has been manually shifted to the left for plotting purposes. This figure clearly shows that the API sand curve captures the overall shape of the experimental p-y curve. It will be discussed later how the stiffness of the API sand

curves was reduced to better match the experimental results. Similar comparisons were performed for other soil units and at various depths, and these results will be presented next.

Figure 3 presents a comparison between the back-calculated experimental static p-y curves and the API relationships for the back pile and front pile in SMS02 and JCB01 at depths of ~ 1*D*, 3*D*, 5*D* and 7*D*. Comparing the values for ultimate resistance in the API curves with those of the back-calculated p-y curves show that at a depth of ~ 1*D*, the API relationships underestimate the ultimate resistance of the p-y curve. This observation is consistent with the experimental results reported by Wilson (1998) for depths that are less than approximately three times the pile diameter. The comparison is relatively reasonable at depths of 3*D* to 5*D*. However, at depths of 5D to 7*D*, the ultimate resistance values in the experimental curves were not fully mobilized due to small pile deflections.

6.4.1 Modifications to API sand p-y curves

The initial stiffness in the API sand curve (k_T) is the product of the depth below the ground surface and the modulus of the subgrade reaction (k). The initial stiffness in loose sand, dense sand and rockfill were back-calculated from the experimental static p-y curves. The back-calculated initial stiffness values are plotted versus depth in Figure 4. Each data point in this plot represents the initial stiffness calculated from an experimental p-y curve shown in Figure 3. No clear slope effect was observed for the initial stiffness of the p-y curves in the landward and bayward directions for the two front piles in SMS02 and JCB01 located along the face of the rockfill slopes. Therefore, the initial stiffness values plotted in Figure 4 are

calculated based on the average values in the landward and bayward directions. These initial stiffness values were then divided by the corresponding depth to obtain the modulus of subgrade reaction (*k*) for different soil units. The initial stiffness values recommended by API for loose sand, dense sand and rockfill are also plotted in this figure for comparison. It can be observed that the initial stiffness values calculated from experimental p-y curves were smaller than the values recommended by API. This reduction might be attributed to the aging effects between the soils in field and freshly deposited sands in the centrifuge. It could also be due to the uncertainties in back-calculating the initial stiffness at shallower depths where small variations in the modeling parameters (i.e. friction angle and/or pseudo cohesion for rockfill) may have a large impact. Despite the differences between the back-calculated moduli of subgrade reaction from centrifuge tests and those recommended by API, the results of centrifuge tests are applicable in evaluating the effects of liquefaction on p-y behavior since the comparisons are made between the static and dynamic p-y curves that are driven from the same centrifuge tests.

In order to account for additional resistance caused by the interlocking and movement of rock particles near the ground surface, a pseudo-cohesion value of 15 kPa was applied to rockfill as suggested by McCullough and Dickenson (2004). This pseudo-cohesion was incorporated in our analysis by using the cemented c-phi p-y curves implemented in *LPILE*. In the current implementation of the cemented c-phi curves in *LPILE* (version 2016.9.10; Ensoft, Inc.), the difference between API sand and c-phi curves are not significant when the initial stiffness is

reduced as evidenced from the p-y curves plotted for rockfill in Figure 3. Table 1 lists the input parameters for p-y curves to approximate the experimental p-y curves from static piles. No significant difference was observed in the back-calculated subgrade reaction moduli between loose and dense sands; therefore, the same modulus is recommended for simplicity.

6.4.2 Validation using lateral pile response

The effectiveness of the API sand curves in predicting the lateral pile response is investigated by comparing the pile demands measured from static piles in the centrifuge tests to those computed using p-y models in *LPILE*. The shear load and bending moment at the pile head were back-calculated directly from the centrifuge tests and applied as pile head loading conditions in *LPILE*. The p-y curves were developed for loose sand, dense sand, and rockfill based on the input parameters reported in Table 1.

Figure 5 presents the comparison of lateral pile responses measured in the centrifuge and computed using *LPILE* for the front static pile in JCB01, which is selected for comparison purposes because it penetrates through all three soil units and is located on a slope. The *LPILE* results are shown for a case using the original API sand curves and a case with the modifications discussed earlier (i.e., reduced stiffness in all soil layers and a pseudo cohesion of 15 kPa in rockfill). While both models capture the maximum bending moment reasonably well, the model with reduced stiffness better captures the bending moment profile with depth as well as the maximum shear, soil reaction and pile displacement. Similar comparisons were made for the back pile in JCB01 and the back and front piles in SMS02. Figure 6

shows the bending moment comparisons between measured and estimated values using *LPILE* for all four static piles in both tests. The results shown in this figure confirm that the modifications made to API input parameters improve the predictions of the bending moment profiles, although it does not change the magnitude of the maximum moment along the pile.

Figure 7 shows the comparison of measured and predicted pile head load–displacement response in both the back and front piles in SMS02 and JCB01. As shown in this figure, the predicted pile head responses are in good agreement with the responses back-calculated from the centrifuge tests (the secant stiffness in the models with *LPILE* with modification is up to 15% softer than the original *LPILE* results (e.g. JCB01, static back pile, bayward direction.) It is observed that the two *LPILE* models (with and without modifications) do not vary significantly in predicting the pile head response for the static piles.. However, it will be shown later that using these modifications significantly improves the prediction of the bending moments for dynamic piles.

6.5 EXPERIMENTAL P-Y CURVES FROM DYNAMIC PILES

Experimental p-y curves were also derived from centrifuge tests for piles supporting the wharf deck. These piles were subjected to wharf inertia during shaking, combined with varying magnitudes of ground deformation induced by partial/full liquefaction and slope instability. These dynamic p-y curves were then compared to the static p-y curves to investigate the effects of excess pore water pressure in liquefiable soils on the lateral response of piles and p-y curves.

Figure 8 presents a comparison of static versus dynamic p-y curves for loose sand (D_R = 40%). The static p-y curve shown in this figure was derived from the front static pile in JCB01 (the same curve shown in Figure 2). The dynamic p-y curve was derived from Pile #3 in JCB01 during the first earthquake motion. Both static and dynamic p-y curves are extracted at the same depth (3.05 m below the ground surface) and normalized by the same pile diameter (0.64 m). Overlapped on Figure 8 are two API sand curves that approximate the p-y responses under static and dynamic conditions. The API sand curve for the static condition is developed using the input parameters in Table 1. The API sand curve for the liquefied condition was developed by modifying the static API curve using a *p*-multiplier (P_m) to approximately envelop the dynamic experimental p-y curve. The p-multiplier was adjusted until it was visually a best fit to the measured response, and in this case was calculated as 0.21. The p-multiplier approach accounts for the first-order effects of liquefaction on p-y behavior.

The experimental dynamic p-y behavior is complex and is affected by contraction and dilation of loose sand, the inertial demand from the superstructure during earthquake loading, as well as factors such as strain rate, stress condition, and ground slope. The last three cycles of loading for the experimental dynamic p-y curve presented in the previous figure are plotted in Figure 9a using different colors to help understand the effect of the transient dilation of liquefied sand on the p-y response. The relative movement shown in Figure 9 is all in the bayward direction. The corresponding time windows for cycles A, B and C are shown with colored areas in the time histories in Figures 9b and 9c corresponding to the same

colors shown earlier in Figure 9a for each cycle. These time histories illustrate the lateral soil resistance (p), relative lateral displacement between soil and pile (y), and excess pore water pressure ratio (R_u) in the loose sand. It can be observed that as the excess pore water pressure ratio builds up in the loose sand in sloping ground, lateral spreading occurs that exerts lateral loads on the pile. It is also observed that the lateral soil reaction (p) in liquefied soil exhibits sudden spikes in the bayward direction as shown by the dashed lines. Careful examination of the spikes in p reveals that they follow transient drops in R_u implying that they might be attributed to the dilative response of sand combined with an increase in the relative displacement between the soil and pile driven by the inertial demand from the wharf deck. However, the magnitude of the spikes in p are not very large (they are approximately 20% of P_{ult} of the static p-y curve), suggesting that a simple p-multiplier approach could be an effective choice for modifying the static p-y curve to represent the complex behavior of dynamic p-y curve in liquefied soil.

To further investigate the softening effect of liquefaction on the dynamic p-y curves, similar comparisons were made between the back-calculated static and dynamic p-y curves in loose sand as plotted in Figure 10. This figure includes static and dynamic p-y curves at depths of 5D and 7D below ground surface for Pile #3 and Pile #5 in JCB01 for two shaking events and at depth of 11D below ground surface for Pile #3 in NJM02 for one shaking event. These depths are selected because the loose sand layer was shallow enough that a direct comparison between static and dynamic p-y curves was possible. The p-multipliers were calculated as the ratio of the ultimate soil reaction in the dynamic curve to the

ultimate soil reaction of the static p-y curve. For p-y curves at shallow depths (5*D*), p_{ult} is accurately captured by the API sand curve. However, for p-y curves at deeper locations (7*D*), the p_{ult} of the experimental static p-y curve is smaller than the p_{ult} of the API sand curve. This could be because the p_{ult} of the experimental static p-y curve is not yet mobilized at the displacements observed in the static tests at greater depths. Therefore, for these cases, the *p*-multipliers are divided by the p_{ult} from the API sand curve instead of the maximum soil reaction in the experimental static p-y curve.

Other researchers have shown that P_m values are correlated to the pore water pressure ratio (R_u) generated during shaking (e.g., Liu and Dobry 1995; Wilson et al. 2000; Brandenberg 2005; Chang and Hutchinson 2013). Figure 11 shows the back-calculated *p*-multipliers versus R_u during dynamic shaking. The R_u value was calculated using the pore pressure value from the transducer that was closest to the locations where the p-y curves were extracted. In practice, the pore water pressure can be estimated using advanced methods such as effective-stress dynamic analysis or simplified approaches where the excess pore water pressure ratio is correlated with the factor of safety against liquefaction (e.g. Marcuson at al. 1990). Also plotted in this figure are the data suggested by Liu and Dobry (1995) as presented in FHWA (2011). The data points for R_u greater than 0.8 generally follow the data by Liu and Dobry. However, the three data points with R_u between 0.4 to 0.6 exhibited *p*-multipliers that were approximately 0.15, which is much lower than those suggested by Liu and Dobry. These three cases correspond to the p-y curve shown for NJM02 and the two p-y curves from Event 18 for Pile 3 in JCB01.

We hypothesize that close proximity to the highly permeable rockfill layers might have contributed in recording low R_u in these three cases. Additionally, there is more uncertainty in the outlier data point for NJM02 because the p_{ult} of the experimental dynamic p-y curve may not have fully mobilized and there is significant amount of uncertainty in soil displacements as the shear failure plane passes through this location. More work is needed to explain the outlier cases observed in this study. The red line in this figure shows a polynomial fit to the data from Liu and Dobry (1995) combined with data from this study excluding the three outlier data points mentioned earlier. While the trend shows a nonlinear behavior, for simplicity, the *p*-multipliers in this study were calculated using $P_m = 1.2 – 1.1*R_u$ for $R_u > 0.2$ and $P_m = 1.0$ for $R_u \leq 0.2$ as indicated by a dashed line in Figure 11. When R_u is equal to 1.0, the *p*-multiplier is calculated as 0.1 and when R_u is lower than 0.2 the effect of liquefaction is assumed to be negligible and the *p*-multiplier is calculated as 1.0. The R_u threshold of 0.2 corresponds approximately to a factor of safety against liquefaction (FS_{liq}) of 1.4 based on the laboratory test data on granular material by Marcuson at al. (1990). This linear fit was found to be a practice-oriented simplification and the effectiveness of this approach in estimating the pile demands is investigated next.

6.6 VALIDATION AGAINST PILE DEMANDS

The effectiveness of the back-calculated input parameters for the API sand curves and the R_u-proportional *p*-multipliers in liquefiable soils in predicting the lateral response of dynamic piles is investigated by comparing the pile bending moment

profiles measured in the centrifuge tests to those estimated using p-y models in *LPILE*. The *LPILE* models consider combined kinematic and inertial effects, in which the soil displacements were imposed to the end nodes of the p-y springs and wharf inertia was imposed by a shear force at the pile head. The kinematic demands (i.e., soil displacements) and inertial demands (i.e., pile head shear) were directly calculated from the centrifuge tests at the exact time when the bending moments are at their peak values. The p-y curves were developed for each soil unit based on the API relationships with the input parameters listed in Table 1. The p-y curves were then softened using *p*-multipliers correlated to the R_u value using the linear equation described above $P_m = 1.2 – 1.1*R_u$ for $R_u > 0.2$ and $P_m = 1.0$ for $R_u \leq 0.2$.

Figure 12 shows a comparison of the bending moments obtained from the first shaking event in Pile #1 in NJM01 (as a representative case) to those estimated from the *LPILE* analyses. The *LPILE* analyses were performed for four cases to evaluate the effectiveness of the modifications to the p-y curve and the application of a *p*-multiplier in predicting the pile bending moments in a liquefied layer. The best agreement between the measured and predicted pile bending moments was observed in the case where the initial stiffness of the API curve used the back-calculated stiffness values listed in Table 1 and the p-y curves were modified by *p*-multipliers that are a function of the R_u value in granular materials. As expected, the predicted bending moments without applying *p*-multipliers or without reducing the stiffness overestimated the demands. Similar observations can be made for other piles shown in the layout in Figure 13, in which the locations

where large bending moments were observed are color-coded: bending moments above grade are shown in red, and those below grade are shown in blue. A comparison of the bending moments at these locations confirms that the simple *p*-multiplier approach is a reasonable approached to approximate the softer response of p-y curves in fully/partially liquefied zones.

In order to further investigate the applicability of the modified API curves, similar analyses were performed for the piles in all the five centrifuge tests. Figure 14 compares the peak bending moments in each instrumented pile from the centrifuge tests to the corresponding bending moments predicted using *LPILE*. It can be observed that bending moments can be reasonably predicted in piles subjected to liquefaction and lateral spreading loads using the modifications made to the API sand p-y curves. The majority of the peak bending moments from the centrifuge tests occurred when the wharf deck was moving in the bayward direction. In Figure 14, the bending moments below the mudline are plotted in blue and those above the mudline (at the pile head) are plotted in red. On average, the estimated bending moments using *LPILE* are 5% larger than the measured bending moments while the majority of the data points are bounded within the 1:2 and 2:1 lines (with the exception of two data points are very small bending moments). It can be seen that the p-y models were more accurate in estimating the bending moments at the pile head; however, the accuracy relies on the confidence in the estimation of the inertial demand (pile head shear) and kinematic demand (soil displacements).

6.7 CONCLUSIONS

The results of five centrifuge tests on pile-supported wharves in saturated sands were used to back-calculate representative static and dynamic p-y curves for laterally loaded piles. Two types of piles were used in this study: 1) single free-head piles with static cyclic lateral loads at the pile head prior to shaking, and 2) dynamic pile groups with fixed-head condition supporting the wharf deck and subjected to deck inertia loads and liquefaction-induced lateral spreading loads due to earthquake ground shaking. The primary conclusions of the analyses are summarized as follows:

- Back-calculated p-y curves from static piles were approximated using API sand curves. The friction angles of 33°, 37° and 45° were used for loose sand (D_R = 30% to 40%), dense sand (D_R = 70% to 85%) and rockfill, respectively. These friction angles appeared to be adequate for estimating the ultimate lateral resistance (P_{ult}) of the experimental p-y curves, and the overall lateral response of the piles was adequately captured; therefore, no modifications were necessary. The initial stiffness values of the p-y curves that were back-calculated from the centrifuge tests. The back-calculated moduli of subgrade reaction were 3500 kN/m^3, 3500 kN/m^3, and 5200 kN/m^3 for loose sand, dense sand and rockfill, respectively. These values are smaller than the values recommended by API (1993) which might be attributed to the aging effects between soils in the field and freshly deposited sands in the centrifuge tests and the effects of pile driving and installation in the field.

- When *p*-multipliers (P_m) in fully/partially liquefied zones were applied to the API sand curves, the softer response of the soils in liquefied zones was reasonably captured. The *p*-multipliers were calculated based on the excess pore water pressure ratio (R_u) generated during dynamic loading using a simple practice-oriented equation ($P_m = 1.2 – 1.1*R_u$ for $R_u > 0.2$ and $P_m = 1.0$ for $R_u \leq 0.2$).
- The comparison of the recorded pile bending moments and those estimated from *LPILE* demonstrates that the recommended modification of the API sand curves can reasonably predict the maximum pile bending moments in piles that are subjected to a complex combination of liquefaction-induced lateral spreading and superstructure inertial loading.
- The conclusions in this study were derived from the centrifuge tests performed on sands. The applicability of these conclusions to other types of soils that are prone to pore water pressure generation during cyclic loading (e.g. sandy silts and low-plasticity silts) need to be investigated in future studies.

Table 1. Back-calculated input parameters for p-y curves

Soil unit	Total unit weight (kN/m^3)	Friction angle	Modeled in *LPILE*	Modulus of subgrade reaction, k (kN/m^3)
Loose sand (D_R = 30% to 40%)	19.4	33°	API Sand	3500
Dense sand (D_R = 70% to 85%)	20.4	37°	API Sand	3500
Rockfill	20.5	45°	Cemented c-phi with a pseudo cohesion of 15 kPa	5200

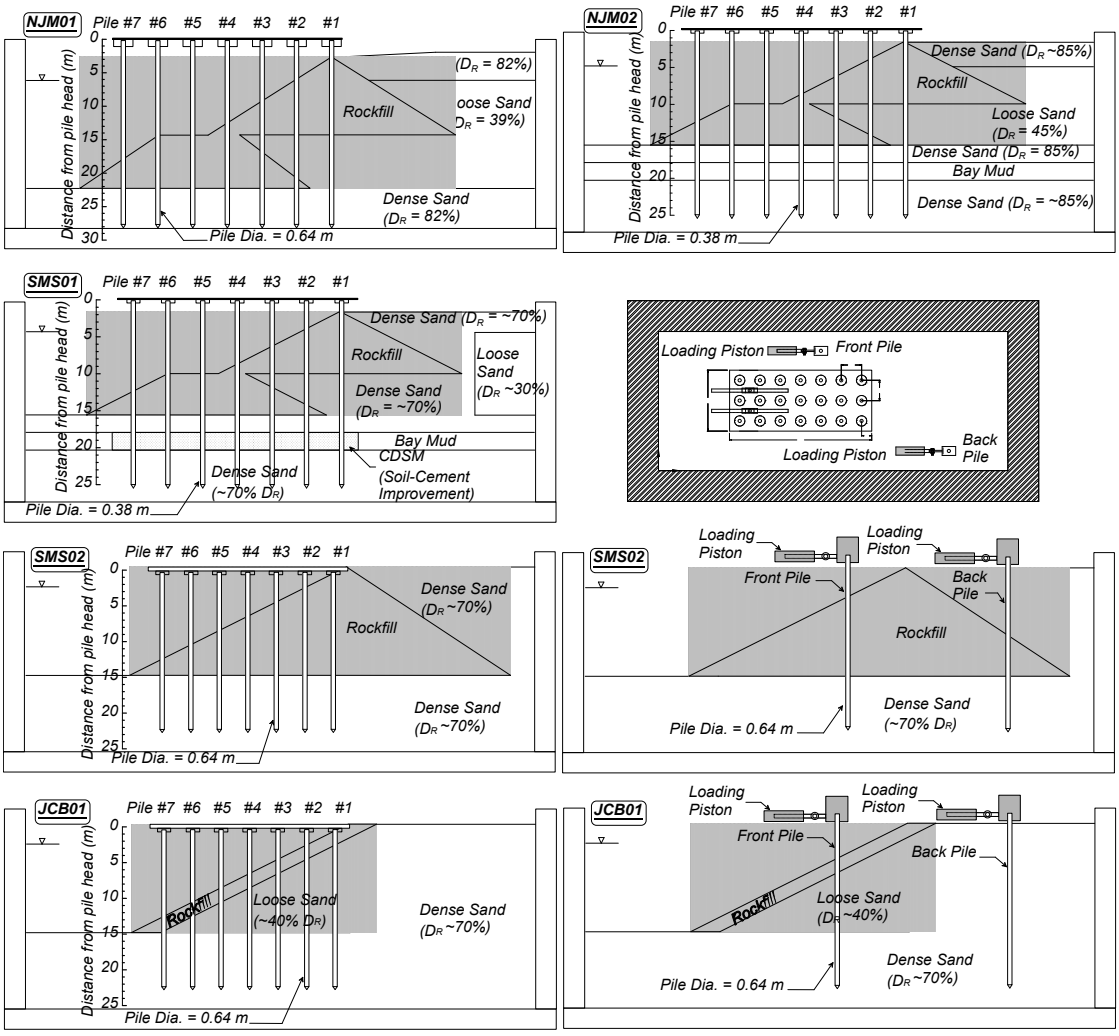

Figure 1. Cross sections and plan view of five centrifuge tests on pile-supported wharves.

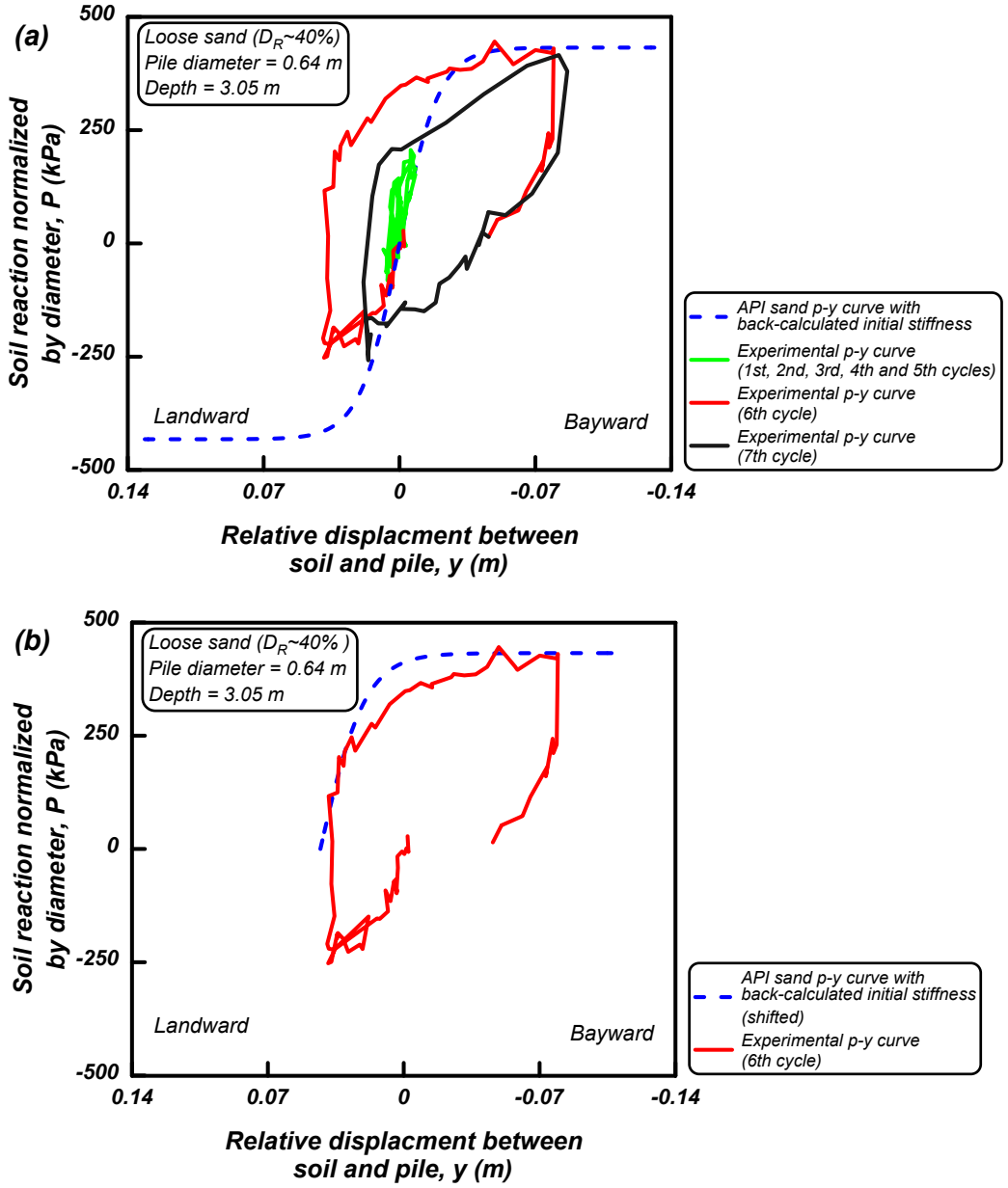

Figure 2. Comparison of an experimental p-y curve for loose sand (DR = 40%) from the front static pile in JCB01 and API sand using back-calculated input parameters

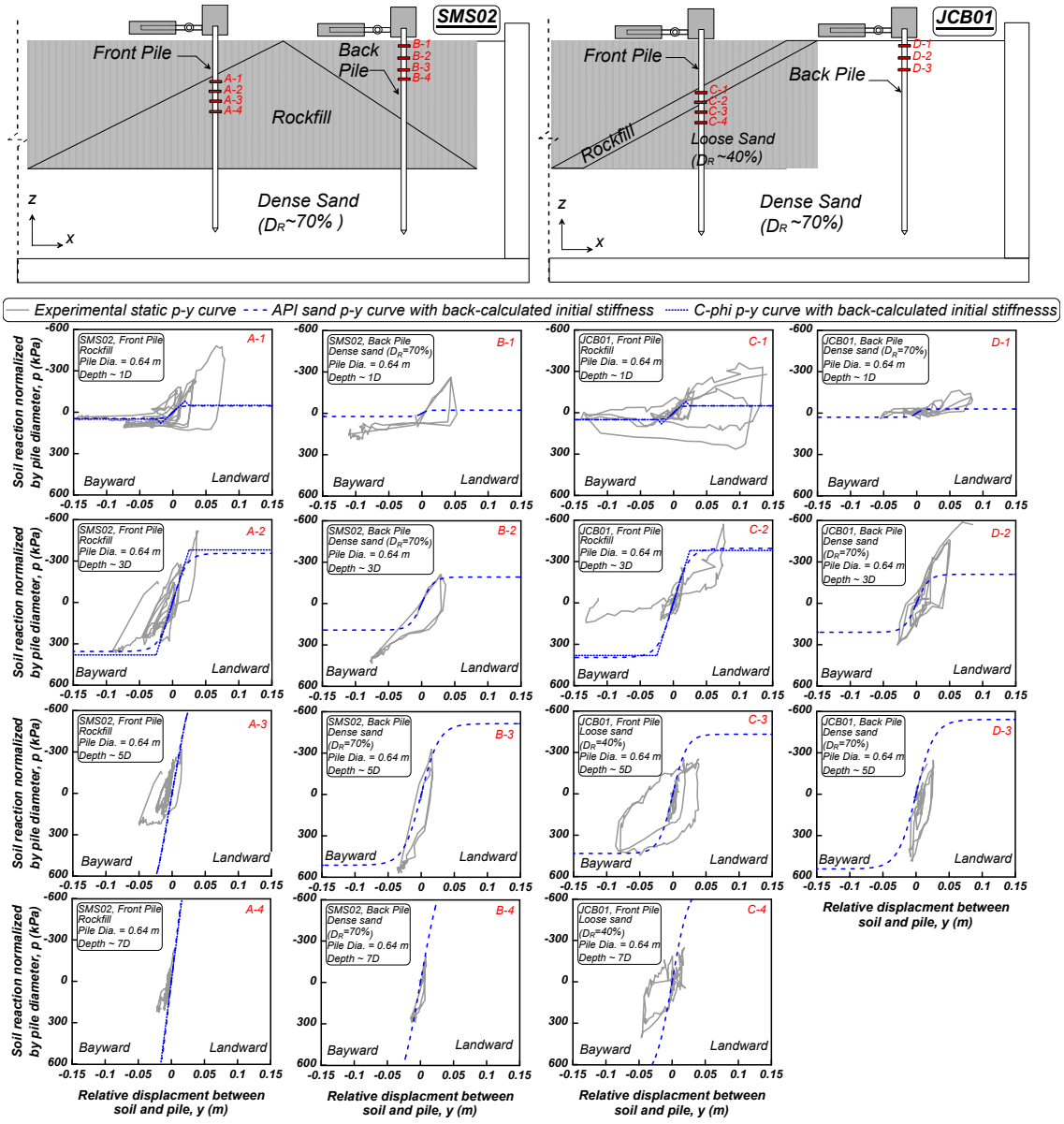

Figure 3. Comparison of experimental p-y curves from static piles in JCB01 and SMS02 and API sand using back-calculated input parameters.

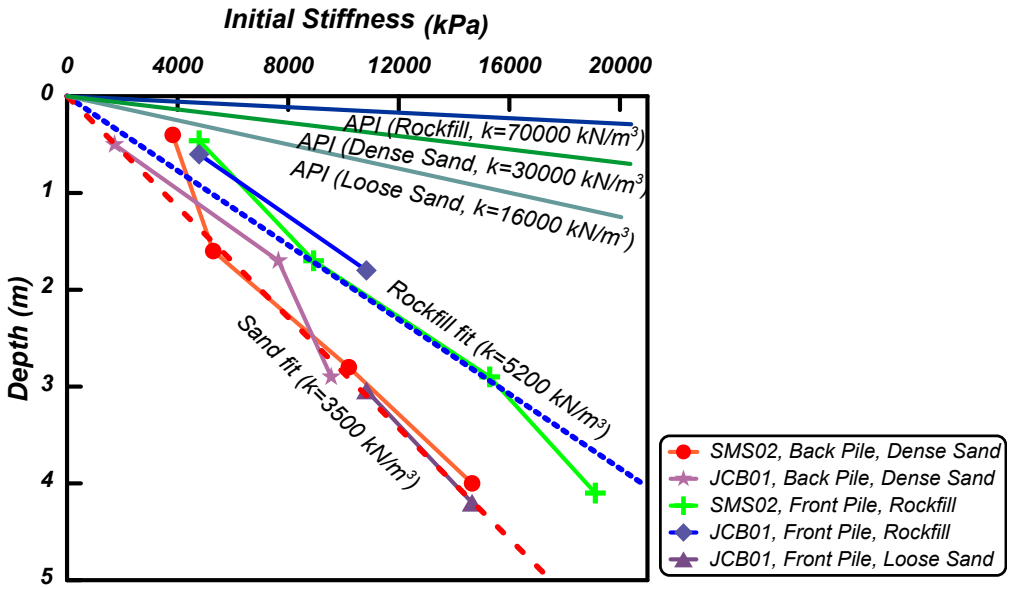

Figure 4. Comparison of initial stiffness back-calculated from experimental static p-y curves and recommended by API

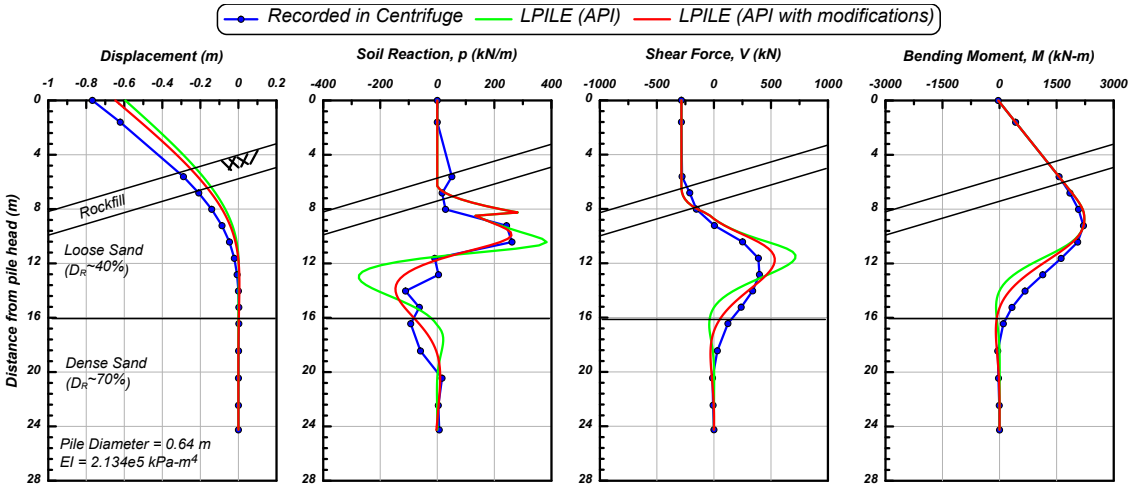

Figure 5. Comparison of recorded and predicted pile lateral responses for the front static pile in JCB01.

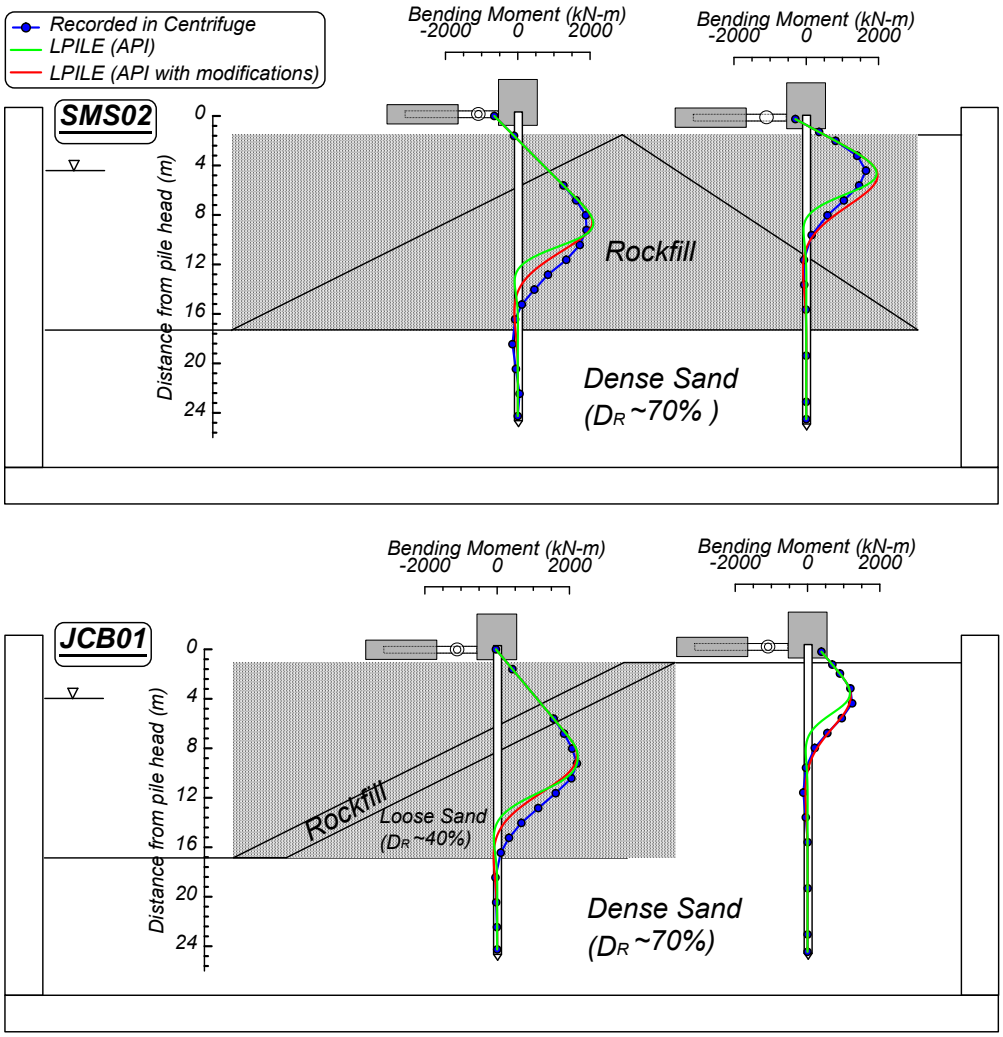

Figure 6. Comparison of recorded and predicted bending moments for static piles SMS02 and JCB01.

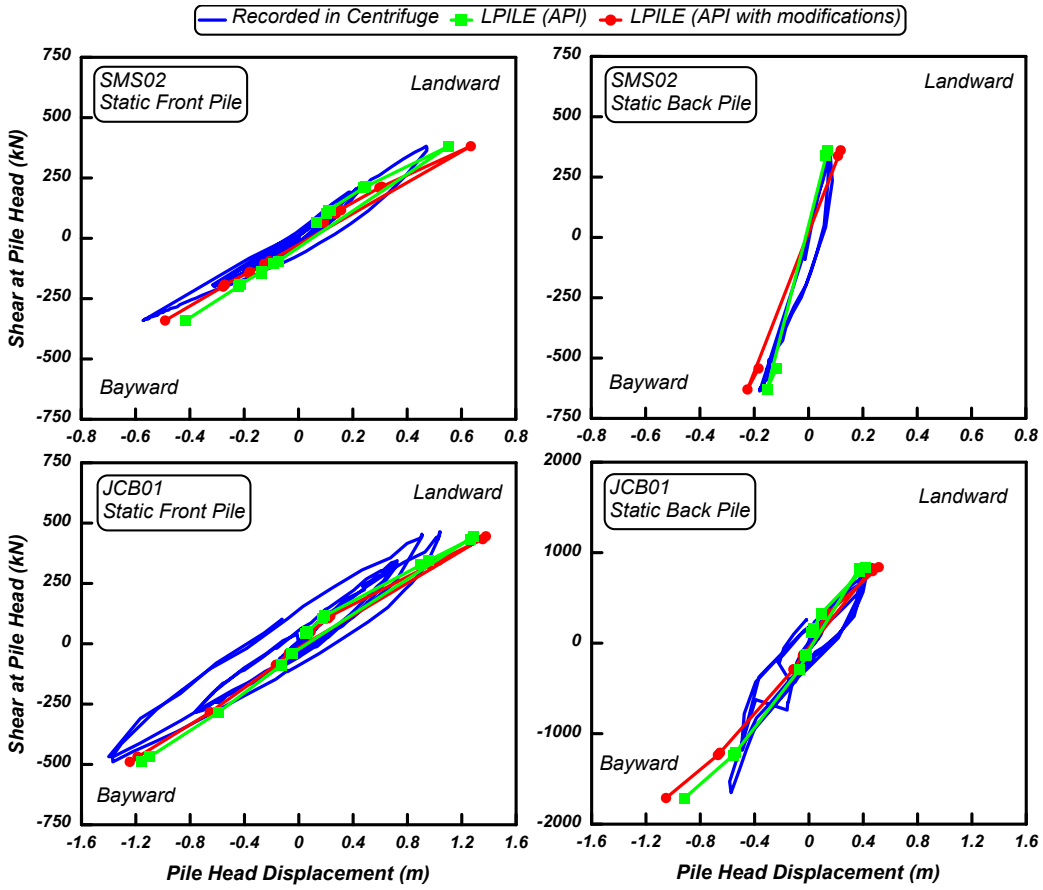

Figure 7. Comparison of recorded and predicted pile head load-displacement response for the static piles in JCB01 and SMS02.

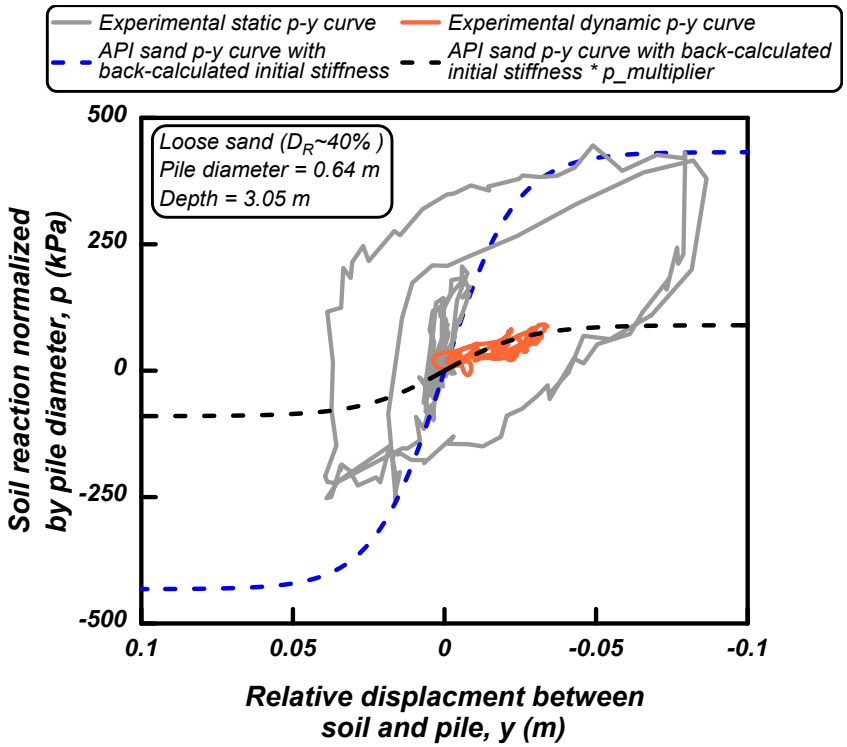

Figure 8. Comparison of static and dynamic p-y curves in loose sand in JCB01

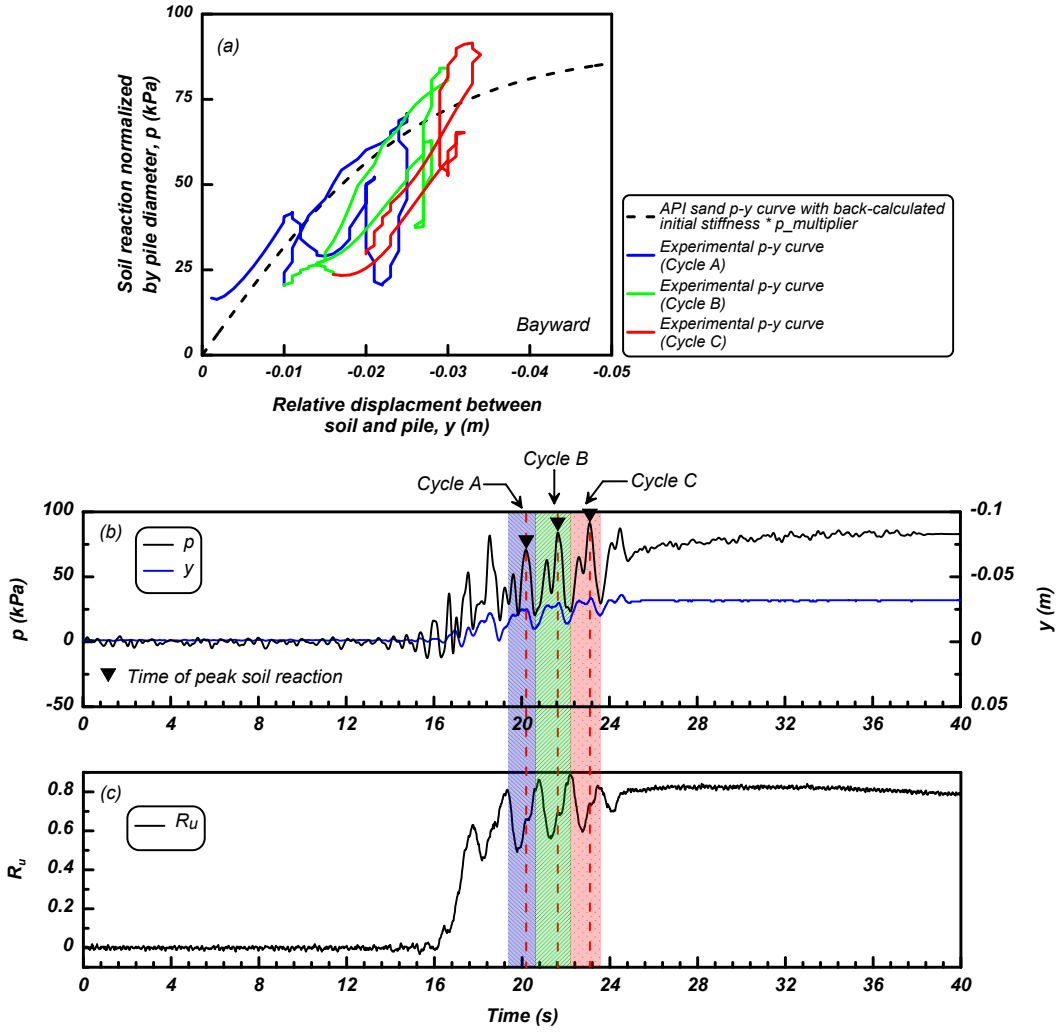

Figure 9. (a) Comparison of dynamic loading cycles in experimental p-y curve and modified API curve for liquefied sand; (b) Time histories of back-calculated soil reaction and relative soil-pile displacement; (c) Excess pore water pressure ratio measured in loose

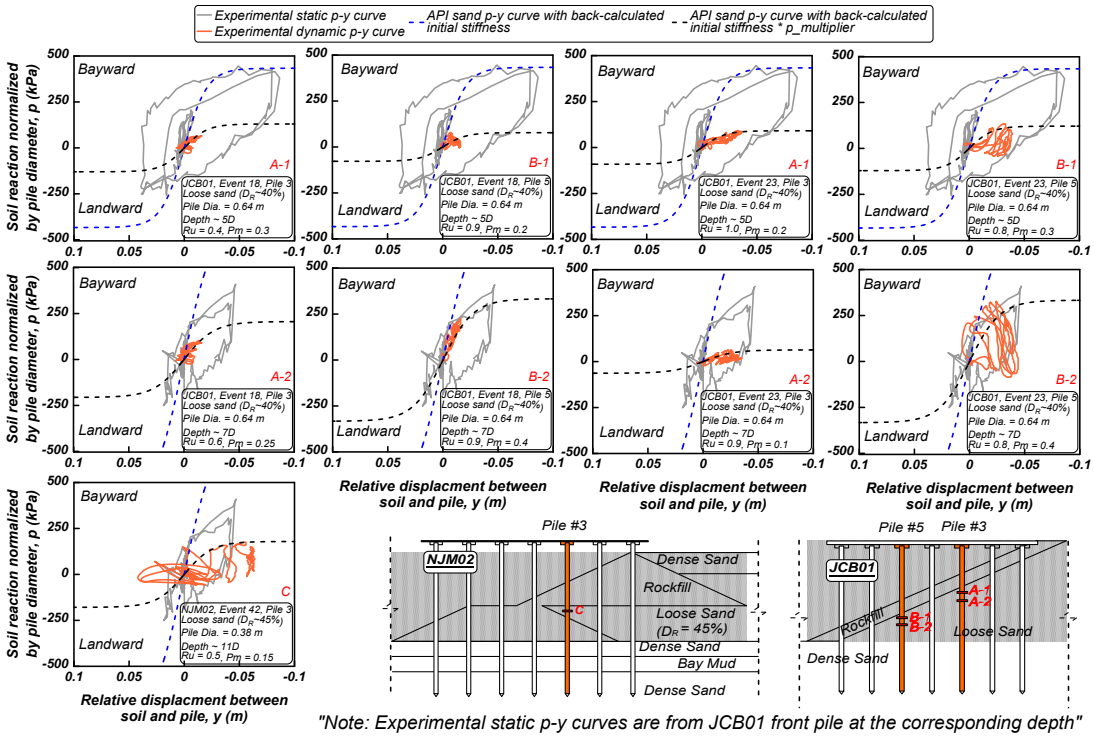

Figure 10. Comparison of static and dynamic p-y curves in loose sand at various depths.

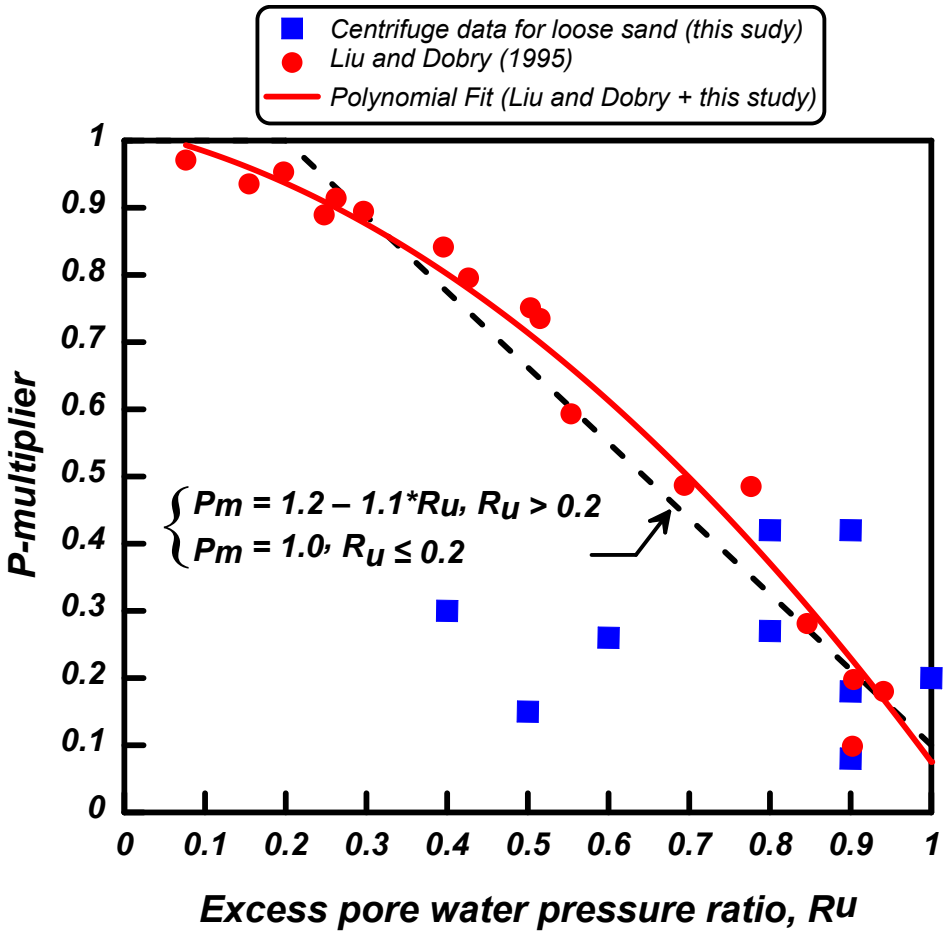

Figure 11. Comparison of back calculated p-multipliers from experimental p-y curves with excess pore water pressure ratio in loose sand and suggested data and relationship by Liu and Dobry (1995) as presented in FHWA (2011)

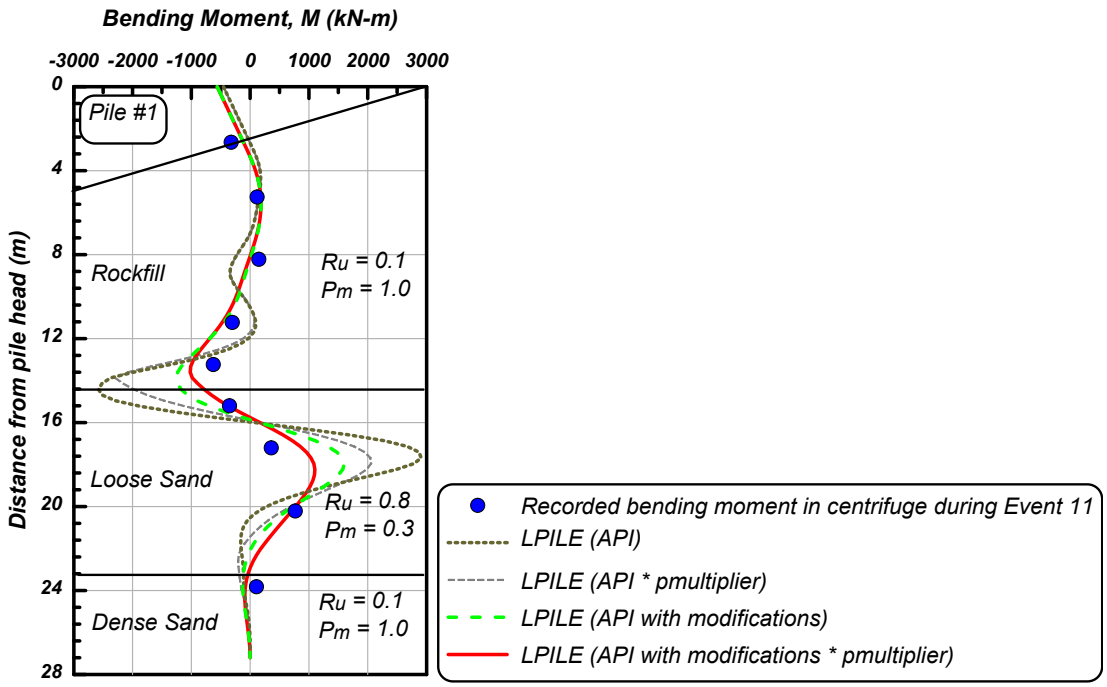

Figure 12. Comparison of recorded and estimated maximum bending moments during shaking event for dynamic Pile #1 in NJM01.

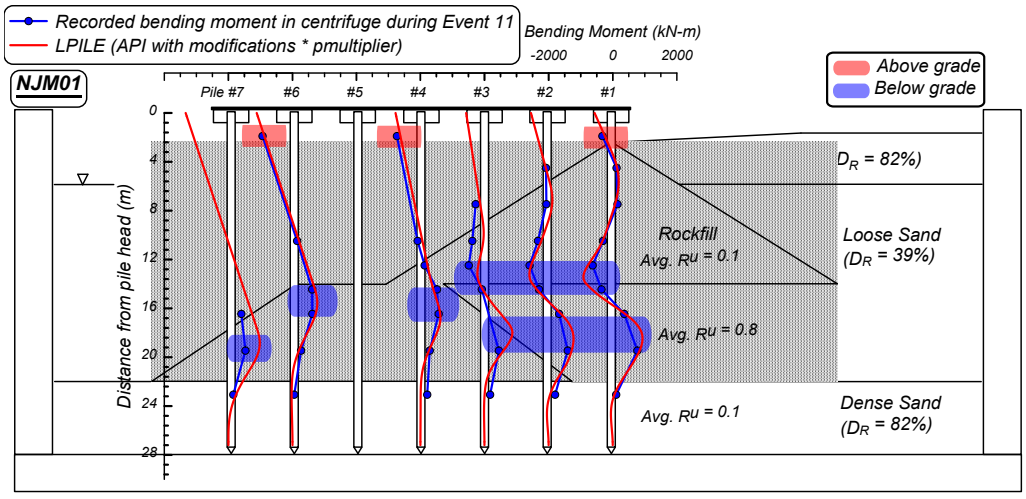

Figure 13. Comparison of recorded and estimated maximum bending moments for all instrumented dynamic piles in NJM01.

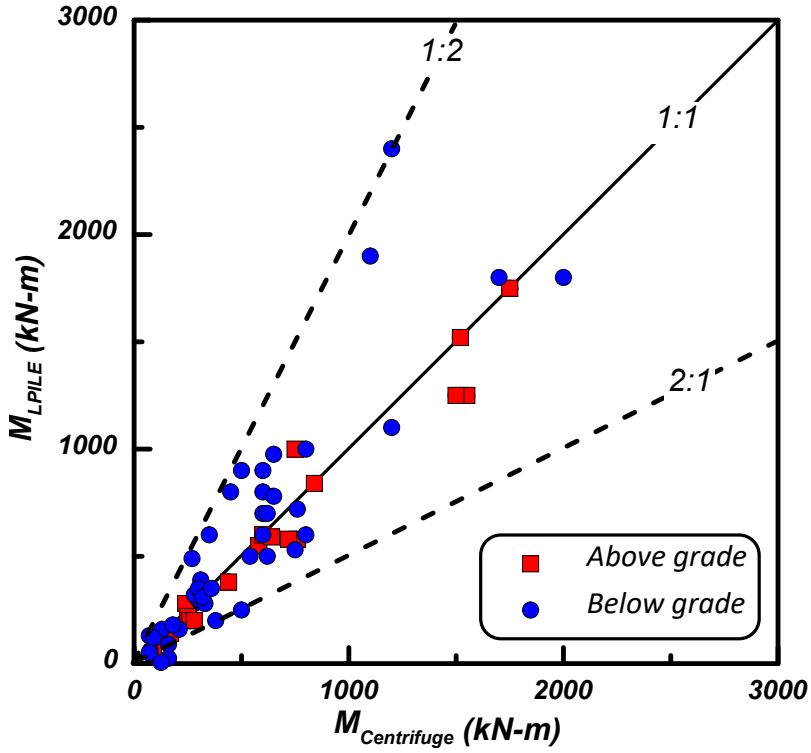

Figure 14. Comparison of maximum bending moments recorded from centrifuge and predicted from the LPILE analyses for all five centrifuge tests.

REFERENCES

Abdoun, T., Dobry, R., O'Rourke, T. D., and Goh, S. H. 2003. Pile response to lateral spreads: Centrifuge modeling. *Journal of Geotechnical and Geoenvironmental Engineering*, 129(10), 869–878.

American Petroleum Institute, API, 1993. Recommended practice for planning, design, and constructing fixed offshore platforms. API RP 2A–WSD, 20th Ed., API, Washington, D.C.

Brandenberg, S. J., Boulanger, R. W., Kutter, B. L., and Chang, D. 2005. Behavior of pile foundations in laterally spreading ground during centrifuge tests. *Journal of Geotechnical and Geoenvironmental Engineering*, 131(11), 1378–1391.

Brandenberg, S.J., Wilson, D.W., and Rashid, M.M., 2010. A Weighted Residual Numerical Differentiation Algorithm Applied to Experimental Bending Moment Data. *Journal of Geotechnical and Geoenvironmental Engineering*, 136(6), 854–863.

Chang, B.J. and Hutchinson, T.C., 2013. Experimental evaluation of p-y curves considering development of liquefaction. *Journal of Geotechnical and Geoenvironmental Engineering,* 139(4), 577–586.

LPILE., 2016. A program for the analysis of piles and drilled shafts under lateral loads. Version 2016.9.10 [computer program]. Austin, Texas: Ensoft Inc.

Federal Highway Administration (FHWA), 2011. LRFD seismic analysis and design of transportation geotechnical features and structural foundations. Publication No. FHWA-NHI-11-032, GEC No. 3. Washington, D.C.: U.S. Department of Transportation.

Franke, K.W. and Rollins, K.M., 2013. Simplified hybrid p-y spring model for liquefied soils. *Journal of Geotechnical and Geoenvironmental Engineering,* 139(4), 564–576.

Haiderali, A. E., and Madabhushi, G., 2016. Evaluation of Curve Fitting Techniques in Deriving p--y Curves for Laterally Loaded Piles. *Geotechnical and Geological Engineering,* 34(5), 1453–1473.

Liu, L., and Dobry, R., 1995. Effect of liquefaction on lateral response of piles by centrifuge model tests. NCEER Bulletin, 91, 7–11.

Marcuson, W. F., Hynes, M. E., and Franklin, A. G., 1990. Evaluation and use of residual strength in seismic safety analysis of embankments, Earthquake Spectra, 6(3), 529–72.

McCullough N. and Dickenson, S., 2004. The Behavior of Piles in Sloping Rock Fill at Marginal Wharves, Proc. Ports 2004, ASCE, May, Houston, TX.

McCullough, N. J., Dickenson, S. E., & Schlechter, S. M., 2001. The seismic performance of piles in waterfront applications. In Ports' 01: America's Ports: Gateway to the Global Economy (pp. 1–10).

McGann R, Arduino P, Mackenzie-Helnwein P., 2011. Applicability of conventional p–y relations to the analysis of piles in laterally spreading soil. *Journal of Geotechnical and Geoenvironmental Engineering,* 137(6):557–567.

Rollins, K. M., Hales, L. J., Ashford, S. A., and Camp, W. M. 2005. P-Y curves for large diameter shafts in liquefied sand from blast liquefaction tests. ASCE Special Publication: Seismic Performance and Simulation of Pile Foundations in Liquefied and Laterally Spreading Ground, 145, 11–23.

Tokimatsu, K. 1999. Performance of pile foundations in laterally spreading soils. Proc., 2nd Int. Conf. of Earthquake Geotechnical Engineering, P. S. Seco e Pinto, ed., Vol. 3, Balkema, Rotterdam, Netherlands, pp. 957–964.

Wang, S-T., and Reese, L. C. 1998. Design of pile foundations in liquefied soils. *Geotechnical earthquake engineering and soil dynamics III, Geotechnical Special Publication No.* 75, Vol. 2, P. Dakoulas, M. Yegian, and R. Holtz, eds., Reston, Va. 1331–1343.

Wilson, D. W. 1998. Soil-Pile-Superstructure Interaction in Liquefying Sand and Soft Clay. Report No. UCD/CGM-98/04 Ph.D. Dissertation, University of California at Davis, Department of Civil & Environmental Engineering, Davis, California.

Wilson, D. W., Boulanger, R. W., and Kutter, B. L. 2000. Observed seismic lateral resistance of liquefying sand. *Journal of Geotechnical and Geoenvironmental Engineering,*126(10), 898–906.

Yang, E. K., Choi, J. I., Kown, S. Y., and Kim, M. M. 2011. Development of dynamic p-y backbone curves for a single pile in dense sand by 1 g shaking table tests. *J. Civ. Eng., 15(5), 813–821.*

Yoo, M. T., Choi, J. I., Han, J. T., and Kim, M. M. 2013. Dynamic p-y curves for dry sand by dynamic centrifuge tests. *J. Earthq. Eng., 17(7), 1082–1102.*

CHAPTER 7

7.0 2D NUMERICAL MODELING OF A CENTRIFUGE TEST ON A PILE-SUPPORTED WHARF SUBJECTED TO LIQUEFACTION-INDUCED GROUND DEFORMATIONS

Note: The contents in this chapter have been submitted as a technical paper to Soil Dynamics and Earthquake Engineering and is currently under review with the following citation:

Souri, M.; Khosravifar, A.; Dickenson, S. E.; Schlechter, S. & McCullough, N. “2D Numerical Modeling of a Centrifuge Test on a Pile-Supported Wharf Subjected to Liquefaction-Induced Ground Deformations.” Soil Dynamics and Earthquake Engineering (under review)

7.1 INTRODUCTION

Previous field case histories on the seismic behavior of pile-supported wharves have repeatedly demonstrated the vulnerability of the foundation system to damage (ranging from minor repairable damage to failure) from ground deformations due to liquefaction or cyclic softening and degradation of foundation soils (e.g. Werner 1998, PIANC 2001, Rathje et al. 2010, Cubrinovski et al. 2017). Due to resources required to prevent slope deformation, small permanent ground deformations are considered acceptable by major design guidelines for wharves and piers (e.g. ASCE/COPRI 61-14). The allowance of small, permanent ground deformations in the context of performance-based seismic design guidelines adopted by major ports highlights the need for calibrated numerical models to reliably predict the ground deformations and the dynamic soil-foundation-structure interaction of the wharf system. Coupled nonlinear dynamic analysis is increasingly

used by practitioners in assessing the seismic performance of existing and new wharf structures. In this type of analysis, the responses of soil, pile and structure are analyzed simultaneously in one unified model, which inherently captures the complex, dynamic interaction between the inertial loads from superstructure mass and kinematic loads from ground deformations. The increased use of coupled dynamic analysis with soil-structure interaction (SSI) effects in practice and research is partly related to the availability of computational platforms that can model soils and structures together (e.g. FLAC, OpenSees, etc.) as well as recent advancements in soil constitutive models that can simulate highly nonlinear, undrained cyclic responses of liquefiable soils (e.g. PM4Sand/PM4Silt, UBCSAND-904aR, PDMY03, SANISAND-MSf, etc.)

While 3D dynamic simulations provide valuable insights on problems involving soil-pile interaction particularly in the near field around the piles (e.g. Chaloulos et al. 2014, Qui et al. 2020), 2D dynamic modeling remains to be used by practitioners and researchers to study the global response of structures subjected to ground deformations, though with some practical simplifications (e.g. Armstrong et al. 2013, Chang et al. 2013). More specifically, FLAC (Itasca, 2016), in various iterations and with various constitutive models, has been used to adequately capture global response and displacements for field case histories. Dickenson and McCullough (2006) used 2D nonlinear, effective stress models in FLAC to simulate the response of five centrifuge tests on pile-supported wharves and a case history on the deformations and damages induced to Port of Oakland during the 1989 Loma Prieta earthquake; these centrifuge tests augment a very sparse collection

of well-documented case histories of pile supported wharf and pier responses. They provided the strengths and limitations of the numerical model in predicting the soil and wharf displacements, bending moments, and excess pore pressure generations. Their model was used as a basis in this study with updates that reflect the new advancements in constitutive modeling of liquefiable soils, and modified soil-pile interface properties based on back-calculated p-y relationships from the five centrifuge tests.

There are several challenges with simulating the dynamic response of piles in liquefiable soils using 2D models. The soil-pile interaction should be modeled in such a way that it would allow large relative displacements to form between the pile and the laterally spreading ground. The soil-pile interface elements (i.e., p-y springs) should capture, to some extent, the softening effects of soil liquefaction on the lateral response of piles as well as the momentarily stiffened response during dilative cycles. More specifically, the 2D models should be able to approximate the out-of-plane geometry of the wharf deck, centrifuge container, and pile spacing (perpendicular to the plane). The study presented here, adopts commonly used methods to approximate the abovementioned aspects of dynamic response in a 2D model and evaluates the effectiveness of these methods against measured data from a centrifuge test. The centrifuge and simulation results are compared for near- and far-field soil responses and the dynamic behavior of the piles, wharf deck and centrifuge container. The limitations of these simplifications in predicting the dynamic response of the wharf system are discussed.

The objective of the numerical analysis was to create a 2D numerical model that captures key responses of the soil, pile and wharf behaviors (e.g. displacements, accelerations, excess pore water pressures, and bending moments). Rather than adjusting the numerical model to exactly match the centrifuge results, the model was created based on data that is commonly available to practicing engineers, namely subsurface stratigraphy, relative densities of soil units, and pile and wharf deck properties. A few modifications had to be made to the 2D model to bring the simulation results closer to the measurements. These modifications include reducing the modulus of subgrade reaction of p-y curves in nonliquefied conditions, using a larger damping ratio for structural response, and adjusting the elastic modulus of the rubber rings of the centrifuge box. These modifications and their effect on the overall responses of the wharf are discussed.

The following sections provide a brief overview of the centrifuge test that was used in the calibration of the numerical model, a discussion of the development of the numerical model, and a comparison of the results of the nonlinear dynamic analysis to the experimental data. Insights derived from the results of the nonlinear dynamic analysis are presented and discussed in detail.

7.2 CENTRIFUGE TEST

A series of five centrifuge tests on pile-supported wharves were performed by McCullough et al. (2001) and were analyzed to investigate the interaction of inertial and kinematic demands on piles in Souri et al. (2019). The results from one of these tests (NJM01) was used to calibrate the numerical model in this study.

Details about this centrifuge test can be found in a data report in McCullough et al. (2000).

Figure 1 presents the cross section, plan view, and photograph of centrifuge model NJM01 before shaking. The centrifuge model configuration in this test consisted of a multi-lift rock dike, a dry dense sand layer, overlying a liquefiable loose sand layer (relative density, D_R = 39%), overlying a dense sand layer (D_R = 82%). A set of 21 piles in a 7-by-3 configuration support the wharf deck as depicted in the plan view in Figure 1. The piles were made with aluminum pipes having an outer diameter of 0.64 m (in prototype scale). The model was subjected to a sequence of shaking with different amplitudes at a centrifugal acceleration of 40.1 g. The first large shaking (Event 11) was used in the calibration study. The potential failure surfaces are interpreted from the peak transient soil displacements obtained from accelerometer arrays. The key characteristics of soil, pile, wharf deck and input motion are listed in Table 1.

7.3 NONLINEAR DYNAMIC ANALYSIS

A two-dimensional numerical model was developed using *FLAC* numerical modeling software (Itasca, 2016) and was calibrated against key responses for centrifuge test NJM01 where the piles were subjected to combined effects of superstructure inertial load and liquefaction-induced lateral ground deformations.

7.3.1 Numerical Model

Two-dimensional (2D) nonlinear dynamic analyses (NDA) were conducted in *FLAC*. In the model geometry and discretization of the soil mesh shown in Figure

2, the soil and container of the centrifuge test were modeled by 2D continuum elements. The wharf deck was modeled using elastic beam elements. The piles were modeled using elastic pile elements, since the piles exhibited elastic behavior in the centrifuge test.

7.3.2 Soil Constitutive Model

The pressure-dependent multi-yield surface model (PDMY03) was used to model the cyclic shear behavior of sands and rockfill with different relative densities during the earthquake motion. The original model was developed and calibrated against a dataset of laboratory and centrifuge tests by Elgamal et al. (2003) and was updated by Khosravifar et al. (2018). The yield criteria in the employed soil model is described using a multi-surface plasticity framework. The model incorporates a non-associative flow rule in order to simulate the mechanism for the post-liquefaction accumulation of shear strains and the subsequent dilation in liquefied soils.

The primary focus in the calibration of the soil model was to capture the triggering of liquefaction and post-liquefaction accumulation of shear strain. The loose and dense sands were calibrated to trigger liquefaction (defined here as 3% single amplitude shear strain) in 15 cycles at the cyclic stress resistance (CRR) value estimated from the correlations by Idriss and Boulanger (2008). Figure 3 provides as an example the results for a single-element undrained cyclic direct simple shear (DSS) simulation for sand with D_R = 39% (corresponding to $(N_1)_{60}$ of 7) under vertical effective stress of 100 kPa. Figure 3a shows the cyclic stress ratio (CSR)

versus the number of uniform loading cycles, which was calibrated to trigger liquefaction at the desired CSR in 15 cycles. The stress–strain loops and the stress path responses are shown in Figures 3b and 3c, respectively. The results for cyclic stress ratio versus shear strain that are shown in these figures indicate that the model is capable of reasonably capturing post-liquefaction cyclic softening and plastic shear strain accumulation (approximately 1% to 1.5% shear strain per cycle after liquefaction is triggered). While there is a considerable uncertainty in predicting post-liquefaction shear strain accumulation (e.g. Wu 2002, Zhang et al. 2004, Tasiopoulou et al. 2020), the analysis performed in this study shows that the constitutive model calibrated based on a relative density and commonly used empirical correlations (i.e. Idriss and Boulanger 2008) reasonably estimated the deformations in a boundary-value problem as will be shown later by comparing the simulation results to measurements from a centrifuge test. However, it is recommended to use soil-specific cyclic shear data to calibrate soil constitutive models when such data is available; this is specifically important when the soil types are very different from those used in the development of empirical correlations.

The model was also calibrated for cyclic behavior in drained conditions to simulate the behavior of loose sand prior to liquefaction and the behaviors of dense sand and rockfill whose dynamic behavior was primarily nonliquefied. The small strain shear modulus (G_{max}) values were defined as stress-dependent based on the Seed and Idriss (1970) relationship, using the K_{2max} values reported in Table 2. The shear wave velocity (Vs) profile calculated using these shear moduli generally

agreed with the Vs measurements in the centrifuge test. The modulus reduction curve (G/G_{max}) and the equivalent damping curve derived from single element drained cyclic DSS simulations are shown in Figure 4 along with the empirical relationships recommended by EPRI (1990) for sands and Gazetas and Dakoulas (1992) for rockfill. The Gazetas and Dakoulas (1992) curve was used as input in PDMY03 to model rockfill whose dynamic behavior was primarily nonliquefied; however, the automatically generated backbone curve was used to model sands, as it works better with the pore pressure generation features in the model. The soil model input parameters for the loose sand, dense sand, and rockfill are summarized in Table 2. More details for each input parameter can be found in Khosravifar et al. (2018).

The initial static stresses were established in the model by assigning a Mohr–Coulomb constitutive model with stress-dependent stiffness to all materials and allowing the model to reach equilibrium under gravity. The shear moduli for all soil zones were calculated based on the mean effective stress at each depth. Once the initial equilibrium was established, the soil model was switched to PDMY03 and the model was solved again to reach equilibrium. During the shaking phase, the acceleration time history that was recorded at the base of the centrifuge box was directly applied at the base of the model as a fixed base. Simulations in *FLAC* were performed in large strain mode to allow for geometry update during the shaking process.

7.3.3 Pile Elements

A total of 21 piles, configured in three rows of seven piles, supported the wharf deck in centrifuge test NJM01. The piles were equally spaced at approximately 10 diameters (10*D*; equivalent to 6.1 m) center-to-center in the out-of-plane direction and 8 diameters (8*D*; equivalent to 5.1 m) in the longitudinal direction. The piles were modeled using pile elements, and the wharf deck was modeled using beam elements with the dimensions and properties listed in Table 1. Considering the rigidity of the deck and the connections to the piles, the pile head connection to the wharf deck was modeled as rigid against rotation. The pile tip was fixed in the vertical direction but was free to rotate. In the 2D *FLAC* model, it was assumed that the mass of the deck was equally distributed between the three rows of piles. To implement this assumption in the 2D model, the deck was defined with 1/3 of the actual total mass, and the spacing was set to 6.1 m which was the pile spacing in the out-of-plane direction. To account for the out-of-plane spacing between the piles, the piles were modeled in *FLAC* using the actual pile properties, and the spacing was set to 6.1 m. The pile elements were modeled as elastic to represent the elastic aluminum tube piles that were used in the centrifuge test.

7.3.4 Soil-Pile Interface Elements

The pile nodes in the 2D model were connected to the soil elements using nonlinear p-y springs. The p-y spring properties were selected based on American Petroleum Institute (API 1993) recommendations for sand; however, the moduli of the subgrade reaction were modified from API based on four pseudo-static lateral

load tests that were performed in two centrifuge tests by McCullough et al. (2001). The modulus of subgrade reaction was selected to be 3500 kN/m^3 for the loose and dense sand and 5200 kN/m^3 for rockfill. More details on the back-calculation of the moduli of subgrade reaction from the centrifuge tests are provided in Souri et al. (2020). The p-y strengths (i.e. P_{ult}) are developed based on the friction angles reported in Table 2. A pseudo-cohesion of 15 kPa was incorporated in calculating the ultimate soil reaction in rockfill to account for additional resistance caused by the interlocking and movement of rock particles near the ground surface (McCullough and Dickenson 2004). The influence of this pseudo-cohesion decreases rapidly with depth due to the high friction angle of the rockfill. Incorporation of this pseudo-cohesion results in minor to moderately better computed near-surface soil-pile interaction as shown in McCullough and Dickenson (2004) and was confirmed using back-calculated p-y springs from centrifuge tests in Souri et al. (2020). Slope effects on the stiffness of p-y springs were accounted for as described in McCullough and Dickenson (2004). No additional multipliers were applied in the liquefiable soils, as the first-order softening effects of liquefaction were assumed to be captured by the soil elements connected to the free end of the p-y springs. This modeling approach resulted in a reasonable match between the numerical model and the centrifuge test results, as will be explained in a later section. Table 3 shows the properties used in developing the p-y relationships and their corresponding p-multipliers. Figure 5 presents the comparisons between the API p-y curves (modified with the back-calculated

moduli of subgrade reactions reported above) and the bi-linear p-y curve defined in *FLAC* for the mid-depth in loose sand, dense sand, and rockfill.

7.3.5 Centrifuge Container

Modeling the centrifuge container in a 2D model is challenging, and it requires that some assumptions be made. The approach presented by Armstrong (2010) and Boulanger et al. (2018) was followed to calculate the equivalent 2D properties of the centrifuge container. The equivalent 2D properties were then calibrated to reasonably match the displacement time histories recorded at different elevations along the container in the centrifuge test. The flexible shear beam container, which was designed to have six rigid aluminum rings separated by a 12-mm (model scale) soft layer of 20-durometer neoprene rubber, allowed the container to deform as shear beams. The container nodes with the same elevation on the left and right sides of the model were attached to have identical vertical and horizontal movements. The aluminum ring and rubber rings were modeled as linear elastic materials. The mass of the upper three aluminum rings was one half of the lower three rings and was modeled as such. The equivalent density and shear moduli of the rubber rings were calculated as their actual properties divided by the out-of-plane width of the enclosed soil ($Width_{container}$ = 0.685 m). The shear modulus of the rubber (G_{rubber}) was calibrated to a value of 1.2 MPa based on sensitivity analyses to match the displacements recorded for the container during shaking. The equivalent 2D shear modulus was calculated as $G_{rubber,2D} = (G_{rubber} \times Area_{rubber}) / (Width_{container} \times Area_{rubber,2D})$ where the $Area_{rubber}$ is the actual area of the rubber

ring used in the centrifuge test and $Area_{rubber,2D}$ is equal to the width of the rubber on both sides of the 2D model.

It was important to model the interface between the soil elements and the container elements in a way that allows for slippage and simulates an impermeable boundary between the soil and the container. To do so, extremely flexible beam elements were placed between the soil elements and the container elements in the *FLAC* model. One side of each beam element was attached to a soil element using a frictional interface element with a friction angle of 23 degrees, which was approximately two-thirds of the friction angle in the soil elements. The other side of each beam element was glued to a container element. This modeling approach allowed for relative displacement between soil and beam elements and restricted the relative movement between the beam and container, and it provided an impermeable boundary at the interface. The beam element properties were selected to be extremely flexible such that they would have no effect on the container response.

Figure 6 presents a comparison of the horizontal displacement of the centrifuge container computed from the *FLAC* model against the recorded displacement from the centrifuge test. The location of the sensor in the centrifuge test and the recorder in the *FLAC* model is shown with a symbol and a schematic inside the figure. This figure shows that the numerical model captured some key features of the lateral response of the container including the magnitude and approximate timing of the peak displacement as well as the period of the dynamic response. The numerical model also captured the sign of the residual, end-of-motion displacement (which

was upslope); however, the magnitude of the residual displacement was overestimated. Displacements presented in this figure are relative to the base of the model.

7.3.6 Damping

Two different Rayleigh damping were used for the soil elements and the structural elements. A relatively low level of Rayleigh damping (0.5%) was employed in the soil elements at a center frequency of 1.25 Hz corresponding to the natural frequency of the wharf system, with the main soil damping coming from the soil nonlinear hysteresis behavior modeled by the constitutive model. Past studies have shown the importance of accounting for additional damping along the piles to capture the radiation damping and the complex interaction between the soil, structure and fluid (e.g. Wang et al. 1998). While in a more rigorous modeling, the dashpots are defined along the piles with the p-y springs (e.g. Brandenberg et al. 2013), this damping was approximated in the 2D model in this study based on the available tools in *FLAC* and was modeled using an additional Rayleigh damping with an equivalent damping ratio of 15% assigned to the structural elements only. Using this damping ratio resulted in a better match with centrifuge recordings as explained later in the sensitivity analysis.

7.4 COMPARISON BETWEEN CENTRIFUGE AND NUMERICAL MODEL

This section presents comparisons of recorded responses from the centrifuge test and simulated responses from the nonlinear dynamic analysis. The results from

FLAC are reported for the same locations where the instruments were placed in the centrifuge test.

7.4.1 Soil and Wharf Responses

Figure 7 presents the contours of the horizontal soil displacements back-calculated from centrifuge test as well as those computed from simulation. The displacements are shown at the critical cycle (a snapshot in time) when the soil displacements are at their peak values. The soil displacements in the centrifuge test were calculated by combining the transient and permanent components of the soil displacement. The transient displacements were calculated by double-integrating the recorded accelerations and applying a high-pass Butterworth filter to maintain only the high-frequency component. The permanent displacements were calculated by applying a low-pass Butterworth filter to the displacements measured using a linear variable differential transformer (LVDT) mounted to the ground surface. The permanent displacements were distributed with depth using a profile developed based on the shape of the peak transient displacements with depth. No permanent displacements were considered below the shear failure plane (shown as a red dashed line in the cross section in Figure 1). While the magnitude of peak soil displacement is under-predicted in simulations, the patterns of soil displacements near the ground surface, in the upper rock dike, and in the areas adjacent to the wharf are in a reasonable agreement with the displacements recorded in the centrifuge test.

Figure 8 presents a comparison of the time histories of the key dynamic responses computed from *FLAC* against those measured in the centrifuge test. The figure illustrates (from bottom to top) horizontal acceleration at the base, excess pore pressure ratio (r_u) in the middle of the loose sand layer, horizontal acceleration and displacement at the wharf deck, and horizontal acceleration and displacement at or near the ground surface. All reported displacements are relative to the base of the model.

It can be noticed from this figure that the computed soil and wharf displacements slightly under-predict the peak recorded soil and wharf displacements in the bayward direction; however, the computed permanent displacements for both soil and wharf deck are in close agreement with the recorded data from centrifuge test. The pattern of computed displacements with time reasonably predicts the recorded displacements from the centrifuge test, including the timing of the critical cycle(s) and the apparent natural period of the soil profile and the pile–wharf system. The simulation results do not predict the strong transient response in the centrifuge recordings, exhibited by large cycles in the upslope direction. Our sensitivity analysis showed that the transient behavior can be improved by softening the lower dense sand (i.e. modeling it with a lower relative density); however, we decided to keep the baseline numerical model based on relative density of D_R = 82% which was calculated during the construction of the centrifuge model. A comparison of the measured and computed horizontal acceleration time histories at a location near the surface indicate that the main cycles and period are captured reasonably well. However, the simulations do have stronger high-frequency

components, which resulted in over-predicting the magnitude of peak ground acceleration (PGA) by a factor of 1.2. As explained later in the comparisons shown for the far-field soil responses, this high frequency component appears close to the ground surface and is likely attributed to the dynamic response of the top rings of the container in the *FLAC* simulations (results of sensitivity analysis with free-field conditions, excluding the container did not exhibit this high frequency). The simulated and measured horizontal accelerations at the wharf deck are in close agreement in terms of both amplitude and frequency. The comparison at the base of the model confirms that the input base excitations from the simulation and the centrifuge test were identical, as expected as the recorded accelerations were input as a fixed base in the *FLAC* model.

It can also be noticed from Figure 8 that the pore pressure ratio computed by *FLAC* reasonably matched the recorded pore pressure ratio in the centrifuge test. The difference between the computed and recorded maximum pore water pressure ratios is attributed to the drainage of the excess pore water pressure into the rockfill, which has a higher permeability during shaking as indicated by the decline in pore pressure ratio towards the end of motion in the centrifuge test. It is worth noting that drainage (flow) was not permitted during the dynamic simulations in *FLAC*.

7.4.2 Far-field Soil Response

Figure 9 presents the soil response in the far field behind the wharf. The plots in this figure compare the simulations results from *FLAC* and recorded data from

centrifuge test. The plots show the change in accelerations, spectra, and excess pore water pressure as the waves propagate from the base of the model to the ground surface. The location of each sensor and recorder is shown in the schematic inside each figure. The acceleration time histories show that the simulations capture the critical cycles reasonably well. The simulations predicted the spectral accelerations at a dominant period of 1.3 sec reasonably well; however, they overestimated the spectral accelerations at smaller periods; the peak acceleration near the ground surface is slightly underestimated (i.e. 0.18 g in simulation versus 0.15 g in centrifuge). The excess pore pressures time histories are captured reasonably well in the middle of the lower dense sand and at two locations along the loose sand. The *ru* in the top half of the loose sand reaches 100% indicating triggering of liquefaction, while *ru* in the lower half of the loose sand only reaches to 55% to 65%. The lower dense sand does not liquefy as indicated by low *ru* in both centrifuge and simulations.

7.4.3 Pile Response

The accuracy of the *FLAC* model in capturing the lateral behavior of the piles during dynamic loading was evaluated by comparing the lateral response of a pile at the critical loading cycle in the simulation against measured and back-calculated response from centrifuge test NJM01. The results are shown in Figure 10 for Pile #1 as an example. The critical loading cycle corresponds to the time when the peak bending moment occurs along the pile. The centrifuge bending moments were recorded at discrete locations along the pile where strain gauges were mounted.

The bending moments were then interpolated along the length of the pile and were double-integrated to estimate the pile lateral displacements. The shear force and lateral soil reactions were estimated by differentiating and double-differentiating the bending moment profile, respectively. As shown in the figure, the peak response parameters (bending moment, lateral soil reaction, and shear forces) generally occur in the vicinity of the boundary between the rockfill and the loose sand and the boundary between the loose sand and the lower dense sand. The magnitude of the peak response parameters is predicted reasonably well; however, the locations of the predicted peak values are sometimes found at distances of up to 5 diameters away from the locations of the peak values measured in the centrifuge test. This is largely attributed to the difference between the soil displacement profile in the centrifuge test and the computed soil displacement profile from *FLAC*, as indicated by the dashed lines in the leftmost plot in Fig. 10. As a result of the differences in the imposed soil displacements, the simulated pile curvatures are different from those in the centrifuge test. The accumulated shear strains in the loose sand (indicated by the slope of the soil displacement with depth) is reasonably predicted in simulation using the PDMY03 soil model compared to the centrifuge results.

7.5 SENSITIVITY ANALYSIS

Additional dynamic analyses were performed to evaluate the effects of some of the modifications that were made in this modeling effort with respect to the modeling assumptions that are commonly made in practice in 2D modeling of slopes with

SSI effects. Comparing the results of these sensitivity analyses with measured data from the centrifuge test provided a method to objectively assess the effectiveness of these modifications.

7.5.1 P-Y Spring Properties

The softening effects of soil liquefaction on the lateral response of piles is often approximated in practice by modifying the p-y springs in loose liquefiable sands using liquefaction p-multipliers (e.g. Liu and Dobry 1995, Brandenberg 2005, Franke and Rollins 2013). While applying liquefaction p-multipliers is necessary in a pseudo-static analysis (as shown in Souri et al. 2020 using *LPILE* models), their application in the coupled dynamic analysis in this study did not improve the predicted lateral pile responses. This is likely because the soil elements in a coupled analysis capture the softening effects of soil liquefaction during the dynamic analysis to some extent. Figure 11 shows the comparison of the bending moment profile in Pile #1 at the critical cycle recorded in centrifuge and simulated in FLAC. The baseline case represents the p-y properties shown in Table 3 while the sensitivity analysis includes additional liquefaction p-multiplier of 0.1 in the loose sand (selected approximately based on the range of p-multipliers reported in Caltrans (2012) for a sand with D_R = 39% or $(N_1)_{60}$ = 7). The comparison shows that the analysis with additional liquefaction p-multiplier under-predicts the bending moments compared to the centrifuge test. As explained earlier, the moduli of subgrade reaction used in the baseline analysis (and listed in Table 3) were back-calculated from four static lateral load tests described in Souri et al. (2020) which

were found to be softer than the API values that are commonly used in practice. An additional sensitivity analysis was performed using the moduli of subgrade reaction by API (70400 kN/m^3 for rockfill, 16000 kN/m^3 for loose sand and 29000 kN/m^3 for dense sand) in combination with a liquefaction p-multiplier of 0.1 in the loose sand. The comparison in Figure 11 shows that using API curves in combination with a liquefaction multiplier of 0.1 results in similar bending moments as the baseline analysis which has a softer p-y curve but with no additional liquefaction p-multiplier.

7.5.2 Structural Damping

While a damping ratio of 5% is typically used in practice as the basis for defining the spectral acceleration at the fundamental period of vibration of the wharf structure, the modeling performed in this study revealed that larger damping ratios are required to reasonably predict the peak accelerations at the wharf. This is likely due to the combined effects of radiation damping and the complex soil, pile, and fluid interactions during the dynamic response of pile-supported wharves. Figure 12 shows the time histories of wharf accelerations recorded in centrifuge and simulated in FLAC using 5% and 15% Rayleigh damping ratios defined at a center frequency of 1.25 Hz. The comparison shows that the peak wharf acceleration is overestimated by a factor of 1.4 when using 5% damping (0.4 g compared to 0.28 g), however it is reasonably estimated using 15% damping.

7.6 CONCLUDING REMARKS

A two-dimensional model was developed using the program *FLAC* to simulate the results of a centrifuge test on a pile-supported wharf subjected to liquefaction-induced lateral ground deformations. The purpose of the analysis was to follow commonly used, practice-oriented approaches in 2D modeling of seismic slope deformations with SSI effects, compare the results with measurements from centrifuge tests, and make reasonable modifications to improve the simulation predictions. The soil elements were modeled using the PDMY03 constitute model which was calibrated based on the relative density (D_R) of different soil units and empirical correlations for liquefaction triggering. The pile and wharf deck were modeled using elastic elements and were connected to the soil mesh using p-y springs that were developed generally based on API recommendations with some modifications as listed in Table 3. The primary conclusions of the numerical analyses are summarized as follows:

- The PDMY03 model reasonably captured key soil responses, including the development of excess water pressure, triggering of liquefaction, and post-liquefaction accumulation of shear strains. The transient and permanent soil displacements showed reasonable agreement with centrifuge measurements. The ground surface spectral accelerations at the natural period of the site agreed well with the centrifuge measurements; however, the spectral accelerations at short periods (e.g. PGA) were over-predicted. The rate of pore pressure generation

within the loose soil agreed well with the centrifuge measurements. However, the drainage of excess pore pressure in loose liquefied sand into the rockfill with high permeability was not modeled in simulations which resulted in higher pore pressure ratios in simulations in the vicinity of rockfill.

- The wharf deck peak displacement and acceleration were reasonably captured in simulations. The wharf deck showed a strong transient response (oscillations during the dynamic motion) in the centrifuge test which is attributed to the dynamic response of the centrifuge container.
- The pile lateral responses from simulations (displacements, bending moments, shear forces, and lateral soil reactions) agreed well with centrifuge measurements; however, this agreement is likely due to the availability of lateral load tests which were used in calibration of p-y parameters. In practical applications where such data is not available, it is recommended to consider the uncertainty in p-y properties.
- The first order softening effect of liquefaction on lateral pile response was captured in the analysis here by the soil constitutive model, i.e. no additional liquefaction p-multipliers were used to alter the p-y springs. However, the availability of lateral load tests in this study enabled calibrating the modulus of subgrade reactions in the p-y springs (which were found to be softer than the moduli recommended by API). The sensitivity analysis showed that the peak bending moments are

captured equally well if the p-y springs are modeled based on API in addition to a liquefaction p-multiplier of 0.1 in the loose sand.

- The analysis performed in this study supports the use of higher damping ratios for the structural response, i.e. 15% damping ratio as opposed to the 5% damping ratio that is routinely used in practice. The sensitivity analysis showed that using 5% damping ratio overestimated the peak wharf deck acceleration by a factor of 1.4 while using 15% damping estimated the peak acceleration well both in terms of amplitude and timing.

Table 1. Pile, superstructure, and soil properties and ground motion in centrifuge test NJM01 (in prototype scale)

Test ID	Pile properties	Superstructure properties	Soil properties	Applied ground motions at base
NJM01	Pile D = 0.64 m t = 0.036 m L = 27.2 m EI = 2.1e5 kPa-m^4	Wharf deck 33.7 m × 15.2 m × 0.25 m, mass = 714.8 Mg	Nevada loose sand, D_R = 39% Nevada dense sand, D_R = 82% Rockfill, friction angle = 45 deg	Event 11 - 1989 Loma Prieta Outer Harbor Station scaled to PGA = 0.15g

Table 2. Soil properties in the PDMY03 constitutive model

Model parameters	Loose sand	Lower and upper dense sands	Rockfill
Relative density, D_R [a]	39%	82%	N.A.
Cyclic resistance ratio, $CRR_{\sigma'v=1, M=7.5}$ [a]	0.1	N.A.	N.A.
Density, ρ	1.94 Mg/m^3	2.04 Mg/m^3	2.05 Mg/m^3
Reference mean effective pressure, p'_r	101 kPa	101 kPa	101 kPa
$K_{2,max}$ [a]	38	65	170
Small-strain shear modulus at reference pressure, $G_{max, r}$	69.6 MPa	111.9 MPa	154.7 MPa
Maximum shear strain at reference pressure, $\gamma_{max, r}$	0.1	0.1	0.1
Bulk modulus at reference pressure, B_r	209 MPa	242.5 MPa	206.3 MPa
Pressure dependent coefficient, d	0.5	0.5	0.5
DSS Friction angle, φ_{DSS} [a]	33°	37°	45°
Model friction angle, φ	28.3°	32.4°	42.2°
Phase transformation angle, φ_{PT}	23.3°	27.4°	32.2°
Contraction coefficient, c_a	0.063	0.001	0.001
Contraction coefficient, c_b	5.0	0.5	0.5
Contraction coefficient, c_c	0.2	0.0	0.0
Contraction coefficient, c_d	0.0	0.0	0.0
Contraction coefficient, c_e	0.0	0.0	0.0
Dilation coefficient, d_a	0.15	0.4	0.4
Dilation coefficient, d_b	3.0	3.0	3.0
Dilation coefficient, d_c	0.0	0.0	0.0
Number of yield surfaces, NYS	20	20	20
S_0	1.73 kPa	1.73 kPa	13.0 kPa [b]

[a] These parameters were calculated during calibration of the model and were not directly input to the constitutive model.

[b] A pseudo-cohesion of 15 kPa was added to the soil elements for rockfill (equivalent to 13 kPa in the octahedral space)

Table 3. P-Y relationship properties and modifications

Soil unit	P-Y relationship	Modulus of subgrade reaction	Ultimate strength (P_{ult}) based on	P-multiplier
Loose sand	API Sand	3500 kN/m^3	API Sand with ϕ = 33°	*Pm* = 0.1 in bayward direction
Rockfill	API Sand	5200 kN/m^3	API Sand with ϕ = 45° and pseud-cohesion = 15 kPa	*Pm* = 0.1 in bayward direction
Lower dense sand	API Sand	3500 kN/m^3	API Sand with ϕ = 37°	No p-multipliers

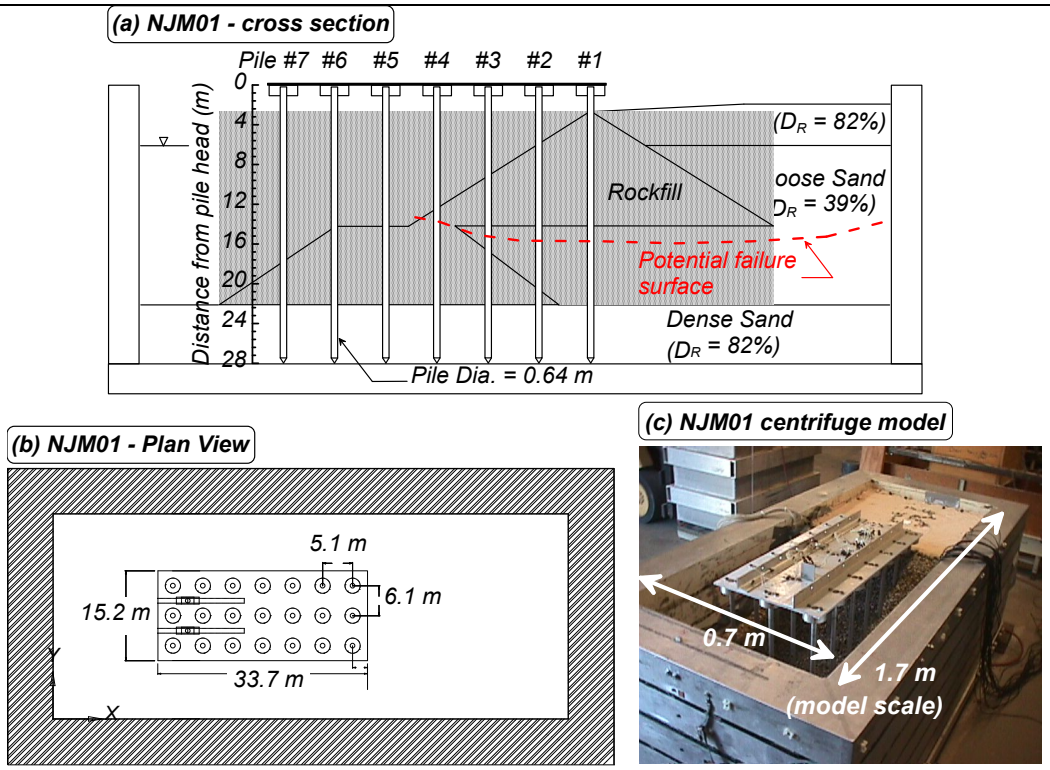

Figure 1. Centrifuge test NJM01 layout properties: (a) Cross section, (b) plan view, and (c) experimental model.

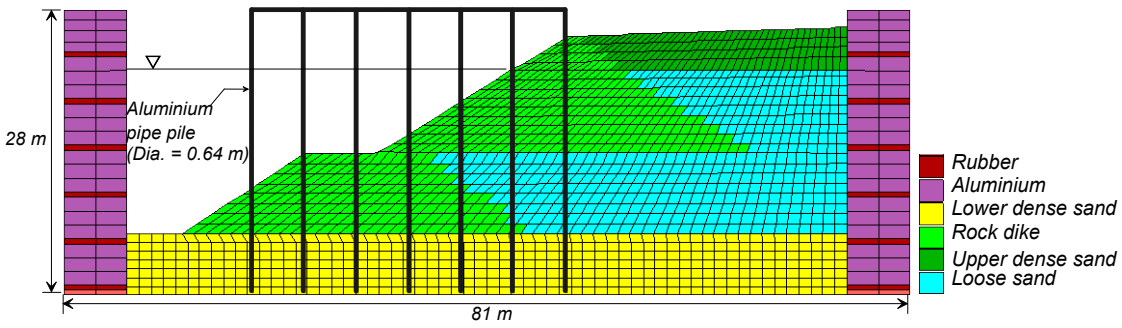

Figure 2. The 2D FLAC model of centrifuge test NJM01.

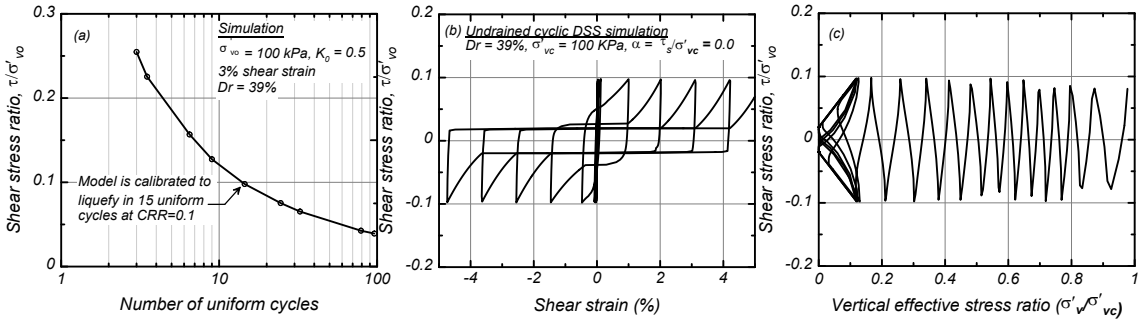

Figure 3. Response of the soil constitutive model in undrained cyclic direct simple shear (DSS) simulation on sand with DR = 39%.

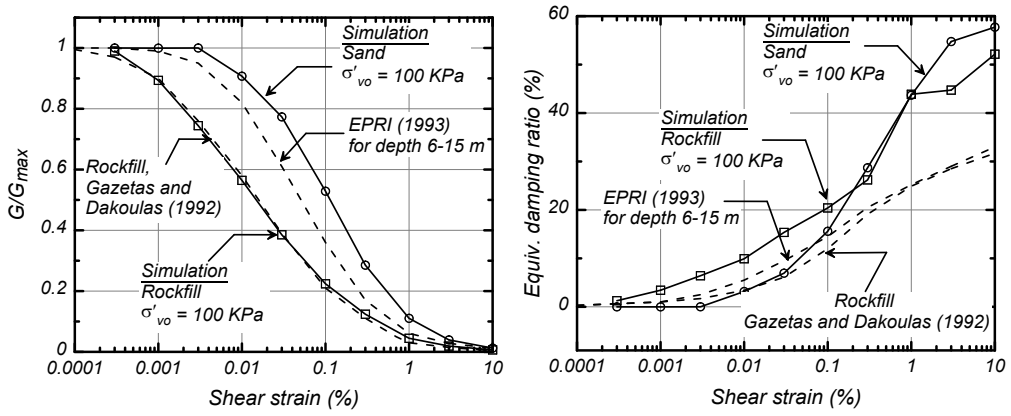

Figure 4. G/Gmax and damping ratios with shear strain in nonliquefied conditions.

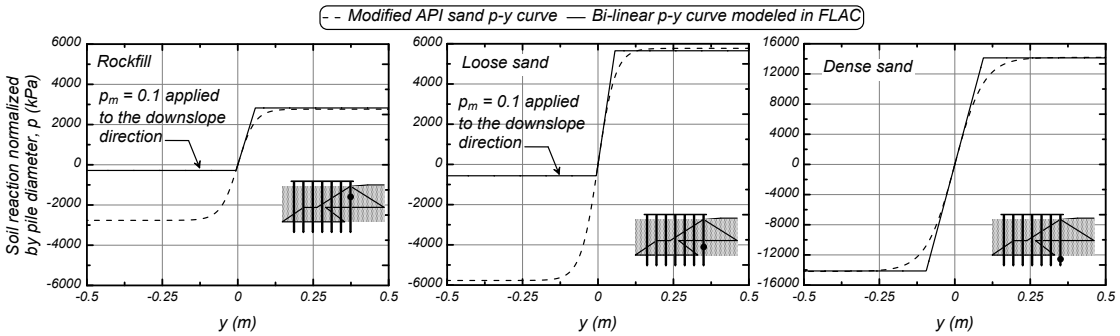

Figure 5. Comparison of target API p-y curves and specified bi-linear p-y curves in FLAC.

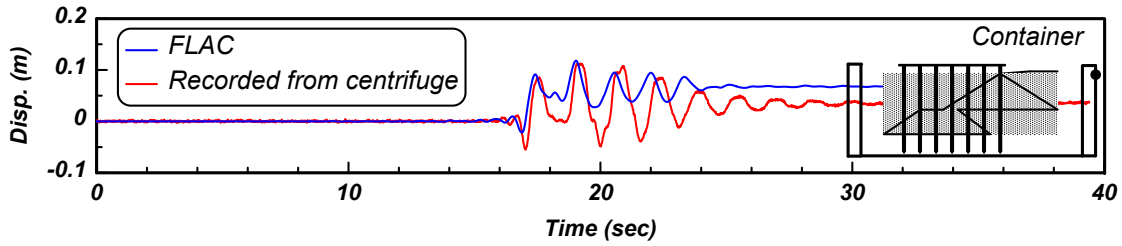

Figure 6. Comparison of lateral displacement of the centrifuge container computed from FLAC against recorded from centrifuge. The location of the sensor is shown on the centrifuge schematic.

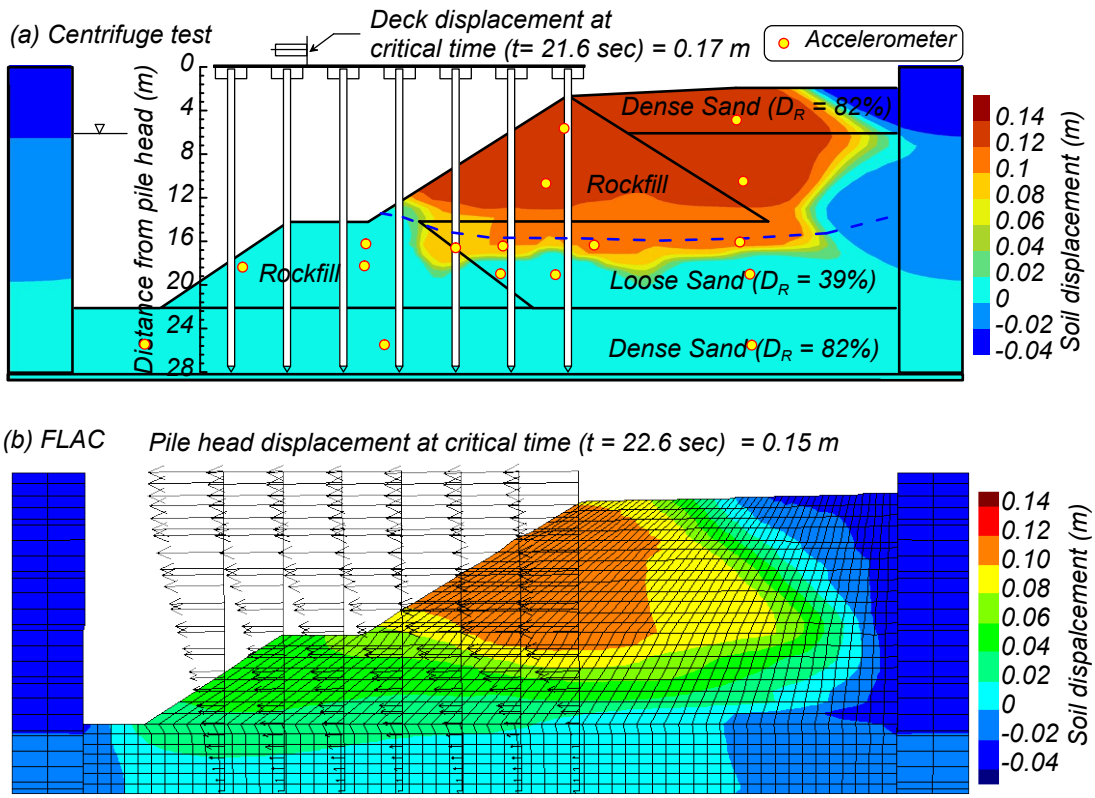

Figure 7. Contour of horizontal soil displacements at the critical time: (a) back calculated from centrifuge test at t = 21.6 sec, (b) computed from FLAC at t = 22.6 sec.

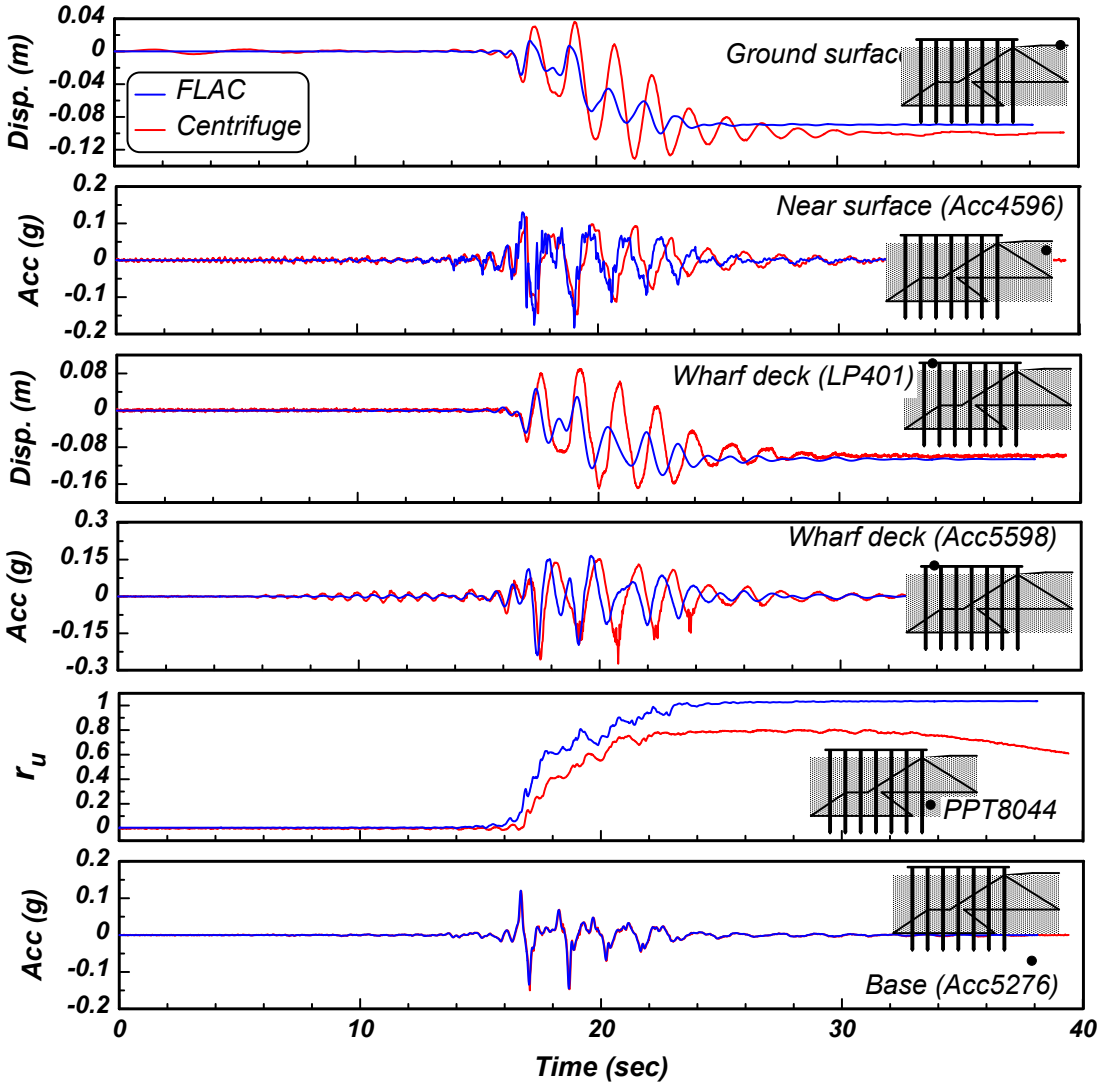

Figure 8. Comparison of measured and computed near-field dynamic response.

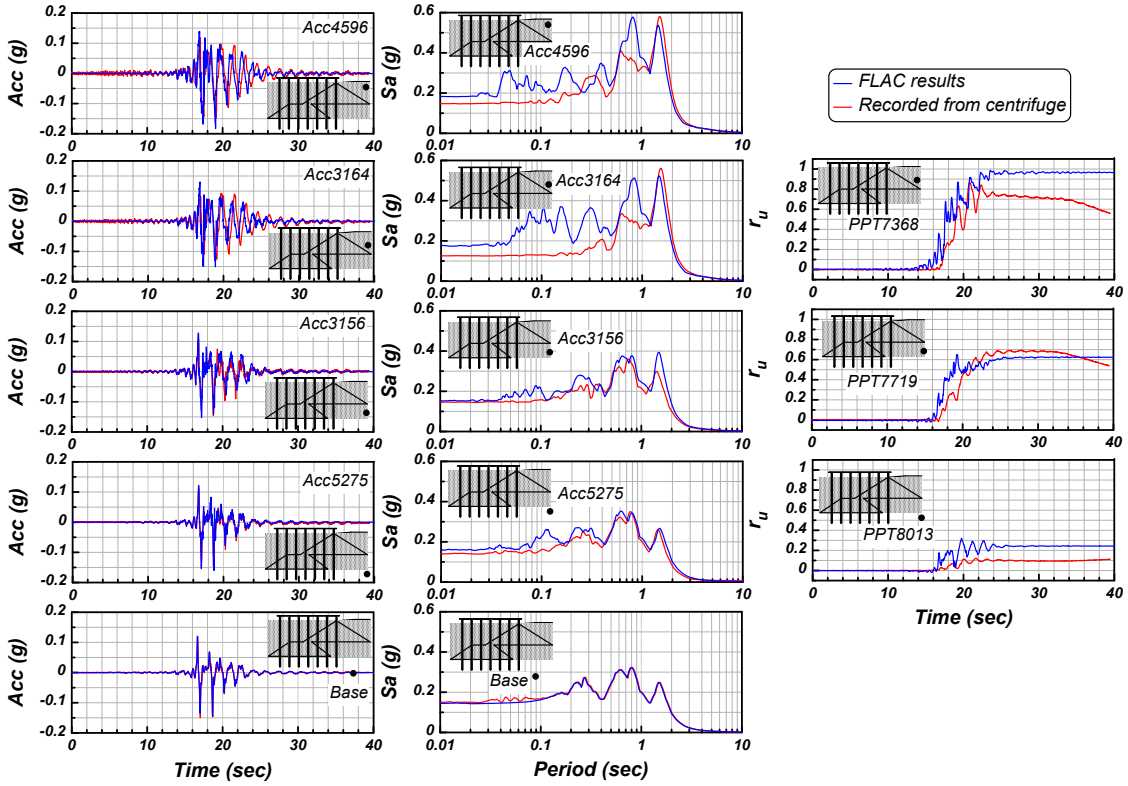

Figure 9. Comparison of measured and computed far-field dynamic soil response

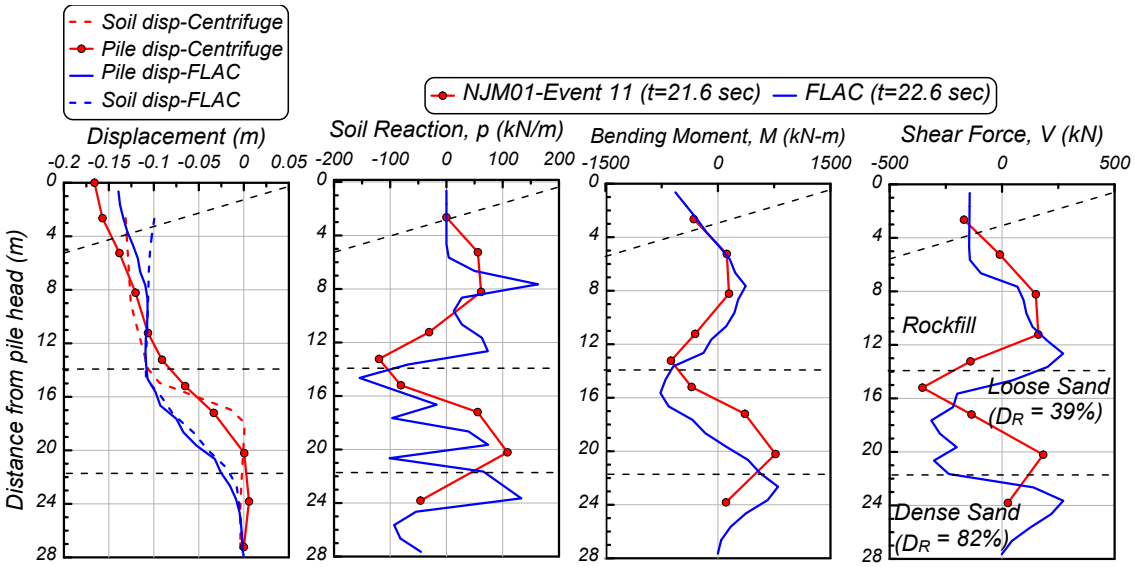

Figure 10. Comparison of profile of soil and pile displacements, soil reactions, bending moments, and shear forces at the critical time recorded from centrifuge test versus computed from FLAC at Pile #1.

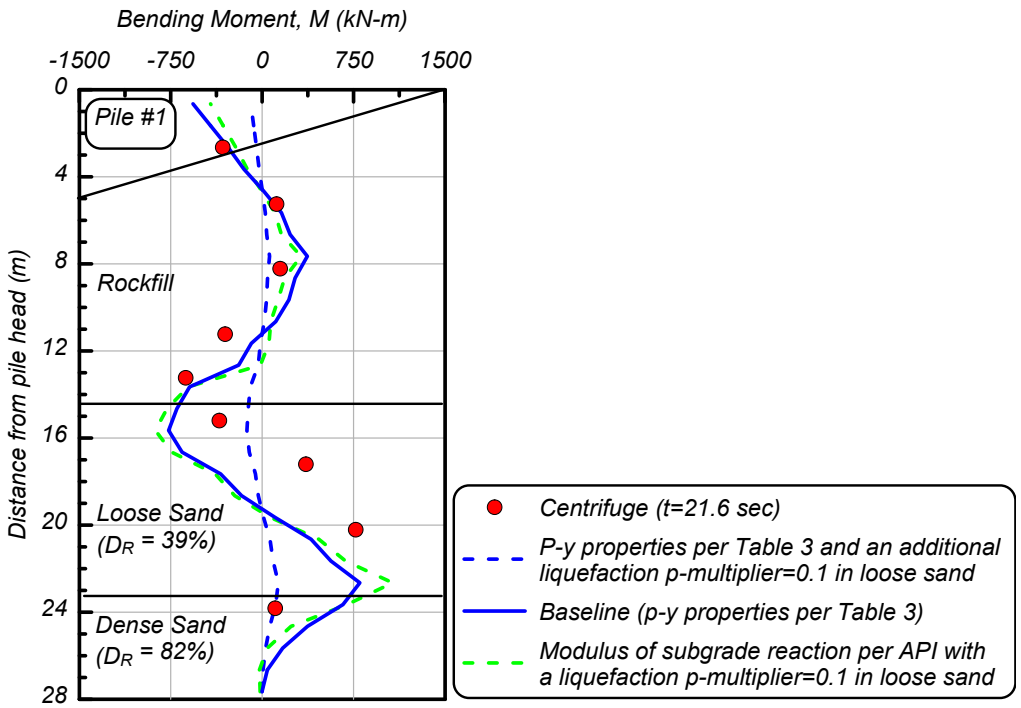

Figure 11. Comparison of bending moment profile in Pile #1 at the critical cycle recorded from centrifuge versus computed from FLAC using different assumptions on p-y spring properties.

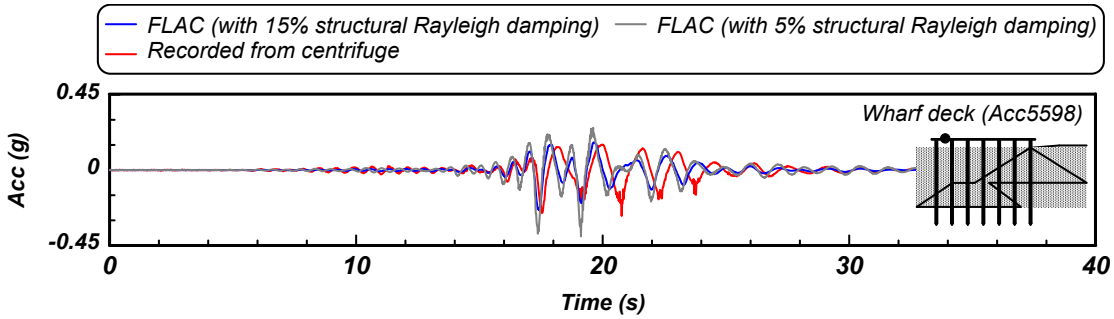

Figure 12. Comparison of wharf acceleration time history recorded from centrifuge versus computed from FLAC using different Rayleigh damping ratios.

REFERENCES

API (American Petroleum Institute), 1993. “Recommended practice for planning, design, and constructing fixed offshore platforms, 20th ed. API RP 2A-WSD.” API Publishing Services, Washington, DC.

Armstrong, R. J., 2010. “Evaluation of the performance of piled bridge abutments affected by liquefaction-induced ground deformations through centrifuge tests and numerical analysis tools.” Ph.D. dissertation, Univ. of California, Davis, CA.

Armstrong, R.J., Boulanger, R.W. and Beaty, M.H., 2013. “Liquefaction effects on piled bridge abutments: Centrifuge tests and numerical analyses.” Journal of geotechnical and geoenvironmental engineering, 139(3), pp.433-443.

ASCE (American Society of Civil Engineers), 2014. “Seismic Design of Piers and Wharves, ASCE/COPRI 61-14.” ASCE Standards Committee on Seismic Design of Piers and Wharves. Reston, Va.: ASCE. https://doi.org/10.1061/9780784413487.

Boulanger RW, Khosravi M, Khosravi A, Wilson DW, 2018. “Remediation of liquefaction effects for an embankment using soil-cement walls: centrifuge and numerical modeling.” Soil Dyn Earthq Eng 114:38–50.

Brandenberg, S.J., 2005, “Behavior of pile foundations in liquefied and laterally spreading ground.” Ph.D. dissertation, University of California, Davis.

Brandenberg, S.J., Zhao, M. and Kashighandi, P., 2013. “Analysis of three bridges that exhibited various performance levels in liquefied and laterally spreading ground.” Journal of geotechnical and geoenvironmental engineering, 139(7), pp.1035-1048.

Caltrans (California Department of Transportation), 2012. “Guidelines for Foundation Loading and Deformation Due to Liquefaction Induced Lateral Spreading.” Sacramento, CA: Caltrans.

Chaloulos, Y. K., Bouckovalas, G. D., & Karamitros, D. K., 2014. “Analysis of liquefaction effects on ultimate pile reaction to lateral spreading.” Journal of Geotechnical and Geoenvironmental Engineering, 140(3), 04013035.

Chang, D., Boulanger, R., Brandenberg, S., & Kutter, B., 2013. “FEM analysis of dynamic soil-pile-structure interaction in liquefied and laterally spreading ground.” Earthquake Spectra, 29(3), 733-755.

Cubrinovski, M., Bray, J. D., de la Torre, C., Olsen, M. J., Bradley, B. A., Chiaro, G., Stocks, E. and L. Wotherspoon, 2017. “Liquefaction effects and associated damages observed at the Wellington Centreport from the 2016 Kaikoura earthquake.” Bull. N. Z. Soc. Earthq. Eng., 50 (2): 152–173.

Dickenson, S.E. and McCullough, N.J., 2006. “Modeling the Seismic Performance of Pile Foundations for Port and Coastal Infrastructure.” In Seismic

Performance and Simulation of Pile Foundations in Liquefied and Laterally Spreading Ground (pp. 173-191).

Elgamal A, Yang Z, Parra E, Ragheb A., 2003 “Modeling of cyclic mobility in saturated cohesionless soils.” Int J Plast;19(6):883–905.

Electric Power Research Institute (EPRI), 1990. “Manual on Estimating Soil Properties for Foundation Design.” Electric Power Research Institute, Palo Alto, California, 308 pp.

Franke, K.W. and Rollins, K.M., 2013. “Simplified hybrid p-y spring model for liquefied soils.” Journal of Geotechnical and Geoenvironmental Engineering, 139(4), 564–576.

Gazetas, G., and Dakoulas, P., 1992. “Seismic analysis and design of rockfill dams: state-of-the-art.” Soil Dynamics and Earthquake Engineering, 11(1), 27-61.

Idriss IM, Boulanger RW., 2008 “Soil liquefaction during earthquakes. Monograph” MNO-12. Oakland, CA: Earthquake Engineering Research Institute; [261p].

Itasca, 2016. “FLAC, Fast Lagrangian Analysis of Continua, User's Guide, Version 8.0.” Minneapolis, MN: Itasca Consulting Group, Inc.

Khosravifar, A., Elgamal, A., Lu, Jinchi, Li, John, 2018. “A 3D model for earthquake-induced liquefaction triggering and post-liquefaction response” Soil Dynamics and Earthquake Engineering, 110, pp. 43–52 https://doi.org/10.1016/j.soildyn.2018.04.008

Liu, L., and Dobry, R., 1995. “Effect of liquefaction on lateral response of piles by centrifuge model tests.” NCEER Bulletin, 91, 7–11.

McCullough, N.J., S.E. Dickenson, B. L. Kutter, and D.W. Wilson, 2000. “Pile-Supported Wharf — Centrifuge Model NJM01. Report No. GEG01-2000.” Oregon State University/University of California at Davis.

McCullough, N., and S. Dickenson. 2004. “The Behavior of Piles in Sloping Rock Fill at Marginal Wharves.” In Proc. Ports Conference 2004, Reston, VA: ASCE. https://doi.org/10.1061/40727(2004)86

McCullough, N. J., S. E. Dickenson, and S. M. Schlechter. 2001. “The seismic performance of piles in waterfront applications.” In Ports Conference 2001, 1–10. Reston, VA: ASCE. https://doi.org/10.1061/40555(2001)83

PIANC (International Navigation Association). 2001. “Seismic Design Guidelines for Port Structures." International Navigation Association Working Group No. 34. A.A. Balkema.

Qiu, Z., Ebeido, A., Almutairi, A., Lu, J., Elgamal, A., Shing, P. B., & Martin, G., 2020. “Aspects of bridge-ground seismic response and liquefaction-induced deformations.” Earthquake Engineering & Structural Dynamics, 49(4), 375-393.

Rathje, E., Bachhuber, J., Cox, B., French, J., Green, R., Olson, S., Rix, G., Wells, D., and Suncar, O., 2010. “Geotechnical engineering reconnaissance of the 2010 Haiti earthquake.” GEER Association, Report No. GEER-021.

Seed, H. B., and Idriss, I. M., 1970. ‘‘Soil moduli and damping factors for dynamic response analysis.’’ Rep. No. UCB/EERC-70/10, Earthquake Engrg. Res. Ctr., University of California, Berkeley, Calif.

Souri, M., Khosravifar, A., Schlechter, S., McCullough, N. and S. E. Dickenson, 2019. “Seismic Performance of Pile-Supported Piers and Wharves Subjected to Foundation Deformations.” In PORTS ’19. Reston, VA: ASCE. https://doi.org/10.1061/9780784482612.058

Souri, M., Khosravifar, A., Schlechter, S., McCullough, N. and S. E. Dickenson, 2020. “Development of experimental p-y curves from centrifuge tests for piles subjected to static loading and liquefaction-induced lateral spreading.” DFI Journal 14 (1), 1–15

Tasiopoulou, P., Ziotopoulou, K., Humire, F., Giannakou, A., Chacko, J. and Travasarou, T., 2020. “Development and implementation of semiempirical framework for modeling postliquefaction shear deformation accumulation in sands.” Journal of Geotechnical and Geoenvironmental Engineering, 146(1), p.04019120.

Wang, S., Kutter, B.L., Chacko, M.J., Wilson, D.W, Boulanger, R.W., and A. Abghari, 1998. “Nonlinear Seismic Soil-Pile Structure Interaction.” Earthquake Spectra 14(2): 377–396.

Werner, S.D. (Editor), 1998. “Seismic Guidelines for Ports.” ASCE Technical Council on Lifeline Earthquake Engineering. Monograph No. 12. March 1998. ASCE, Reston, VA.

Wu, J., 2002. “Liquefaction triggering and post-liquefaction deformation of Monterey 0/30 sand under uni-directional cyclic simple shear loading.” Ph.D. dissertation, Dept. of Civil and Environmental Engineering, Univ. of California, Berkeley

Zhang, G., Robertson, P.K. and Brachman, R.W.I., 2004. “Estimating liquefaction-induced lateral displacements using the standard penetration test or cone penetration test.” Journal of Geotechnical and Geoenvironmental Engineering, 130(8), pp.861-871.

CHAPTER 8

8.0 EFFECTS OF LONG DURATION EARTHQUAKES ON THE INTERACTION OF INERTIAL AND LIQUEFACTION-INDUCED KINEMATIC DEMANDS ON PILE-SUPPORTED WHARVES

Note: The contents in this chapter have been submitted as a technical paper to Soil Dynamics and Earthquake Engineering and is currently under review with the following citation:

Souri, M.; Khosravifar, A.; Dickenson, S. E.; Schlechter, S. & McCullough, N. “Effects of Long Duration Earthquakes on the Interaction of Inertial and Liquefaction-Induced Kinematic Demands on Pile-Supported Wharves.” Soil Dynamics and Earthquake Engineering (under review)

8.1 INTRODUCTION

Lateral ground deformations due to liquefaction or cyclic softening and degradation in foundation soils could cause severe damage to pile foundations (e.g. Hamada et al. 1986, Egan and Wang 1991, Werner et al. 1997, Finn 2005, Rathje et al. 2010, Turner et al. 2016, and Cubrinovski et al. 2017). Pile-supported wharves in liquefiable soils are subjected to kinematic loads due to large lateral ground deformation and inertial load associated with wharf deck seismic response. Uncoupled methods are often used in design where the inertial and kinematic demands on piles are estimated separately. There is currently no consensus in seismic design guidelines on how to combine the inertial and kinematic loads in uncoupled methods. This is due in part to the site- and project-specific nature of the interaction between inertial and kinematic demands as evidenced in varying recommendations provided by maritime and highway transportation agencies (e.g.

ASCE 2014, POLB 2015, POA 2017, AASHTO 2014, MCEER 2003, Caltrans 2012, ODOT 2014, and WSDOT 2015).

It is also recognized that while most design codes do not provide specific recommendations on the effects of earthquake motion duration on the interaction of inertial and kinematic loads, some design codes acknowledge that the two loads are more likely to interact during long-duration motions in large-magnitude earthquakes (e.g. AASHTO 2014 and MCEER 2003). This is particularly important in highly seismic regions like the Pacific Northwest of the United States, where the hazard is predominately associated with a Magnitude 9 earthquake along the Cascadia Subduction Zone, which is expected to produce long-duration ground motions. Khosravifar et al. (2014) and Nasr and Khosravifar (2018) studied the effects of ground motion duration on inelastic pile demands on a relatively stiff large diameter shaft in liquefied soil and found that inelastic pile demands are amplified in long-duration earthquakes due to incremental yielding in the plastic hinge. Dickenson et al. (2014) examined the effects of long-duration motions on the seismic performance of a wharf structure at the Port of Los Angeles in a testbed study and found that plastic hinges in piles (0.6 m concrete piles) formed generally once the ground displacements passed a threshold of approximately 0.3 m. They found that for CLE level motions, this threshold occurred after approximately 4 to 10 seconds of significant shaking and Arias Intensity of 0.9 to 1.2 m/sec. The present study extends the breadth of the previous studies by investigating the effects of ground motion duration on the interaction of inertial and kinematic demands for relatively flexible piles in a pile group that supports a wharf structure.

It will be described later that, unlike large-diameter stiff piles, the performance of small-diameter flexible piles in long duration motions is heavily influenced by kinematic demands and less influenced by inertial demands.

The primary objective of the present study is to investigate the effects of inertial and kinematic load interaction on pile foundations subjected to short- and long-duration earthquake motions. This objective is achieved by first calibrating a numerical model against a centrifuge test on a pile-supported wharf subjected to short-duration earthquake shaking and then subjecting the calibrated numerical model to a suite of spectrally matched ground motions covering a wide range of strong motion durations. The constitutive model parameters were calibrated in order to capture key mechanisms that are important to study the interaction of inertial and kinematic demands. The calibration of the numerical model against the centrifuge test is described in detail in (Souri et al. 2021a) and is not repeated here for brevity. The nonlinear dynamic analyses were performed for three loading cases: (a) a case with combined effects of liquefaction-induced lateral spreading and wharf deck inertia, (b) a case with liquefaction but without wharf deck inertia, and (c) a case with inertia only in the absence of liquefaction. Incremental dynamic analyses were performed by linearly scaling seven motions that were spectrally matched to have the same response spectra. These dynamic analyses provided insights on the effects of motion duration on the contribution of soil lateral spreading and wharf deck inertia in pile demands.

The following sections provide a brief overview of the development of the numerical model. Insights derived from the results of the incremental dynamic

analyses are presented and discussed in detail. Finally, the difference between the interaction of inertial and kinematic demands for small- and large-diameter piles are discussed by comparing the results of the analyses conducted in this study to the results in Khosravifar et al. (2014).

8.2 NONLINEAR DYNAMIC ANALYSIS

8.2.1 Numerical Model and Calibration against Centrifuge Test

A two-dimensional numerical model was developed using *FLAC* numerical modeling software (Itasca, 2016) and was calibrated against key responses for a centrifuge test on pile-supported wharf (Test NJM01 in McCullough et al. 2000). The centrifuge model configuration in this test consisted of a multi-lift rock dike, a dry dense sand layer (relative density, D_R = 82%), overlying a liquefiable loose sand layer (D_R = 39%), overlying a dense sand layer (D_R = 82%). A set of 21 piles in a 7-by-3 configuration support the wharf deck. The piles were made with aluminum pipes having an outer diameter of 0.64 m (in prototype scale). The main objective in the calibration of the numerical model was to reasonably capture key responses that are important to study the interaction of inertial and kinematic demands, such as the amplitude and timing of peak accelerations and peak displacements at the wharf deck and soil surface, triggering of liquefaction in the loose sand, the mechanism of slope failure, and the induced bending moments in piles. Details about the calibration process and comparison of simulations and experiment results are provided in Souri et al. (2021a).

8.2.2 Model Geometry

The calibrated model was modified for the incremental dynamic analysis in this study to better replicate the real field condition. The centrifuge container walls were removed and the right and left boundaries of the model were extended in order to minimize the boundary effects on the cyclic response of the soil adjacent to the wharf. The far boundaries were modeled as free-field conditions. A rock layer with a shear wave velocity (*Vs*) of 760 m/s was added to the base of the model, and input ground motions were applied as outcrop motions using the compliant-base procedure of Mejia and Dawson (2006). The pile properties were changed to nonlinear behavior. The modified model was then subjected to a suite of spectrally matched short- and long-duration motions to investigate the effects of long-duration motions on the interaction of inertial and kinematic demands. Fig. 1 shows the *FLAC* model used in the incremental dynamic analysis. The key characteristics of soil, pile and wharf deck are listed in Table 1.

8.2.3 Soil Constitutive Model

The pressure-dependent multi-yield surface model (PDMY03) was used to model the cyclic shear behavior of sands and rockfill with different relative densities during the earthquake motion. The primary focus in the calibration of the soil model was to capture the triggering of liquefaction and post-liquefaction accumulation of shear strain. The loose sand was calibrated to trigger liquefaction (defined here as 3% single amplitude shear strain) in 15 cycles at a cyclic resistance ratio (CRR) of 0.10 estimated from the correlations by Idriss and Boulanger (2008). The shear

moduli of the soil units were defined based on the Seed and Idriss (1970) relationship, using the K_{2max} values reported in Table 1. The shear wave velocity (Vs) profile calculated using these shear moduli generally agreed with the Vs measurements from the centrifuge test. Details about the input parameters for the soil model are provided in Khosravifar et al. (2018) and Souri et al. (2021a).

8.2.4 Pile Elements

The wharf modeled in this study is supported on a total of 21 piles, configured in three rows in the out-of-plane direction and seven rows in the longitudinal direction. The piles were modeled using pile elements, and the wharf deck was modeled using beam elements with the dimensions and properties listed in Table 1. The pile elements were modeled as inelastic with a bending moment capacity of 600 kN-m to represent the target prestressed concrete piles that are typically used in marginal wharves with similar geometries.

8.2.5 Soil Interface Elements

The structural nodes in the 2D model were connected to the soil elements using nonlinear p-y springs. The p-y spring properties were selected based on American Petroleum Institute (API 1993) recommendations for sand. However, the moduli of the subgrade reaction were modified from API to match the centrifuge results (3500 kN/m^3 for loose sand and 5200 kN/m^3 for dense sand and rockfill). More details on the back-calculation of the moduli of subgrade reaction from the centrifuge tests are provided in Souri et al. (2020). Slope effects on the stiffness of p-y springs were accounted for as described in McCullough and Dickenson (2004).

8.2.6 Damping

A relatively small Rayleigh damping (0.5%) was employed in soil elements at a center frequency of 1.25 Hz corresponding to the natural period of the wharf system, assuming that the main soil damping is produced from the soil nonlinear hysteresis behavior. Past studies have shown the importance of including additional damping to capture the radiation damping and the complex interaction between the soil, structure, and fluid (e.g. Wang et al. 1998). While some studies, have included this damping using distributed dashpots along the piles (e.g. Brandenberg at el. 2013), this damping was approximated in the 2D analysis in this study using an additional Rayleigh damping ratio of 15% only applied to the structural elements. Sensitivity analysis showed that this relatively large damping for structural elements provided a better match between wharf accelerations computed from simulations and recorded in centrifuge test (Souri et al. 2021a).

8.3 INCREMENTAL DYNAMIC ANALYSIS

In order to investigate the effects of ground motion duration on the contribution of inertial and kinematic loads to the pile demands, the calibrated model was subjected to a suite of seven shallow crustal and subduction earthquakes covering a wide range of significant duration ($D_{5\text{-}95}$ ranging from 4 sec to 86 sec). While the intensity measures that incorporate both amplitude and duration of acceleration (e.g., Arias Intensity and CAV) have been shown to be better indicators of liquefaction effects on structures (e.g. Kramer and Mitchell 2006, Dickenson et al. 2014, Bullock et al. 2020), the significant duration ($D_{5\text{-}95}$) is used in this study as a

simple indicator to investigate the interaction of inertial and kinematic demands when subjected to short- and long-duration motions. The seven motions were spectrally matched; therefore, the inertial demands were relatively constant among the seven motions. However, the varying durations provided different magnitudes of kinematic demands. The spectrally matched motions were used for the incremental dynamic analysis (IDA), in which the intensity of ground motions was increased linearly by three different scale factors (creating a total of 21 input motions) to provide varying levels of inelastic demands on piles. Each input motion was used in three loading conditions: (a) combined inertial and kinematic loading, (b) inertial loading only (in the absence of liquefaction), and (c) kinematic loading only (in the absence of deck mass).

8.3.1 Input Ground Motions

The ground motions included a set of seven short and long duration time series which were spectrally matched to the risk-targeted, maximum considered earthquake (MCE_R) spectrum developed using the site-specific ground motion procedures as the basis for the Design Earthquake spectrum of ASCE 61-14 for a site located in Portland, Oregon. The MCE_R seismic hazard level is representative of ground motions having a 2% probability of exceedance in 50 years (i.e., 2,475-year Average Return Period). These motions are indicated as “IDA 1.0” in subsequent plots. The spectrally matched motions were then linearly scaled by factors of 0.6 (IDA 0.6) and 1.5 (IDA 1.5). The scaled ground motions in IDA 0.6 represent the 975-year return period level of shaking which is approximately equal to the Design Earthquake spectrum per ASCE 61-14. The scaled ground motions

in IDA 1.5 were used to impose larger inelastic demands on the piles to evaluate the effects of pile inelasticity on the interaction of inertial and kinematic demands. While, it is acknowledged that the IDA 1.5 motions are significantly larger than the ground motions considered based on ASCE 61-14 for a hypothetical site in Portland, OR, these ground motions are comparable to the design ground motions at the Oregon coast which is approximately 10 km away from the Cascadia Subduction Zone (i.e. the PGA at MCE_R level of shaking is approximately 0.8 g in Astoria, OR); therefore, the IDA 1.5 motions are considered relevant in evaluating the performance of port structures in highly seismic regions. Acceleration response spectra for the three levels of dynamic shaking along with the time histories of the spectrally matched motions are shown in Fig. 2. Using the probability of pulse motions per Hayden et al. (2014), two of the four selected crustal motions contained velocity pulses. Additional details on the selection of ground motions and the matching process are provided in Khosravifar and Nasr (2018) for an investigation of the interaction of inertial and kinematic demands on a bridge structure.

8.3.2 Loading Conditions

Each nonlinear dynamic analysis (NDA) was performed for three loading conditions, as illustrated in Fig. 3. Case A represents the full combination of inertial and kinematic loads, in which liquefaction-induced soil displacements applies kinematic lateral loads on the piles and where the deck mass applies inertial loads during shaking. In Case B, which considers only the inertial load, the loose sand

was modeled as nonliquefiable by setting the contraction parameters in the PDMY03 model equal to zero. In this case, the excess pore pressure generation was precluded, and the model was subjected to minimal kinematic loads. For Case C, in which only the kinematic loads are considered, the inertial effects of the wharf deck were precluded by assigning the mass of the deck to zero. The soil parameters in Case C were kept the same as those in Case A.

The results for the three loading scenarios will provide insights into the relative contributions of the inertial and liquefaction-induced kinematic loads on the overall demand of the pile-supported wharf. However, it should be noted that the interaction of inertia and kinematics is a complex and nonlinear dynamic problem. As triggering liquefaction affects the dynamic response of the soil profile, the magnitude of the inertial demand in the liquefied condition is different from that in the nonliquefied condition. Nevertheless, analyzing the nonliquefied case provides a reasonable estimate of the inertial load–induced demands, which is frequently considered in pile design.

8.3.3 Free-field Site Response

Acceleration response spectra and the corresponding amplification ratios at the ground surface are plotted in Fig. 4 for the loading cases with liquefaction (Cases A and C) and without liquefaction (Case B). The response spectra correspond to the computed horizontal acceleration at the ground surface at a location far away from the wharf (at a distance of 40 meters) as shown by a circle symbol in the schematic in Fig. 4a. The results in this figure are shown for the seven ground

motions in IDA 1.0 (matched to the MCE_R level spectra) as an example. The median PGA is approximately 0.4 g in the nonliquefied condition, and it drops to approximately 0.2 g in the liquefied condition. The spectral accelerations in the condition with liquefaction for periods shorter than 1 sec are noticeably lower than those where liquefaction is absent. The amplification ratios were computed as the ratio of the acceleration response spectra at the ground surface to the outcrop spectra at the base of the model. The mean amplification curve in the absence of liquefaction shows that on average, the maximum amplification occurred at a period of approximately 0.6 sec; in the condition with liquefaction, the maximum amplification occurred at periods greater than 1 sec due to the softening effects from liquefaction. These periods correspond to the natural period of the soil profile in the free-field.

8.3.4 Effects of Liquefaction on Peak Kinematic Demands

Figure 5 shows the peak horizontal ground displacement versus significant duration of the input motion, $D_{5\text{-}95}$ (Fig. 5a) and versus the peak base acceleration (Fig. 5b). The displacements correspond to the ground surface at the backland (approximately 14 m behind the wharf) relative to the base of the model. The plotted data include the results of the analyses performed for the liquefied conditions (Case A) and nonliquefied conditions (Case B) for all ground motions in the incremental dynamic analyses. Data from five centrifuge tests on pile-supported wharves are also included for comparison purposes. Details about the series of five centrifuge tests are provided in McCullough et al. (2001) and the

corresponding centrifuge data reports. As noted in the legend, each centrifuge test includes multiple shaking events with various amplitudes. The ground motions in all five centrifuge tests were short-duration motions (i.e. less than 10 sec). All centrifuge tests represent liquefied conditions except for test SMS02, which includes a single, monolithic rock deck supported by a layer of dense sand and represents a nonliquefiable soil profile. The results of the numerical analysis in *FLAC* are generally comparable to the centrifuge results in the short-duration range (particularly when compared to the first shaking event in NJM01, which was used to calibrate the *FLAC* model). The simulations using long-duration motions provide insights on the effects of motion duration on kinematic effects in liquefied and nonliquefied conditions.

Fig. 5a shows that, as expected, the peak ground displacements (and the corresponding kinematic effects) are significantly larger under liquefied conditions as compared to nonliquefied conditions. The peak ground displacements in the liquefied condition are positively correlated with ground motion duration. This finding indicates that while all the ground motions were spectrally matched, the soil profile incrementally accumulated more shear strains in long-duration motions. It is noted that specifically in the case of 2011 Tohoku motions, significant duration is a poor indicator of significant energy due to multiple sections of strong shaking that are separated in time as shown by Walling et al. (2018). In contrast, the nonliquefied cases show relatively little correlation with motion duration; this is expected, as all seven ground motions were spectrally matched to the same target spectra. It is worth noting that separate limit equilibrium analysis showed that the

yield acceleration is approximately 0.57 g for this slope using nonliquefied soil properties which is larger than the PGA of the input motions indicating that the slope does not yield in nonliquefied conditions which explains the lack of correlation with motion duration.

The variations in the peak ground displacements for a given motion duration shown in Fig. 5a are attributed to the varying intensity of the input motions, as revealed from the plot in Fig. 5b. As expected, the peak ground surface displacements increase with peak base acceleration under both liquefied and nonliquefied conditions. The peak displacements from the simulations reasonably match the distribution of the data from the centrifuge tests for the liquefied cases.

8.3.5 Effects of Liquefaction on Peak Inertial Demands

As shown earlier in Fig. 4, the acceleration response spectra are reduced in the liquefied conditions as compared to nonliquefied conditions. The natural period of the soil-wharf system was approximately 0.9 sec in nonliquefied conditions and elongated to approximately 1 sec in liquefied conditions (as estimated from pushover analyses; Souri et al. 2021b). According to Fig. 4, the spectral accelerations at the mentioned periods of 0.9 sec to 1 sec reduced by a factor of 0.6 to 0.7 due to soil liquefaction. Therefore, it is expected that the peak inertial loads are also reduced due to liquefaction. Fig. 6 shows the ratio of the peak wharf accelerations in liquefied conditions (Case A) to that for nonliquefied conditions (Case B). This ratio is denoted as C_{liq} in this figure and is plotted against (a) significant duration, $D_{5\text{-}95}$, and (b) peak base acceleration. For a majority of the

cases, the C_{liq} ratio is below one, which indicates that the peak inertial demands produced in liquefied conditions are smaller than those in the absence of liquefaction. The C_{liq} shows a slightly increasing trend with motion duration and a slightly decreasing trend with peak base acceleration. The C_{liq} values calculated in this study range from 0.7 to 1.1. For comparison, the C_{liq} values reported by Boulanger et al. (2007) from a series of centrifuge tests for highway bridge foundations range from 0.35 to 1.4 and the C_{liq} values calculated from the results of a series of shake table tests by Tokimatsu et al. (2005) range from 0.2 to 0.3. The wide range of liquefaction effects on peak inertial loads observed in this study and reported in the literature highlights the complex effects of liquefaction on the soil–foundation–structure behavior. These complex behaviors are affected by the timing of liquefaction triggering with respect to the timing of peak inertia as discussed in the next section.

8.3.6 Timing of Liquefaction and Peak Inertia

As described in the previous section, the effects of liquefaction on inertial demands depend on the timing of liquefaction triggering and peak inertial loads — which, in turn, are influenced by the characteristics of input motion, the rate of pore pressure generation and subsequent development of kinematic loads. These effects are discussed in this section with respect to the motion duration. The dynamic responses of the soil and wharf are plotted in Fig. 7 for two motions that are spectrally matched to MCE_R design spectra but have distinctly different durations. The short-duration, shallow crustal motion corresponds to the 1992 Cape Mendocino earthquake (CPM station) and the long-duration subduction motion

corresponds to 2011 Tohoku earthquake (MYGH06 station). Fig. 7 shows the representative time histories of ground surface displacement, wharf deck acceleration and displacement, and excess pore pressure ratio (r_u) in the middle of the loose sand layer (used here to indicate the triggering of liquefaction). The time of the peak response is marked in each plot with a vertical dashed line and a triangle. In the short-duration motion (CPM), the peak wharf acceleration occurred prior to the triggering of liquefaction (3.5 sec versus 9.5 sec.) However, in the long-duration motion (MYGH06), the peak wharf acceleration occurred after liquefaction was triggered (68 sec versus 24 sec). It is also noticeable that while the ground displacements in the long-duration motion continued to accumulate following the triggering of liquefaction and reached a peak value at around 78 sec, those in the short-duration motion did not increase further after liquefaction was triggered. These behaviors are indicative of cyclic mobility and the accumulation of shear strains during cyclic loading. This phenomenon is different than the flow liquefaction reported in other studies, where large lateral spreading displacements develop towards the end of motion due to instability of the slope under a static shear stress. It is also important to note that the peak deck displacements are heavily correlated with the peak soil displacements in both motions for the relatively flexible piles in this study, where the piles follow the soil displacements closely. This behavior may be different when considering relatively stiff piles, such as the large-diameter shafts typically used in highway bridges.

The observations from the example motions in Fig. 7 are summarized for all motions in Fig. 8, where the relative timing of the peak inertial load (indicated by

the wharf deck acceleration) is plotted against the timing of liquefaction triggering and the timing of maximum ground displacement. Fig. 8a shows that the majority of the long-duration motions (those having a $D_{5\text{-}95}$ greater than 26 sec) fall close to or above the 1:1 line, which indicates that peak wharf acceleration occurred after the triggering of liquefaction. In contrast, in short-duration motions, the peak wharf acceleration occurred prior to the triggering of liquefaction.

While it is important to consider the timing of liquefaction triggering, it is equally important to consider the timing of the peak ground displacements, as it was shown in the example time histories in Fig. 7 that the timing of maximum demands on the piles (i.e., peak wharf deck displacement) is highly correlated with the timing of maximum ground displacements. Fig. 8b shows that the maximum wharf accelerations occurred before the ground displacements reached their peak values in all motions studied here (both short- and long-duration motions). This is important, as it will be shown later that for relatively flexible piles, that the wharf and pile behaviors are dominated by the large ground displacements that develop in long-duration motions.

8.3.7 Contribution of Inertial Load During the Critical Cycle

As discussed previously, the peak inertial load occurs at a different time than the peak kinematic load. The relative contribution of the peak inertial load and the peak kinematic load during the critical cycle is characterized in this section using three approaches that are sometimes used in practice. Fig. 9 shows the normalized wharf deck acceleration (acceleration at time t divided by the peak wharf

acceleration) with motion duration. In Fig. 9a, the time *t* was selected at the critical cycle during which the peak transient ground displacement occurred. As suggested by the relatively low acceleration ratios, in most cases, the peak ground displacement and peak wharf deck acceleration are less likely to occur during the same cycle. These low ratios are also affected by the small time lag (approximately 0.1 sec) between the peak deck acceleration and the peak ground displacement during the critical cycle; therefore, as a more conservative approach for design, it is sometimes desirable to select the maximum acceleration that the structure experiences from the time of peak ground displacement until the end of shaking (e.g. maximum deck acceleration between 78 sec and 130 sec for MYGH06 motion in Fig. 7b). Fig. 9b presents the wharf acceleration ratios calculated using the latter approach; the results show noticeably larger ratios than those shown in Fig. 9a. Regardless of the approach used to calculate the wharf acceleration ratio, both figures show an increasing trend with motion duration, indicating that there is a larger likelihood for peak deck acceleration to interact constructively with peak kinematic loads during long-duration motions compared to short-duration motions. Despite the larger likelihood of inertia and kinematic interaction in long-duration motions, it will be shown later that for small-diameter flexible piles, this interaction becomes less relevant to the design of the piles as the magnitude and influence of kinematic loads on relatively flexible piles become significantly larger than the inertial contribution in long-duration motions.

Figure 10 shows an alternative approach to characterize the interaction of inertial loads and kinematic demands. The calculated normalized wharf deck acceleration

(acceleration at time *t* divided by the peak wharf acceleration) shown in this figure occurs at the time when the pile bending moments are at their maximum. Data from the first shaking event in the five centrifuge tests are presented in this figure as well. First, key locations where large bending moments developed among all piles were determined. The locations of large bending moments were generally located at the connection of pile head and the wharf deck, at the boundary between rockfill and loose sand, and the boundary between loose sand and lower dense sand. Then, the wharf accelerations were extracted at the time when the bending moment in each key location was at the peak value (the maximum bending moments did not necessarily occur at the same time in all locations). Finally, the extracted wharf accelerations were normalized by the peak wharf acceleration. For plotting purposes, only the average of all acceleration ratios is plotted for each ground motion and centrifuge test in this figure.

For the short-duration motions (those with a $D_{5\text{-}95}$ shorter than 10 sec), the *FLAC* simulations suggest acceleration ratios ranging between 0.45 to 0.85, which are within the range observed in centrifuge tests NJM01, NJM02 and SMS01 which had soil profiles that were similar to the one modeled in the *FLAC* simulations. It is noticeable that centrifuge tests SMS02 and JCB01 show acceleration ratios of approximately 0.95; these ratios are significantly larger than those in the other tests. The difference is attributed to the very different soil profiles in these two tests as compared to the others, which highlights the site- and project-specific nature of the interaction of inertial and kinematic demands. The soil profiles in NJM01, NJM02, SMS01, and *FLAC* simulations are characterized as configurations that

include deep-seated liquefaction underlying significant non-liquefiable crust (i.e. rockfill), while the soil profiles in SMS02 and JCB01 are characterized as configurations that include generally smaller kinematic demands/loads associated with either non-liquefiable profile or weak/softened soils closer to the ground surface, and thin non-liquefiable crust (i.e. sliver rockfill). More details about the dependency of the inertial contribution factors to the soil profiles in the centrifuge tests are provided in Souri et al. (2021b).

The computed acceleration ratios in Figure 10 are also comparable to the fraction of the maximum inertial load with liquefaction that occurs at the critical loading cycle (C_{cc}) values recommended by Boulanger at al. (2007), which range from 0.65 to 0.85 as marked by the dotted dashed line in Fig. 10. Similar to Fig. 9, the data from the incremental dynamic analyses presented in this figure suggest that the acceleration ratios increase with the duration of motion.

8.3.8 Contribution of Inertial and Kinematic Demands on Overall Wharf Response

The relative contribution of inertial and kinematic demands on the overall wharf response was evaluated by performing the incremental dynamic analyses for three load conditions. The schematics of the three loading conditions presented earlier in Fig. 3 include combined inertial and kinematic effects (Case A), inertial loading only in the absence of liquefaction (Case B), and kinematic loading only in the absence of wharf deck inertia (Case C). Soil–foundation–structure interaction with liquefaction is a highly nonlinear problem and the effects of inertial and kinematic

demands cannot be truly decoupled. However, the three loading conditions analyzed here provide an insight on the relative contribution of each demand on the overall responses. This modeling approach was also used in Khosravifar et al. (2014) to evaluate the behavior of single-pile bridge foundations in liquefiable soils.

In Fig. 11, the maximum wharf deck displacements in the three loading conditions are compared against input motion duration for IDA 0.6, 1.0 and 1.5. As indicated by the fitted curves shown by the dashed lines, the pile demands in liquefied cases (with or without inertial loads) increase with the duration of motion, whereas the pile demands in the nonliquefied case (inertia only) show no correlation with motion duration. This is somewhat expected, considering that the ground motions used in these analyses are spectrally matched to the same target spectra. For the short-duration motions, the inertial demands are smaller but comparable to the demands in the analyses for kinematics only and the combined case. In contrast, for long-duration motions, the demands in the combined case are much larger than the inertial demands and are primarily governed by the kinematic demands. This finding suggests that despite the higher likelihood of interaction between the inertial and kinematic loads in long-duration motions (as shown previously in Figures 9 and 10), the contribution of the inertial loads in the overall demands is much smaller, and the kinematic demands seem to govern the design. This finding highlights the differences in the assumptions that need to be made in combining the inertial and kinematic demands when designing for short-duration or long-duration events.

The data in Fig. 11 are replotted in Fig. 12 to provide more insight on the relative contribution of inertial and kinematic loads in the overall demands on the wharf. The horizontal axes in the top two plots in this figure show the maximum deck displacements under the combined effects of inertial and kinematic loads (Case A). The vertical axes in Figs. 12a and 12b show the maximum deck displacements under inertial loads only (Case B) and under kinematic loads only (Case C), respectively. Fig. 12a shows that the maximum deck displacements could be significantly underpredicted (by an average factor of 0.33) by only considering the inertial effects in the absence of liquefaction. Fig. 12b shows that the maximum deck displacements could be slightly underpredicted (by an average factor of 0.9) by only considering the kinematic effects. It will be shown in the next figure that these ratios are correlated with motion duration.

The horizontal axes in Figures 12c and 12d show the significant duration of input motion $D_{5\text{-}95}$, and the vertical axes show the ratio of maximum deck displacements in the inertia only (Case B) or kinematics only (Case C) versus those considering combined inertial and kinematic loading (Case A). Fig. 12c shows that as the motion duration increases, the contribution of inertial loads to the overall wharf demands decreases. On the other hand, Fig. 12d shows that the contribution of kinematic loads on the overall wharf demands slightly increases with motion duration. The response of the wharf structure modeled here is heavily influenced by kinematic demands, as the relatively flexible piles tend to follow the pattern of ground deformations; these deformations increase with motion duration such that in long-duration motions, the wharf demands become primarily governed by

kinematic loads and less so by inertial loads. This response contrasts with that for large-diameter pile shafts that are typically used for highway bridge structures, where the kinematic loads on piles do not increase further once the relative displacements between the pile and soil exceed a certain value (i.e., y_{ult} in p-y springs).

The relative contribution of inertial and kinematic demands for a wharf subjected to short- and long-duration motions is examined further using the two motions shown in Fig. 13. The time histories of the wharf deck displacements are plotted for the combined inertial and kinematic loads (Case A) as well as for inertia only (Case B) and kinematics only (Case C) and are compared for a short-duration motion (CPM) and a long-duration motion (MYGH06). The magnitude of maximum deck displacements under inertial load only (Case B) are similar in both motions (i.e. 0.09 m), as both motions are spectrally matched to MCE_R spectra. The wharf displacements under kinematic load only (Case C) closely follow the pattern in the combined case (Case A) in both motions. However, the magnitude of displacements in Cases C and A are much larger for the long-duration motion than for the short-duration motion. As shown in the time histories for the long-duration motion, the structure continues to experience strong inertial cycles throughout the motion (note the large inertial cycles at around 70 sec), however the relative contribution of these loads becomes less significant as the kinematic demands begin to dominate the wharf response.

8.4 DISCUSSION

In this section, the differences and similarities between the inelastic response of a wharf structure modeled in this study supported on relatively flexible, small diameter group of piles under combined inertial and kinematic loads and the response of an intermediate bridge bent supported on a single large diameter (2-m) RC shaft are discussed. The data used for the large-diameter case are results from a 2D numerical analysis in a multi-layer soil profile (5 m non-liquefiable crust, overlying 3 m liquefiable soil, overlying 12 m non-liquefiable competent soil in a gently sloped ground) from Khosravifar et al. (2014). The results of over 2000 nonlinear dynamic analyses are presented in Fig. 14a, in which the horizontal axis of the plot indicates the earthquake duration, and the vertical axis indicates the ratio of maximum deck displacement under combined loading (Case A), divided by the summation (linear superposition) of maximum deck displacements under inertia only (Case B) and kinematics only (Case C). The results of the dynamic analyses performed in this study for pile-supported wharves is shown in Fig. 14b. Higher ratios on the vertical axes in these two figures indicate more interaction between inertial and kinematic loads. Ratios higher than one indicate the amplification of demands due to the interaction of inertial and kinematic loads to the extent where maximum displacements under combined loading are larger than the linear superposition of demands (i.e. maximum displacement in Case B plus maximum displacement in Case C).

The results of the dynamic analyses for both types of structures show that the interaction of inertial and kinematic loads increases slightly with motion duration.

However, an alarming number of cases of large-diameter shafts show that the combination of inertia and lateral spreading would excessively amplify the inelastic demands to the point where structure collapse would occur. We found that most cases involving collapse (which are indicated by red squares in Fig. 14a) correspond to long-duration and high-intensity motions characterized by a cumulative absolute velocity (CAV_5) greater than 3 g/s. Two cases were selected for further analysis as shown in Fig. 15:

- The 1999 Hector Mine earthquake (M 7.1) scaled to a PGA of 0.6 g featured short-duration motion, where demands under combined loading can be reasonably estimated by linear superposition (summing) of demands from individual loads alone (with no amplification).
- The 1999 Chi-Chi earthquake (M 7.6) scaled to a PGA of 0.4 g featured long-duration motion, where the structure collapsed under combined loading even though its performance under individual loads was satisfactory.

A possible explanation for the fundamentally different responses is that the combination of cyclic inertia and semi-static downslope lateral spreading load resulted in incremental yielding (ratcheting) in the plastic hinge during the long-duration motion, as shown in Fig. 15. In this figure, input acceleration time histories are plotted for the short-duration and long-duration motions (note the significant difference in the durations of these motions). A plastic hinge formed at the bottom of the liquefied layer at a depth of 8 m (4 diameters) in both cases. The moment–

curvature in the plastic hinge is plotted in Fig. 15 (*center*). The incremental yielding in the plastic hinge results in excessive inelastic deformation to the point where the additional moments from the structure gravity (the p-Δ effect) exceeds the moment capacity of the pile, resulting in eventual collapse.

The collapse mechanism described for the large-diameter single shafts supporting an intermediate bridge bent was not observed in the analyses performed for the wharf structure supported by a group of small-diameter piles. This is attributed to the redundancy in the load-carrying mechanism in the pile group supporting the wharf deck and the lack of overlap in the location of plastic hinges from inertial and kinematic loads. Fig. 16 shows the locations of the plastic hinges formed in the wharf structure during the dynamic analysis under inertia only (Case B) and under kinematics only (Case C). In Case B, the plastic hinges formed in Piles 1, 2, and 3 at the deck level and shallow locations (<10*D*) below the ground surface, which is above the typical depth of fixity for piles loaded at top (Fig. 16a). The remaining piles remained elastic in this analysis. In Case C, most plastic hinges formed at greater depths (>10*D*) mostly at the boundaries between the loose liquefied sand, the rock dikes, and the lower dense sand (Fig. 16b). This figure indicates that there is no overlap between the location of plastic hinges that form due to deck inertial loads in the absence of liquefaction (Case B) and those in Case C, where the model is only subjected to the kinematic soil displacements due to liquefaction. This observation provides a possible reason for the differences between the amplification of inelastic demands in large-diameter single shafts supporting bridge

bents and small-diameter pile groups supporting wharf structures subjected to combined inertial and kinematic loading.

8.5 CONCLUDING REMARKS

A calibrated two-dimensional model of a pile-supported wharf was used in nonlinear dynamic analyses to investigate the effects of earthquake duration on the interaction of inertial loads and liquefaction-induced lateral spreading loads. The calibration process was performed against a centrifuge test and is presented in Souri et al. (2021a). The 2D model was subjected to a suite of spectrally matched ground motions with varying motion durations to evaluate the relative contribution of inertial and kinematic loads on the response of the wharf. The analyses were performed for three loading conditions including combined effects of inertial loads from the wharf deck and kinematic ground deformations, inertial load only in the absence of liquefaction, and kinematic load only in the absence of deck mass. The primary conclusions of the numerical analyses are summarized as follows:

- The deck displacement demands due to combined effects of inertial and kinematic loads in liquefied conditions were larger than the demands due to inertial loads only in non-liquefied conditions.
- It was recognized that the response of the wharf supported on relatively flexible piles was heavily influenced by lateral soil displacements. The lateral soil displacements were found to be strongly correlated with motion duration due to accumulation of shear strain in liquefied soil in

many loading cycles. Consequently, the wharf demands were found to be strongly correlated with motion durations as well even for the spectrally matched ground motions with almost identical response spectra.

- The wharf demands in non-liquefied conditions were primarily driven by the inertial loads associated with the deck mass and did not vary with motion duration for the spectrally matched motions used in this study. This was due, in large part, to the small seismically-induced slope deformations computed for the non-liquefaction cases.

- For the wharf structure modeled in this study, the occurrence of liquefaction reduced the peak inertial load from the wharf deck in most cases (C_{liq} parameters ranged from approximately 0.7 to 1.1) and showed a slightly increasing trend with motion duration.

- The analyses in this study suggest that the likelihood of inertial load interacting with kinematic load (characterized by the ratio of inertial load at the critical cycle to the peak inertial load during the entire motion) increased with motion duration. However, it was found that the behavior of wharf structures supported on relatively flexible, small-diameter piles, such as the ones studied here, is heavily influenced by the kinematic loads in long duration motions and less so by the inertial loads.

- Comparison of data produced in this study for wharf structures supported on small-diameter pile groups and those by Khosravifar et al.

(2014) for intermediate bridge bents supported on large-diameter single shafts highlights the similarities and differences in the dynamic response under combined inertial and kinematic loads. It was found that for both types of structures, the interaction of inertial and kinematic loads slightly increases with motion duration. The excessive incremental yielding (ratcheting) in the plastic hinge in large-diameter single shafts during long-duration motions was found to be the reason for cases where the structure collapsed under combined loads but performed satisfactory under both inertial load only and kinematic load only conditions. In contrast, the lack of excessive yielding in pile-supported wharves subjected to long-duration motions was attributed to the lack of overlap between the plastic hinges that form due to inertial loads versus kinematic loads as well as the redundancy in the lateral and vertical load carrying mechanisms (i.e., the plastic hinge development at depth in a row of piles for a wharf does not necessarily lead to collapse of the structure). It was observed that the inertial loads tend to develop plastic hinges at pile head and shallow depths (<10*D*) on landward piles and kinematic loads tend to develop plastic hinges at deeper locations (>10*D*) for the soil profile and geometries studied here.

- The results of numerical analyses and centrifuge experiments used in this study suggest that design recommendations for highway bridge foundations that consist of single drilled shafts or small group of large

diameter piles should be used judiciously when applied to wharves structures supported on large number of usually smaller diameter piles.

Table 1. Pile, superstructure, and soil properties

Pile properties	Superstructure properties	Soil properties
Pile D = 0.64 m t = 0.036 m L = 27.2 m EI = 2.1e5 kPa-m^4 Yield moment, My = 600 kN-m Out-of-plane spacing = 6.1 m [a]	Wharf deck 33.7 m × 15.2 m × 0.25 m, mass = 714.8 Mg Out-of-plane spacing = 6.1 m [b]	Nevada loose sand, D_R = 39%, friction angle = 33°, K_{2max} = 38, CRR = 0.10, ρ = 1.94 Mg/m^3 Nevada dense sand (upper dense sand), D_R = 82%, friction angle = 37°, K_{2max} = 65, CRR = N/A (Nonliquefiable), ρ = 2.04 Mg/m^3 Nevada dense sand (lower dense sand), D_R = 82%, friction angle = 37°, K_{2max} = 56, CRR = N/A (Nonliquefiable), ρ = 2.04 Mg/m^3 Rockfill, friction angle = 45°, K_{2max} = 170, CRR = N/A (Nonliquefiable), ρ = 2.05 Mg/m^3 Base rock (elastic half space), Vs = 760 m/s, ρ = 2.04 Mg/m^3

[a] The piles were modeled using the actual pile properties, and the spacing was set to 6.1 m.
[b] The deck was defined with 1/3 of the actual total mass to account for 3 rows of piles, and the spacing was set to 6.1 m which was the pile spacing in the out-of-plane direction.

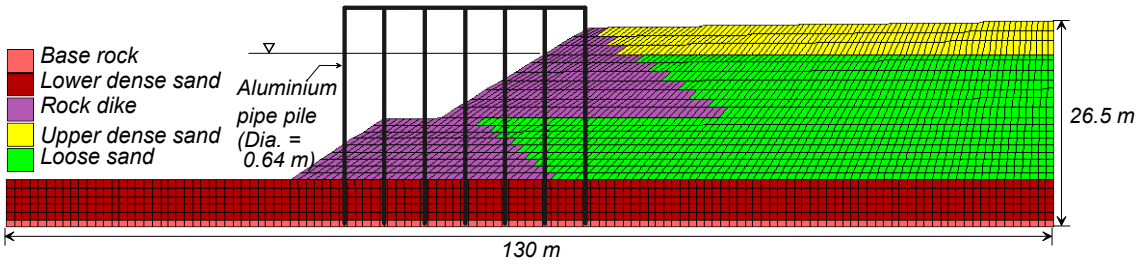

Figure 1. Soil mesh discretization and material zones in the FLAC model used for incremental dynamic analysis.

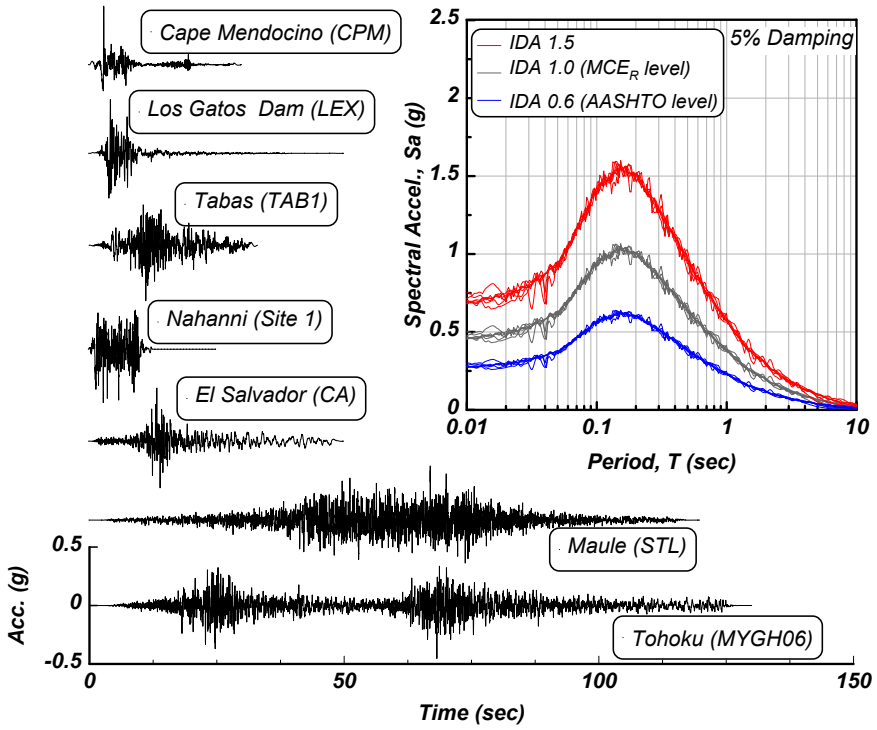

Figure 2. Spectrally matched input motions used in the incremental dynamic analyses.

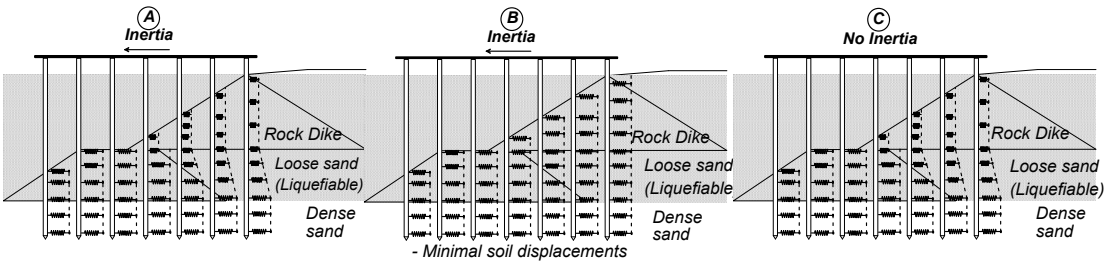

Figure 3. Schematic of three loading conditions in nonlinear dynamic analysis: (a) combined inertia and kinematics, (b) inertia only in the absence of liquefaction, and (c) kinematics only in the absence of deck mass.

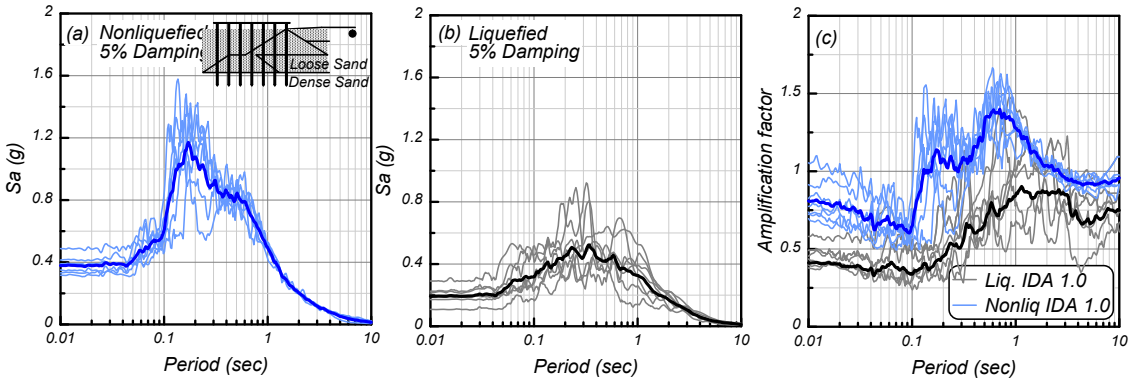

Figure 4. Acceleration response spectra (5% damping) and amplification factor at the ground surface for (a) nonliquefied and (b) liquefied conditions; (c) amplification ratios with and without liquefaction. All three plots correspond to the seven ground motions i

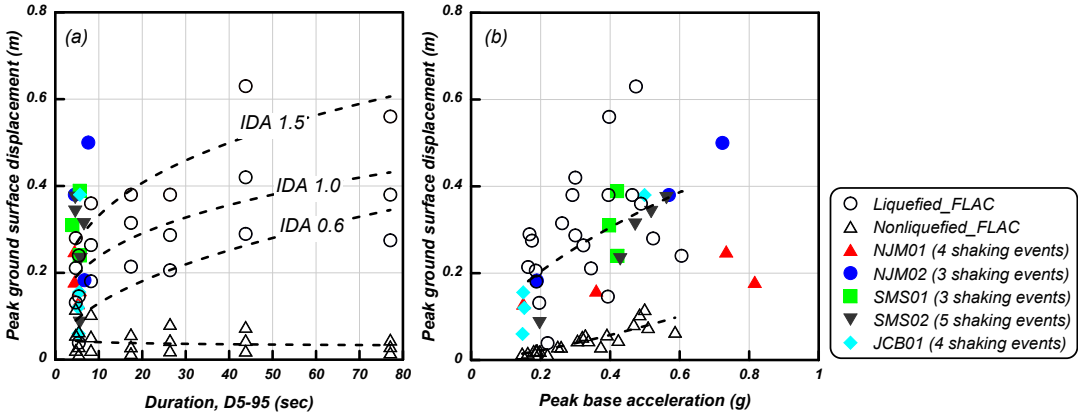

Figure 5. Peak ground surface displacement against: (a) significant duration, D5-95, and (b) peak base acceleration for all motions in the incremental dynamic analyses along with data from five centrifuge tests.

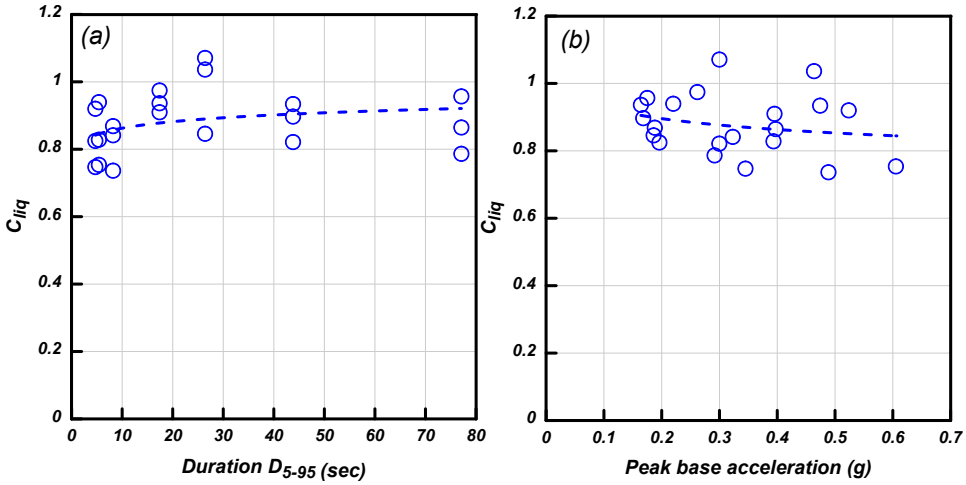

Figure 6. Dependence of the Cliq ratio on (a) ground motion duration (D5-95) and (b) peak base acceleration.

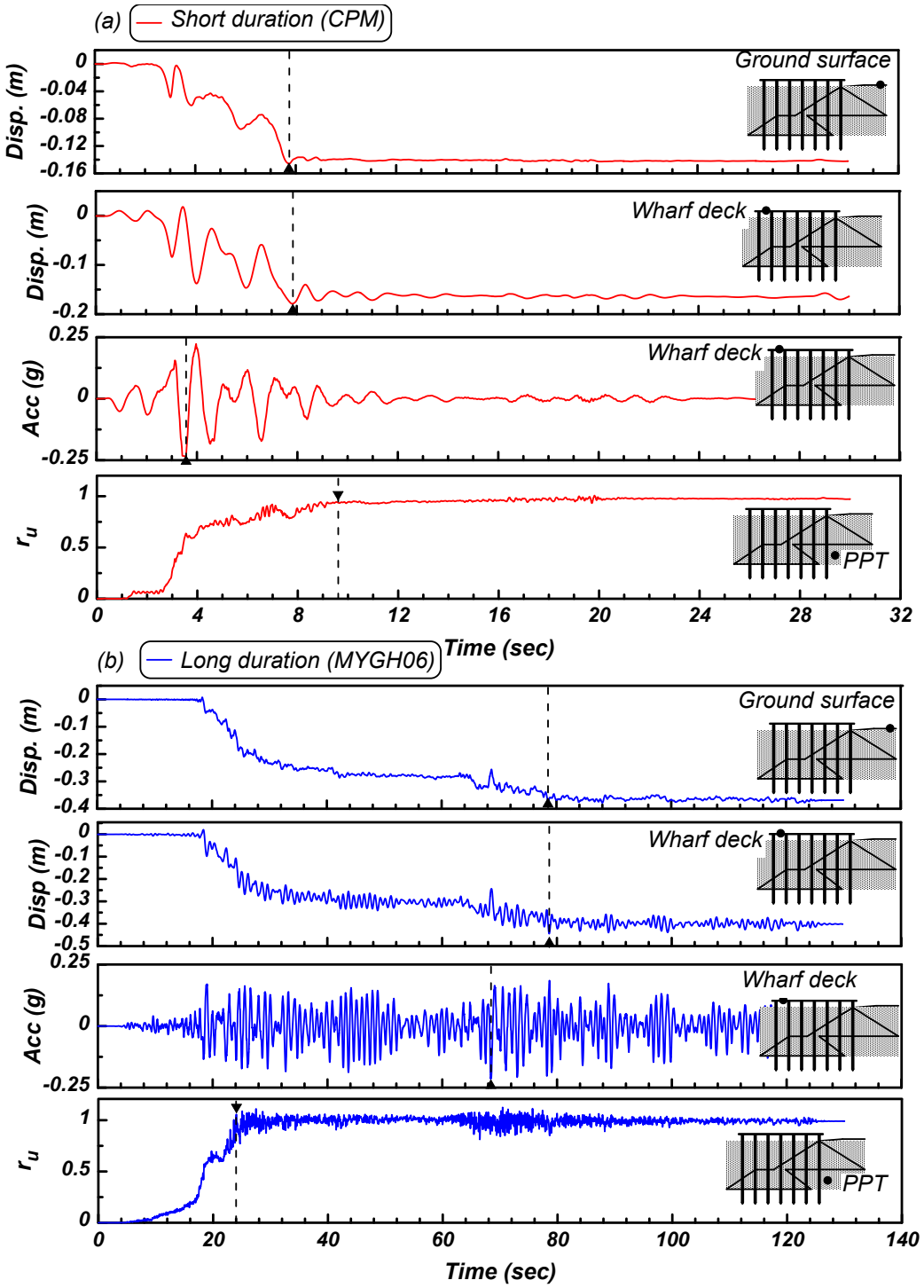

Figure 7. Representative dynamic time histories for piles subjected to combined inertial and kinematic loads in (a) short-duration motions and (b) long-duration motions.

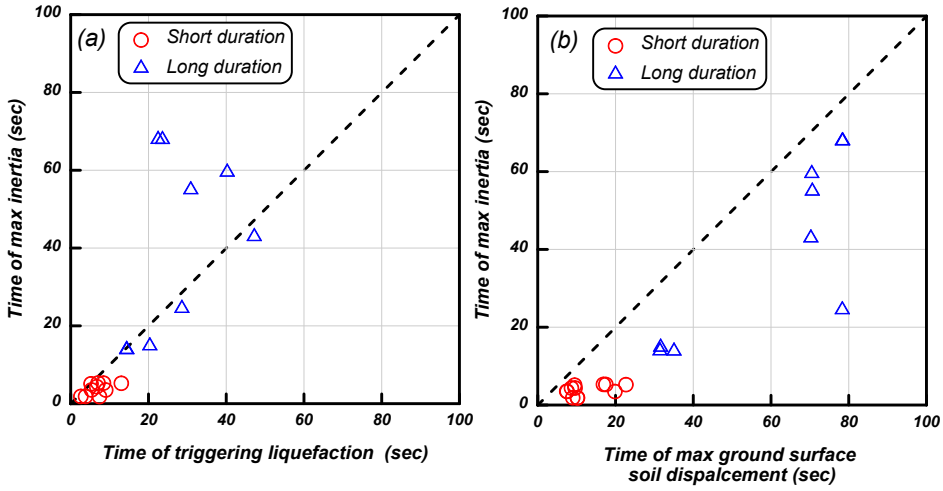

Figure 8. Time of maximum wharf deck acceleration versus (a) time at which liquefaction is triggered, and (b) time of maximum ground surface displacement.

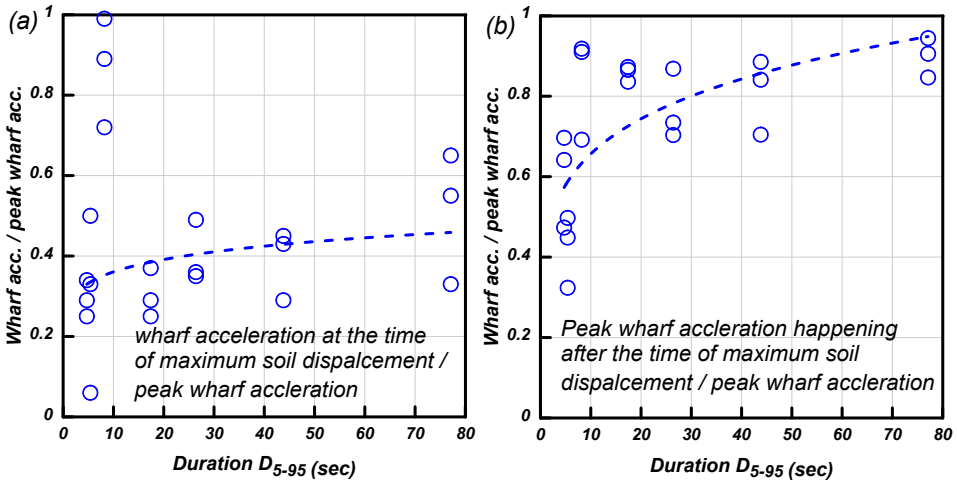

Figure 9. Normalized wharf deck accelerations against significant motion duration (D5-95): (a) at the time of peak soil displacements, and (b) following the time of peak soil displacements

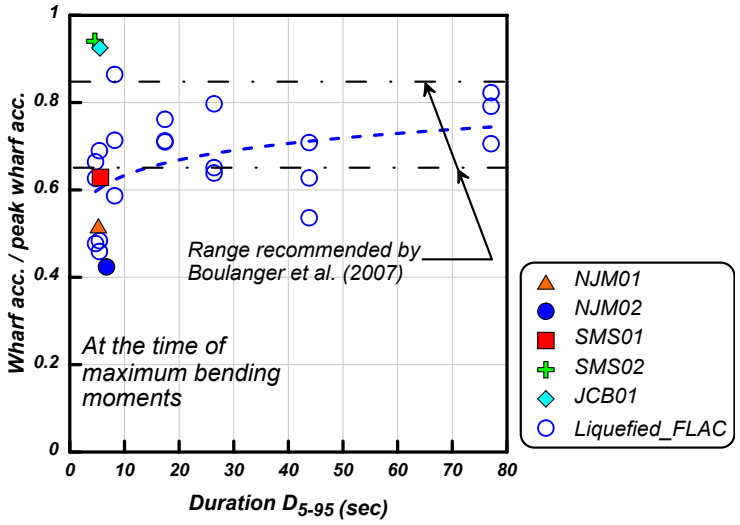

Figure 10. Normalized wharf deck accelerations against significant motion duration (D5-95) at the time of maximum pile bending moments

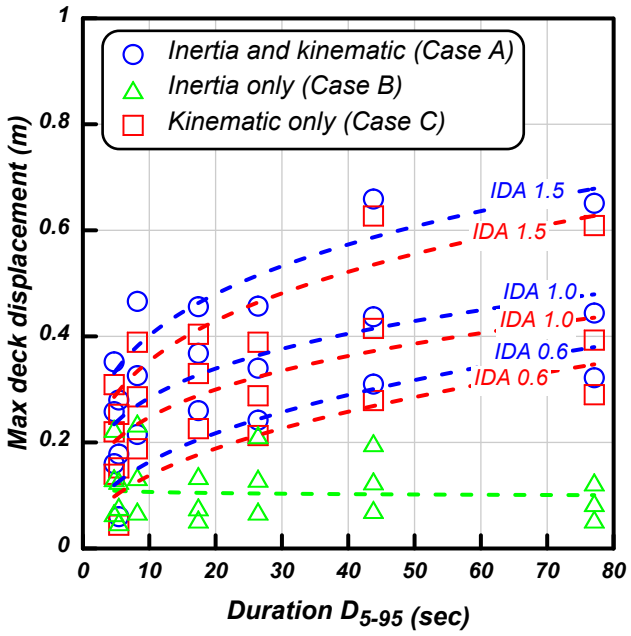

Figure 11. Comparison of maximum wharf deck displacement against motion duration for combined inertia and kinematics (Case A), inertia only (Case B), and kinematics only (Case C).

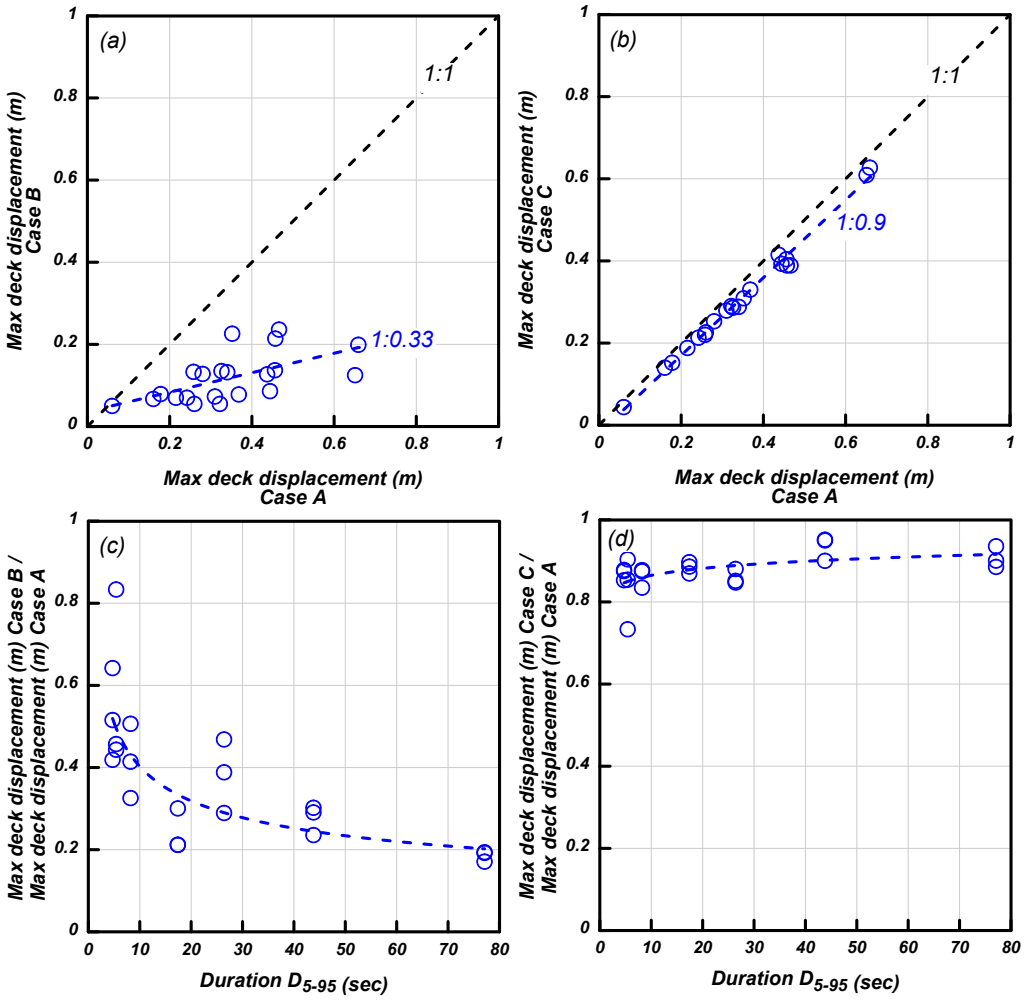

Figure 12. Comparison of maximum wharf deck displacement in incremental dynamic analyses for combined inertia and kinematics (Case A), inertia only (Case B), and kinematics only (Case C).

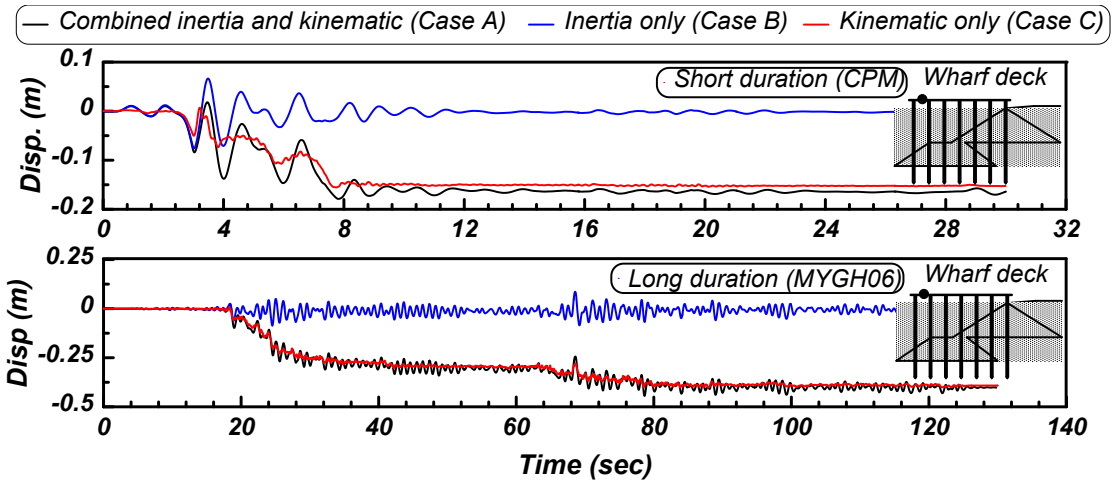

Figure 13. Comparison of wharf deck displacements in a short and long-duration motions for the cases of combined inertia and kinematic (Case A), inertia only (Case B), and kinematic only (Case C).

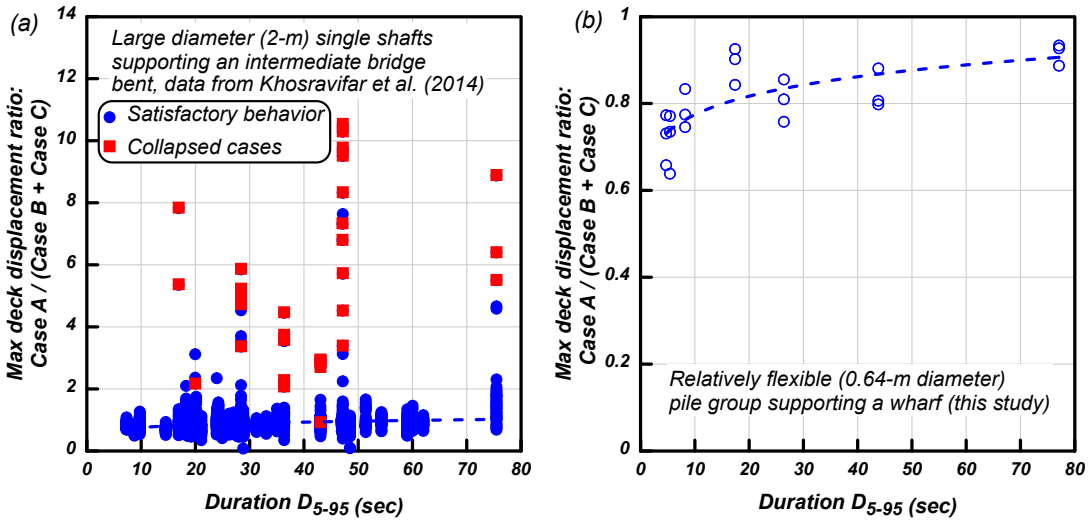

Figure 14. Amplification of deck inelastic displacements due to the interaction of inertial and kinematic demands with respect to motion duration for (a) large-diameter single piles supporting an intermediate bridge bent and (b) relatively flexible pile groups sup

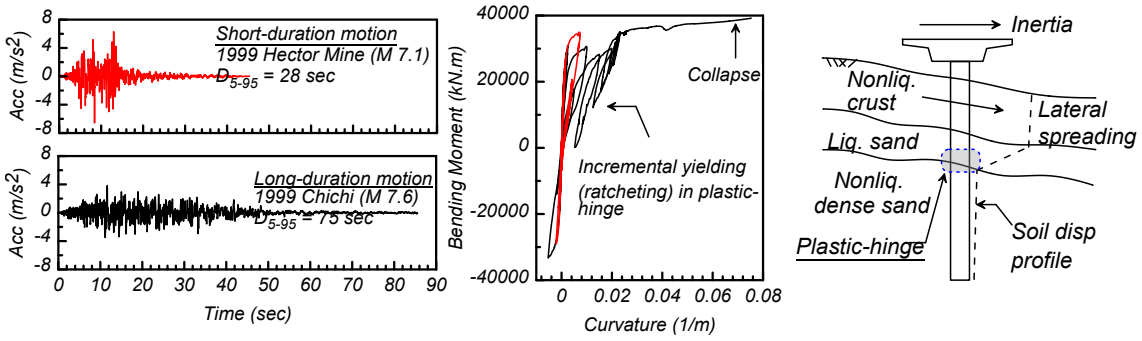

Figure 15. Comparison of input time histories and moment–curvature in plastic hinge between a short-duration motion (red), and a long-duration motion (black).

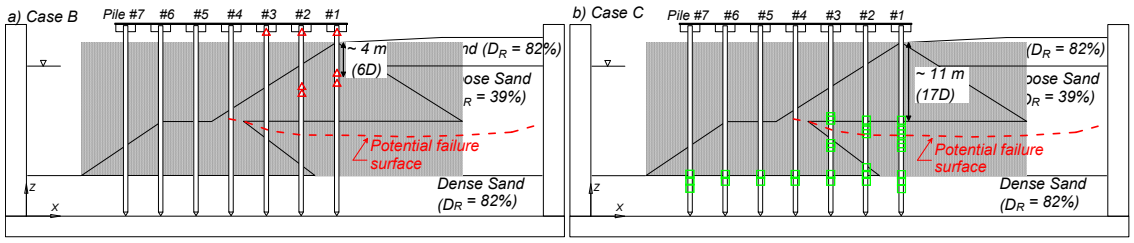

Figure 16. Location of plastic hinges formed along the inelastic piles during incremental dynamic analyses in cases with (a) inertia only in the absence of liquefaction (Case B), and (b) kinematics only (Case C).

REFERENCES

AASHTO (American Association of State Highway and Transportation Officials). 2014. *Guide Specifications for LRFD Seismic Bridge Design*. 2nd ed. with 2014 Interim. Washington, DC: AASHTO.

API (American Petroleum Institute). 1993. Recommended practice for planning, design, and constructing fixed offshore platforms, 20th ed. API RP 2A-WSD. API Publishing Services, Washington, DC.

ASCE (American Society of Civil Engineers). 2014. *Seismic Design of Piers and Wharves,* ASCE/COPRI 61-14. ASCE Standards Committee on Seismic Design of Piers and Wharves. Reston, Va.: ASCE. https://doi.org/10.1061/9780784413487.

Boulanger, R. W., Chang, D., Brandenberg, S. J., Armstrong, R. J., and B. L. Kutter. 2007. "Seismic design of pile foundations for liquefaction effects." In *Proc. of 4th International Conference on Earthquake Geotechnical Engineering*, 277–302. Dordrecht, Germany: Springer. https://doi.org/10.1007/978-1-4020-5893-6_12.

Brandenberg, S. J., Zhao, M., and Kashighandi, P. (2013). "Analysis of three bridges that exhibited various performance levels in liquefied and laterally spreading ground." J. Geotech. Geoenviron. Eng., *139*(7), pp.1035-1048.

Bullock, Z., Liel, A.B., Dashti, S. and Porter, K.A., 2020. A suite of ground motion prediction equations for cumulative absolute velocity in shallow crustal earthquakes including epistemic uncertainty. *Earthquake Spectra*, p.8755293020957342.

Caltrans (California Department of Transportation). 2012. *Guidelines for Foundation Loading and Deformation Due to Liquefaction Induced Lateral Spreading*. Sacramento, CA: Caltrans.

Cubrinovski, M., Bray, J. D., de la Torre, C., Olsen, M. J., Bradley, B. A., Chiaro, G., Stocks, E. and L. Wotherspoon. 2017. "Liquefaction effects and associated damages observed at the Wellington Centreport from the 2016 Kaikoura earthquake." *Bull. N. Z. Soc. Earthq. Eng*., 50 (2): 152–173.

Dickenson, S., Yang, S., Schwarm, D., Rees, M., Hill, C. and Swindon, U.K., 2014. "Seismic performance analysis of pile-supported wharves subjected to long-duration ground motions." In *SMIP14 Proceedings of Seminar on Utilization of Strong-Motion Data, Los Angeles, California* (pp. 63-82).

Egan, J. A., and Wang, Z. L. 1991. "Liquefaction-related ground deformation and effects on facilities at Treasure Island, San Francisco, during the 17 October 1989 Loma Prieta Earthquake." In Proceedings of the 3rd Japan–US workshop on earthquake resistant design of lifeline facilities and countermeasures for soil liquefaction. Technical Report NCEER-91–0001 (pp. 57–76).

Electric Power Research Institute (EPRI), 1990. Manual on Estimating Soil Properties for Foundation Design. Electric Power Research Institute, Palo Alto, California, 308 pp.

Finn, W. D. L. 2005. “A study of piles during earthquakes: Issues of design and analysis.”
B. Earthq. Eng., 3(2), 141–234. https://doi.org/10.1007/s10518-005-1241-3

Hamada, M., Yasuda, S., Isoyama, R., and Emoto, K. 1986. ‘‘Study on liquefaction induced permanent ground displacements.’’ Research Rep., Association for Development of Earthquake Prediction, Japan, November, 87.

Hayden, C. P., Bray J. D. and Abrahamson, N. A. 2014. “Selection of near-fault pulse motions.” Journal of Geotechnical and Geoenvironmental Engineering, 140(7), 04014030.

Idriss IM, Boulanger RW., 2008 “Soil liquefaction during earthquakes. Monograph” MNO-12. Oakland, CA: Earthquake Engineering Research Institute; [261p].

Itasca. 2016. FLAC, Fast Lagrangian Analysis of Continua, User's Guide, Version 8.0. Minneapolis, MN: Itasca Consulting Group, Inc.

Khosravifar, A., Boulanger, R. W. and Kunnath, S. K. 2014. “Effects of liquefaction on inelastic demands on extended pile shafts.” Earthquake Spectra, 30(4), 1749–1773. https://doi.org/10.1193/032412EQS105M

Khosravifar, A., Elgamal, A., Lu, Jinchi, Li, John, 2018 “A 3D model for earthquake-induced liquefaction triggering and post-liquefaction response” Soil Dynamics and Earthquake Engineering, 110, pp. 43–52 https://doi.org/10.1016/j.soildyn.2018.04.008

Khosravifar, A. and Nasr, J., 2017. “Modified design procedures for bridge pile foundations subjected to liquefaction-induced lateral spreading.” *DFI Journal-The Journal of the Deep Foundations Institute*, *11*(2-3), pp.114-127.

Kramer, S.L. and Mitchell, R.A., 2006. “Ground motion intensity measures for liquefaction hazard evaluation.” *Earthquake Spectra*, *22*(2), pp.413-438.

McCullough, N.J., S.E. Dickenson, B. L. Kutter, and D.W. Wilson. 2000. *Pile-Supported Wharf — Centrifuge Model NJM01. Report No. GEG01-2000*. Oregon State University/University of California at Davis.

McCullough, N., and S. Dickenson. 2004. “The Behavior of Piles in Sloping Rock Fill at Marginal Wharves.” In *Proc. Ports Conference 2004*, Reston, VA: ASCE. https://doi.org/10.1061/40727(2004)86

McCullough, N. J., S. E. Dickenson, and S. M. Schlechter. 2001. “The seismic performance of piles in waterfront applications.” In *Ports Conference 2001*, 1–10. Reston, VA: ASCE. https://doi.org/10.1061/40555(2001)83

MCEER (Multidisciplinary Center for Earthquake Engineering Research). 2003. *Recommended LRFD Guidelines for the Seismic Design of Highway Bridges.*

MCEER/ATC-49, Report No. MCEER-03-SP03. Buffalo, N.Y.: University at Buffalo.

Mejia, L. H. and Dawson, E. M. 2006. Earthquake deconvolution for FLAC. Proceedings of fourth international FLAC symposium on numerical modeling in geomechanics, Madrid.

Nasr, J., and A. Khosravifar. 2018. “The Effects of Long-Duration Subduction Earthquakes on Inelastic Behavior of Bridge Pile Foundations Subjected to Liquefaction-Induced Lateral Spreading.” In *Proc. Geotechnical Earthquake Engineering and Soil Dynamics V*, Geotechnical Special Publication 290, Brandenberg, S. J. and M. T. Manzari, eds., 617–625, Reston, VA: ASCE.

ODOT (Oregon Department of Transportation). 2014. *Geotechnical Design Manual.* Tech. Services Branch, Salem, OR

POA (Port of Anchorage). 2017. “Anchorage Port Modernization Project Seismic Design Manual”.

POLB (Port of Long Beach). 2015. “Port of Long Beach Wharf Design Criteria,” Version 4.0 (May). Long Beach, CA: POLB.

Rathje, E., Bachhuber, J., Cox, B., French, J., Green, R., Olson, S., Rix, G., Wells, D., and Suncar, O. 2010. “Geotechnical engineering reconnaissance of the 2010 Haiti earthquake.” GEER Association, Report No. GEER-021.

Seed, H. B., and Idriss, I. M. (1970). ‘‘Soil moduli and damping factors for dynamic response analysis.’’ Rep. No. UCB/EERC-70/10, Earthquake Engrg. Res. Ctr., University of California, Berkeley, Calif.

Souri, M., Khosravifar, A., Schlechter, S., McCullough, N. and S. E. Dickenson. 2020. “Development of experimental p-y curves from centrifuge tests for piles subjected to static loading and liquefaction-induced lateral spreading.” *DFI Journal* 14 (1), 1–15

Souri, M., Khosravifar, A., McCullough, N., Dickenson, S., and S. Schlechter. 2021a. “Design guidelines for pile foundations subjected to liquefaction-induced lateral spreading.” Final Project Report, Deep Foundations Institute Seismic and Lateral Loads Committee.

Souri, M.; Khosravifar, A.; Dickenson, S. E.; Schlechter, S. & McCullough, N. 2021b “Pile-supported wharves subjected to inertial loads and lateral ground deformations: design recommendation” Submitted to ASCE Journal of Geotechnical and Geoenvironmental Engineering (under review)

Tokimatsu, K., Suzuki, H., and M. Sato. 2005. “Effects of inertial and kinematic interaction on seismic behavior of pile with embedded foundation.” *Soil Dyn. Earthq. Eng.* 25 (7–10): 753–762. https://doi.org/10.1016/j.soildyn.2004.11.018

Turner, B. J., Brandenberg, S. J., and J. P. Stewart. 2016. “Case study of parallel bridges affected by liquefaction and lateral spreading.” *J. Geotech. Geoenviron. Eng.* 142.7 (2016): 05016001.

Walling, M., Kuehn, N. and Mazzoni, S., 2018. “Regional ground motion duration prediction model for subduction regions.” In *11th National Conference in Earthquake Engineering*.

Wang, S., Kutter, B.L., Chacko, M.J., Wilson, D.W, Boulanger, R.W., and A. Abghari. 1998. “Nonlinear Seismic Soil-Pile Structure Interaction.” Earthquake Spectra 14(2): 377–396.

Werner, S. D., Dickenson, S. E., and Taylor, C. E. (1997). “Seismic risk reduction at ports: Case studies and acceptable risk evaluation.” Journal of waterway, port, coastal, and ocean engineering, 123(6), 337-346.

WSDOT (Washington Department of Transportation). 2015. *Geotechnical Design Manual.* M 46-03.11, May 2015.

CHAPTER 9

8.6 SUMMARY AND CONCLUSIONS

The research presented in this dissertation is composed of the following major components:

(1) The combination of inertial and kinematic demands in pile foundations subjected to liquefaction-induced lateral spreading was investigated using the experimental data from five centrifuge tests on pile-supported wharves.

(2) The results of the five centrifuge tests were used to back-calculate representative static and dynamic p-y curves for laterally loaded piles and were used to develop practice-oriented p-multipliers (*Pm*) for design.

(3) The pile demands estimated from Equivalent Static Analysis (ESA) were compared to the peak pile demands measured in the centrifuge tests. The peak kinematic demands were estimated from the Newmark sliding block method using recorded accelerations time histories in centrifuge tests. The peak inertial demands were estimated using the natural period of the wharf–foundation system and the spectral acceleration at the ground surface. The analysis was performed for three loading cases: soil displacement only, peak inertia only, and soil displacement combined with 85% of peak inertia. The comparison provided a systematic way to evaluate the accuracy of the proposed load combinations in estimating bending moments demands and provided insights on the circumstances under which each load combination controls the pile design.

(4) A two-dimensional nonlinear dynamic model of a pile-supported wharf was created and calibrated using recorded data from a centrifuge test. The purpose of the analysis was to follow commonly used, practice-oriented approaches in 2D modeling of seismic slope deformations with SSI effects, compare the results with measurements from centrifuge tests, and make reasonable modifications to improve the simulation predictions.

(5) The calibrated numerical model was then subjected to a suite of spectrally matched ground motions covering a wide range of strong motion durations. The analyses were performed for three loading conditions including (a) combined effects of inertial loads from the wharf deck and kinematic ground deformations, (b) inertial load only in the absence of liquefaction, and (c) kinematic load only in the absence of deck mass. These dynamic analyses provided insights on the effects of motion duration on the contribution of soil lateral spreading and wharf deck inertia in pile demands.

The primary conclusions of the analyses are summarized as follows.

- Bending moments adjacent to the pile head can be reasonably estimated by applying the peak inertial load only, while bending moments at deep locations (>10D) can be reasonably estimated by applying the kinematic demands only.
- Bending moments at shallow locations (<10D) can be reasonably estimated by combining kinematic demands with a portion of peak deck inertial load. The portion of the peak inertia that was acting at the deck during the critical cycle

(*Ccc*) ranged from 0.2 to 1.0, and appeared to be generally correlated with soil profile and the dynamic response of each soil unit.

- The wide range of Inertial multipliers (*Ccc*) values observed in this research highlights the benefit of performing coupled nonlinear dynamic analysis that capture complex soil-pile-structure interaction for varying soil profiles.
- Median soil displacements calculated using the Newmark sliding block method are well correlated with permanent displacements from the centrifuge tests, but underestimate the peak transient displacements. Newmark median + 1σ values are better correlated with the peak transient displacements from the centrifuge tests. It is recommended that the median displacements computed using Newmark-type analysis be applied in combination with an idealized soil displacement profile with distinct transitions.
- There is considerable uncertainty in predicting the pattern of soil displacement with depth, and this significantly affects the estimated bending moments in the equivalent static analysis of flexible piles. The distribution of soil displacements in multi-layered soils based on the expected maximum shear strain in each layer resulted in idealized soil displacement profiles with distinct transitions. The overestimation of bending moments due to distinct transitions in idealized soil displacement profiles, when combined with the underestimation of peak transient soil displacements using the Newmark mean values, resulted in a reasonably accurate estimation of the maximum bending moments below grade.

- The peak deck accelerations and the peak shear forces at pile head were reasonably estimated by ESA methods using pushover analyses for both liquefied and nonliquefied conditions.
- The deck displacement demands due to combined effects of inertial and kinematic loads in liquefied conditions were larger than the demands due to inertial loads only in non-liquefied conditions.
- It was recognized that the response of the wharf supported on relatively flexible piles was heavily influenced by lateral soil displacements. The lateral soil displacements were found to be strongly correlated with motion duration due to accumulation of shear strain in liquefied soil in many loading cycles. Consequently, the wharf demands were found to be strongly correlated with motion durations as well even for the spectrally matched ground motions with almost identical response spectra.
- The wharf demands in non-liquefied conditions were primarily driven by the inertial loads form the deck mass and did not vary with motion duration for the spectrally matched motions used in this study. This was due, in large part, to the small seismically-induced slope deformations computed for the non-liquefaction cases.
- For the wharf structure modeled in this study, the occurrence of liquefaction reduced the peak inertial load associated with the wharf deck in most cases (Cliq parameters ranged from approximately 0.7 to 1.1) and showed a slightly increasing trend with motion duration.

- The analyses in this study suggest that the likelihood of inertial load interacting with kinematic load (characterized by the ratio of inertial load at the critical cycle to the peak inertial load during the entire motion) increased with motion duration. However, it was found that the behavior of wharf structures supported on relatively flexible, small-diameter piles, such as the ones studied here, is heavily influenced by the kinematic loads in long duration motions and less so by the inertial loads.
- The modeling completed in this investigation supports the use of damping ratios significantly greater than the 5% routinely used in practice as the basis for defining the spectral acceleration at the fundamental period of vibration of the wharf structure. This appears to reflect the combined influence of radiation damping, nonlinear soil behavior and inelastic pile performance consistent with the cyclically-induced permanent deformations. Given the range of tolerable and anticipated displacements defined in port standards and codes for design-level ground motions, a damping ratio of approximately 10% to 15% appears to more suitably represent aspects of wharf – pile foundation – soil behavior. Project-specific estimates of the structural damping deemed representative of the response of the wharf structure, and therefore the inertial loading, should be made in conjunction with structural analysis.
- Comparison of data produced in this study for wharf structures supported on small-diameter pile groups and those by Khosravifar et al. (2014) for intermediate bridge bents supported on large-diameter single shafts highlights

the similarities and differences in the dynamic response under combined inertial and kinematic loads. It was found that for both types of structures, the interaction of inertial and kinematic loads slightly increases with motion duration. The excessive incremental yielding (ratcheting) in the plastic hinge in large-diameter single shafts during long-duration motions was found to be the reason for cases where the structure collapsed under combined loads but performed satisfactory under both inertial load only and kinematic load only conditions. In contrast, the lack of excessive yielding in pile-supported wharves subjected to long-duration motions was attributed to the lack of overlap between the plastic hinges that form due to inertial loads versus kinematic loads as well as the redundancy in the lateral and vertical load carrying mechanisms (i.e., the plastic hinge development at depth in a row of piles for a wharf does not necessarily lead to collapse of the structure). It was observed that the inertial loads tend to develop plastic hinges at pile head and shallow depths (<10D) on landward piles and kinematic loads tend to develop plastic hinges at deeper locations (>10D) for the soil profile and geometries studied here.

- The load combination factors proposed here are appropriate for decoupled analysis using the p-y spring approach and are not necessarily appropriate for use with the simplified equivalent fluid pressure for lateral spreading load.
- The results of numerical analyses and centrifuge experiments used in this study suggest that design recommendations for highway bridge foundations

that consist of single drilled shafts or small group of large diameter piles should be used judiciously when applied to wharves structures supported on large number of usually smaller diameter piles.

8.7 RECOMMENDATIONS FOR FUTURE WORK

Based on the work presented in this research, there are several avenues for future studies as follows.

- The centrifuge tests studied in this research were all subjected to a series of short duration motions. It would be worthwhile for future centrifuge tests on pile supported wharves to include a series of long duration subduction zone earthquakes.

- The conclusions in this study were derived from the centrifuge tests performed on sands. The applicability of these conclusions to other types of soils that are prone to pore water pressure generation during cyclic loading (e.g. sandy silts and low-plasticity silts) needs to be investigated in future studies.

- These conclusions are applicable only for relatively flexible piles with small diameters (up to about 0.7 m). • It would be worthwhile for future centrifuge tests and numerical modeling to evaluate interaction of inertial and kinematic loads for pile shafts with larger diameters.

- Incorporating uncertainties in design (e.g. uncertainties associated with estimating ground motions) may introduce error in estimating inertial demands

that could affect how the inertial and kinematic demands are combined. The sensitivity of the proposed load combinations to these uncertainties is an important issue that needs to be evaluated in future studies.

- Despite the reasonably good agreement between the nonlinear dynamic analysis performed in this study and the centrifuge test, it is recommended to perform additional analysis using an alternative numerical platform and constitutive models in future studies to evaluate the sensitivity of the concnlusions to the numerical analysis tools. .

- It would be worthwhile for future centrifuge tests and numerical modeling to evaluate the effect of seismic retrofit on the interaction of inertial and kinematic demands in wharf systems.

REFERENCES

Khosravifar, A., Boulanger, R. W., and S. K. Kunnath. 2014. “Design of Extended Pile Shafts for the Effects of Liquefaction.” *Earthq. Spectra* 30 (4): 1775–1799. https://doi.org/10.1193/032512EQS107M